Optical prediction models of whey protein denaturation in thermally treated milk for the development of an inline sensor

HEATHER TATERKA

Universitat Autònoma de Barcelona

Department of Animal and Food Science

Universitat Autònoma de Barcelona

Optical prediction models of whey protein denaturation in thermally treated milk for the development of an inline sensor

PhD in Food Science

HEATHER TATERKA

Bellaterra (Cerdanyola del Vallès), 2016

Planta de Tecnologia dels Aliments UAB

XaRTA
Xarxa de Referència en Tecnologia dels Aliments de la Generalitat de Catalunya

Dr. MANUEL CASTILLO ZAMBUDIO, professor titular del Departament de Ciència Animal i dels Aliments de la Universitat Autònoma de Barcelona (UAB),

FA CONSTAR que HEATHER TATERKA ha realitzat, sota la seva direcció, en el àrea de Tecnologia dels Aliments de la Universitat Autonòma de Barcelona (UAB), el treball titulat "Optical prediction models of whey protein denaturation in thermally treated milk for the development of an inline sensor" que presenta per optar al grau de Doctor en Ciència dels Aliments.

I perquè així consti, signa el present document a:

Bellaterra, Cerdanyola del Vallès, 15 de Juliol del 2016.

Dr. Manuel Castillo Zambudio

Research of this thesis has been financed by a Marie Curie International Reintegration Grant (IRG) 268281 FP7-PEOPLE- 2010-RG: "Development of an optical backscatter sensor for determining thermal denaturation of whey proteins during milk processing".

To my father,

who wanted me to be a pharmacist

“I know one thing: that I know nothing"

Acknowledgements

Thanks is in order, foremost, to my director Dr. Manuel Castillo. Even in the most stressful of times, you have always been supportive. Thank you for your assistance in many areas, personal and professional. I am grateful for your patience and kindness and instilling in me passion for our work. I only hope that one day I can find that sort of dedication.

I would also like to thank Dr. Ted Labuza, for allowing me the opportunity to work again in your laboratory with your very talented group, in particular Dr. Qinchun Rao, who kept me on my feet and helped me gain some excellent laboratory techniques and practice. As well, I would like to thank Dr. Tonya Schoenfuss for her assistance on experimental design and techniques, as well as her valuable conversation on the topic.

For their laboratory assistance in this project, I would like to thank Petri Winkelmolen, Maggie Nitti and Jasper Obers.

Thank you to the faculty and staff of the Food Science department at UAB for their assistance as support throughout this project.

To the colleagues at UAB who gave were there for comedic relief, when necessary. A special thank you, Aida, Claudia, Cristina and Joan.

For all of the friends who have personally supported me through this journey, I am very thankful. If I had to name you all I'd need another book, and for that I consider myself very lucky.

To my mother, thank you for always being there.

And to my favorite reason for sticking around here in Barcelona, Christian. Thank you for supporting me in pretty much every way imaginable. You've encouraged me to be my best, even when I'm at my worst. I couldn't have survived this without you.

Publications

Analysis of the preferential mechanisms of denaturation of whey protein variants as a function of temperature and pH for the development of an optical sensor. International Journal of Dairy Technology (accepted May 2016) Authors: Heather Taterka, Manuel Castillo

Heather Taterka, Manuel Castillo. 2015. **The effect of whey protein denaturation on light backscatter and particle size of the casein micelle as a function of pH and heat-treatment temperature.** International Dairy Journal, 48, 53-59.

Presentations related to this thesis

Zamora, A., Hebishy, E., Rocha, A., Taterka, H., González, C., Ayala, N., Gallardo, J., Saldo, J., Castillo, M. Application of native fluorescence tracers for quick quantification of milk damage during milk processing. ICEF 12, Québec, Canada, June14-18, 2015.

Zamora, A., Ayala, N., Gràcia-Julià, A., Rocha, A., Taterka, H., Gonzalez, C., Gallardo, J., Saldo, J., Castillo, M. Rapid quantification of milk damage during milk processing using native fluorescence tracers. 29th EFFoST International Conference. Food Science Research and Innovation: Delivering sustainable solutions to the global economy and society, Athens, Greece, November 10-12, 2015.

Taterka, Fernández-Avila, C., Castillo, M. Modeling the light backscatter response signal as a function of the denaturation of whey proteins in heat treated milk for the development of an inline optical sensor. EFFoST, 7th International Conference on Food Factory for the Future. Uppsala, Sweden, November 25-28, 2014.

Taterka H., Castillo M. Analysis of the preferential mechanisms of denaturation of whey protein variants in heat treated milk as a function of temperature and pH for the development of an optical sensor. 7th International Whey Conference, Rotterdam, Netherlands. September 7-9, 2014.

Taterka H., Rao Q., Labuza TP., Castillo M. Kinetic analysis of the pH-specific mechanisms of denatured whey protein interaction for the development of an optical light backscatter sensor. 7th International Whey Conference, Rotterdam, Netherlands. September 7-9, 2014.

Taterka H, Castillo M. Desnaturalización de las proteínas del suero en leche desnatada reconstituida: dispersión de luz y tamaño de la micela de caseína en función del pH y la temperatura de tratamiento. CIBIA 9 2014 Valencia, Spain.

Gallardo-Chacón JJ, Taterka H, Zamora A, Rocha Humboldt AV, Liu J, Saldo J, Castillo M. Aplicación de indicadores nativos de fluorescencia para la cuantificación rápida de daño térmico durante el procesado de la leche. CIBIA 9 2014 Valencia, Spain.

Taterka H, Castillo M. Evaluación óptica de la formación pH dependiente de complejos entre micelas de caseína y proteínas séricas desnaturalizadas mediante calor. Congreso Español de Ingeniería de Alimentos CESIA 2012 Ciudad Real, Spain.

Taterka H, Castillo M. A review of the pH influenced casein-whey protein interactions in heated milk. American Dairy Science Association (ADSA) Conference, Phoenix, Arizona 2012

Abstract

An inline whey protein denaturation sensor would be of interest to the dairy industry to monitor milk batch variations and to achieve the highest quality products. It has been well-established that whey protein denaturation is a pH-dependent mechanism, in which proteins at lower pH values (pH 6.3) tend to form complexes with κ-casein on the surface of the casein micelle, and at higher pH values (pH 7.1) the preference is for unfolded whey proteins to for serum complexes, in general, with other denatured whey proteins. The objective of this PhD was to develop successful prediction models of whey protein denaturation variables utilizing an optical sensor set-up with the potential for inline implementation during thermal processing.

The optical sensor system was developed with inline implementation in mind, with the goal being to measure the effects of temperature, pH and time on the changes in light scatter of thermal treated skim milk and relate these changes to the denaturation of whey proteins. Variables to be compared to the optical light backscatter response were particle size and the whey protein concentration of the three whey protein configurations that occur in milk after thermal treatment: native, micelle-bound and soluble aggregate whey protein. In the second and third experiments, tryptophan front-face fluorescence spectroscopy was also tested with the potential for sensor development and compared to light backscatter technology.

Results of the first experiment showed a relationship between light backscatter intensity and particle size, in particular at pH 6.3 whereas at pH 7.1 no notable changes in the light backscatter intensity or particle size were observed with an increasing in heat treatment temperature. In the second experiment, curves of LB and FFF intensity versus time at pH 6.3 resembled curves of particle size and bound whey protein, and their first-order kinetic rate constants were not statistically different. The third experiment included a range of fat percentages (<0.5%, 1.3% and 3.7%) and exhibited a noticeably greater amount of light scatter and larger particle size with increasing fat content.

Model equations showed successful predictions of particle size as a function of light backscatter. In the second experiment, models of bound whey protein at pH 6.3 were best fit to models as a function of the light backscatter spectra, whereas soluble aggregate whey protein content showed best fit when using tryptophan fluorescence measurements. Light

backscatter regions which corresponding to best-fit models for particle size and bound whey protein models were near the maximum intensity wavelength (540-600 nm) or included a ratio combination of a numerator value between 387-569 nm and denominator from 963-1033 nm. Front-face fluorescence models also exhibited good R^2 values near the maximum intensity wavelength, however a ratio of numerator near 340 nm combined with a denominator around 390 nm yielded models with a better fit. An interesting finding was the relationship exhibited by particle size models as a function of light backscatter, which exhibited an exponential character using an equation with the intercept value similar to the initial particle size. Combined models over a range of pH values (6.3, 6.7 and 7.1) predicted particle size as a function of light backscatter, giving promise to the development of an optical inline backscatter sensor technology.

Resumen

Un sensor de proteínas del lactosuero desnaturalizadas, en línea, sería de gran interés en la industria láctea para monitorizar las variaciones entre lotes de leche durante el procesado y obtener productos de alta calidad. Se ha demostrado que el mecanismo de desnaturalización de las proteínas del suero depende del pH; a pH más bajo (pH 6,3) las proteínas desnaturalizadas tienden a formar complejos con la κ-caseína en la superficie micelar, mientras que a valores de pH más altos (pH 7,1) las proteínas de suero desplegadas forman preferentemente complejos de carácter soluble con otras proteínas de suero desnaturalizadas. El objetivo de esta tesis doctoral ha sido desarrollar con éxito modelos de predicción de las diferentes conformaciones que presentan las proteínas de suero en leche tratada termicamente mediante parámetros obtenidos empleando un sistema óptico de medida con potencial para la aplicación en línea durante el procesado térmico de leche.

El sistema óptico de medida fue desarrollado con vistas a su aplicación en línea, con el objetivo de determinar los efectos de la temperatura, el pH y el tiempo sobre los cambios en la dispersión de luz observados en la leche desnatada tratada térmicamente, y relacionar dichos cambios con la desnaturalización de las proteínas del lactosuero. Las variables a correlacionar con la señal de dispersión de luz fueron el tamaño de partícula y la concentración de las diferentes configuraciones de proteína sérica que se producen en la leche después del tratamiento térmico: proteínas nativas, proteínas desplegadas unidas a la superficie de la micela y agregados solubles de seroproteínas desnaturalizadas. En el segundo y tercer experimento, se evaluó la espectroscopia de fluorescencia *front-face* del triptófano para comparar dicha tecnología optica con las medidas de dispersión de luz.

Los resultados del primer experimento mostraron una correlación entre la intensidad de dispersión de luz y el tamaño de partícula, concretamente a pH 6,3, mientras que a pH 7,1 no se observaron cambios notables en la intensidad de dispersión de luz ni en el tamaño de partícula con el aumento de la temperatura del tratamiento térmico. En el segundo experimento, las curvas de dispersión y fluorescencia *versus* tiempo a pH 6,3 fueron similares a las curvas de tamaño de partícula y de proteína de suero unida a la micela, no observándose diferencias significativas entre sus constantes cinéticas de primer orden. El tercer experimento incluyó un rango de porcentajes de grasa (<0,5%, 1,3% y 3,7%) y exhibió una intensidad de dispersión de luz y de tamaño de partícula notablemente mayor al aumentar el contenido en grasa.

Se obtuvieron con éxito modelos de predicción del tamaño de partícula en función de la dispersión de luz. Los modelos de interación de proteína de suero-caseína a pH 6,3 se ajustaron mejor a los parametros obtenidos a partir de los espectros de dispersión de luz, mientras que los modelos de predicción del contenido de agregados solubles de proteína de suero desnaturalizada se ajustaron mejor a las determinaciones de fluorescencia de triptófano. Un hallazgo significativo fue la correlación exponencial obtenida entre el tamaño de partícula y la intensidad de dispersión de luz, que permitió obtener una ordenada en el origen que se corresponde bastante fielmente con los valores medios iniciales de tamaño de las micelas de caseína antes del tratamiento térmico. Un modelo combinado en un rango de pH 6,3, 6,7 y 7,1 permitió predecir el tamaño de partícula en función de valores de intesidad de dispersión de luz, mostrando potencial para el desarrollo de un sensor de dispersión óptica en línea que permitiría estimar el tamaño de partícula dentro de un rango de valores de pH y de intesidades de tratamiento térmico.

Resum

Un sensor de desnaturalització de les proteïnes de sèrum de llet en línia seria de gran interès a la indústria làctica per a monitoritzar les variacions entre diferents lots de llet i obtenir productes d'alta qualitat. S'ha demostrat que el mecanisme de desnaturalització de les proteïnes del sèrum làctic és depenent del pH; les proteïnes amb valors de pH més baixos (pH 6,3) tendeixen a formar complexos amb la κ-caseïna a la superfície de la micel·la de caseïna, mentre que a valors de pH més alts (pH 7,1) les proteïnes de sèrum desplegades formen preferentment, i en general, complexos amb altres proteïnes de sèrum desnaturalitzades de caràcter soluble. L'objectiu d'aquesta tesi doctoral ha estat desenvolupar amb èxit els models de predicció de les diferents conformacions que presenten les proteïnes de sèrum en llet tractada tèrmicament mitjançant paràmetres òptics obtinguts mitjançant un sistema òptic de mesura amb potencial per a l'aplicació en línia durant el processament tèrmic de la llet.

El sistema òptic de mesura va ser desenvolupat amb vista a la seva aplicació en línia, amb l'objectiu de determinar els efectes de la temperatura, el pH i el temps sobre els canvis en la dispersió de llum observats en la llet descremada tractada tèrmicament, i relacionar aquests canvis amb la desnaturalització de les proteïnes del lactosèrum. Les variables a correlacionar amb el senyal de dispersió de llum van ser la grandària de partícula i la concentració de les diferents configuracions de proteïna sèrica que es produeixen en la llet després del tractament tèrmic: proteïnes natives, proteïnes desplegades unides a la superfície de la micel·la i agregats solubles de seroproteïnes desnaturalitzades. En el segon i tercer experiment, també es va avaluar l'espectroscòpia de fluorescència front-face del triptòfan a fi de comparar aquesta tecnologia òptica amb la de dispersió de llum i avaluar el potencial per al desenvolupament d'un sensor en línia.

Els resultats del primer experiment van mostrar una correlació entre la intensitat de dispersió de llum i la grandària de partícula, en particular a pH 6,3, mentre que a pH 7,1 no es van observar canvis notables en la intensitat de dispersió de llum ni en la grandària de partícula amb l'augment de la temperatura del tractament tèrmic. En el segon experiment, les corbes de LB i FFF *versus* temps a pH 6,3 van ser similars a les corbes de grandària de partícula i de proteïna de sèrum unida a la micel·la, no observant-se diferències significatives entre les seves constants cinètiques de primer ordre. El tercer experiment va incloure un rang de percentatges de greix (<0,5%, 1,3% i 3,7%) i va exhibir una intensitat de dispersió de llum i de grandària de partícula notablement major en augmentar el contingut en greix.

Es van obtenir amb èxit models de predicció de la grandària de partícula en funció de la dispersió de llum. En el segon experiment, els models de interacció de proteïna de sèrum-caseïna a pH 6,3 es varen ajustar millor als models en funció dels espectres de dispersió de llum, mentre que els models de predicció del contingut d'agregats solubles de proteïna de sèrum desnaturalitzada es van ajustar millor a les determinacions de fluorescència de triptòfan. Les regions de dispersió de llum que corresponen als models de millor ajust per a la grandària de partícula i la proteïna de sèrum associada a les micel·les van emprar longituds d'ona properes a la longitud d'ona de màxima intensitat (540-600 nm) o a una ràtio de longituds d'ona amb valors d'intensitat obtinguts entre 387-569 nm en el numerador i entre 963-1033 nm en el cas del denominador. Els models de fluorescència front-face també van mostrar bons valors de R2 a longituds d'ona properes a la d'intensitat màxima, no obstant això, una ràtio de intensitats a 340 nm (numerador) i 390 nm (denominador) va proporcionar models amb un millor ajust. Una troballa de interès va ser la correlació exponencial obtinguda entre la grandària de partícula i la intensitat de dispersió de llum, que va permetre obtenir una ordenada en l'origen que es correspon bastant fidelment amb els valors mitjans inicials de grandària de les micel·les de caseïna abans del tractament tèrmic. Un model combinat en un rang de pH 6,3, 6,7 i 7,1 va permetre predir la grandària de partícula en funció de valors de intensitat de dispersió de llum emprant valors experimentals corresponents als experiments segon i tercer, mostrant potencial per al desenvolupament d'un sensor de dispersió òptica en línia que permetria estimar la grandària de partícula dins d'un rang de valors de pH i de intensitats de tractament tèrmic.

Table of Contents

Abbreviations

ANOVA	Analysis of variance
AWP	Aggregate whey proteins
BCA	Bicinchoninic acid
BSA	Bovine serum albumin
BWP	Bound whey proteins
CCP	Colloidal calcium phosphate
CL	Confidence limit
CMP	Caseinmacropeptide
CORR	Correlation procedure
CP	Centrifuged whey proteins
DF	Degrees of freedom
DLS	Dynamic light scattering
DO	Denominación de origen
DWS	Diffusing wave spectroscopy
E_{gap}	Band gap energy
FFF	Front-face fluorescence
GLM	General linear model
HHP	High hydrostatic pressure
HPLC	High performance liquid chromatography
HTST	High temperature short time processing
I_d	Light backscatter intensity of the ratio denominator
IgG	Immunoglobulin
I_m	Maximum light backscatter intensity
I_n	Light backscatter intensity of the ratio numerator
IR	Infrared
k	Rate of change
LB	Light backscatter
LSM	Least square means
ME	2-mercaptoethanol
MFGM	Milk fat globule membrane
MIR	Mid-infrared
$n_{D,20}$	Refractive index
NIR	Near-infrared
NLIN	Non-linear regression
NWP	Heated native whey proteins
$NWP_{initial}$	Unheated native whey proteins
PAGE	Polyacrylamide electrophoresis
PARAFAC	Parallel factor analysis
PCA	Principal component analysis
PDCASS	Protein digestibility-corrected amino acid score
PDO	Protected designation of origin
PLS	Partial least squares
PS	Particle size z-average
RP-HPLC	Reverse phase high performance liquid chromatography

SAS	Statistical Analysis System
SDS	Sodium dodecyl sulfate
T	Temperature
t	Time
Trp	Tryptophan
UHT	Ultra-high temperature processing
WP	Whey protein
WPC	Whey protein concentrate
a-LA	Alpha-lactalbumin
αs-CN	Alpha s casein
β-CN	Beta-casein
β-LG	Beta-lactoglobulin
ϰ-CN	Kappa-casein
λ_{max}	Maximum wavelength

CHAPTER 1: Interest of Study

The heat treatment of milk is an essential step in industrial dairy food processes to eliminate pathogens, reduce the number of microorganisms and inactivate enzymes in order to improve conservation time and/or modify milk functional properties. On the other hand, milk heat treatment may impart some undesirable consequences such as browning reactions, the production of off-flavors, the inactivation of nutrients and bacterial growth inhibitors and whey protein denaturation. Some of the negative effects that whey protein denaturation may have on cheese production is a slower gelation time and looser gel structure (Alloggio et al., 2000), the formation of a highly networked protein structure (Schorsch et al., 2001) and an increase in moisture content which may lead to poorly ripened cheese. However, for industrial purposes, whey protein denaturation in milk may or may not be desirable, depending on the product to be manufactured. An effect of whey protein denaturation is an increase in reactive amino acid side chains; thus increasing protein-protein interactions. As a result, there is an increase in water holding capacity in the gel structure, which has been found to decrease the occurrence of "wheying off" and may act to improve the final texture of yogurt (Mottar et al., 1989). Therefore, early prediction of the potential gelling strength of milk would allow milk batches to be used for their most suitable purposes. From a market standpoint, real time measurement of milk whey protein denaturation could allow for more consistent high quality dairy products. If milk with a high degree of whey protein denaturation is used in cheese making; time and raw materials, such as milk, calcium and rennet may be wasted if the cheese produced is unsuitable for sales. Alternatively, this milk could have been used to produce a successful yogurt.

To date, no rapid, inexpensive methods exist for the inline determination of whey protein denaturation in processed milk. The theory behind the development of our sensor proposal utilizes optical light backscatter technology and the scattering properties of casein micelles. The use of an optical light backscatter technique for the determination of whey protein denaturation has first been reported by Lamb et al., (2013) based on the assumption that denatured whey proteins attach to the surface of the casein micelle and result in a change in the size of the casein micelle. Lamb et al. (2013) was able to model β-LG denaturation in milk during heat treatments as a function of optical data, in which a correlation between these two was found. However, it should be considered that the binding of denatured whey proteins to the surface of the casein micelle has been found to be highly pH specific, in which

maximum binding occurs at a low milk pH (6.3) whereas at higher pH values (7.1) there seems to be a preference for the formation of soluble whey protein aggregates that remain in the serum portion of the milk matrix (Vasbinder & de Kruif, 2003). The formation of a whey protein/casein complex on the surface of the casein micelle has been found to increase the size of the casein micelle, however at higher pH values, little to no change in casein micelle particle size has been observed (Anema & Li, 2003a). This change in preference of attachment for denatured whey proteins as a function of milk pH should result in different light scatter properties of the casein micelle. As milk characterisics, such as pH, may vary depending on certain factors such as breed of cow, season and feed (Linn, 1988), among other parameters, it is necessary to consider pH an important variable for the development of an optical sensor based on this mechanism. As a result, our study aimed to target the pH-dependence of whey protein denaturation mechanisms, and in particular, the consequence of the attachment of denatured whey proteins to the micelle with respect to changes in the optical light backscatter signal intensity. Therefore the interest of this study lies in the inline determination of the extent of whey protein denaturation in heat treated milk, which would allow the dairy industry to use specific milk batches for their optimal purpose.

CHAPTER 2: Literature Review

2.1 Milk

Milk consumption began during the Neolithic agricultural revolution and the domestication of cattle in Southwest Asia, which later spread to Europe around 7000 BC (Beja-Pereira et al., 2006). It has been historically considered a high value animal product. Once being established as nutritionally useful to humans, milk became a culturally significant food source in many regions. With an increase in milk consumption, milk pasteurization became common practice to reduce tuberculosis and other important infections from raw milk (HowStuffWorks, 2015). Industrial production began around the mid-19th century and milk has been a wide-spread consumer good ever since. Milk is distribution as a liquid beverage or other dairy product such as cheese, yogurt, cream and butter.

2.1.1 Milk composition

Milk contains a complex mixture of lactose, fat, protein and minerals. Its main components are summarized in Table 2.1. Lactose, which is a reducing sugar consisting of glucose and galactose, is found in milk at somewhere close to 5% *w*/*w* content. From a nutritional standpoint, it is commonly known to be one of the "problem" components of milk. Many people (up to 70% worldwide) are found to be absent of the enzyme lactase which may lead to chronic digestion problems (Lomer et al., 2008). As a result, dairy markets have aimed toward producing "lactose-free" products which, despite labeling tactics, generally do contain lactose plus the lactase enzyme added in order to aid in proper digestion. Another milk component is milk fat, which exists as a mixture of fatty acid chains, phospholipids, and mono and diglycerides. Milk fat globules are storage centers for many vital nutritional components to be transferred from mother to baby, and are therefore animal-specific. For example, human milk fat has been found to contain protective components to aid infants in building proper gut flora and protecting against microorganisms (Hamosh et al., 1999). Another aspect of milk fat globules is their composition and size, for instance goat milk fat globules are found to contain significantly higher levels of nutritious short and medium chain fatty acids and, in general, a smaller globule size that may promote

easy digestion in human consumption (Haenlein, 2004). Fat globule size is also sufficiently large to impact the light backscatter properties of milk.

Table 2.1 Approximate composition of cow milk

Component	Average content in milk (%*w*/*w*)	Range (%*w*/*w*)	Average content in dry matter (%*w*/*w*)
Water	87.1	85.3-88.7	--
Lactose	4.6	3.8-5.3	36
Fat	4.0	2.5-5.5	31
Protein	3.3	2.3-4.4	25
Casein	2.6	1.7-3.5	20
Mineral substance	0.7	0.57-0.83	5.4
Organic acids	0.17	0.12-0.21	1.3
Miscellaneous	0.15	--	1.2

Adapted from Walstra et al. (2005)

The main protein component found in milk is casein, followed by whey proteins and smaller amounts of other protein components, such as enzymes. Casein is largely important in dairy products as many dairy foods involve the enzymatic and/or acid-induced coagulation of casein, such as cheese and yogurt. Briefly, this process involves destabilization of the casein micelle further causing the promotion of interactions on the micellar interface, which induce the formation of a three/dimensional casein matrix. Then liquid portion is then expelled from the more tightly structured matrix of casein, retaining fat and minerals. This process is called syneresis. Historically the liquid, or whey, was considered a waste by-product of cheesemaking and other dairy products. Now whey is also considered a nutritionally important protein source with an even higher quality protein digestibility-corrected amino acid score (PDCAAS) than casein (Pasin & Miller, 2000). Since milk proteins are of a very high quality, caseins and whey proteins are commonly used as nutritional supplements, and are promoted for use in exercise focused groups for consumption as shakes and bars (Pasin & Miller, 2000). An important consideration, which may be overlooked, is that depending on the origin (casein, whey, soy, egg, etc.) proteins have varying amino acid composition as well as digestion characteristics.

Mineral substances present in milk are K^+, Na^+, Ca^{2+}, Mg^{2+}, Cl^-, and phosphate. These minerals aid in pH equilibrium and are generally associated to each other and/or with protein components in both the aqueous and micellar phase (Gaucheron, 2005). Other constituents

include organic acids and trace miscellaneous components. It should be noted that the content of the various components may vary depending on cow breed, season and feeding habits. For example, differences in casein and calcium content have been found between various cow breeds in which a lower casein/calcium content was associated with lower coagulation strength (Macheboeuf et al., 2006) which has been found to result in differences in cheese quality (De Marchi et al., 2008). Thus Table 2.1 represents approximate composition of milk based on average content values for milk components.

2.1.2 Milk structure

As a polydisperse colloidal solution, milk contains components with a range of sizes, charges and composition. Therefore it is essential to understand the varying components and how they interact within the milk matrix. Depending on the component, different structural aspects should be considered. For example, fat is the largest particle in milk with a diameter of approximately 0.1-10 μm, thus with respect to the remaining portions of milk it is considered an oil-in-water emulsion (Table 2.2). Fat molecules are relatively easy to separate from the remaining portion of milk; referred to as milk plasma (Table 2.2) (Figure 2.1).

Table 2.2 Structural elements of milk (adapted from Walstra et al., 2005).

	Milk			
		Plasma		
			Serum	
	Fat Globules	Casein Micelles	Globular proteins	Lipoprotein particles
Main component	Fat	Casein, water, salts	Serum protein	Lipids, proteins
Colloidal status	Emulsion	Fine dispersion	Colloidal solution	Colloidal dispersion
Particle diameter	0.1−10 μm	20−500 nm*	3−6 nm	10 nm
Visible with	Microscope	Ultramicroscope	----	Electron microscope
Isoelectric point	~3.8	~4.6	4−5	~4

*(McMahon & Brown, 1984; Walstra et al., 2005)

On the other hand, casein micelles are considered a dispersion in the liquid (whey or serum portion) of milk. Casein micelles contain a large portion of water and, internally, contain calcium phosphate or colloidal calcium phosphate (CCP). The surface of the casein molecule is negatively charged allowing interactions with minerals, such as calcium and

magnesium. The continuous phase which casein micelles and fat molecules are dispersed is called milk serum (Table 2.2) (Figure 2.1). Within the serum portion there are smaller globular proteins (whey or serum proteins) and lipoproteins which, in general, contain residues of mammary secretions (Walstra et al., 2005). Thus it is important to perceive milk with regard to the milk portion in question considering that milk can be classified as both an oil-in-water emulsion and a dispersion of various particles.

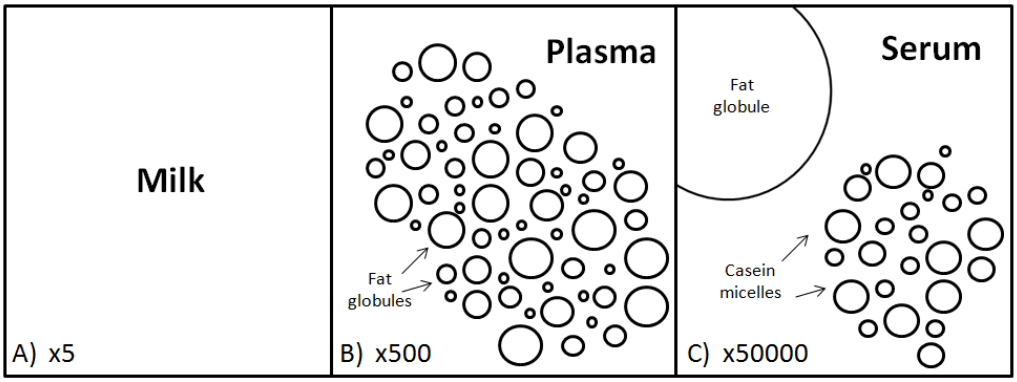

Figure 2.1 Images of milk components at various levels of magnification, adapted from Walstra et al. (2005).

2.2 Whey protein structure and functionality

Whey proteins are the second major protein source in milk, after casein, comprising approximately 20% of total milk protein. Whey proteins can be defined as protein which does not precipitate upon acidification at pH 4.6, and may also be referred to as serum proteins or non-casein nitrogen. The major constituents, *β*-lactoglobulin and *α*-lactalbumin, make up approximately 80% of the total whey protein mass proportion. The remainder of whey protein comes from bovine serum albumin (BSA), immunoglobulin G and lactoferrin (Table 2.3). In the production of most dairy products, whey proteins are not present in the final product and are instead considered a waste by-product. Until realized that whey proteins contained high quality protein profiles, the whey containing waste portion was disposed of during industrial dairy productions. Currently, whey tends to be considered a useful by-product of high value in the production of dairy goods.

Table 2.3 Typical protein composition of whey (adapted from Farrell et al., 2004).

Protein	Proportion by mass (%)	No. Amino acids	Molecular mass (Da)	Disulfide bonds/thiols
β-Lactoglobulin	60	162	18,363[a]	2/1
a-Lactalbumin	20	123	14,178	4/0
Bovine serum albumin (BSA)	3	583	66,399	17/1
Immunoglobulin G (IgG)	10	>500	161,000[b]	--
Lactoferrin (Lf)	<0.1	689	76,110	17/0

[a]Molar mass from A variant

[b]IgA most prevalent isoform

*From Boland, Singh, & Thompson (2014)

Whey proteins are, in general, sensitive to heat treatment and will denature upon temperatures above 60 °C exposing reactive side chains, which may promote protein-protein interactions within the milk matrix. As a result of their unique characteristics and varying amount of disulfide and/or thiol groups (Table 2.3), their respective reactivity after denaturation is unique. As discussed further in Section 2.5.4, each type of whey protein has different variant types, which gives them each a specific reactivity dependent on their structure.

2.2.1 Beta-lactoglobulin

Sixty percent of the mass proportion of whey protein comes from *β*-lactoglobulin (*β*-LG) (Table 2.3). Structurally, *β*-LG is very similar to serum retinol binding protein, in that the eight-strand *β*-barrel aids in binding, helping *β*- LG to act as an efficient carrier protein (Creamer et al., 2011). The primary structure of *β*-LG includes a disulfide bonds at Cys 106-119 and Cys 66-160 and a free thiol group at Cys 121 (Figure 2.2). Even so, the free thiol group is buried deep within the protein structure, thus rendering it relatively unreactive in the native form. The secondary structure is estimated to be around 50% *β*-sheet and 10% *a*-helix. *Beta*-lactoglobulin generally exists in equilibrium of both the monomeric and dimeric form at room temperature (20 °C), however, with heat treatment (>30 °C) it is found primarily in the monomeric form (Fox & McSweeney, 1998). As well, there exist three genetic variants of *β*- LG; A, B, and C, nevertheless the C variant is found in very small proportions in bovine milk. Variants differ by specific amino acid substitutions. Between the two variant types A and B, there are only minor amino acid substitutions. For example, Ala in the B

variant is substituted for Val at 118 in the A, and at 64 Gly in B substituted for Asp in A (Creamer et al., 2011). Although these are only minor substitutions, they have been found to contribute to alterations in functionality and can affect the rate of protein denaturation and the promotion of protein-protein interactions (Section 2.4.5).

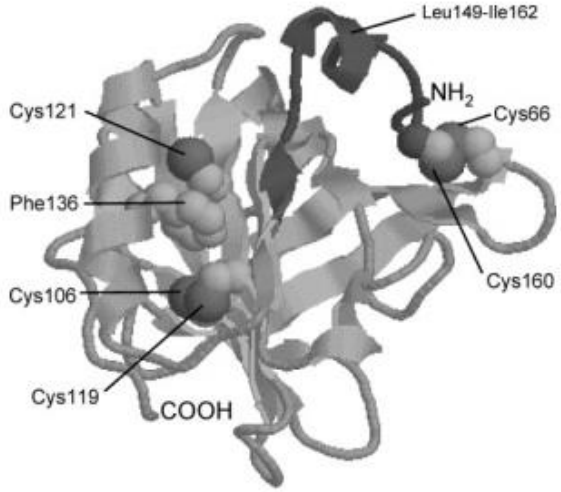

Figure 2.2. *Beta*-lactoglobulin three-dimensional structure (Creamer et al., 2004).

A closer look at the *β*-LG structure allows the observation of a highly hydrophobic region of the molecule in which there are five cysteine residues (Figure 2.2). Once heat-induced monomerization of *β*-LG occurs and partial unfolding exposes the free sulfhydryl group of Cys 121, further aggregation reactions may be triggered (Mulvihill & Donovan, 1987). Once exposed, Croguennec et al., (2003) found that the free sulfhydryl on Cys 121 readily reacts with Cys106-119, resulting in a reversible Cys 106-121 disulfide bond with a free thiol on Cys 119. They hypothesized that this was an "activation" step leading to further protein-protein interactions, including interactions with other disulfide bond containing proteins. On the other hand, it has also been suggested that the Cys 121 residue alone is responsible for irreversible aggregation, as recombinant mutant Cys 121 was found to favor an unfolded configuration of the protein after heat-induced interactions, thus Cys 121 plays a vital role in the formation of aggregates (Jayat et al., 2004). Another observation is that the sulfhydryl groups of *β*-LG become highly sensitive to heat-induced interactions as pH increases from 3 to 7.5, hence pH is an important consideration in heat-induced interactions (Singh, 2004). Nonetheless, comprehending aggregation mechanisms in a more complex system, such as milk, has proven to be an even greater challenge.

2.2.2 Alpha-lactalbumin

The second most abundant whey protein in milk (around 20%) is *a*-lactalbumin (*a*-LA). Using circular dichroism it was found that the secondary structure of *a*-LA contains briefly 26% *a*-helix, 14% *β*-sheet and 60% ordered structure (Bottomley et al., 1990). Four disulfide bonds are found in *a*-LA (Cys 6-120, Cys 28-111, Cys 61-77, Cys 73-91) (Brew, 2003) (Table 2.3). The main function of *a*-LA is as a coenzyme (along with galactosyltransferase) for catalyzing the lactose synthesis pathway. Another key constituent of *a*-LA is calcium, which contributes to the thermal stabilization of the protein structure (Rodríguez et al., 2014). Besides weakening of the protein configuration by disulfide bond cleavage, *a*-LA may also become susceptible to unfolding if calcium is removed from the internal structure (Walstra et al., 2005). Bovine *a*-LA has two genetic variants A and B, however only the B variant is found in Western milk (Prasad et al., 1982).

2.2.3 Other whey proteins present in milk

Other less prevalent whey proteins include bovine serum albumin (BSA), immunoglobulins and lactoferrin. Bovine serum albumin, which exists as a result of leakage from the blood, is a large protein, however only present in small quantities in milk (Table 2.3) (Walstra et al., 2005). The natural purpose of immunoglobulins in milk is the immunization effects they hold. In early stages of growth, immunoglobulins are absorbed by the calf into the blood stream for protective effects. Structurally, immunoglobulins are classified as Immunoglobulin A, M or G. Immunoglobulin G (IgG) specifically exists as a polymer containing two heavy and one light chain, whereas immunoglobulin M is a macromolecule containing various IgG-like molecules attached in a somewhat pentameric form (Walstra et al., 2005). Lactoferrin is present in milk as a bacterial inhibitor, and is found in very low concentration in milk. There are more than 100 additional proteins/enzymes, found in lower concentration (Rodríguez et al., 2014).

2.3 Casein micelle structure and functionality

Casein micelles are negatively charged molecules accounting for ~80% of the protein content in milk. They tend to have a dense hydrophobic core containing the majority of the hydrophobic portions of casein, whereas the surface of the micelle contains hydrophilic portions. Their high charge is in part a result of containing many phosphate groups which allow them to stay in solution and form hydrophobic bonds with other casein micelles and/or other milk components. Phosphate groups bind Ca^{2+} which acts to stabilize the micelle. On a dry matter basis, casein micelles contain 94% protein and 6% low molecular weight species, referred to as colloidal calcium phosphate (CCP), consisting of calcium, magnesium, phosphate and citrate (Fox & McSweeney, 1998). Micelles are voluminous and have the potential to bind about 2.0 g H_2O g^{-1} protein. Their diameters range from 20-500 nm (McMahon & Brown, 1984; Walstra et al., 2005), with an average of 200 nm (de Kruif, 1998). In fact, κ-CN content may be an indicator of micelle size in that the amount of κ-CN has been found to be inversely related to casein micelle diameter (Dalgleish et al., 1989). In general, size variation occurs between milk from each specific animal but, as expected, tends to be more consistent than the variation which is found among different individual animals and/or breeds (Walstra et al., 2005).

The four peptide chains involved in casein micelles α_{s1}, α_{s2}, β and κ, which are found in proportions of approximately 38%, 10% 36% and 13%, by weight; and several minor proteins, including γ-caseins (proteolytic fragments of β-casein) and proteose-peptones found in the serum portion (Davies & Law, 1983). The order of hydrophobicity of caseins is $\beta > as1 > \kappa > as2$ (Walstra & Jenness, 1984). The αs caseins and β caseins form the inner structure of the casein micelle, whereas κ-casein (κ-CN) is found on the outer surface of the micellar structure allowing micelles to exhibit Brownian motion. As a result, its two cysteine residues are mainly responsible for the formation of intermolecular disulfide bonds, potential aggregation and/or other protein-protein interactions. Moreover, the casein micelle has a high degree of stability under thermal stress conditions, therefore the two cysteine groups of α_{s2}, found internally, are less likely to be influenced by protein-protein interactions. In general the micelle structure (Figure 2.3) is quite rigid. The high content of proline limits the formation of much secondary structure, favoring a more random arrangement and somewhat open structure (Regan et al., 2009).

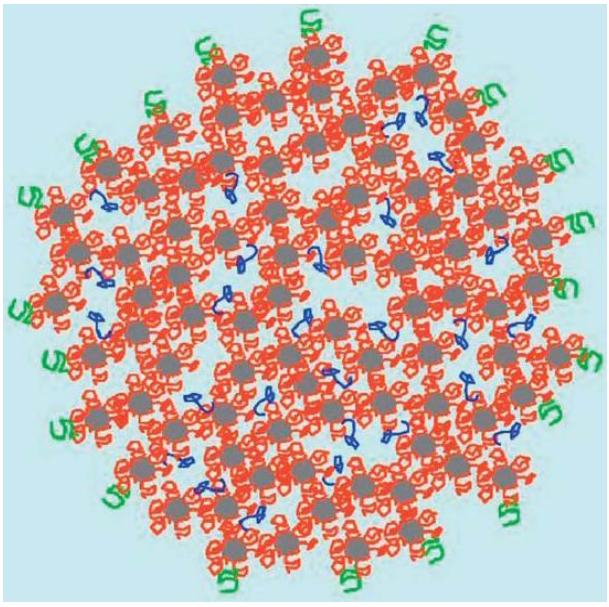

Figure 2.3. General structure of the casein micelle based on the most recent theory by Dalgleish (2011); phosphate nanoclusters (grey) attached to caseins (red), "hydrophobically bound" β caseins and surface κ-CN (green).

Although "micelle" is the term used to define the casein structure in milk, every casein micelle does not have the exact same structure, nor are they exactly assembled in the traditional definition that the word micelle suggests (hydrophobic core and hydrophilic tail on the surface). What is clear is that the internal structure is composed of aggregates of phosphorylated α_s and β caseins held together by calcium phosphate and the surface is composed of κ-CN which aids in stabilization (Dalgleish, 2011; Walstra et al., 2005). However, determining the specific native structure of the casein micelle continues to be a challenge, as its various components have the potential to rearrange according to environmental conditions and stresses. A number of theories regarding casein micelle structure have been proposed, however none have been conclusively accepted. The most recent model, after analysis by electron microscopy, suggests that the casein micelle is made up of calcium phosphate nanoclusters which act to link together casein submicelles (Figure 2.3) (Dalgleish, 2011). This model points out that interactions with large molecules with only surface κ-CN and caseins in the internal portion of the micelle are inaccessible. On the other hand, in some cases smaller molecules are able to react with β casein, such as in observed by Diaz et al. (1996) where trypsin was able to access β casein for cleavage. These trends in reactivity were not considered in previous models, and are one of the reasons, along with others, that this model is believed to be more thorough and comprehensive.

2.4 Protein-protein interactions induced by heat

2.4.1 Effect of heat treatment on whey proteins

Milk whey proteins become denatured when exposed to external stress, such as heat and pressure. In heat treated milk, various factors can contribute to the rate of whey protein denaturation, such as heat treatment time, temperature, pH, protein concentration, protein structure and heat susceptibility (O'Connell & Fox, 2003; Singh, 2004). A greater extent of denaturation reveals more "active" sulfide groups which are otherwise buried within the protein structure, resulting in an increase in casein micelle attachment and/or other protein-protein interactions. Cysteine residues exposed as a result of denaturation tend to be responsible for the formation of aggregate disulfide bonds after heat treatment. For example, when Cys160 is available after heat treatment, it has the potential to form a disulfide bond with κ-CN on the surface of the casein micelle (Lowe et al., 2004).

According to the model for β-lactoglobulin denaturation and aggregation of Roefs & de Kruif (1994) the general propagation of aggregates is a result of a series of reaction mechanisms. The first step (Eqn 2.1) includes the reversible reactions of the β-LG dimer to yield β-LG monomers.

$$B^2 \leftrightharpoons B \qquad \text{(Eqn 2.1)}$$

where B^2 is a β-LG dimer and B is a native β-LG monomer.

The more proper initiation reaction is the first-order monomer reaction with a β-LG molecule containing a reactive sulfhydryl group (Eqn 2.2).

$$B \overset{k_1}{\rightarrow} B^* \qquad \text{(Eqn 2.2)}$$

where B^* is a β-LG molecule with a reactive sulfhydryl group and k_1 is the reaction rate constant.

After the Eqn 2.2 reaction, the following step would be the propagation of aggregate formation, shown in Eqn 2.3, where the disulfide bond of one intramolecular disulfide of

native *β*-LG and one of the reactive free sulfhydryl groups of either a single *β*-LG molecule with reactive sulfhydryl, or a polymer of *β*-LG molecules react with one another.

$$B + B_i^* \overset{k_2}{\rightarrow} B_{i+1}^* \qquad \text{(Eqn 2.3)}$$

where B_i^* is either a *β*-LG monomer or polymer with reactive sulfhydryl group, B_{i+1}^* is a polymer with new reactive sulfhydryl and k_2 is the reaction rate constant.

Taking into account the conformational changes of *β*-LG, Roefs & de Kruif (1994) deduced that only one of the two intramolecular disulfide bonds of a *β*-LG monomer and one sulfhydryl group is reactive. Thus the propagation step should result in the formation of linear aggregates. In the case that *a*-lactalbumin is a part of the protein mixture, an extra propagation step should be included to account for the incorporation of *a*-LA into the linear aggregates (Roefs & de Kruif, 1994). Finally, the termination step (Eqn 2.4) occurs when the linear polymer no longer contains unreacted sulfhydryl groups.

$$B_i^* + B_j^* \overset{k_3}{\rightarrow} B_{i+j} \qquad \text{(Eqn 2.4)}$$

where B_i^* and B_j^* are reactive intermediates, B_{i+j} is a linear polymer with no unreacted sulfhydryl groups and k_3 is the reaction rate constant.

The total reaction rate (k´) can be calculated by Eqn 2.5, which takes into account the three irreversible steps of the denaturation and aggregation reactions.

$$k' = k_2 \left(\frac{k_1}{2k_3}\right)^{1/2} \qquad \text{(Eqn 2.5)}$$

where k_1 corresponds with the reaction of Eqn 2.2, k_2 with Eqn 2.3, and k_3 with Eqn 2.4.

It should be considered that k' is highly dependent on the diffusional motion of reactants as well as the viscosity of medium. In fact, k_1 follows first-order kinetics and

remains relatively unchanged with an increase in polymer particles (Painter & Coleman, 2008). On the other hand, the resulting increase in viscosity of solution causes a slight decrease in the rate of propagation (k_2) (Eqn 3). Also, as termination is dependent on the diffusion of larger particles, there is a noticeable decrease in the rate of termination (k_3) (Eqn 2.4). As well, Oldfield et al. (1998) proposed a similar model to that of Roefs & de Kruif (1994), however included the potential for the formation of hydrophobic bonds between whey protein groups (*β*-LG or *a*-LA) which may have the potential to be converted to disulfide bonds upon heating temperature greater than 75 °C.

2.4.2 Effect of heat treatment on casein micelles

One of the main heat effects of casein micelles is aggregation, and in general the formation of a gel. Casein micelles are molecules which are reasonably heat stable, and do not undergo major heat induced changes under 100 °C or more (Goff, 2016). As the *κ*-CN hairs on the surface are a source of stability for the micelle, removal or collapse of them may lead to casein micellar aggregation. The alteration of the milk environment by addition of ethanol or excess calcium can also lead to micelle instability and result in aggregation (Walstra et al., 2005). The formation of Ca salt bridges may occur as well as covalent bond formation of negatively charged amino groups of which may be revealed during high temperature treatment. Thus casein micelle aggregation is a result of the formation of various types of bonding and is highly dependent on electrostatic and steric repulsions at specific milk conditions (Walstra, 1990).

2.4.3 Protein- protein interactions induced by heat

One of the main protein-protein interactions that occur in heat-treated milk is the formation of disulfide bonds. Of particular interest is the attachment of denatured whey proteins to the surface of the casein micelle. In order for whey proteins to attach to casein micelle, two steps need to occur. First, *β*-lactoglobulin (*β*-LG), one of the major whey proteins, must unfold to expose its sulfhydryl groups, and then the protein must form a disulphide bond with *κ*-casein (*κ*-CN). It is generally accepted that the other major whey protein, *a*-lactalbumin (*a*-LA), is not involved until after the initial formation of the association between *β*-LG and *κ*-CN; attributed to its lack of a free thiol group (Corredig & Dalgleish, 1999; Donato & Guyomarc'h, 2009; Mulvihill & Donovan, 1987) (Table 2.3).

Alternatively, whey proteins may attach to each other and remain in the serum portion as whey protein aggregates (Donato and Guyomarc'h, 2009; Jean et al., 2006; Vasbinder and de Kruif, 2003; Guyomarc'h et al., 2003). Thus, after heat-treatment, the milk matrix is composed of a mixture of three types of whey proteins: native whey proteins, soluble whey protein aggregates and aggregates that have formed an association on the surface of the casein micelle (Figure 2.4).

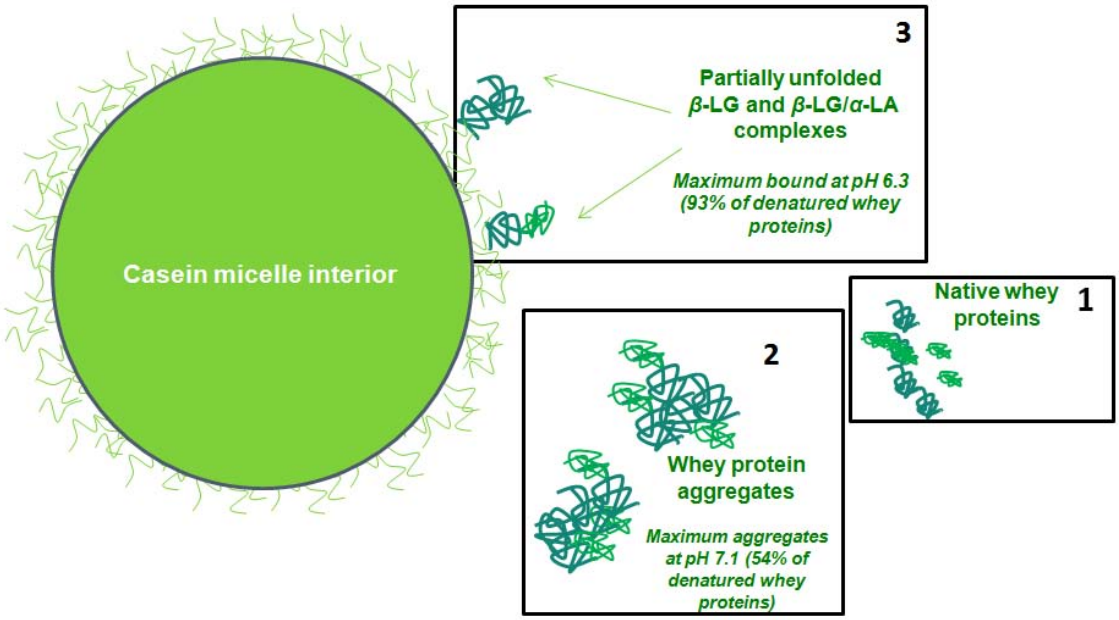

Figure 2.4. Three types of whey proteins in heat-treated milk.

One point to keep in mind is that the WP/κ-CN attachment mechanism is not fully understood, therefore various pathways have been suggested. Generally accepted is that the WP/κ-CN complex is first formed via attachment of β -LG to κ-CN, whereas *a*-LA may later form a linkage with β-LG. The next consideration is the location of the formation of the WP/κ-CN complex. As κ-CN is located externally on the casein micelle, it has generally been assumed that κ-CN acts as a nucleation site in the attachment of whey proteins (Dalgleish, 1990) . However, studies have found that in certain cases, WP/κ-CN complexes can be found in the serum portion (Anema, 2008a; Guyomarc'h et al., 2003), thus complicating this notion. Furthermore, it is unknown whether whey proteins attach to κ-CN in the serum and then reattach to the casein micelle, or that the WP/κ-CN complex dissociates from the casein micelle and then is further found in the serum. Another concern is if the formation of whey protein aggregates (β-LG/β-LG or β-LG/*a*-LA aggregates) precedes or follows the formation

of the *β*-LG/*κ*-CN complex. Since Corredig and Dalgleish (1999) found equal proportions of *β*-LG and *a*-LA bound to the surface of the casein micelle, it was thus proposed that primary aggregates were formed prior to whey protein interactions with *κ*-CN. On the other hand, Euber and Brunner (1982) were able to reproduce a direct covalent bond formation of an individual *β*-LG/*κ*-CN complex, even though this was an in-vitro experiment. As well, studies have found a relationship between the amount of denatured whey protein and *κ*-CN found in the serum (Anema, 2007; Singh, 2004), which may suggest *κ*-CN dissociation as a prerequisite for the formation of a complex. Donato and Guyomarc'h (2009) have suggested four distinct pathways utilizing the information found in these studies as a basis. They are summarized as follows (Figure 2.5):

A) Primary whey protein aggregates are formed in the serum portion and later attach to *κ*-CN either on the surface of the casein micelle or in the serum portion.
B) Denatured *β*-LG associates with *κ*-CN on the surface of the casein micelle, *β*-LG and/or *a*-LA later attach to the *β*-LG/*κ*-CN complex on the micelle via *β*-LG.
C) *β*-LG and/or primary serum whey protein aggregates attach to *κ*-CN which has dissociated into the serum portion.
D) *β*-LG/*κ*-CN and/or whey protein/*κ*-CN complex is formed on the surface of the casein micelle and later dissociates as serum complexes, where they may interact further with denatured whey proteins and/or whey protein aggregates.

These four mechanisms are further illustrated in Figure 2.5. However, it should be noted that current research has not been able to fully prove or disprove any of these theories.

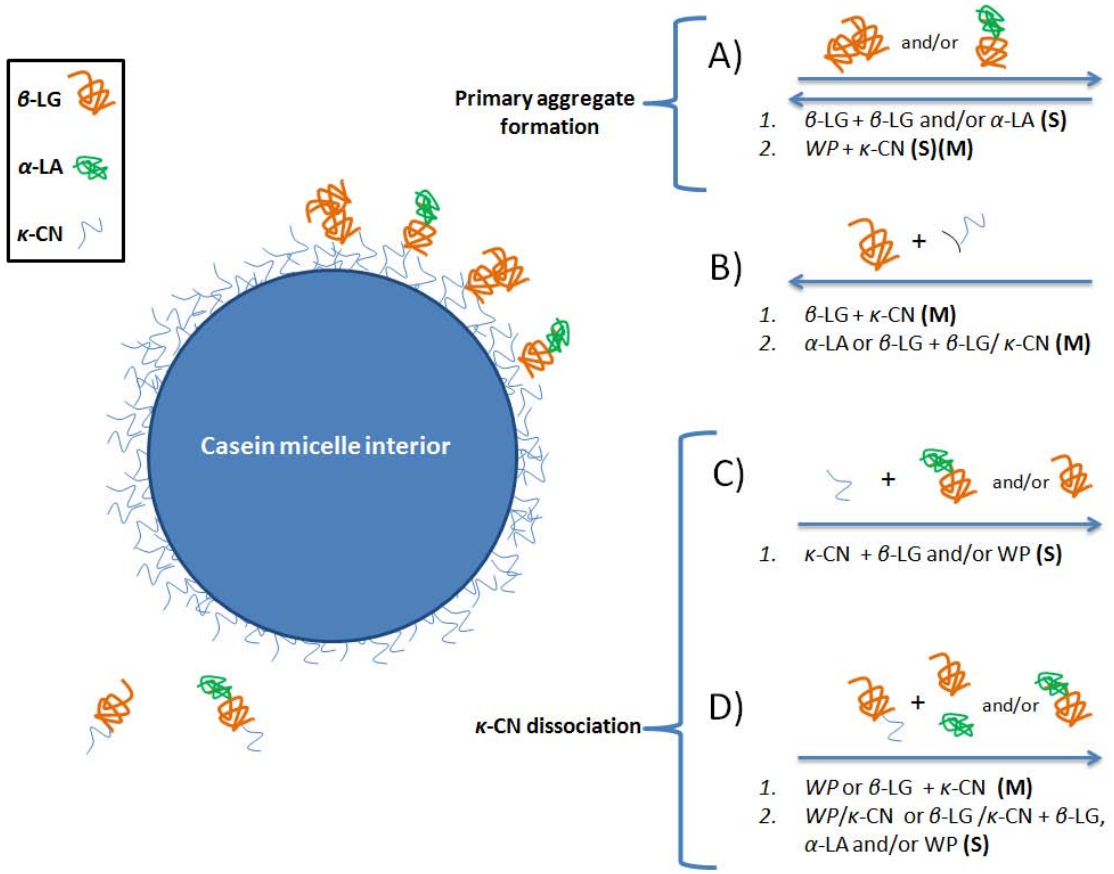

Figure 2.5. The four proposed pathways of formation of whey protein/*κ*-CN complexes (adapted from Donato and Guyomarc'h (2009)); *β*-LG=single denatured *β*-LG; *a*-LA=single denatured *a*-LA; *κ*-CN= *κ*-casein molecule; WP=*β*-LG-*β*-LG or *β*-LG-*a*-LA aggregate; *β*-LG/*κ*-CN=*β*-LG/*κ*-CN complex; WP/*κ*-CN=*β*-LG-*β*-LG or *β*-LG-*a*-LA aggregate/*κ*-CN complex; (M)=interaction occurs on micelle surface; (S)=interaction occurs in serum; arrows represent where the formation of the advanced WP aggregates takes place.

2.4.4 Role of pH

The attachment of whey proteins to the casein micelle has been found to be highly dependent on pH. In short, there is a maximum attachment at pH ~6.3 and a minimum at pH ~7.1 (Figure 2.6) (Donato & Guyomarc'h, 2009). In a series of studies, the said relationship between whey protein interactions and their associations with casein micelles regarding pH dependence was supported, in which low pH (~6.3) denatured whey proteins tend to form associations with the casein micelle and at high pH (~7.1) denatured whey proteins have a preference to form soluble aggregates in the serum (Anema & Li, 2003a, 2003b; Anema, Lowe, & Li, 2004; Anema, 2007). Using reconstituted skim milk at pH 6.5 and 7.1 heated at 90 °C for 20-30 min, it was exhibited that at pH 6.5 ~85% of denatured

whey proteins were associated with the casein micelle and at pH 7.1 only ~15% were associated (Anema, 2007). In a similar study, Kethireddipalli, Hill, & Dalgleish (2010) heat treated milk at pH 6.3, 6.7, and 7.1 at 90 °C for 10 min and found percentages of bound proteins to be 82.2%, 30%, and 0-5%, respectively. As a result, it has been found that at low milk pH there is a greater change in casein micelle size when compared to higher milk pH. This relationship is also dependent on the temperature of heat treatment, in which a greater increase in particle size is seen with higher heat treatment temperatures, as more denaturation would have occurred (Anema et al., 2004).

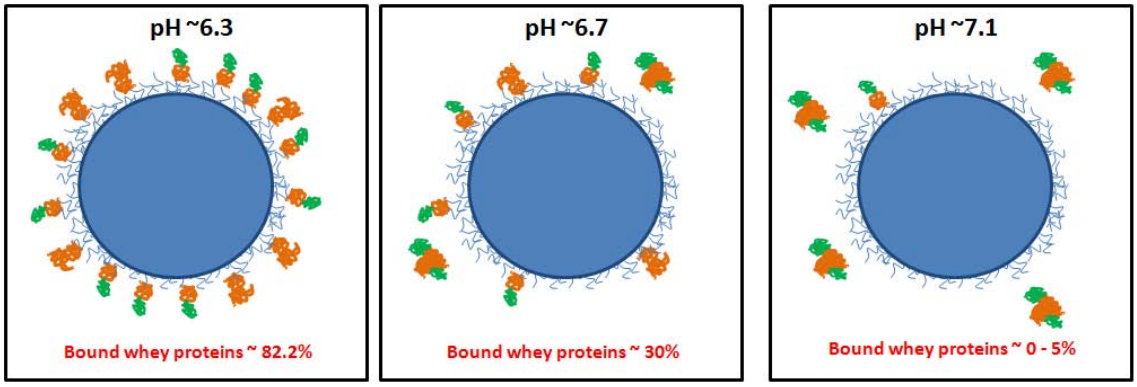

Figure 2.6. The pH dependence of denatured whey protein attachment to the casein micelle.

In heat treated milk, it has been shown that the whey protein/casein micelle complex is responsible for an increase in casein micelle particle size (up to 30-35 nm change in diameter) (Anema & Li, 2003a), with a maximum attachment at approximately pH 6.3 and a minimum at approximately pH 7.1, as it can be observed in Figure 2.5 (Kethireddipalli et al., 2010; Vasbinder & de Kruif, 2003). Consequently, a greater change in casein micelle particle size has been found to occur in lower pH milk when compared to higher pH milk after heat treatment (Anema & Li, 2003b; Donato & Guyomarc'h, 2009; Kethireddipalli, Hill, & Dalgleish, 2011; Vasbinder & de Kruif, 2003). Moreover, this mechanism should exhibit temperature dependence, where a greater increase in particle size should be seen at higher heat treatment temperatures, as more protein denaturation occurs and therefore increases the amount of free sulfide groups with the potential to form protein-protein interactions (Anema, Lowe, & Lee, 2004; Vasbinder, Alting, & de Kruif, 2003).

2.4.5 Whey protein variant denaturation characteristics

The major whey proteins, *β*-LG and *a*-LA have varying degrees of heat-stability with respect to their tendency to denature and potentially react with other components in the milk matrix. In general, *β*-LG is less heat stable than *a*-LA, however neither denatures to a significant extent below 70°C (Anema, 2008b). In addition, *a*-LA can unfold and refold back into its native state (Rüegg, Moor, & Blanc, 1977). Law and Leaver (2000) have observed an increase in thermal denaturation of *a*-LA upon adding 2-mercaptoethanol (ME), which may have acted to prevent the reformation of intramolecular disulfide bonding. Therefore the ability of *a*-LA to refold may be a contributing factor to the observation of a less extent of denaturation in *a*-LA than *β*-LG which, in most cases, undergoes irreversible denaturation. In fact, *a*-LA does generally not refold once it has been denatured to the point of exposing reactive sulfide groups, instead tending toward the potential for protein-protein interactions (Rüegg et al., 1977). As a consequence of its greater facility to denature and expose its reactive side chains, denatured *β*-LG tends to incorporate into the micellar portion of the milk matrix before and to a greater extent than *a*-LA (Noh & Richardson, 1989).

The genetic variants of *β*-LG, the most abundant being *β*-LG A and *β*-LG B, are distinct in that they differ by two amino acid substitutions, which consequently alter their susceptibility to heat induced denaturation and reactivity (Bello et al., 2011). It has been observed that the B variant of *β*-LG denatures to a greater extent than *β*-LG A (Anema & McKenna, 1996). Furthermore, it has been suggested that the amino acid substitution Ala/Val118 of the B variant causes a cavity from the loss of two methyl groups which increases access to the sulfide group of Cys121, resulting in a greater reactivity of the B variant compared to the A variant (de la Fuente et al., 2002; Qin et al., 1999). In the case of rennet gel formation (Meza-Nieto et al., 2013; Meza-Nieto et al., 2007) variant B was found to be predominant in the internal structure of the gel made from pasteurized milk. This may infer that *β*-LG B is involved in colloidal interactions to a greater extent than the A variant of *β*-LG. Alternatively, the lower E_a and ΔH values of *β*-LG A are related to a preference for aggregation (Anema & McKenna, 1996).

2.5 Industrial implications of heat treatment of milk

2.5.1 Typical industrial thermal treatments

The heat treatment of milk is an essential step in industrial dairy food processes to reduce the number of microorganisms and improve milk quality characteristics by inactivation of enzymes which may reduce milk stability. The most common heat treatment technique used for the production of dairy products is pasteurization, accomplished by combining a certain temperature and hold time, generally corresponding to the inactivation of pathogenic and spoilage microorganisms. Industrial pasteurization is accomplished via a batch or continuous method (Goff, 2016). Batch pasteurization or vat pasteurization includes a jacketed vat with heating method such as circulating water, steam or heat coils. During batch pasteurization milk is stirred to promote even heating. On the other hand, the continuous method or high temperature short time (HTST) pasteurization includes specialized heat plates in order to ensure maximum heat transfer and uniform heat treatment. In addition to pasteurization and HTST, other methods of thermalization used in milk are shown in Table 2.4.

Table 2.4. The main categories of heat treatment in the dairy industry (*Dairy processing handbook*, 1995).

Process	Temperature	Time
Thermization	63 – 65°C	15 s
LTLT pasteurization of milk	63°C	30 min
HTST pasteurization of milk	72 – 75°C	15 – 20 s
HTST pasteurization of cream etc.	>80°C	1 – 5 s
Ultra pasteurization	125 – 138°C	2 – 4 s
UHT (flow sterilization)	135 – 140°C	a few seconds
Sterilization in container	115 – 120°C	20 – 30 min

During the production of dairy products such as yogurt and cheese, standard procedures are required as well as some general manufacturing steps, which may vary depending on the type of product and/or the manufacturer. After receiving raw milk, a series of steps may occur such as milk standardization, homogenization, pasteurization, and addition of bacterial cultures. The order of these steps is dependent of the product and its desired characteristics (Tamime & Robinson, 1999).

Milk standardization is useful in order to obtain ideal quality characteristics of the finished product, as well as for economic purposes. Manipulation of fat content and total solids are the most common standardization techniques which take place during the production of cheese and yogurt. Fat content in cow milk can range from 2-7 kg/hL, however the average for a Holstein is 3.9 kg/hL (Goff, 2016). Fat removal may occur via centrifugal separation techniques followed by milk fat standardized by re-addition. The addition of milk solids can be accomplished by evaporation and or the addition of milk powder. Different procedures are followed in the production of yogurt versus cheese and are further discussed in the following sections (2.5.2 and 2.5.3).

2.5.2 Thermal treatment in yogurt manufacture

Yogurts are essentially formed as a milk fermentation using specific bacteria, usually a mixture of a mixture of *Streptococcus thermophilus* and *Lactobacillus delbrueckii* subsp. *bulgaricus* (WHO & FAO, 2011). The basic manufacturing steps of yogurt follows a general scheme involving the receiving of the raw milk, standardization, homogenization, pasteurization, inoculation and fermentation. A step-wise diagram showing the fundamental steps of yogurt processing are shown in Figure 2.7. As well, it is important to note that certain quality control steps are required during the manufacture of yogurt (Tamime & Robinson, 1999). Steps which require quality control points are highlighted in Figure 2.7.

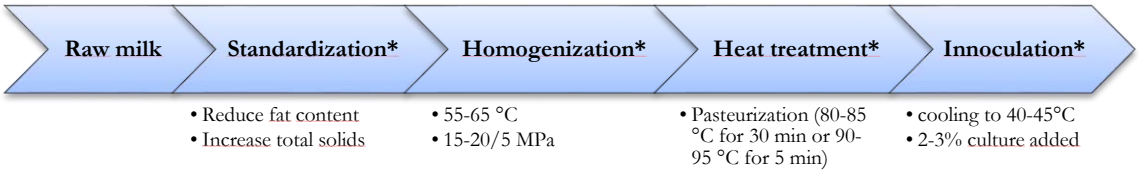

Figure 2.7. Industrial yogurt process diagram (adapted from Lee and Lucey, (2010). Steps requiring quality control checkpoint are labelled with an asterisk (*).

Before yogurt production, milk is usually standardized to promote consistency among products. Typically, industrial products regulations generally require a minimum of 17.5% milk solids-not-fat contents and a protein content of 2.7% (WHO & FAO, 2011). On the other hand, yogurt may also experience "wheying-off", which may occur when water

within the yogurt matrix leeches out forming a liquid layer, which may be perceived as a negative attribute from a consumer standpoint. Pectins or gelatins may be added as stabilizing agents to reduce the occurrence of this phenomenon and assist in general product consistency (Tamime & Robinson, 1999). However in some cases these quality control measures may give rise to negative effects, such as a yogurt which is too firm.

Homogenization is also an important step in the pre-production of yogurt. The main goal in homogenization is the breaking down of larger fat globules into more consistent, and generally smaller, size (Walstra et al., 2005). This is generally accomplished using dual heat and pressure treatments of 55-65 °C and 15-20/5 MPa. Such as the addition of pectins/gelatins, this function aids in producing a consistent product texture and promotes product stabilization during storage.

As in the case of most non-cured dairy products, milk heat treatment is a critical part of yogurt making. Not only is heat treatment used for eliminating pathogenic microorganisms and fermentation-competing bacteria, but also assists specific physical and chemical changes that have come to be expected in commercial product. For example, heat treatment may promote partial denaturation of whey proteins, which may result in the reduction of wheying-off. Heat treatment for milk used in the production of yogurt is usually accomplished using treatments of 80-85 °C for 30 min or 90-95 °C for 5 min (Lee & Lucey, 2010). In some cases, yogurts have been produced using UHT pre-treated milk. No significant differences were found in initial texture and consistency, however after storage, product quality appeared to be of a lower value than yogurts produced using milk pre-treated by established heat-treatment methods (Krasaekoopt, 2004).

After heat treatment, milk is cooled to incubation temperature (40-45 °C) that promotes the growth of bacterial cultures. Milk is inoculated using *Streptococcus thermophilus* and *Lactobacillus delbrueckii* subsp. *bulgaricus*. Fermentation results in a significant decrease in pH (from 6.7 to less than 4.6) as a result of the conversion of lactose into lactic acid. The production of lactic acid is responsible for giving yogurt its characteristic acidic flavor, however other compounds are also associated with typical flavor profiles of yogurt, such as certain fatty acids, amino acids and aldehydes (Tamime & Robinson, 1999). As the pH drops, acid gelation occurs causing the formation of a milk-gel matrix. Once pH 4.6 has been reached, the product is cooled to about 20 °C and stored at refrigeration temperature (4-6 °C) (Lee & Lucey, 2010).

2.5.3 Thermal treatment in cheese manufacture

Compared to yogurt, there are a wider variety of types of cheeses that are produced on an industrial level worldwide. Cheeses are known to have much variety that can be attributed in part as a result of the specific milk characteristics, such as the animal (cow, goat, sheep, etc.) and the region in which the animal is found (Fox, 2002). As well, there is a long history of cheesemaking in that some cheeses have a protected designation of origin (PDO), referred to as "*denominación de origen" (DO)* in Spain. This label has been established by the European Union and refers to products which have roots to certain regions, typically products such as meats, cheeses, olives certain vinegars and wines (European Commission, 2015). In order to carry the PDO approved name, the product must be produced in the specified region and comply with certain procedures.

Cheese production follows a similar milk pre-treatment scheme as yogurt, with some exceptions. For example, the addition of $CaCl_2$ is essential to optimize the coagulation process after heat treatment while addition of milk starter culture is required to effectively lower the pH of the milk and aid in the ripening process (Fox, 2002). Also, pasteurization may not occur in the case of cured cheeses which are to be "held at 20 °C or more for a period of 60 days or more from the date of the beginning of the manufacturing process," according to Food and Drugs Act and Regulations Sections B.08.030 and B.08.043." However this regulation varies depending on the region the cheese is to be made, for example in Catalonia there are specific aging regulations regarding cheese to be aged for less than 60 days and may require a statement on their label (Alimentaria, 2007). A description of the general cheese making steps can be found in Figure 2.8.

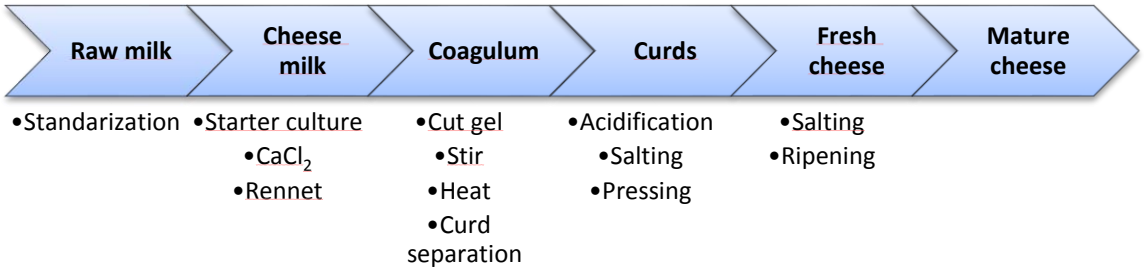

Figure 2.8. Cheese process diagram. Adapted from Fox (2002).

In an industrial scale operation, cheese production occurs in a vat process including acidification, coagulation and whey expulsion. Acidification occurs naturally as lactose converts to lactic acid or by means of the addition of lactic acid bacteria (generally *Lactobacillus* spp.) (Fox & McSweeney, 1998). Acidification is necessary in order to ensure milk has the specific coagulation characteristics as well as the appropriate bacteria to inhibit pathogenic growth as well as to promote the production of cultures for optimal flavor and texture. As well this step helps to ensure suitable gel strength of the cheese matrix. Coagulation is generally achieved by the addition of rennet, however some cheeses have acid induced coagulation (lowering pH to 4.6), combined acid (lower pH to 5.2) and heat treatment (90 °C) and mixed coagulation (acid + rennet) (Fox, 2002). Coagulation is caused by the destabilization of the casein micelle which promotes the formation of a stable gel. However, upon cutting and stirring, the milk gel undergoes syneresis in which whey is expelled, thus concentrating casein and fat (known as curd). At this point the curd may be pressed, salted or stored for ripening, depending on the desired cheese type.

2.5.4 Effect of heat-induced whey protein denaturation on milk properties

Heating of milk causes various side effects which may be beneficial, such as deactivation of enzymes and destruction of microorganism, whereas the production of off-flavors and increased reactivity of amino groups may be detrimental. Protein unfolding to expose reactive cysteine groups occurs at temperatures of 60 °C and above. For industrial purposes, whey protein denaturation in milk may or may not be desirable, depending on the product to be manufactured. For example, during cheese manufacturing, milk that has been denatured can impair rennet-induced gelation and yield curd with high moisture content and a less firm gel structure (Singh & Waungana, 2001; Waungana, Singh, & Bennett, 1996); however a degree of whey denaturation may act to improve the final texture of yogurt (Mottar et al., 1989).

A critical step during cheese production is rennet coagulation, in which two processes take place: enzymatic hydrolysis and secondary aggregation. Enzymatic hydrolysis occurs when rennet causes $\varkappa$-CN hydrolysis at the Phe_{105}-Met_{106} bond resulting in the formation of para-casein and caseinmacropeptide. This causes instability and the formation of casein aggregates, likely via Ca^{2+} bridges, van der Waals and hydrophobic interactions (Walstra, 1990). However the formation of the whey protein/$\varkappa$-CN complex has been shown to

potentially block rennet from cleaving at Phe_{105}-Met_{106} thus causing a less complex gel structure with a higher moisture content (Fox & McSweeney, 2003; Walstra & Jenness, 1984). This decrease in rennet effectiveness may be a result of steric hindrance from the formation of longer whey protein aggregate chains formed on the surface of the casein micelle. On the other hand some authors have found no difference in enzyme hydrolysis of milk gels in heat treated milk, but the secondary aggregation step was found to be affected whether or not denatured whey proteins attached to the micelle (Anema, Lee, & Klostermeyer, 2007; Vasbinder et al., 2003). Bremer et al. (1989) observed a consistent fractal floc formation exists in casein micelle gels, thus exhibiting the importance in understanding the structure of the casein micelle and how its packing arrangement affects interactions in heated milk gels. For example, it can be observed that using heat treated milk results in a protein gel with a denser casein-whey network (Figure 2.9).

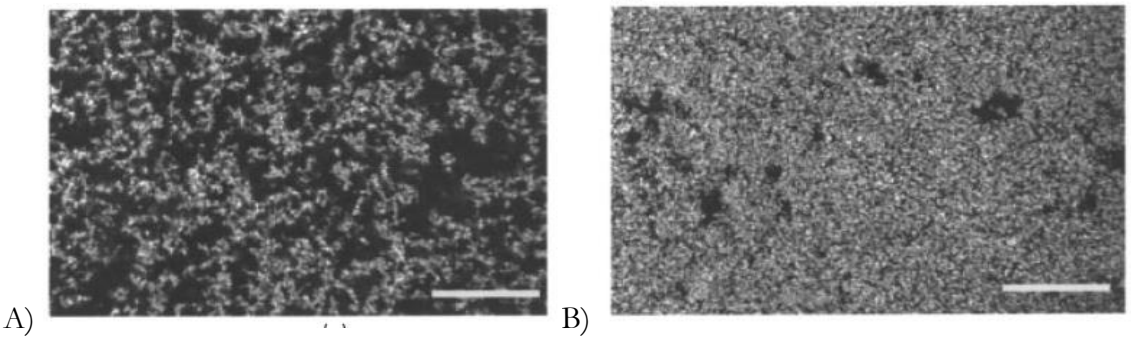

Figure 2.9. Comparison of confocal micrographs of milk gels from Schorsch et al. (2001) A) Unheated milk; B) Milk heated at 80 °C for 30 min.

In the case of yogurt production, partially denatured whey proteins have been found to trap water within the matrix, therefore increasing texture consistency and storage stability (Guyomarc'h et al., 2003). Dannenberg and Kessler (1988) also found that an increase in whey protein denaturation resulted in an increase in yogurt firmness, though at very high levels of denaturation (>95%) yogurt quality and firmness tended to decrease. Firmness in acid gels has been found to be pH-specific, in that the formation of a gel was found to begin at a higher pH in gels where milk was heated at a higher initial milk pH (Anema, Lowe, et al., 2004). Complementary, it was suggested that serum whey proteins significantly increased the acid gel firmness when compared to gels in which whey proteins formed a complex on the surface of the casein micelle (Anema et al., 2004). As previously discussed in detail, the

preference for denatured whey proteins to form a complex on the casein micelle or remain in the serum portion is highly related to initial pH, and consequently should be considered an essential concern in the formation of acid gels.

Denatured whey proteins also have an effect on milk fat globules. When immunoglobulin M (agglutinins) interacts with the fat membrane surface, fat globule aggregation is more likely to occur and result in creaming (Fox, 2000). As a consequence, the heat-induced denaturation of this protein acts to reduce the effect of creaming by inhibition of this interaction. Whey proteins have also been found to form interactions with the fat globule membrane. The presence of both *β*-LG and *a*-LA on the fat globule membrane has been observed in fat containing heat-treated milk, however *β*-LG was found to be more prevalent (Lee & Sherbon, 2002; Ye et al., 2004). This may be a result of the lower heat sensitivity of *a*-LA, its lack of a free thiol group and/or its lower concentration in bovine milk. Lee and Sherbon (2002) also found that percentage of whey protein bound to the fat globule to be higher in milk that was both homogenized and heated, however proposed that this may be a result of the increase in fat globule surface area during homogenization.

2.6 Determining whey protein denaturation and fractionation

2.6.1 Separation of protein fractions

Early milk protein separation techniques were formed via basic chemical methods, shown in Figure 2.10. Separation from bovine milk began with the standard acid separation of protein components, casein and whey, via isoelectric precipitation to pH 4.6. The whey portion was then further separated by $MgSO_4$ saturation leading to the precipitation of a lactoglobulin portion and a soluble albumin portion. From the albumin portion the two main whey proteins were found: *β*-LG and *a*-LA. Further addition of $(NH_4)_2SO_4$ to the albumin portion causes BSA to crystallize (Creamer et al., 2011; O'Mahony & Fox, 2014). These physico-chemical separation methods have been improved and/or facilitated using other techniques such as membrane separation or chromatographic separation methods.

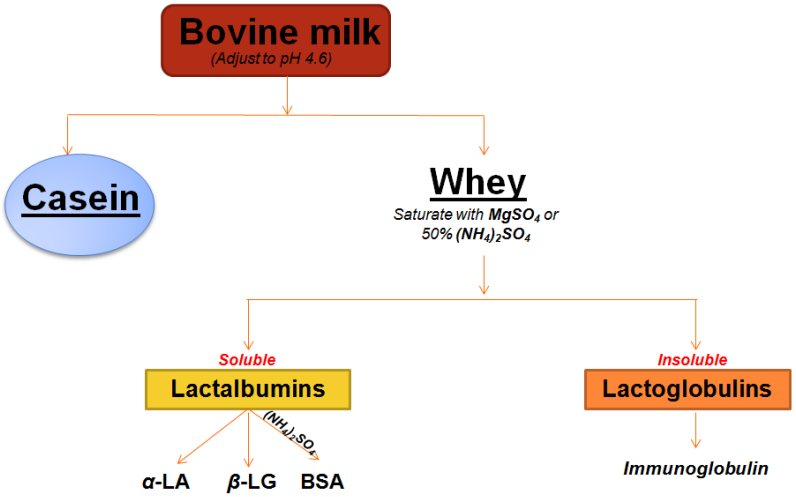

Figure 2.10. Conventional separation technique of whey protein fractions from bovine milk (Creamer et al., 2011; O'Mahony & Fox, 2014).

The generally accepted method of separation by reducing milk pH to 4.6 using acid is useful to isolate native proteins from casein (IDF 178: 2005), and is still commonly used in industrial and laboratory practice. During acid fractionation, the instability of the casein micelles occurs as a result of the decrease in pH wherein casein micelles and soluble aggregates of denatured whey proteins are precipitated. However, if the isolation of whey proteins involved in complex protein-protein interactions is desirable, other methods may be useful. Some alternative separation techniques are briefly summarized below (O'Mahony & Fox, 2014).

- *Isoelectric precipitation* to pH 4.6 in which precipitate is filtered and/or lightly centrifuged. In this technique casein (sedimented portion) and native whey protein fractions may be collected.
- *Ultracentrifugation* at 100,000 g for 1 hr allows caseins to sediment with native and heat denatured whey proteins remaining in the serum portion. This technique is solely based on high centrifugal force (high speed and/or extended time) (Kethireddipalli et al., 2010).
- *Salting-out methods* usually by $(NH_4)_2SO_4$ at 260 gL^{-1} causing the precipitation of casein and immunoglobulins.
- *Ultrafiltration and microfiltration* using specified membranes according to the size of the desired milk component.

- *Gel filtration* is based on size and separates casein and whey protein portions by permeation chromatography.
- *Rennet coagulation* occurs when rennet cleaves κ-casein into caseinmacropeptide (CMP) and para-casein, causing micellar instability resulting in flocculation of the casein micelles (Vasbinder & de Kruif, 2003; Vasbinder et al., 2003).

2.6.2 Protein determination

The determination of whey protein content can be accomplished using various techniques, of which there are either direct or indirect methods (Fox & McSweeney, 2003). Direct methods quantify nitrogen content of a sample. There are two types of direct methods for determination of whey protein content; Kjeldahl and Dumas methods. Kjeldahl is a chemical titration technique and is the most commonly accepted protein determination technique used in foods. However it is often not the most desirable technique, as it is time consuming and requires the use of concentrated sulfuric acid at high temperatures. An alternative direct technique, simpler than Kjeldahl, is the Dumas method. This combustion technique is less time consuming, however the required equipment is costly. Direct techniques clearly have some disadvantages, thus indirect techniques have been developed which offer, in general, a more affordable and at times more sensitive alternative.

Indirect protein determination techniques are called such as they do not measure nitrogen content. Instead they convert a given test sample into a protein value which is determined by comparison with a directly related measurement. This is accomplished using a reference measure or calibration curve. As a consequence, they do include some extent of estimation error. Nonetheless many of these methods are regularly used and well-accepted. Some commonly used indirect techniques include high performance liquid chromatography, dye-binding and gel electrophoresis, which are discussed further in the next sections.

2.6.2.1 High Performance Liquid Chromatography

Liquid chromatography is often used for protein analysis when various fractions are difficult to separate. Mobile and stationary phases separate components based on adsorption affinity. High Performance Liquid Chromatography (HPLC) is a standard separation technique based on protein hydrophobicity, however it should be noted that the elution of

complex protein conformations may be less predictable (Katzenstein et al., 1986). HPLC includes a polar stationary phase and a non-polar mobile phase. More commonly used for whey protein separations is reverse phase HPLC (RP-HPLC) which includes a non-polar stationary phase and polar mobile phase (Nollet, 2004). When a sample passes through the column, highly non-polar molecules bind strongly to the stationary phase. Polar molecules elude early on the chromatogram and non-polar molecules leave the column later. Since most mixtures include a varying degree of polar and non-polar molecules, a solvent gradient is utilized so all molecules elude during a given sample run.

While each sample passes through the column, a UV detector is set at a specific wavelength (or wavelengths) in order to detect the absorption of the molecules of interest. Quantification of protein content can be accomplished using computer software which generates a chromatogram to measure various characteristics of the sample including retention time, peak height or area under the curve. Retention time is useful as an indicator of the component to be measured, in that various components elude at different times. For example in the chromatogram in Figure 2.11 the elution time of the three main whey protein variants *a*-LA and *β*-LG A and B are shown.

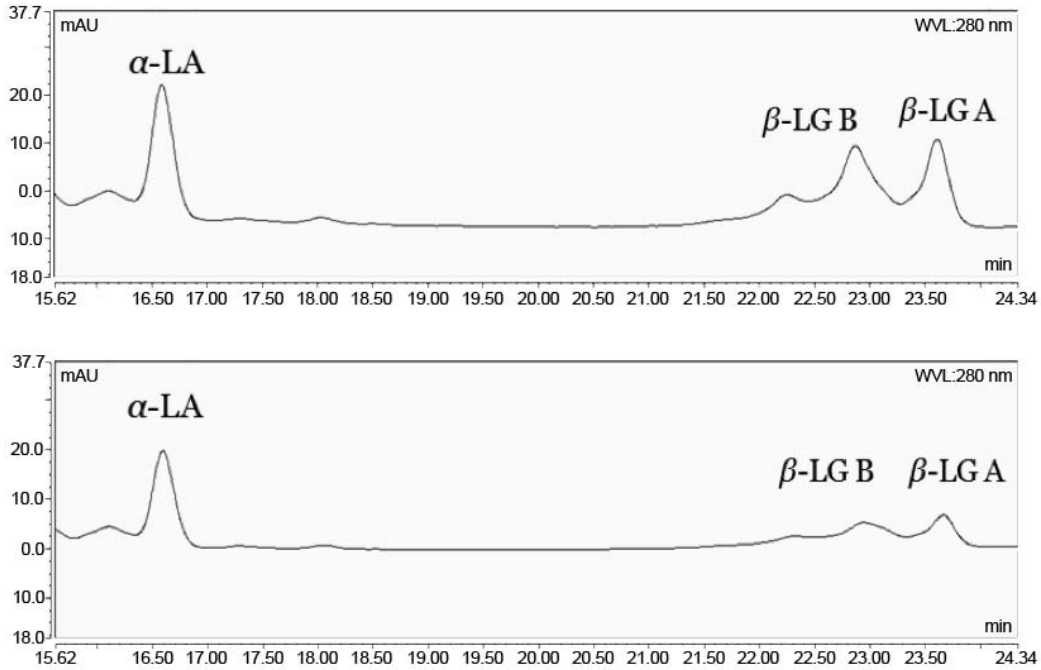

Figure 2.11. HPLC of acid-separated serum portion of pH 6.7 milk unheated (upper image) and heat treated at 80°C for 10 min (lower image).

Sample estimation of protein content is based on comparison to whey protein reference samples by development of a standard curve. RP-HPLC was evaluated for the quantification of whey protein denaturation in comparison to the standard Kjeldahl method with great reproducibility and favorable results (Parris, Purcell, & Ptashkin, 1991). As well a standard ISO technique for acid-whey determination has been developed (IDF, 2005).

2.6.2.2 Dye-binding chemical techniques

Various techniques have been developed for protein determination based on colorimetric dye-binding principles. Some common dye-binding techniques include Bradford, Biuret, Lowry and bicinchoninic acid (BCA) assays. Depending on the solution to be tested, one of these assay may be preferable as a result of certain chemical interferences. Briefly, the Bradford assay uses Coomassie Blue G-250 dye which acts to bind protein residues via hydrophobic interactions (de Moreno, Smith, & Smith, 1986). This assay is fast, reagents are inexpensive and the technique is quite sensitive, however there are many interfering components which may cause inaccurate readings (Noble & Bailey, 2009).

Another technique is the Biuret method which uses a copper reduction of Cu^{2+} to Cu^{+}. Color change occurs when three or more amino acid residues are found within a protein forming a copper complex (Pierce Biotechnology, 2015a). This technique was improved using Folin-Ciocalteu reagent. This reagent increases the assay sensitivity 100 times, and although the exact mechanism is not fully understood, it is believed to be a result of the transfer of electrons from the copper complex to the reagent complex. The initial formation is said to result in an unstable blue-colored complex but after a 30 min incubation, this complex becomes more stable (Pierce Biotechnology, 2015a). The complete method is called the Lowry assay. The blue-colored solution has an absorbance maximum at 750 nm (Lowry et al., 1951). Color is produced by the formation of a complex with any one of the peptides tyrosine, tryptophan, cysteine, histidine and asparagine (Pierce Biotechnology, 2015a). As well, it is an end-point assay, in that it reaches a final reaction point in which no further color development occurs. This is beneficial in that it allows a degree of comparison to previous test runs. Nonetheless this technique is still time consuming, and therefore an alternative, the Bicinchoninic assay, was developed replacing the Folin-Cioalteu reagent in the secondary step with bicinchoninic acid (BCA). The BCA assay requires around 32 min whereas the Lowry assay four times as long (~122 min) (Pierce Biotechnology, 2015b). In comparison to

the blue colored complex of the Lowry assay, BCA yields a final purple colored solution by the binding of two BCA molecules with one cuprous ion. Absorbance at 562 nm yields a relatively straight and increasing line with protein content (Pierce Biotechnology, 2015b). Unlike other protein assays, it maintains accurate results with up to 5% detergents in the solution, allowing even less potential for test interference (Smith et al., 1985). The amino acids which interact with BCA are cysteine/cystine, tyrosine and tryptophan.

2.6.2.3 Gel electrophoresis

Protein electrophoresis is a common technique in which charged molecules separate by being exposed to an electric field, thus positively charged particles move toward the cathode and negative particles toward the anode. Polyacrylamide gel electrophoresis (PAGE) forms a gel matrix by using a combination of bisacrylamine linked to two acrylamide molecules (Farrell, 2005). The speed at which the molecules migrate through the gel is a function of their protein characteristics (size, shape and charge), the electric field strength, temperature and/or pH.

In the case of SDS-PAGE, sodium dodecyl sulphate (SDS) is added in order to denature the protein tertiary and secondary structure and apply a negative charge to the molecules. This alteration to the sample allows separation based on molecular mass. Protein concentration can be assessed based on comparison to a reference standard, chosen appropriately according to the test sample. Proteins accumulate in bands on the gel with an equivalent distance in each respective lane based on their mass. Bands can be visualized by applying a stain, such as the commonly used dye Coomassie blue (Berg, Tymoczko, & Stryer, 2002). Later, band protein concentration can be estimated using imaging software of the band intensity.

2.7 Optical properties of milk

The way light moves with respect to its interaction with particles can be defined by various phenomena such as absorption, refraction, diffraction and reflection (Figure 2.12). Light photons may be absorbed so that they disappear entirely or are re-emitted at a different wavelength. Light is reflected when direction is changed such that the angle of incidence is equivalent to the angle of reflection. Diffracted light is the result of light bending around an

obstacle as it encounters a slit or an obstacle. And light may be refracted by passing through the particle and changing direction as a result of this interaction. The refractive index is a dimensionless measure of how light propagates through a medium, usually defined as *n*, and is dependent on temperature and light wavelength (Walstra & Jenness, 1984). Typically the refractive index is measured at the sodium wavelength, indicated by the symbol D at 20 °C, thus the notation $n_{D,20}$ is commonly used.

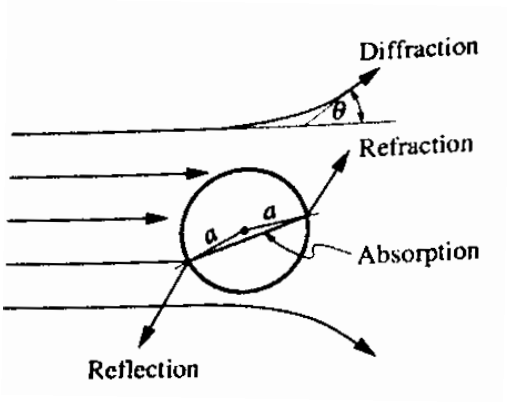

Figure 12. Electromagnetic wave interactions (adapted from Modest, 2003).

Milk has a refractive index ($n_{D,20}$) somewhere between 1.3440 - 1.3485 in which the main contributor is water (1.3330) (Fox & McSweeney, 2003). Milk fat has a refractive index of 1.4620, however only particles smaller than 0.1 μm have been found to affect the total milk refractive index. As shown in Eqn 2.6, the amount of increase in the refractive index compared to solvent, or refractive increment (Δn), of a solution is directly proportional to its volume fraction (Walstra & Jenness, 1984).

$$\Delta n = n(solution) - n(solvent) = \rho \sum r_i m_i \qquad \text{(Eqn 2.6)}$$

ρ is product density, m is the mass fraction of solute and r is the specific increment of the refractive index corresponding to the solute.

Thus from Eqn 2.6, the milk refractive index can be calculated using these refractive index specific increments or r values (mL g^{-1}) for milk components from Walstra and Jenness

(1984) at 589.3 nm and 20 °C: casein micelles (0.207), serum proteins (0.187), lactose (0.140), sucrose (0.141) and other dissolved milk components (0.170).

Light scatter is defined when photons change direction after a collision with a particle (Øgendal, 2013). In milk, fat globules and casein micelles exhibit light scatter as a result of their large size in comparison to other milk components. As a result of their larger size, fat particles scatter more light than casein micelles. Once contact occurs, light is scattered in all directions and in general involves multiple scattering events, 1000 times or more in undiluted milk (Walstra & Jenness, 1984). In addition, the light scattering properties of the casein micelles are the main reason for the white color of milk, which becomes clear if the micelles are disrupted. In particular the creamy appearance of milk is a result of the β-carotene content in milk fat (Walstra & Jenness, 1984), whereas the slightly blue appearance comes from the short wavelength scatter of casein micelles (Fox & McSweeney, 2003). It should be noted that light scatter is closely related to turbidity, and in some cases these two units of measures may be comparable.

2.7.1 Particle size measurement based on dynamic light scattering

Among different measurement techniques based on light scatter, dynamic light scattering (DLS) is commonly used to measure particle size. Since this measurement occurs over a range of micelle sizes, light scatter is found to be representative of the average micelle size of a sample. As well, changes in size may occur when using different solutions for suspension during DLS measurement as a result of alterations in the native pH and ionic environment (Beliciu & Moraru, 2009).

The general measurement using DLS is a calculation of effective diameter, which is an averaged value of the hydrodynamic diameter, based on the intensity of scattered light using the Stokes-Einstein equation (Eqn 2.7) shown below.

$$D = \frac{k_B T}{3\pi\eta D_t} \qquad \text{(Eqn 2.7)}$$

where D is diameter, D_t is diffusion coefficient, k_B is the Boltzmann constant, T is temperature and η is dynamic viscosity.

It should be noted that after the signal is received by DLS systems may be interpreted in terms of an autocorrelation function, as intensity measurements are affected by the normal Brownian motion of particles (Alexander & Dalgleish, 2006).

2.7.2 Light scatter using fiber optics

Using the light scatter principles of milk, optical sensors systems have been implemented for applications in dairy processing. As seen in Figure 2.13, using a light source with a backscatter detector configuration, the light scatter of casein micelles in skim milk has been measured at an angle of 180°. This technique is thus referred to as light backscatter, in which light is sent via optical fibers into a sample cell containing skim milk. The scatted light is sent back to a detector allowing the scattered light to be quantified as a signal response.

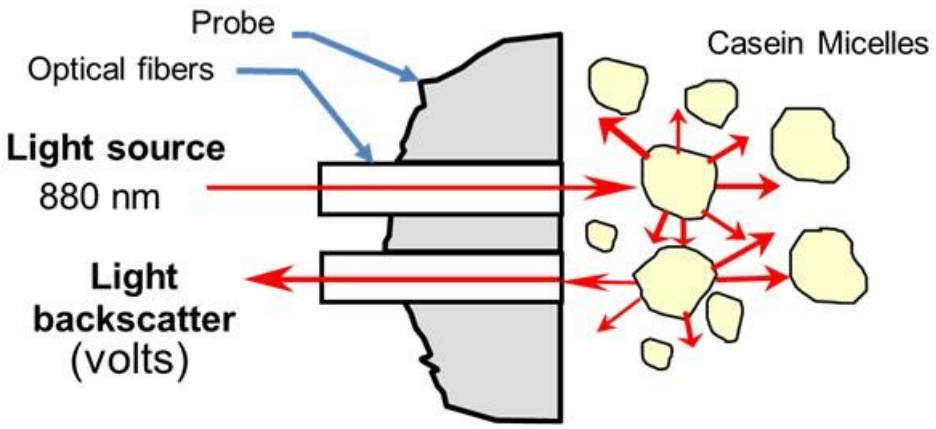

Figure 2.13. Light backscatter measurement using optical fibers From Lamb et al. (2013).

In certain cases light side scatter or transmission may also be used, however Lamb et al. (2013) found that light backscatter best suited protein denaturation measurements. Further information regarding optical sensors can be found in Section 2.8 and 2.9.

2.8 Optical sensor components

An optical sensor system typically requires at least three major components: optical fibers, light source and detector. Optical fibers are essential to transfer light long distances

with minimal light scatter and absorbance losses. Thus, the material components and configuration of optical fibers can optimize various characteristics of the desired signal transfer. For example, the refractive index of the medium is essential for the amount of reflection and/or refraction of which the light travels through the optical fiber. In general, optical fibers are composed of two dielectric mediums, an internal core surrounded by a cladding layer, composed of plastic or glass, which depending on the respective refractive index can allow for various modes of light transfer. The configuration can be single-mode, multi-mode step-index and multi-mode graded-index (Figure 2.14). Single-mode light is the simpler form, which propagates just one light mode whereas multi-mode has a number of light modes. Step-index consists of a consistent refractive index throughout the core and graded-index results in variable refractive index with a change in distance from the fiber (Kwan, 2002).

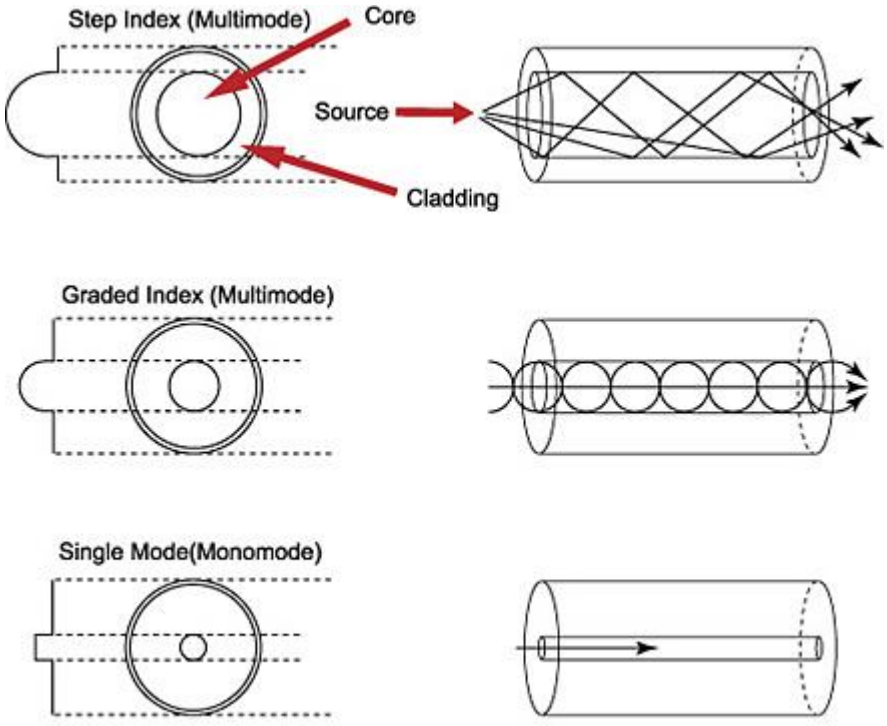

Figure 2.14. Optical fiber light modes ("Fiber Optic Cables," 2016).

The spectral region of the signal is dependent on the light source characteristics. In the case that the desired response lies in various spectral ranges (i.e. UV, visible, IR, etc.)

specific light sources can be chosen within regions. For example, the use of a H_2 or 2D lamp lies mostly in the UV region (approximately 100-400 nm), whereas a tungsten lamp would allow for quantification partially in the UV range, visible and IR region (approximately 350-2500 nm) (Figure 2.15). The light source is responsible for transferring the signal to the spectrometer where it is quantified after transforming light components into measurable readings.

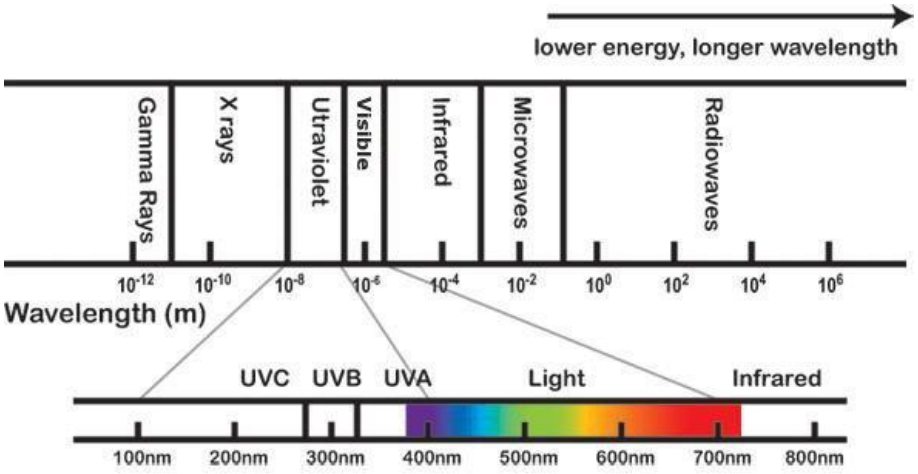

Figure 2.15. Electromagnetic spectrum. Adapted from Skoog et al. (2007)

The spectrometer receives light via optical fibers. The function of the spectrometer is to convert light readings into spectral components as a function of wavelength and create an image display of these measurements ("Spectrometer Knowledge," 2015). Important spectrometer characteristics include the slit width which is important for the amount of light allowed to the detector and grating, which determines the wavelength range of measurements. Various components may be used in detectors, and should be chosen depending on based on the band gap energy (E_{gap}) of the semiconductor material. This information is essential in order to determine the maximum wavelength (λ_{max}) detection limit, as defined by Eqn 2.8 ("Spectrometer Knowledge," 2015).

$$\lambda_{max} = \frac{hc}{E_{gap}} \qquad \text{(Eqn 2.8)}$$

where h is Planck's constant and c is the speed of light.

Common semiconductors used in detectors are silicon with a band gap of 1.11 eV and germanium with a band gap of 0.36 eV at 300K (Kittel, 1986). Detectors read-outs are often susceptible to a certain extent of noise, depending on the integration time and other factors. It has been shown that in some cases noise may be reduced by incorporating a cooling unit ("Spectrometer Knowledge," 2015).

2.9 Application of optical sensors in dairy food process control

Automation of dairy production facilities is of interest to the industry to improve quality processing and production control. As milk must undergo certain processing steps prior to dairy manufacturing, it could be of interest to implement monitorization techniques inline in order to minimize interference and analysis time and gain feedback for process optimization. For this reason, optical sensors can be useful in that they give the opportunity for minimal interference, and little to no product loss, as measurements have no negative effect on the product. Various groups discussed in this section have studied the possibilities for the potential development of inline optical sensors for the dairy industry, and show promise for the implementation of these techniques.

For example, optical sensors for dairy food products have been developed to analyze milk coagulation and syneresis (Castillo et al., 2000; Fagan et al., 2007; Fagan et al., 2008) and milk and whey fat (Crofcheck et al., 2000; Castillo et al., 2005;) concentration for improved monitoring and quality control in industrial processes using only simple optical sensor techniques, whether it be light backscatter/sidescatter (180°/90°, respectively) or light transmission (0°). These studies all utilized a simple, non-destructive technique using a relatively inexpensive measurement system. Combining the knowledge of optical sensor technology and the light scatter properties of casein micelles, an optical light backscatter technique has been developed based on the assumption that denatured whey proteins attach to the surface of the casein micelle and give rise to a measurable change in the size of the casein micelle (Lamb et al., 2013). Utilizing the hypothesis that denatured whey proteins attach to the casein micelle resulting in an increase in the diameter of the casein micelle, Lamb et al. (2013) modelled the extent of β-LG denaturation in milk during heat treatments as a function of specific spectral information in the range of 200-1100 nm. Analyses have indicated that a correlation exists between the light backscatter ratio response in heat-treated

milk and the degree of denaturation of its whey proteins, however did not take into account the pH dependence of the formation of the denatured WP/κ-CN complex.

2.10 Fluorescence measurement and configuration

Fluorescence occurs when the electrons of a fluorophore are excited to a higher energy level and emit light energy during relaxation. Fluorophores are usually aromatic compounds or molecules which contain many pi bonds. As shown in Figure 2.16 (Jablonski diagram), fluorescence occurs when an electron is excited from the ground state (s_0) to an excited state (s_1') (1). During non-radiative energy loss to a more relaxed excited state (s_1), heat may be given off (Figure 2.16, 2). Fluorescence only occurs when the electron returns to its ground state during radiative emission in which light energy is released (Figure 2.16, 3).

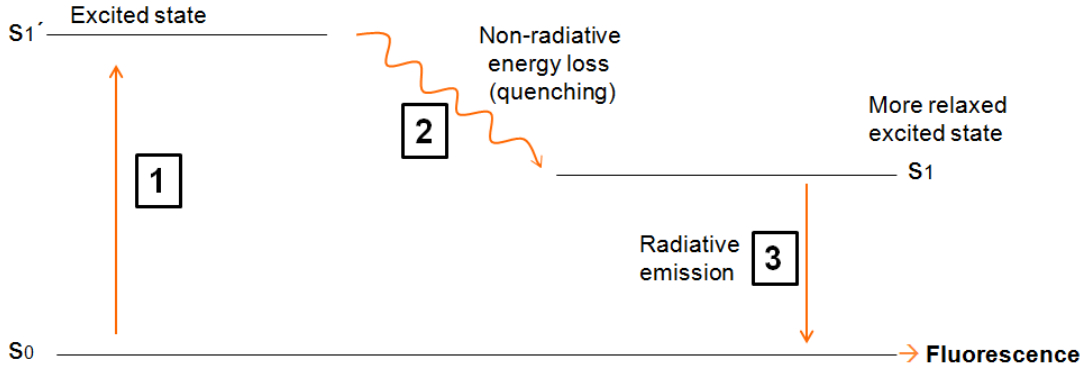

Figure 2.16. Electron transitions during fluorescence, s_0 ground state, s_1' excited state, s_1 more relaxed excited state.

Fluorescent spectroscopy involves quantification of the light energy emitted during fluorescence. In general, the two basic spectral configurations for fluorescent measurements are emission and excitation spectra. Emission spectra is an intensity reading taken at a constant excitation wavelength spanning across a range of emission spectra, whereas excitation spectra has a constant emission wavelength and a range of excitation wavelengths. Dairy products contain a number of fluorophores such as riboflavin, vitamin A, amino acids and the product of various reactions such as oxidation and Maillard browning. As seen in Figure 2.17, fluorophores may have overlapping emission and excitation wavelengths, thus

in some cases fluorescence quantification may include intensity contributions from numerous fluorophores.

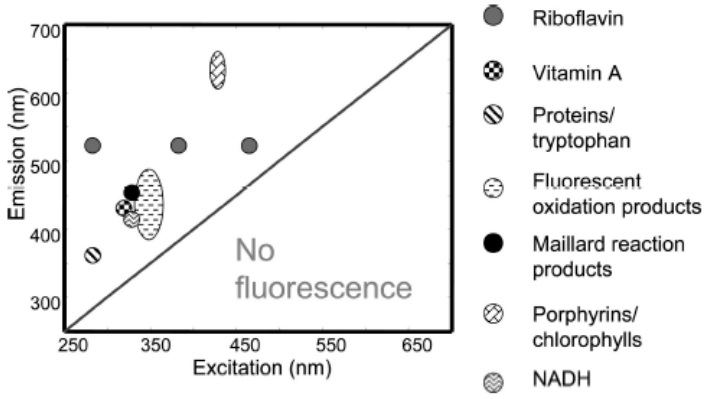

Figure 2.17. Excitation and emission maxima of fluorphores found in dairy products according to Wolfbeis, (1985), Duggan et al. (1957) and Christensen, Nørgaard, Bro, & Engelsen (2006)

Fluorophores are generally characterized to have well-known maximum intensity values for their respective emission/excitation spectra. However, alterations of the electronic environment of the solvent and protein configuration may result in a wavelength shift corresponding to the peak intensity. A shift to lower energy and higher wavelength results in a red shift, whereas a shift to a higher energy and lower wavelength is called a blue shift. Vivian and Callis (2001) investigated tryptophan fluorescence and found shifting characteristics to be a result of various factors; mainly due to the presence of water and/or protein in the environment as well as an alteration of charge (presence/absence as well as location). For example, a blue shift occurred when a positive charge was found on the pyrrole ring and negative on benzene, with the opposite resulting in a red shift. Also, the presence of water usually showed a red shift, however this effect was less when the protein was in a buried state (not exposed to water). Interpretation of the maximum intensity shift of tryptophan fluorescence is complex, but nonetheless may be useful for certain characterization of protein configuration and charge locations.

Results can be further complicated by the interference of quenching components which may cause a decrease in the fluorescence intensity of a molecule. However, quenching also depends on the molecular state of the fluorescent compound. For example, tryptophan

fluorescence involved a certain level of quenching by tyrosine during measurements of protein *β*-LG (2 Trp, 4 Tyr) in its native state, but in the unfolded state quenching is not observed (Lakowicz, 2013). Dynamic quenching is when the fluorophore collides with a quencher, whereas static quenching may also occur when a fluorophore forms a stable complex with another non-fluorescent molecule. Using the Stern-Volmer equation shown below in Eqn 2.9, we see that the total intensity (I) is dependent on the intensity of the quencher (I_0) and the quencher concentration ($[Q]$). Thus it is possible to calculate the quenching effect using the Stern-Volmer constant (k_{SV}).

$$\frac{I_0}{I} = 1 + k_{SV}[Q] \qquad \text{(Eqn 2.9)}$$

The primary amino acid fluorophore is tryptophan, with negligible emissions from tyrosine and phenylalanine (Lakowicz, 2013), therefore, protein fluorescence is generally referred to as tryptophan (Trp) fluorescence. The specific tryptophan residues found in milk are from: *β*-LG (Trp-19 and Trp-61), *a*-LA (Trp- 60, Trp-104 and Trp-118), *κ*-CN (Trp-143 and Trp-76), a_{s1}-CN (Trp-164 and Trp-199) and a_{s2}-CN (Trp-109 and Trp-193) (Barman & Perry, 1977; Moro, Gatti, & Delorenzi, 2001; Rahimi Yazdi & Corredig, 2012). Thus total Trp fluorescence in milk should be a result of the location, conformation and availability/unavailability of these residues. Trp fluorescence can be interpreted by change in intensity, which should be a result of fluorophore availability, or as a result of red/blue shifting due to the location of the fluorophore. For example, initially a highly folded native protein would move from a nonpolar to a polar environment during heat-induced denaturation, and likely result in a red-shift (in which the max intensity occurs at a longer wavelength). On the contrary, a blue-shift may occur if the protein is initially found in a polar environment and moves to a nonpolar environment, as in the case of embedded in a micellar structure (Caputo & London, 2003), in which a shift to a shorter wavelength would occur.

Improvement in fluorescence techniques has been established by changing the measurement angle. In the case of concentrated or opaque samples, the use of front-face fluorescence (FFF) may offer advantages to traditional fluorescence. During measurements at 90°, highly concentrated samples may undergo self-absorption and beam attenuatation resulting in undetectable or distorted readings (Horiba, 2007). Front-face fluorescence can

often resolve these issues by changing the angle (30-60°) and allowing the light to travel across the surface of the liquid sample, and thus reducing the above-mentioned negative effects (Figure 2.18).

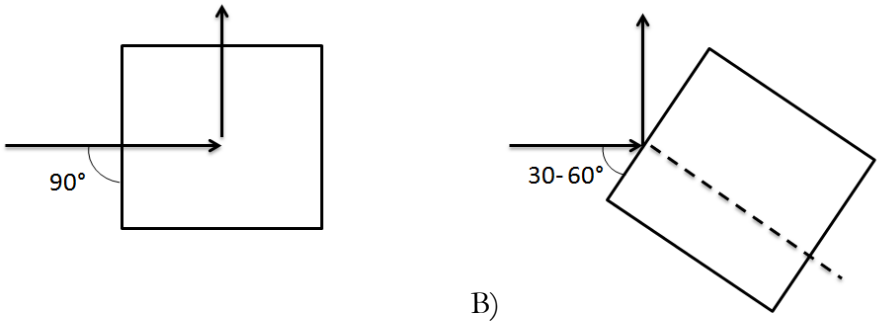

Figure 2.18. A) Traditional fluorescence and B) Front-face fluorescence configurations.

The use of FFFS has been reported in the literature to measure characteristic changes in dairy products during heat treatment and/or other processing methods. For example, Dufour and Riaublanc (1997) used FFFS of tryptophan and vitamin A to differentiate between raw, heated milk and homogenized milks. Kulmyrzaev et al. (2005) were able to successfully distinguish between heat treatment times by correlating native β-LG and alkaline phosphate content to various fluorescent markers (Trp, NADH and FADH). Secondary reactions have also been investigated using FFFS such as Maillard browning in milk (Schamberger & Labuza, 2006), oxidation in dairy products (Wold, Jørgensen, & Lundby, 2002), and the effects of cheese ripening (Herbert, Riou, & Devaux, 2000). Fluorescence spectroscopy involves the consideration of many factors and has potential interfering aspects. Nevertheless a high degree of sensitivity, considerable degree of reproducibility and the potential to gain information on various mechanisms are some of the reasons fluorescence spectroscopy is widely used as an analytical measurement technique for changes in dairy products.

CHAPTER 3: Objectives and working plan

The main objective of the study is to develop an inexpensive method for assessing the extent of heat-induced whey protein denaturation in milk products that could be used for inline processing. The specific objectives throughout the work include:

1. Determine the concentration of the three configurations of heated whey protein (native, whey protein aggregates, and whey proteins attached to the casein micelle) in skim milk heat treated at different processing temperatures, times and pH values.
2. Correlate changes in concentration of the three whey protein configurations with changes in particle size and the optical light backscatter response.
3. Determine the nature of the optical signal based on the relationship between particle size and changes in light backscatter in samples as a function of (A) pH and (B) the concentration of bound whey proteins and/or (C) formation of soluble whey protein aggregates within the heat treated skim milk matrix.
4. Compare the light backscatter technique to front-face fluorescence measurements as an alternative and/or complementary technique for modeling whey protein denaturation.
5. Investigate the potential for developing a kinetic model of whey protein denaturation using the following optical and reference methods: light backscatter, fluorescence, particle size, and whey protein concentration (whey protein variants by HPLC and total whey protein by BCA assay).
6. Test the main hypotheses, previously evaluated in skim milk, in milk with a range of fat percentages (~0.5, ~1.5 and ~3%).
7. Effectively model whey protein denaturation in milk as a function of light backscatter signal.

3.1 Working plan

The experimental work was performed using three separate studies, summarized below.

3.1.1 Experiment I

The first experiment was run entirely at the *Universitat Autònoma de Barcelona* (UAB) using 3 milk pH values (6.3, 6.7 and 7.1) for the heat treatment at two different temperatures (80°C and 90°C) for 10 min. Unheated control samples were also analyzed after adjusting to the three milk pH values. In total, there were 3 replications of each respective sample, therefore the experiment included 18 heated samples (n = 3·3·2) and 9 unheated control samples. Some data analysis and model development was done in collaboration with the *Servei d'Estadística* at the *Universitat Autonoma de Barcelona* (UAB). The objectives that were accomplished during this experiment include 1, 2 and 3.

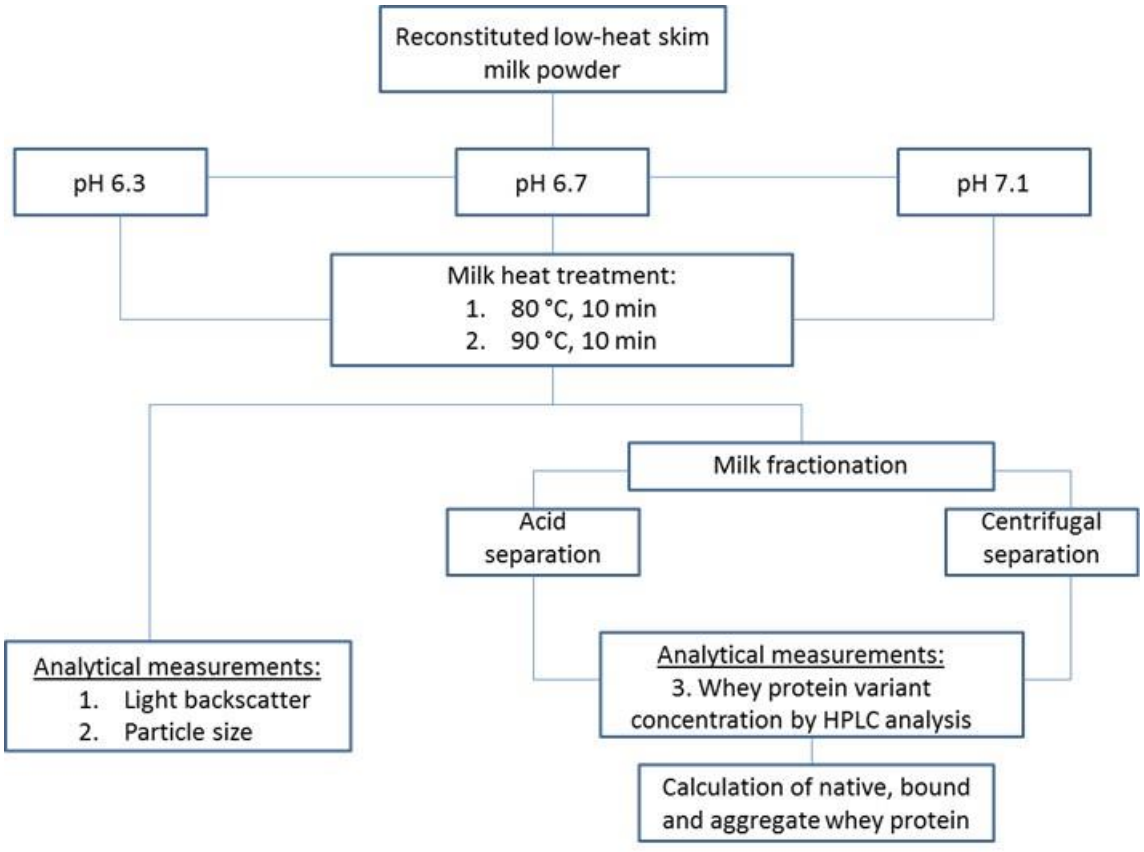

Figure 3.1. Experimental design of the first experiment: Whey protein variant denaturation in reconstituted skim milk. Light backscatter and particle size of the casein micelle as a function of pH and heat-treatment temperature. (*Published:* Taterka, H. & Castillo, M., 2015. The effect of whey protein denaturation on light backscatter and particle size of the casein micelle as a function of pH and heat-treatment temperature. *International Dairy Journal*, 48, pp.53–59).

3.1.2 Experiment II

The second experiment was run at the University of Minnesota with the financial support of a grant ("Ajuts per a estades de curta durada fora de Catalunya per a l'any 2012 pels becaris de les convocatòries PIF de la UAB") for a short research stay abroad. The experiment included 2 milk pH values (6.3 and 7.1) for the heat treatment at 80°C for 0, 3, 5, 7, 12 and 25 min in order to develop estimates of the kinetic rate constants for both binding (pH 6.3) and soluble aggregate formation (pH 7.1). In total there were 3 replications of each respective sample, therefore the experiment included 36 samples (n = 2·6·3). Some data analysis and model development was accomplished at *Universitat Autonoma de Barcelona* (UAB) in collaboration with the *Servei d'Estadística*. The objectives that were accomplished during this experiment include 1, 2, 3, 4 and 5.

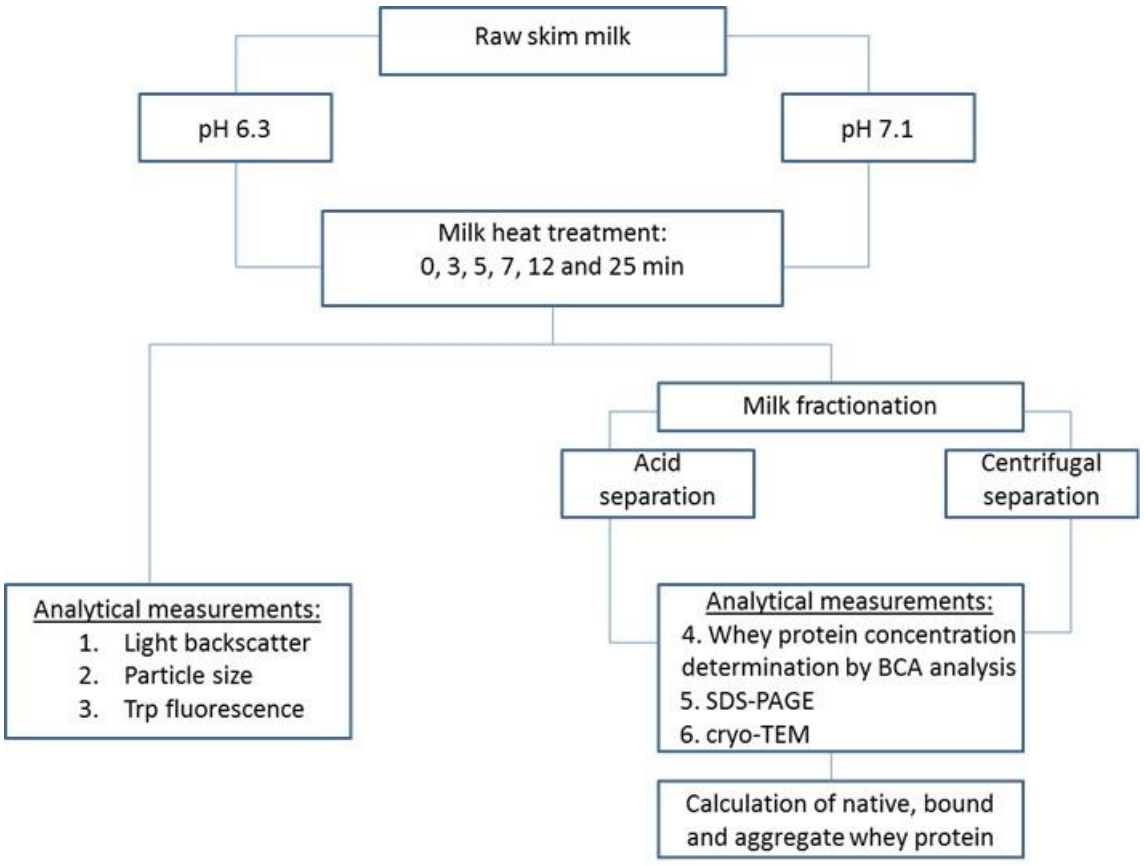

Figure 3.2. Experimental design of the second experiment: Kinetic analysis of the pH-specific mechanisms of denatured whey protein interaction for the development of an optical light backscatter sensor.

3.1.3 Experiment III

The third experiment was run at the *Universitat Autònoma de Barcelona* (UAB) with the assistance of the Erasmus student J. Obers who came to do an internship for his final school project at HAS University of Applied Sciences in the Netherlands. The experiment included pH 6.3 milk for the heat treatment at 80°C for 0, 3, 5, 7, 12 and 25 min with 3 different fat levels of milk (0, 1.3 and 3.7%). In total, there were 3 replications of each respective sample, therefore the experiment included 54 milk samples (n = 3·6·3). In addition fat and skim portions were fractionated thus 36 fat portion samples and 36 skim portion samples were also analyzed. The objectives that were accomplished during this experiment include 3, 4, 5 and 6.

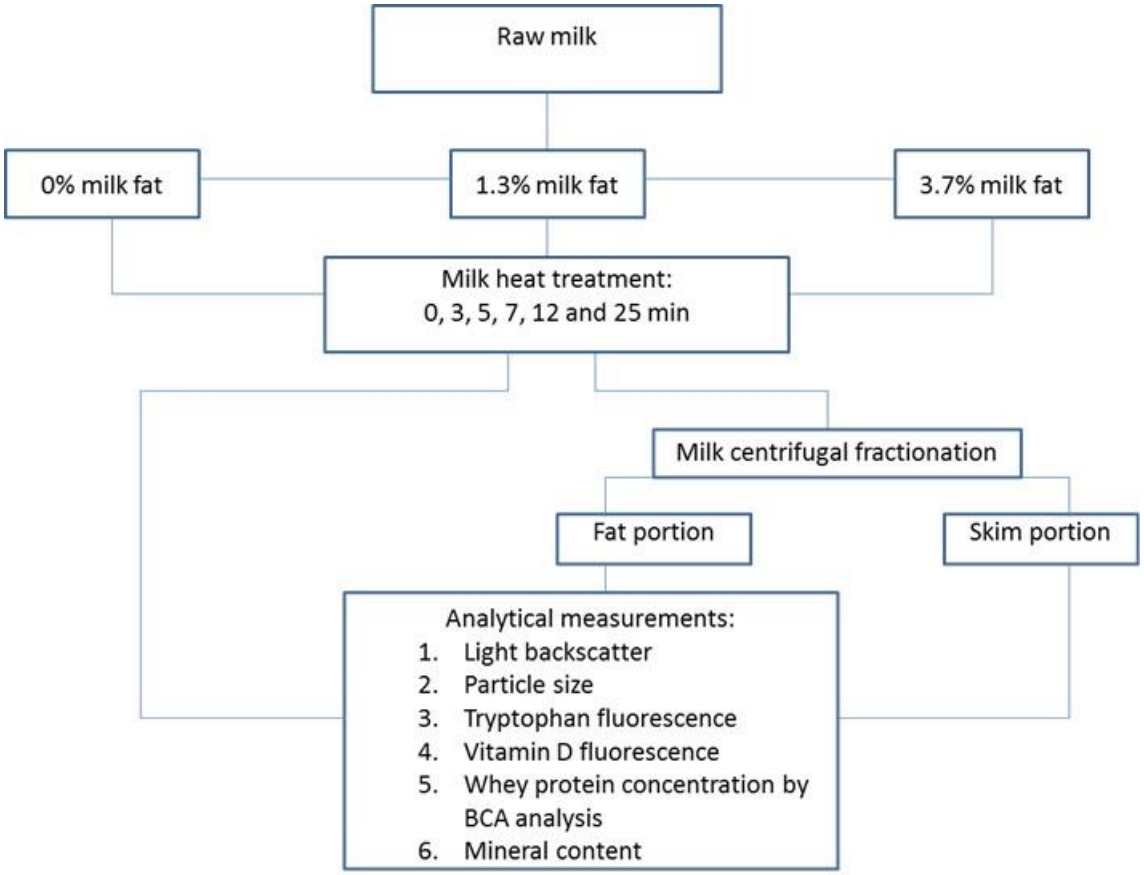

Figure 3.3. Experimental design of the third experiment: Kinetic analysis of the mechanisms of denatured whey protein interaction as a function of milk fat for the development of an optical light backscatter sensor.

CHAPTER 4: Materials and Methods

4.1 Milk preparation techniques

4.1.1 Reconstituted milk and pH adjustment

Low-heat skim milk powder (Chr. Hansen, Barcelona, Spain) was chosen for the experiment to minimize prior whey denaturation during processing and to ensure consistency among the various experimental trials (i.e., reduce experimental variability). The milk was standard skimmed milk powder of excellent functional and microbiological quality (low-heat, spray-dried skim milk powder; pH = 6.5, solubility = 99%, WPNI ≥ 7 mg g^{-1}, 800 cfu g^{-1}) supplied by Chr. Hansen SL (Barcelona, Spain). Milk was reconstituted by dispersion in Type I Milli-Q water (Conductivity at 25 °C) to a final solids content of 12% (*w*/*w*). Reconstituted milk, initially at pH 6.55 (± 0.015), was pH-adjusted at 21°C using 0.5 M HCl or 0.5 M NaOH, stirring well. Re-adjusted milk samples were allowed to equilibrate for 2 h in a dark place, before final pH reading and minor re-adjustments. Reconstituted milk following this procedure was used during Experiment I.

4.1.2 Fresh raw skim milk

All trials were run using the same batch of raw skim milk, obtained from the University of Minnesota Food Science and Nutrition pilot plant in Experiment II and from the Universitat Autònoma de Barcelona pilot plant in Experiment III. Milk was then pH adjusted at 21 °C to 6.3 and 7.1 using 1 M HCl or 1 M NaOH, stirring well. After 2 hour equilibration in a dark place, milk was measured for final pH readings and minor pH re-adjustments. Raw skim milk using this procedure was used during Experiment II and III.

4.2 Heat treatment

4.2.1 Plate heat treatment

After final pH re-adjustments, 80 mL of room temperature (21°C) equilibrated milk was poured into a stainless steel plate consisting of two thin rectangular plates 6 mm width apart, designed with a high surface area in order for consistent heat distribution (Figure 4.1). The plate was then placed into an OvanTherm C water bath maintaining proper temperature

control using an OvanTherm TC00 unit (resolution 0.1, stability ±0.1°C) (Suministros Grupo Esper, S.L., Badalona, Spain) at either 80°C or 90°C for 10 min. Thermal treatment was stopped by removing the heat plate from the circulating water bath and rapidly placing it in a 0°C ice-water bath for 3 min. The milk samples were removed from the heating vessel, placed in a test tube, and refrigerated at 4°C for no more than 2 days before further analysis. Samples were re-equilibrated to 21°C before analysis. This heat treatment method was used during Experiment I and III.

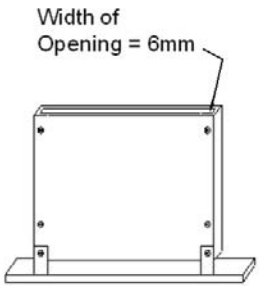

Figure 4.1. Parallel plate vessel used to hold milk sample for heat treatment.

4.2.2 Autosampler heat treatment

After final pH readjustments, 12 mL of room temperature (21 °C) milk was poured into individual 15 mL vials and capped with magnetic crimp caps with septa (Gerstel Inc., MD, USA). Thermal treatment was accomplished using CombiPAL GC Autosampler (CTCAnalytics, Zwingen Switzerland) (Figure 4.2) by transfer of the vials from an temperature regulated sample rack set to 21 °C via magnetic arm to an isolation chamber set at 80°C with an agitation speed of 500 rpm at times of 0, 3, 5, 7, 12, 25 min. After thermal treatment, each vial was rapidly placed in an ice-water bath for 3 min. Each treatment was replicated three times. This heat treatment was used during Experiment II.

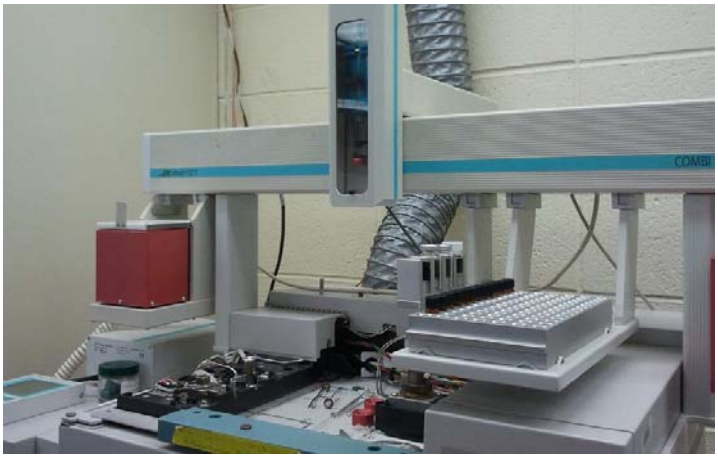

Figure 4.2. CTC Analytics GC Autosampler.

4.3 Light backscatter system and measurements

4.3.1 Optical system setup I

The optical system was set to measure light backscatter (180°) using a Reflectronics light scatter probe (Figure 4.3A) (Reflectronics Inc Lexington, KY, USA) placed inside a fitted slot of a black-walled 20 mL sample well (Figure 4.3B, 4.3C). The sample temperature was controlled by double jacketed walls below the sample well, which was connected to a circulating water bath controlled at 25°C (Figure 4.3B, 4.3C). Two 0.440 mm optical fibers were embedded into the probe, in which one fiber connected to a tungsten halogen light source (LS-1; Ocean Optics, Inc. Dunedin, FL, USA) via SMA connector attached to an optical fiber cable (d~0.8 mm) (Spectran Specialty Optics, Avon, CN, USA), and the other optical fiber of the probe connected to a high resolution miniature spectrometer (Model HR4000; Ocean Optics, Inc. Dunedin, FL, USA) with a detection bandwidth of 200-1100 nm via a UV-NIR optical fiber of 0.6 mm (Ocean Optics, Inc. Dunedin, FL, USA) (Figure 4.3A, 4.3C). At each sample measurement, the spectrometer sent the quantified light backscatter signal to a computer allowing for the generation of an intensity spectrum using Spectra Suite computer software (Ocean Optics, Inc. Dunedin, FL, USA) with scans at an integration time 5 s, boxcar smoothing of 3 and an average of three scans. The full optical system is shown in Figure 4.3C. This optical system was used during Experiment I.

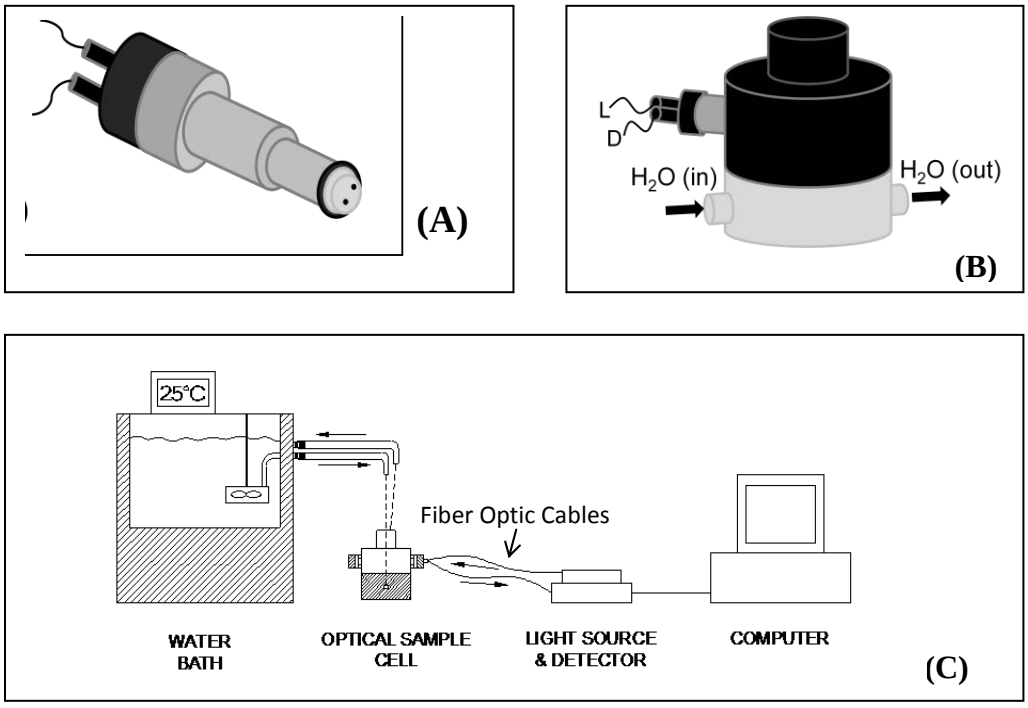

Figure 4.3. (A) Light backscatter probe (B) Optical sample cell: L= Light source, D= Detector (C) The complete optical system (Lamb et al., 2013).

4.3.2 Optical system setup II

The main components of the optical sensor system are shown schematically in Figure 4.3C such as: a tungsten halogen light source (LS-1; Ocean Optics, Inc. Dunedin, FL, USA); two fiber optic cables with a diameter of 0.8 mm, one of which connected the optical system to the light source; and one to the detector of high resolution fiber optic spectrometer (Glacier® X TE Cooled spectrometer, B&W Tek Inc., Delaware, USA) with a detection bandwidth of 200-1050 nm. The optical system was set up to measure light backscatter (reflectance at 180°). The spectral profiles were generated using BWSpec Version 4.01 Spectral software (B&W Tek Inc.) with scans at an integration time of 1 second and an average of three scans.

The sample cell consisted of a 20-mL space with a 2.54 cm diameter fiber optic probe set at 180° (backscatter). Improvements to this system have been developed in comparison to optical system I, including an improved sampling cell with an increased temperature control system (Figure 4.4A) as well as a new spectrometer (BWTEK, Model BCTC112E, B&W Tek Europe GmbH, Germany) with increased sensitivity and detector temperature control. The materials used for the manufacturing of the cell were AISI 316L stainless steel, suitable for use in contact with food and delrin high density polymer. The design was

modified by substantially extending the area of contact with the heated water; and the materials were selected to achieve higher heat transmission efficiency using one water inlet and three outlets (Figure 4.4A, C). A Nerinox oxidation treatment was used inside of the sample cell in order to obtain an intense matte black tone which would prevent any measurement error as a result of light reflection (Figure 4.4C). To fit the pieces of the sampling cell together, stainless steel screws and viton seals were used. A water bath at 25°C was connected to the top of the sample cell in order for water to flow from the bottom of the cell to the top, coming in contact with not only the bottom, but the sides of the sample cell. Additionally, the stainless steel material allows for higher heat transfer, which added to the uniformity of the temperature control (Figure 4.4B). This optical system was used during Experiment II and III.

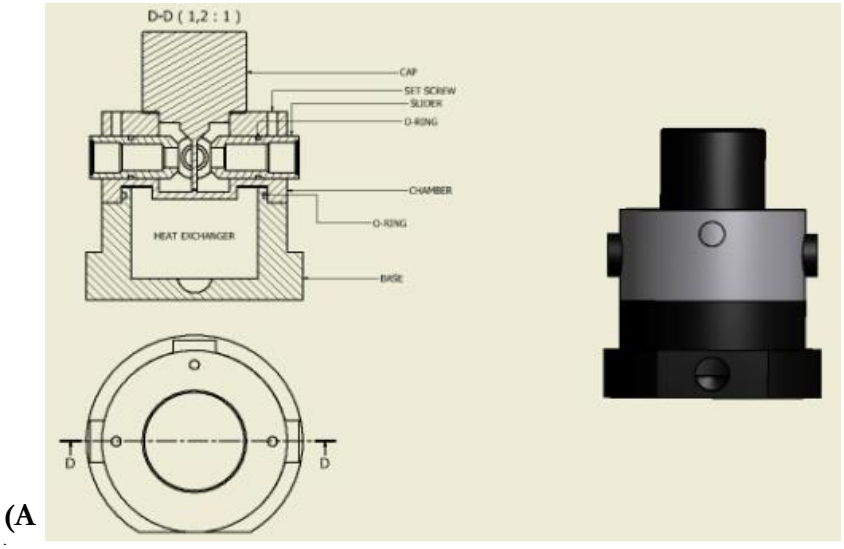

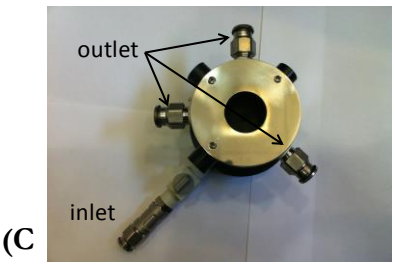

Figure 4.4. (A) Improved sampling cell with increased heat transfer with water circulation around the sample cell walls as well as the bottom (B) Stainless steel sample cell before treatment (C) Sample cell after Nerinox oxidation treatment for decreased light wall reflection.

4.4 Particle size

Particle size z-average was measured at 20 ± 0.5 °C using dynamic light scattering set to 90° and refractive index set to 1.471. A Malvern Zetasizer 4 (Malvern Instruments Ltd., Malvern, Worcs., UK) was used for Experiments I and III, whereas a BIC ZetaPALS system (Brookhaven Instruments Corporation, New York USA) was used in Experiment II. In Experiment I, samples were suspended in Ca/imidazole buffer (20 mM-imidazole, 5 mM-$CaCl_2$, 30 mM-NaCl, pH 7.0) at a concentration of 1:2 in order to suspend the casein micelles and allow stability during measurements (Anema, 1997; Anema & Li, 2003a; Anema, Lowe, et al., 2004). The following experiments (II and III) were suspended in Ca/imidazole buffer with 17 µl milk sample in 4 mL of imidazole buffer after a more thorough investigation of optimal suspension/scattering ratio, however no significant differences were found between recorded z-average measurements from Experiment I and Experiments II and III. Measurements were 3 min each and an average of 3 measurements was taken for each representative sampling.

(A)  **(B)** 

Figure 4.5. (A) Malvern Zetasizer 4 (B) BIC ZetaPALS system.

4.5 Front face fluorescence

4.5.1 Perkin Elmer

Fluorescence measurements were accomplished using a Perkin Elmer Fluorescence Spectrometer LS-50B (Serial #36275, Perkin-Elmer Ltd., Beaconsfield, U.K.) (Figure 4.7A) with front-face accessory to change the measurement angle to 60° (Figure 4.7B) with an attenuation filter of 2% used in the excitation slit to yield a more appropriate signal-to-noise ratio. Samples were measured at an excitation wavelength of 290 nm using an emission

spectra from 305-450 nm; parameters that correspond to tryptophan fluorescence (Schamberger and Labuza, 2006). Each representative measurement was an average of three runs. The above methodology and instrumentation was used in Experiment II.

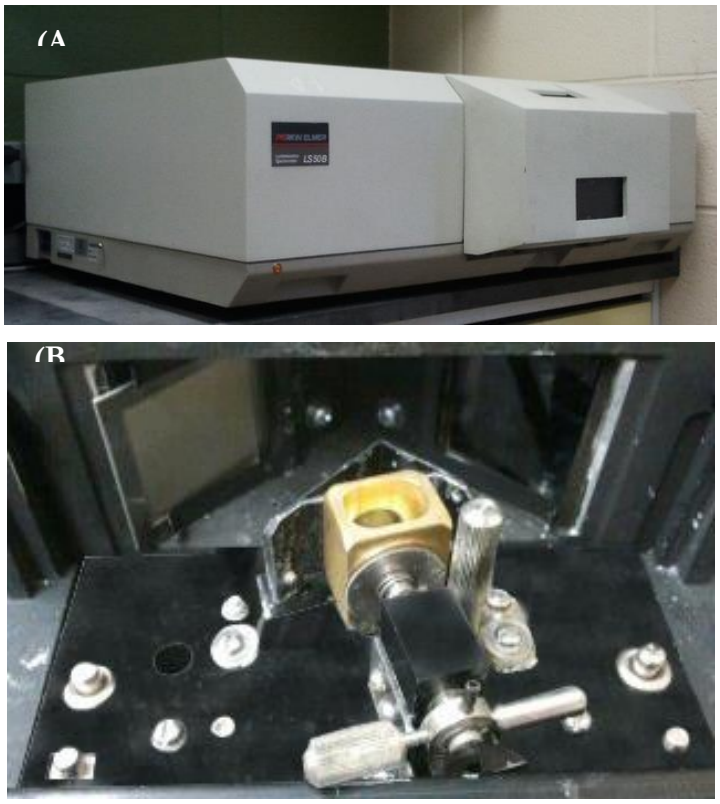

Figure 4.7. (A) LS-50B Fluorescence Spectrometer and (B) Front face fluorescence (FFF) accessory to measure tryptophan fluorescence in milk samples.

4.5.2 Cary Eclipse

Fluorescence measurements were accomplished using a Cary Eclipse Fluorescence Spectrophotometer (Agilent Technologies) (Figure 4.8A) equipped with a plate reading accessory (Figure 4.8B). Samples were measured for tryptophan fluorescence at an excitation wavelength of 290 nm and emission spectra from 305-450 nm (Schamberger and Labuza, 2006). Vitamin A fluorescence was measured at an excitation spectrum of 270- 350 nm at an emission wavelength of 410nm. Each representative measurement was an average of four runs and 3 replications. This methodology and instrumentation was used in Experiment III.

Figure 4.8. (A) Cary Eclipse Fluorescence Spectrophotometer (Agilent Technologies) (B) with a plate reading accessory.

4.6 Milk protein fractionation

4.6.1 Acid precipitation

Native whey proteins were fractionated from milk samples (control samples –i.e., unheated, reconstituted skim milk powder samples-, and heat-treated samples) using acid-induced precipitation, as adapted from the method IDF Standard 178, by adjustment to pH 4.6 by adding 2 M HCl dropwise while mixing continuously. The pH-adjusted milk was centrifuged at 3,000 g for 20 min at 21 °C ("ISO 13875:2005 (IDF 178: 2005) 2005). The supernatant was filtered using Whatman grade 1 paper (Whatman, Maidstone, UK) and the acid whey collected in a test tube. The supernatant from this separation technique is further referred to as heated native whey proteins (HNP). This technique is used in all Experiments (I, II and III).

4.6.2 Centrifugal separation

Centrifugation was used in heat-treated samples to sediment the casein micelles while retaining native whey proteins and smaller complexes of denatured whey proteins in the serum phase, as well as the possibility to find whey protein/κ-casein complexes depending on the mechanism of formation and/or attachment (Donato, Guyomarc'h, Amiot, & Dalgleish, 2007).

Eqn 4.1 (D'Allemand, 1994) was used in order to simulate a centrifugal force equivalent to the methodology of Anema and Li (2003a) (63,000 g for 1 h). A combination of velocity and time to obtain proper separation was used to estimate optimal conditions for the adapted technique.

$$t = \frac{a \cdot b}{c} \qquad \text{Eqn 4.1}$$

where t= calculated run time for the new study,

a = run time from previous study,

b = g-force of rotor from previous study,

c = g-force of the new study.

Since our technique balanced the lower RPM value for an extended time centrifugation, we found it necessary to run preliminary tests to ensure a proper speed/time combination. Various trials of the RCF/time combinations were run in line with Eqn. 4.1 and the previous methodology of Anema and Li (2003a), and it was observed that the optimal combination was 20,000 g for 4 h. After separation of the two phases, the supernatant was re-spun at 3,000 g for 20 min, and then removed and filtered. The supernatant from this separation technique is further referred to as centrifuged whey proteins (CP). This separation technique was used in Experiment I.

4.6.3 Ultracentrifuge separation

As adapted from Jensen et al. (2012) milk was centrifuged at 100,000 for 1 h at 4 °C. The supernatant was removed and analyzed or frozen at -20 °C and thawed for further analysis. This separation technique was used in Experiment II.

4.7 Protein concentration determination

4.7.1 High Performance Liquid Chromatography (HPLC)

Protein concentration in the acid-whey (4.6.1) and centrifuged samples (4.6.2) was determined by HPLC according to IDF Standard 178:1996. The HPLC system consisted of a Teknokroma column (Tracer Excel 300 C8 5µm 25x0.46, Teknokroma Analítica SA., Sant Cugat del Vallés, Spain), a UV/vis detector UVD 170U, ASI-100 Automated Sample Injector

and a TCC-100 thermostatted column compartment (Dionex Corp., Sunnyvale, CA, USA) (Figure 4.9). Whey samples were dissolved in 6M urea/dithiothreitol buffer in a 1:2 dilution. Sample peaks were quantified at 280 nm using Chromeleon software Version 6.70 (Dionex Corp. Sunnyvale, CA, USA) compared against standard dilutions of *a*-lactalbumin and *β*-lactoglobulin (Sigma Aldrich Corp., St. Louis, MO, USA).

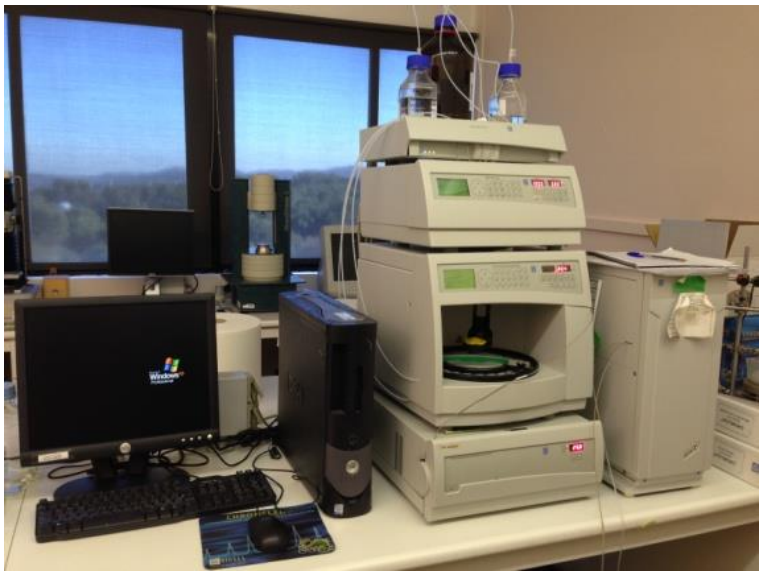

Figure 4.9. Teknokroma HPLC system.

4.7.2 Bicinchoninic Acid (BCA) assay

Total protein concentration in supernatant samples separated by both acid (4.6.1) and ultracentrifuge (4.6.3) methods were analyzed using the bicinchoninic acid assay (BCA assay Kit #23235 Product Instructions, Pierce Chemical Company, Thermo Fisher Scientific Inc., Rockrord IL, USA). As it requires a concentration between 0.5 μg/mL to 1.5 mg/mL, samples were diluted 1:9 with double distilled water. Standard curve and samples were run in duplicate according to the microplate technique in the pamphlet of the BCA Assay Kit method (Thermo Scientific, BCA protein Assay Kit 23225 Instructions).

4.8 Bound and aggregate whey protein content determination

Using the two separation techniques (acid separation and centrifugal separation), all three whey protein configurations were determined using Equation 2 and 3, as shown below.

The separation techniques and quantification of the various types of whey proteins are also shown in Figure 4.10.

$$\text{Heated native whey proteins (NWP)} = \text{NWP} \tag{Eqn. 4.2}$$

$$\text{Aggregate whey proteins (AWP)} = \text{CP} - \text{NWP} \tag{Eqn. 4.3}$$

$$\text{Bound whey proteins (BWP)} = \text{NWP}_{\text{initial}} - \text{CP}$$

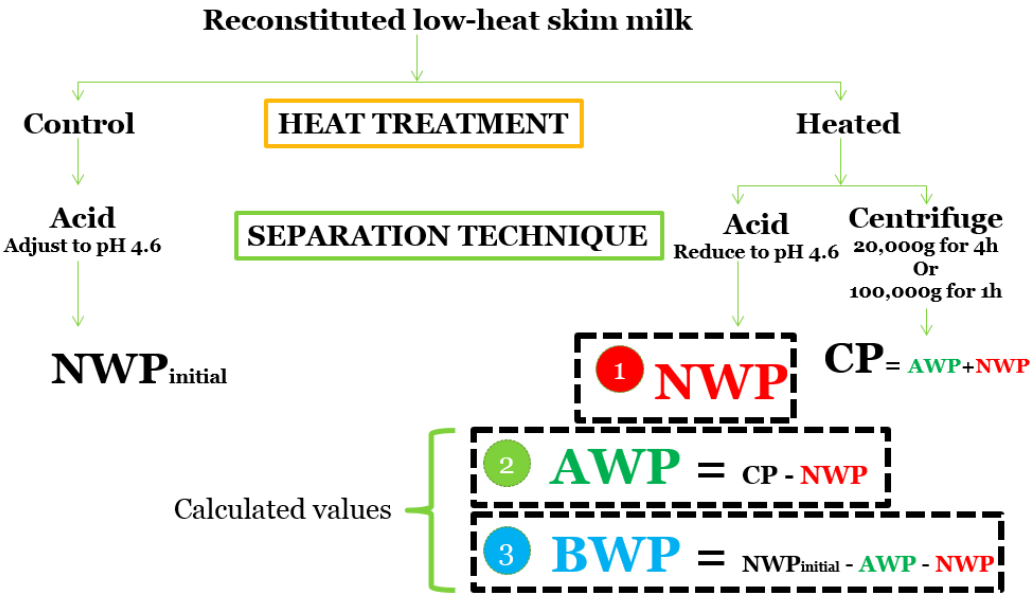

Figure 4.10. Separation scheme and calculation of the various configurations of whey proteins in milk; 1: NWP: heated native whey proteins; 2: AWP: aggregate whey proteins; 3: BWP: bound whey proteins; TP: total whey proteins; CP: centrifuged whey proteins.

4.9 Statistical analysis

4.9.1 Maximum wavelength statistics

Data was analyzed using "Statistical Analysis System" (Experiment I: version 9.2, Experiment II: version 9.3, SAS Institute Inc., Cary, NC, USA, 2013). The linear Pearson correlation coefficients were determined with the Correlation procedure (CORR), while the analysis of variance (ANOVA) was performed using the General Linear Model procedure

(GLM). In Experiment I the linear model used was $Y_i = \mu + E_i + \varepsilon_i$ where Y were the dependent variables studied (Experiment I: light backscatter, PS, NWP, Experiment II: PS, NWP, BWP, AWP), E_i were independent variables (pH, temperature and light backscatter) and ε_i was the error term. Least squares means (LSM) and significance of each treatment were computed using Type IV sum of squares. Independent variables selected as main effects in the statistical model were pH, temperature (T) and the interaction of pH and temperature (pH x T). The effect of replication was not significant and was removed from the model. Differences between means of the various treatments were considered significantly different when $P < 0.05$.

4.9.2 Ratio prediction models

Waveband ratios (Experiment I: 35 nm, Experiment II: 35 nm) were determined from the light backscatter and fluorescence spectra and implemented into linear (Eqn 4.4), quadratic (Eqn 4.5), cubic (Eqn 4.6) and/or exponential (Eqn 4.7) models where y represent dependent variables and x represent independent variables. Further information regarding the techniques used for this experiment can be found in Section 7.3.2.1 (Experiment I) and Section 9.3.2 (Experiment II).

$$y = \beta_0 + \beta_1 x \quad \text{(Eqn. 4.4)}$$

$$y = \beta_0 + \beta_1 x + \beta_2 x^2 \quad \text{(Eqn. 4.5)}$$

$$y = \beta_0 + \beta_1 x + \beta_2 x^2 + \beta_3 x^3 \quad \text{(Eqn. 4.6)}$$

$$y = \beta_0 + e^{(\alpha_0 + \alpha_2 x)} \quad \text{(Eqn. 4.7)}$$

CHAPTER 5: The effect of whey protein denaturation on light backscatter and particle size of the casein micelle as a function of pH and heat-treatment temperature

5.1 Introduction

Various factors can contribute to the rate of whey protein denaturation, such as heat treatment time, temperature, pH, whey protein concentration, protein structure and heat susceptibility (O'Connell & Fox, 2003; Singh, 2004). A greater extent of denaturation exposes more sulfhydryl groups which are otherwise buried within the protein structure, resulting in an increase in casein micelle attachment and/or other protein-protein interactions. In order for whey proteins to attach to the surface of the casein micelle, two steps need to occur. First, *β*-lactoglobulin (*β*-LG), one of the major whey proteins, must unfold to expose its sulfhydryl group, and then the protein must form a disulphide bond with *κ*-casein (*κ*-CN). It is generally accepted that the other major whey protein, *α*-lactalbumin (*α*-LA), is not involved until after the initial formation of the association between *β*-LG and *κ*-casein; attributed to its lack of a free thiol group (Corredig & Dalgleish, 1999; Donato & Guyomarc'h, 2009; Mulvihill & Donovan, 1987). Alternatively, whey proteins may attach to each other and remain in the serum portion as whey protein aggregates (Donato & Guyomarc'h, 2009; Guyomarc'h, Law, & Dalgleish, 2003; Jean, Renan, Famelart, & Guyomarc'h, 2006; Vasbinder & de Kruif, 2003). Thus, after heat-treatment, the milk matrix is composed of a mixture of three types of whey proteins: native whey proteins, soluble whey protein aggregates and aggregates that have formed an association on the surface of the casein micelle.

In heat treated milk, that the whey protein/casein micelle complex has been found to be is responsible for an increase in casein micelle particle size (up to 30-35 nm change in diameter) (Skelte G Anema & Li, 2003a), with a maximum attachment at approximately pH 6.3 and a minimum at approximately pH 7.1 (Kethireddipalli, Hill, & Dalgleish, 2010; Vasbinder & de Kruif, 2003). Consequently, a greater change in casein micelle size has been found to occur in lower pH milk when compared to higher pH milk after heat treatment

(Anema & Li, 2003b; Donato & Guyomarc'h, 2009; Kethireddipalli, Hill, & Dalgleish, 2011; Vasbinder & de Kruif, 2003). Moreover, this mechanism exhibits temperature dependence, where a greater increase in particle size should be seen at higher heat treatment temperatures, as more protein denaturation occurs and therefore increases the amount of free sulfide groups with the potential to form protein-protein interactions (Anema et al., 2004; Vasbinder, Alting, & de Kruif, 2003).

Optical sensors for dairy food products have been developed to analyze milk coagulation and syneresis (Castillo et al., 2000; Fagan et al., 2007, 2008) and milk and whey fat (Castillo, Payne, López, et al., 2005; Crofcheck et al., 2000) concentration for improved monitoring and quality control in industrial processes using only simple optical sensor techniques, whether it be light backscatter/sidescatter (180°/90°, respectively) or light transmission (0°). These studies all utilized a simple, non-destructive technique using a relatively inexpensive measurement system.

To date, no rapid inexpensive methods exist for the inline determination of whey protein denaturation in processed milk. Rapid and non-destructive antibody detection methods have been developed for the determination of *a*-LA denaturation index; however they require a higher cost and preparation compared to optical methods (Dupont & Muller-Renaud, 2006; Dupont, Rolet-Repecaud, & Muller-Renaud, 2004). On the other hand, traditional fluorescence techniques have also been designed providing quick, easy and relatively inexpensive readings of whey protein denaturation, however at the moment these methods involve a certain extent of sample manipulation (Birlouez-Aragon et al., 1998), whereas the incorporation of front-face fluorescence technology may allow for potential inline use (Hougaard, Lawaetz, & Ipsen, 2013). Combining the knowledge of optical sensor technology and the light scatter properties of casein micelles, an optical light backscatter technique has been developed based on the assumption that denatured whey proteins attach to the surface of the casein micelle and give rise to a measurable change in the size of the casein micelle (Lamb et al., 2013). Utilizing the hypothesis that denatured whey proteins attach to the casein micelle resulting in an increase in the diameter of the casein micelle, Lamb et al. (2013) modelled the extent of *β*-LG denaturation in milk during heat treatments as a function of specific spectral information in the range of 200-1100 nm. Analyses have indicated that a correlation exists between the light backscatter ratio response in heat-treated milk and the degree of denaturation of its whey proteins. To further investigate this relationship between optical light backscatter measurements and casein particle size, our

study aimed to target the pH-dependence of whey protein denaturation mechanisms, and in particular, the consequence of the attachment of denatured whey proteins to the micelle with respect to changes in the optical light backscatter signal intensity.

5.2 Materials and Methods

The experiment consisted of a 3x2 factorial design with pH values of 6.3, 6.7 and 7.1 and two heat treatment temperatures: 80 and 90°C. The work plan for Experiment I can be found in Section 3.1.1. Low-heat skim milk powder (Chr. Hansen, Barcelona, Spain) was chosen for the experiment. Reconstitution information and pH adjustment can be found in Section 4.1.1. Time of heat treatment was constant for all measurements at 10 min with samples first equilibrated to a consistent room temperature of 21°C. Each treatment was replicated three times. Heat treatment of milk was accomplished using a stainless steel plate and an OvalTherm C water bath and is summarized in Section 4.2.1. Analytical techniques used in this part of Experiment I include: optical light backscatter, particle size z-average and native whey protein content (NWP) after heat treatment. Optical analysis was accomplished using the full system described in Section 4.3.1 and can be visualized in Figure 4.3. Light backscatter maximum intensity (570 nm) was recorded and used for further analysis. Milk samples for particle size measurements were suspended in a Ca/imidazole buffer (20 mM-imidazole, 5 mM $CaCl_2$, 30 mM NaCl, pH 7.0) and z-average was investigated using the Malvern Zetasizer 4 (Malvern Instruments Ltd., Malvern, UK) (Section 4.4.1). After acid-induced precipitation and fractionation of native whey proteins using pH adjustment to 4.6 (Section 4.6.1), NWP concentration was determined by HPLC and is summarized in Section 4.7.1. All data was analyzed by CORR, ANOVA and GLM using "Statistical Analysis System "(SAS, version 9.2, SAS Institute Inc., Cary, NC, USA, 2013) and least square means (LSM) were considered significantly different when $P < 0.05$.

5.3 Results and Discussion

Heat treated milk samples were analyzed by light backscatter, particle size and whey protein concentration by HPLC analysis. An ANOVA was conducted in order to determine main sources of variation in the dependent variables (Table 5.1), which included light backscatter maximum intensity (at ~570 nm), particle size mean radius (Z-value) by dynamic light scattering, and total whey protein concentration in mg mL^{-1}. The sources of variation

tested were pH, temperature (T) as well as the interaction of pH and temperature (pHxT). The results of the ANOVA exhibited significance in the case of light backscatter and particle size with respect to pH and temperature. The effect of replications is not shown in Table 5.1, as there was no significance for this variable. Additionally, an interaction between pH and temperature was observed in the case of particle size. For total whey protein concentration, only temperature was significant, which is expected as authors have found a minimal effect of pH with respect to whey protein denaturation in intermediate pH ranges (Law & Leaver, 2000; Vasbinder & de Kruif, 2003).

Table 5.1. Analysis of variance and *F* statistic for dependent variables[a]

			Variation source		
	Model		pH (2DF)	T (1DF)	pHxT (2DF)
	R^2	F	F	F	F
LB	0.992	178***	538***	16.6**	2.06ns
PS	0.984	86.9***	245***	92.3***	71.2***
NWP	0.766	4.67*	0.11ns	22.5***	0.520ns

T, temperature; LB, light backscatter intensity at 570nm; PS, particle size diameter; NWP, native whey protein content, R^2, determination coefficient; F, ANOVA F-statistic; DF, degrees of freedom; *P<0.05, **P<0.01, ***P<0.001, ns not significant; N = 18.

5.3.1 The effect of temperature on light backscatter, particle size and whey protein concentration of milk

Differences among treatments with respect to temperature are presented in both Figure 5.1B demonstrating least square means of temperature treatments and Table 5.2 which displays correlation statistics between independent variables (pH and T) and dependent variables (LB, PS and NWP).

Table 5.2. Pearson Correlation between independent variables (pH and Temperature) and dependent variables (light backscatter, particle size and native whey protein content.)

	LB	PS	NWP
PS	0.774***	---	---
pH	-0.984***	-0.745***	-0.080 ns
T	0.122 ns	0.354 ns	-0.793***

T, temperature; LB, light backscatter intensity at 570 nm; PS, particle size diameter; NWP, native whey protein content; R^2, determination coefficient; F, ANOVA F-statistic; DF, degrees of freedom; *P<0.05, **P<0.01, ***P<0.001, ns not significant; N=18.

Notable observations in total acid-soluble whey protein concentration include a significant decrease by nearly 50% (Figure 5.1B) and a significant negative correlation with increasing temperature ($r = -0.79$, $P<0.001$; Table 5.2). As whey protein unfolding induces protein-protein interactions by exposing reactive sulfhydryl groups; in general a greater reaction potential has been observed in samples that withstood a more severe temperature treatment (Mulvihill & Donovan, 1987). Attachment of whey protein to the micelle surface also tends to increase with increasing heat treatment temperature (Anema & Li, 2003a, 2003b; Anema et al., 2004; Corredig & Dalgleish, 1999; Oldfield, Singh, Taylor, & Pearce, 2000; Vasbinder, Rollema, & de Kruif, 2003). Similarly, we observed a significant increase in light backscatter and particle size between heat treatments of 80 and 90 °C (Figure 5.1B), however a significant temperature correlation does not exist in neither light backscatter nor particle size (Table 5.2). Even though we see a general increase in light backscatter and particle size with increasing temperature, it has been found that significant differences in whey protein/casein complex formation did not occur with an increase in temperature in the range of 70-110 °C (Dannenberg & Kessler, 1988).

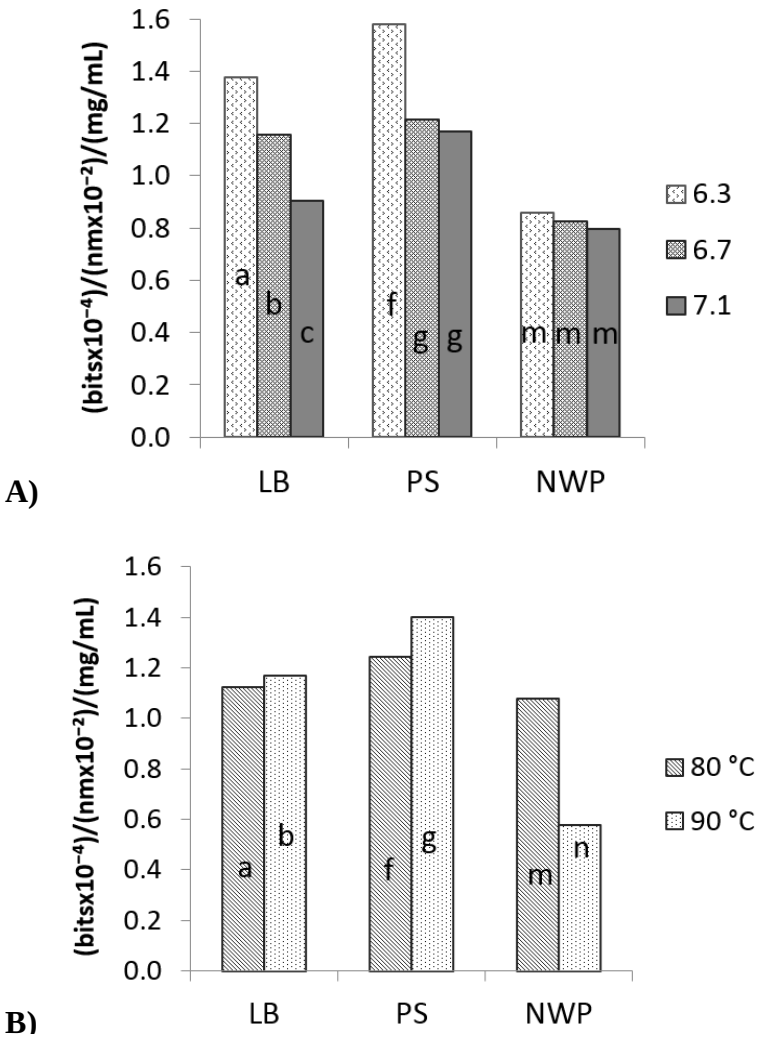

Figure 5.1. Influence of main effects on parameters evaluated: LB, light backscatter intensity at 570nm; PS, particle size diameter; NWP, native whey protein concentration, adjusted parameters according to unit values on y-axis (A) LSM by pH, (B) LSM by temperature, LSM with same letters were not significantly different $p<0.05$; number of replications 3; N=18.

It should also be considered that milk pH tends to reversibly decrease during moderate heat treatment as a result of the incorporation of calcium phosphate in the casein micelle resulting in an increase in H+ ions (Singh, 2004; Walstra et al., 2005). As attachment is the preferential mechanism at lower pH, this additional decrease in pH during heat treatment may play a role in the increased particle size and light scatter response observed from 80 to 90 °C. Nonetheless, Anema et al. (2004) found that milk-pH adjustments after heat treatment had no effect on particle size; thus it is likely that the preference for protein

interactions to result in binding and/or serum aggregates depends to a greater extent on initial milk pH than on pH alterations that occur as a result of heat treatment.

5.3.2 The effect of pH on light backscatter, particle size and whey protein concentration of milk

Least square means and correlation statistics are summarized in Figure 5.1A and Table 5.2, respectively. Quantification of native whey protein content by HPLC showed only a slight negative but not significant trend with an increase in milk pH (Table 5.2). A study by Law and Leaver (2000) determined denaturation rate constants of specific major whey proteins (*α*-LA and *β*-LG) and found relatively constant reaction rates in the milk pH range of our study (6.3-7.1). If the rate of whey protein denaturation is not pH dependent, reactive amino acid groups should occur in the same abundance at all milk pHs, and therefore any preference for whey proteins to adhere to the micelle or form serum aggregates should be a result of a change in side chain reactivity at different pH. For example, the cysteine -SH group, with a pKa of 9.5 at 25°C, is highly reactive in the ionized form exhibiting 0.04, 0.08, and 0.16% dissociation at pH 6.1, 6.4, and 6.7, respectively. As a result, it can be suggested that further dissociation at higher milk pH results in an increased reactivity (Walstra et al., 2005).

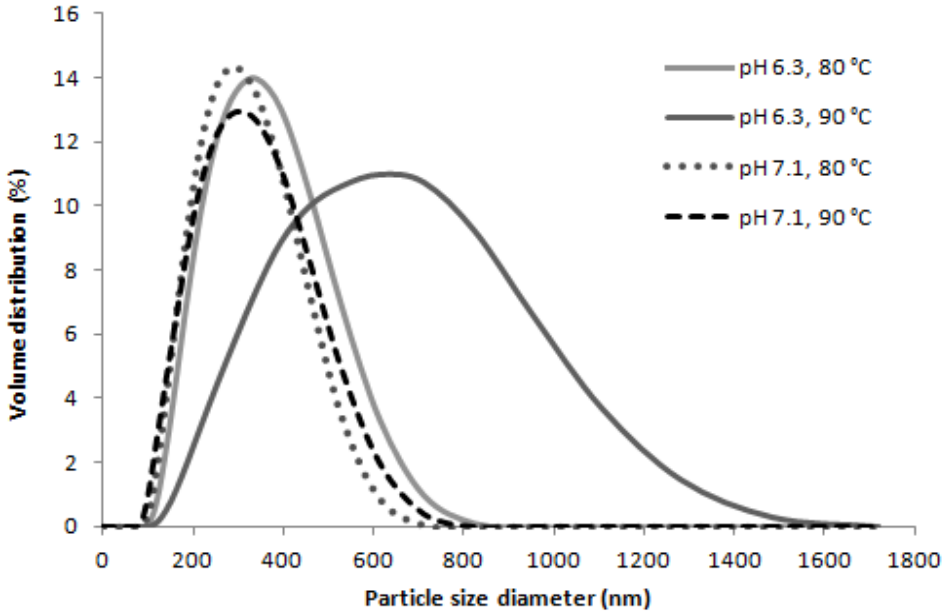

Figure 5.2. Particle size diameter volume distribution in pH adjusted milk (6.3 and 7.1) heated at 80 or 90°C for 10 min.

Consequently, it was of interest to investigate the relationship between light backscatter maximum intensity and particle size with respect to pH in order to form potential correlations for the development of an optical light backscatter sensor. As both of these techniques are based on light scatter, a similar trend was exhibited in which a significant decrease in light backscatter intensity and particle size (Figure 5.1A) and a significant negative correlation ($r = -0.98$ and -0.75, respectively, $P<0.001$; Table 5.2) were observed with respect to increasing pH. Assuming these correlations are a result of an increase in micellar attachment with decreasing pH, these correlations are logical; as it has been previously mentioned that changes in the size of the casein micelle after heat treatment are highly dependent on milk pH (Anema & Li, 2003b; Anema, 2007; Corredig & Dalgleish, 1996; Kethireddipalli et al., 2010; Oldfield et al., 2000; Vasbinder & de Kruif, 2003). In general, these differences in micelle size, which are detected by the two light scatter techniques, have been attributed to the formation of a whey protein/casein micelle complex; the preferable mechanism of denatured whey proteins at lower milk pH values. However, casein micelle aggregation, or as well, the formation of large serum whey protein aggregates, may also result in an increase in average particle size. For particle size analysis we used a Malvern Zetasizer,

which models dynamic light scattering (DLS) as a representative distribution of the different particle sizes in the mixture. Therefore mean size distribution should be a function of all the various particulate components of milk after heat treatment, which have been found to include casein micelles (d~50-600 nm, average d=120 nm) (Maubois & Olliver, 1997), whey protein aggregates (d~60nm) (Vasbinder & de Kruif, 2003) and κ-casein/WP complexes (d~25-70nm) (Jean et al., 2006). At various levels of pH, Anema and Li (2003a; b) observed a 30-35 nm increase in the particle size diameter after heat treatment, and attributed this to the pH-dependent attachment of denatured whey proteins to the surface of the micelle. As casein is in general much larger than other protein components and constitutes ~80% of total skim milk solids, we can expect that changes in particle size are due to an alteration in the size of the casein micelle. At pH 6.3, we observed a significant shift in z-average volume distribution with an increase in heat treatment from 80°C to 90°C (Figure 5.2), which we attribute to the attachment of denatured whey proteins to the surface of the casein micelle as this is the preferred mechanism at low pH. In addition to the formation of micelle/whey protein complexes on the micellar surface, there is the potential for the formation of whey protein aggregates in the serum. In particular, at pH 7.1 large whey protein aggregate formation may contribute to variations in the mean particle size, however, aggregates that exceed the size of the casein micelle have been known to form only when the intrinsic whey protein/casein micelle ratio was increased (Guyomarc'h et al., 2003). Consequently, we did not observe major difference in the particle size volume distribution with an increase in heat treatment in the case of pH 7.1 milk (Figure 5.2) and therefore in standard milk, aggregate formation is unlikely to be a cause for a positive shift in particle size distribution.

Another consideration for an increase in average particle size is the potential for casein micelle aggregation. A bimodal distribution was observed in heated milk DLS distribution curves by (Tran Le, Saveyn, Hoa, & Van der Meeren, 2008), which was attributed to either whey protein attachment to the surface of the casein micelle or casein micellar aggregation in milk. Because the bimodal distribution heavily skewed the mean particle size (~30-200nm) when compared to untreated milk, it was concluded that this shift was a result of casein aggregation, as only a slight augmentation (~30-35nm) and a monomodal distribution in the average particle size has been observed in studies in which the reaction mechanism was dominated by whey protein incorporation on the casein micelle surface (Anema & Li, 2003a, 2003b). Furthermore, a minimum treatment of 140°C for ~5 min is necessary for coagulation within the pH conditions utilized (Walstra et al., 2005) and/or in

studies where the milk-like suspensions were prepared to contain approximately 11% protein (Tran Le et al., 2008). Note that there was no visible coagulation present in our study. Taking into account these considerations, it is recognized that the attachment of denatured whey proteins to the casein micelle is likely to be the main contributor for the positive shift in the mean particle size in our study (Figure 5.2), and other aspects do not play a significant role.

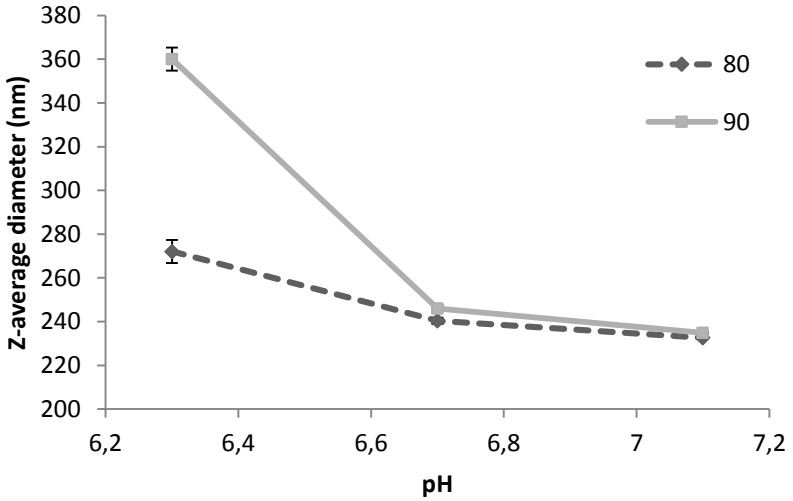

Figure 5.3. Z-average particle size diameter versus pH with respect to heat treatment temperature (°C). Experimental data corresponds to average values (N=3). Error bars correspond to the ± SD.

As discussed in Section 3.1, there is a temperature dependent relationship with respect to NWP, whereas other parameters show no relationship with heat treatment temperature. On the other hand, our analysis clearly shows a pH-dependent relationship in particle size and light backscatter measurements (Table 5.1, 5.2); and a pH x T interaction (Table 5.1, Figure 5.3). Higher heat treatment temperature results in a greater number of reactive whey protein sulfhydryl groups, and attachment is significantly higher at low pH, thus the observed pH x T interaction is clearly a result of these two observed effects (Section 3.2, 3.3). With support from the literature, we consider that the observed pH-dependent relationship exist as a result of the attachment of whey proteins to the surface of the casein micelle.

5.3.3 The relationship of light backscatter and casein micelle particle size separated by milk pH

Statistical relationships among samples at each respective pH value were determined. Figure 5.4 illustrates the least square means values for PS and LB as a function of pH and Table 5.3 summarizes the correlation statistics between PS and LB with respect to heat treatment temperature separated by pH. As mentioned before, there is a strong affinity for the attachment of denatured whey proteins to the surface of the casein micelle at pH 6.3 and for the formation of whey protein aggregates at pH 7.1. Consequently, in the case of light backscatter response, we see a significant difference in intensity at milk pH values of 6.3 and 7.1 with increasing heat treatment temperature (Figure 5.4) and a significant positive temperature correlation with light backscatter ($r > 0.86$, $P<0.05$; Table 5.3). At pH 6.7, however, there are no observable trends or correlations, as it has been observed that only slight micellar association was observed at pH 6.7 (Anema & Li, 2003a). On the other hand, and as expected, with respect to changes in particle size we see a significant difference and a positive correlation with temperature in pH 6.3 milk, only (Figure 5.3, 5.4). These results are well explained, as protein attachment yields a significant change in particle size (Anema & Li, 2003b), whereas the formation of protein aggregates should result in relatively little change in particle size (Guyomarc'h et al., 2003). Likewise, results were presented by Anema et al. (2004) in which particle size at pH 6.5 exhibited a temperature effect, whereas at pH 7.1 particle size was unchanged with respect to varying treatment temperatures.

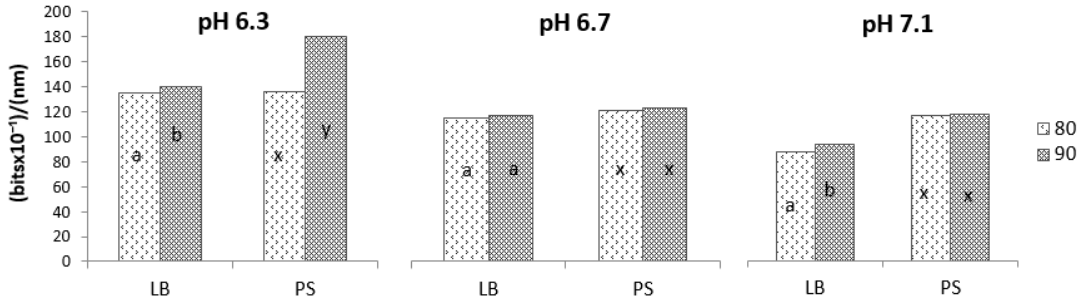

Figure 5.4. Influence of temperature on parameters measured as a function of milk pH, adjusted parameters according to unit values on y-axis. LSM values with same letters were not significantly different $p<0.05$; LB, light backscatter intensity at 570 nm; PS, particle size diameter; number of replications 3; number of observations, N=6.

In general, trends for the light backscatter technique and particle size show many similarities, except at pH 7.1 in which we see a significant positive correlation with temperature in the case of light backscatter ($r = 0.86$, $P<0.05$; Table 5.3) and no significance in particle size ($r = 0.21$, $P\geq0.05$; Table 5.3).

Table 5.3. Pearson Correlation between independent variable (pH) and dependent variables (light backscatter and particle size).

pH		LB	PS
6.3	PS	0.874*	
	T	0.857*	0.984*
6.7	PS	0.150ns	
	T	0.310ns	0.553ns
7.1	PS	0.451ns	
	T	0.862*	0.241ns

T, temperature; LB, light backscatter intensity at 570 nm; PS, particle size diameter; * P<0.05, **P<0.01, ***P<0.001, ns not significant; N=6.

This may be a result of the potential to detect the formation of large whey protein aggregates in the light backscatter spectra. On the other hand, aggregate formation may not contribute to a noticeable change in the mean particle size distribution. As particle size is a mean adjusted value, weighted according to size and frequency, values are highly based on the casein micelle and therefore it is reasonable to assume that binding would be the main contributor to alterations in the mean particle size. Supplementary support to this idea is the positive correlation of light backscatter and particle size; present only in the case of pH 6.3 (Table 5.3). These variations further demonstrate the idea that different mechanisms are involved in the measurement of particle size and light backscatter response. From our observation of a correlation between light backscatter and particle size measurements (Table 5.2), we suggest that our light backscatter sensor may be useful as a simple and inexpensive alternative to more expensive methods of particle size measurement.

5.4 Conclusions

This work utilizes an inexpensive/simple optical light backscatter system to detect changes in casein micelle size with respect to generally-accepted trends of whey protein denaturation. As previously suggested by Lamb et al. (2013), our study implies that changes in light backscatter signal are primarily based on the pH-dependent attachment of denatured whey proteins to the surface of the casein micelle. As a result, sensor development is considerably more complex among a range of milk pHs such that pH should be regarded as a necessary variable for future modelling purposes. Thus the pH dependent formations of whey protein serum aggregates and casein/whey protein complexes should be taken into consideration for the potential inline use of this technology as a tool for the determination of whey protein denaturation during milk heat treatment.

CHAPTER 6: Analysis of the preferential mechanisms of denaturation of whey protein variants as a function of temperature and pH for the development of an optical sensor

6.1 Introduction

The major whey proteins, *β*-lactoglobulin (*β*-LG) and *a*-lactalbumin (*a*-LA), have varying degrees of heat-stability with respect to their tendency to denature and potentially react with other components in the milk matrix. A fundamental difference, which is a critical consideration for heat-induced denaturation and subsequent interactions, is that *β*-LG contains one free sulfhydryl group whereas *a*-LA is absent of a free sulfhydryl. In addition, the genetic variants of *β*-LG, the most abundant being *β*-LG A and *β*-LG B, are distinct in that they differ by two amino acid substitutions, which consequently alter their susceptibility to heat induced denaturation and reactivity (Bello et al., 2011). In general, *β*-LG is less heat stable than *a*-LA, however neither denatures to a significant extent below 70°C (Anema, 2008b). In addition, *a*-LA has a greater potential to unfold and refold back into its native state (Rüegg et al., 1977). Law and Leaver (2000) have observed an increase in thermal denaturation of *a*-LA upon adding 2-mercaptoethanol (ME), a chemical reducing agent, which may have acted to prevent the reformation of intramolecular disulfide bonding. Therefore the ability of *a*-LA to refold may be a contributing factor to the observation of a less extent of denaturation in *a*-LA than *β*-LG, which is more reactive and tends to form covalent bonds once in an unfolded state (Walstra et al., 2005). Still, *a*-LA generally does not refold once it has been denatured to the point of exposing reactive sulfide groups, instead tending toward the potential for protein-protein interactions (Rüegg et al., 1977). As a consequence of its greater facility to denature and react, denatured *β*-LG tends to incorporate into the micellar portion of the milk matrix before and to a greater extent than *a*-LA (Noh & Richardson, 1989).

Heat stability of milk proteins are significantly affected by pH, in which a maximum in stability occurs around pH 6.7 and a minimum at pH 6.9 (Singh, 2004). In a series of studies, the said relationship between whey protein interactions and their associations with

casein micelles regarding pH dependence was supported, in which low pH (~6.3) denatured whey proteins tend to form associations with the casein micelle and high pH (~7.1) denatured whey proteins have a preference to form soluble aggregates in the serum (Anema and Li, 2003a, b; Anema et. al, 2004; Anema 2007). Using reconstituted skim milk at pH 6.5 and 7.1 heated at 90°C for 20-30 min, it was exhibited that at pH 6.5 ~85% of denatured whey proteins were associated with the casein micelle and at pH 7.1 only ~15% were associated (Anema 2007). In a similar study, Kethireddipalli et al. (2010) heat treated milk at pH 6.3, 6.7, and 7.1 at 90°C for 10 min and found percentages of bound proteins to be 82.2%, 30.0%, and 0.0-5.0%, respectively. Consequently, it has also been found that as a result of the association of denatured whey proteins with casein micelle, the size of casein micelles tends to increase in size upon heat treatment (Anema and Li 2003a, b). As casein micelles are known to scatter light in the spectral range of 200-1100 nm (Lamb et al., 2013), optical light backscatter measurements have been developed in order to model the extent of whey protein denaturation in milk during heat treatments. This methodology uses the assumption that denatured whey proteins attach to the casein micelle, resulting in a change in the size of the casein micelle (Lamb et al., 2013). Even though it has been exhibited that attachment is highly related to milk pH, and as well, particle size and light backscatter response exhibit significant relationships with pH, no correlations have been developed so far in relation to the three forms of whey proteins in milk after heat treatment: bound (BWP), soluble aggregates (AWP), and native (NWP). Thus, it is of interest to further investigate this relationship between optical light backscatter measurements and casein particle size as a result of the attachment of denatured whey proteins to the micelle and the formation of soluble aggregates, with the potential for the development of an optical sensor.

6.2 Materials and Methods

Analysis techniques of the study correspond to the data set presented by Taterka & Castillo (2015), where in-depth details of the materials and methods can be found. Here a brief description of the experimental methodology is provided. The experiment consisted of a 3x2 factorial design with pH values of 6.3, 6.7 and 7.1 and two heat treatment temperatures: 80 and 90°C and each treatment was replicated three times (N = 3·3·2). The heat treatment time was constant for all measurements at 10 min with samples first equilibrated to a consistent room temperature of 21°C. The milk used was standard skimmed milk powder of excellent functional and microbiological quality (low-heat, spray-dried skim milk powder; pH

= 6.5, solubility = 99%, WPNI ≥ 7 mg g^{-1}, 800 cfu g^{-1}) supplied by Chr. Hansen SL (Barcelona, Spain). Milk was reconstituted to a final solids content of 12% (*w*/*w*) and pH adjusted at 21°C to 6.3, 6.7, and 7.1 using 0.5M HCl or 0.5M NaOH. Light backscatter and casein particle size z-average were monitored as described by Taterka & Castillo (2015). Native whey proteins were fractionated using an acid-whey technique described in Taterka & Castillo (2015), whereas a centrifugal separation technique (Section 4.6.2) was used to isolate other whey protein fractions. Protein concentration in the acid-whey and centrifuge whey protein was determined by HPLC according to IDF Standard 178:1996. Calculation of bound and aggregate portions is summarized in Section 4.8. Data was analyzed by CORR, ANOVA, GLM and LSM using "Statistical Analysis System" (SAS, version 9.2, SAS Institute Inc., Cary, NC, USA, 2013).

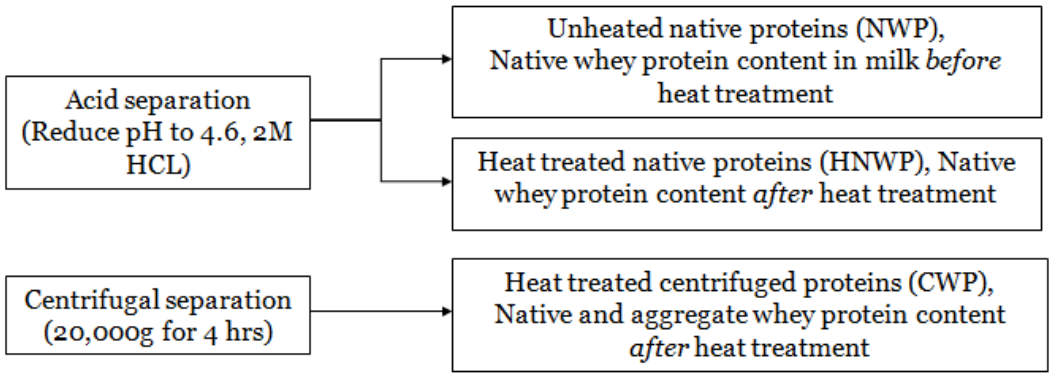

Figure 6.1. Whey protein separation scheme used in this study.

6.3 Results and Discussion

6.3.1 Bound, aggregate and native whey protein distribution with respect to heat treatment temperature and pH

The technique used for quantification of whey protein aggregates (Section 4.8) results in a separation of heat-treated milk colloidal portions by high relative centrifugal force (RCF) with the remaining serum portion containing native whey proteins and soluble protein aggregates (Figure 6.1). Similar studies measured whey protein configurations (native, bound, and aggregate) in milk after heat treatment using an ultracentrifuge technique (with variable speed/time combinations) (Anema & Li, 2003a; Anema et al., 2004). As well, Vasbinder and de Kruif (2003) utilized a technique involving the rennet induced fractionation which yielded results comparable to the ultracentrifuge techniques of other studies. Our method was adapted from (Anema & Li, 2003a) using Eqn. (1) allowing for the adjustment of RCF using revolutions per minute (RPM)/time combinations in order to implement a similar net centrifugal force (D'Allemand, 1994).

Table 6.1 displays some of the general trends observed by various authors which have investigated the attachment of whey proteins to the surface of the casein micelle as a function of pH and temperature of heat treatment. In all cases, authors observed that an increase in temperature of heat treatment resulted in an increase in attachment, however in the case of lower milk pH (6.3-6.55) the increase is more marked than in milk at higher pH (6.8-7.1). Anema et al. (2004) presented a study using high temperature (100, 90 and 80°C) and time (30 min) heat treatment. Assuming intense treatment at 100°C for 30 min would denature all available whey proteins, the maximum amount of whey proteins bound at pH 6.9 was only 35% however at pH 6.5 binding was more prevalent with 85% of whey proteins adhered to the surface of the casein micelle.

Table 6.1. Percent bound denatured whey proteins after 10 min heating.

Temperature	pH	% attached total WP	% attached *α*-LA	% attached *β*-LG	ref
80 °C	6.35		30	78	2
	6.45		28	65	2
	6.55		5	20	4
	6.55	18			5
	6.55		25	55	2
	6.7	25			5
	6.7		20	50	3
	6.7		18	45	2
	6.9		13	28	2
90 °C	6.3	82			6
	6.48		55	95	1
	6.55		30	55	4
	6.55	18			5
	6.6		63	80	1
	6.7	50			5
	6.7		45	63	3
	6.7	30			6
	6.83		20	60	1
	7.1	5			6

1, Oldfield et al. (2000); 2, Vasbinder and Kruif (2003a); 3, Vasbinder and Kruif (2003b); 4, Anema and Li (2003a); 5, Anema and Li (2003b); 6, Kethireddipalli et al. (2010).

Using Eqns. (4.2) and (4.3), aggregate and bound proteins were calculated from acid separated whey and ultracentrifuged samples. There was a clear temperature effect, in that an increase in the heat treatment temperature from 80 to 90°C resulted in a clear increase in the percentage bound (46 and 51%, respectively) and aggregate formations (12 and 22%, respectively) (Figure 6.2). It was observed that 93% denatured whey proteins attached to the casein micelle at pH 6.3, 81% at pH 6.7 and 46% at pH 7.1 after 10 min of heating (Figure 4). Our results are in line with values for binding reported by other authors within the conditions of our study in that up to 82% total whey protein binding occurred at pH 6.3, 30-50% at pH 6.7 and 0-5% at pH 7.1 (Table 6.1). In contrast, there is a greater probability for denatured whey proteins to form soluble whey protein aggregates at higher milk pH (Donato & Guyomarc'h, 2009; Singh, 2004; Vasbinder & de Kruif, 2003; Vasbinder et al., 2003). Our study observed a minimal formation (7%) of whey protein aggregates at low pH (6.3), whereas at higher milk pH (7.1) the level of soluble aggregate formation was much greater (54%) (Figure 6.2). When binding is not the favored mode, denatured whey proteins may instead aggregate with each other in the serum portion.

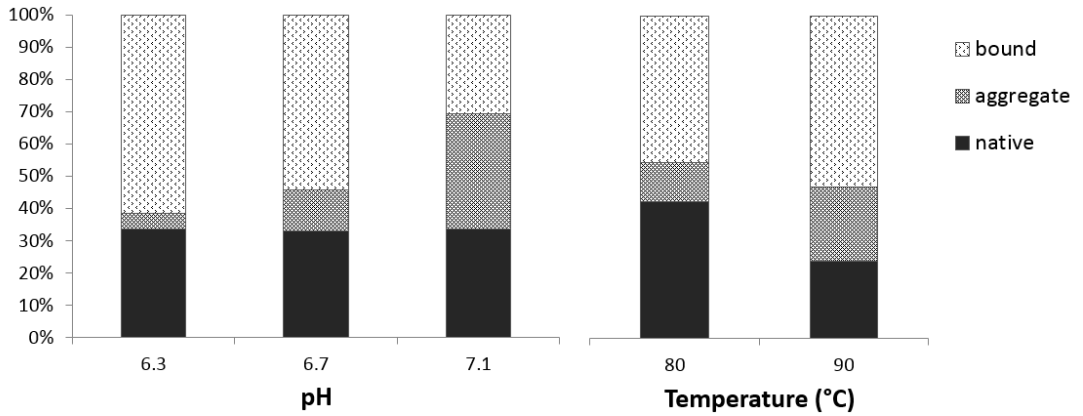

Figure 6.2. Bound, aggregate, and native whey protein content separated by pH and temperature of heat treatment.

Observations to support the potential implementation of a light backscatter sensor were reported by both Lamb et al. (2013), which observed a negative correlation between the light backscatter signal and native *β*-LG and Taterka and Castillo (2015) which found a correlation between the light backscatter signal and changes in particle size with respect to milk at various pH levels. However, the relationship found by Lamb et al. (2013) did not take into account that the mechanism of attachment is highly dependent on pH, whereas the results of Taterka and Castillo (2015) did not look at soluble aggregate and bound whey protein content.

An ANOVA analysis was run in order to determine main sources of variation in the dependent variables (Table 6.2), aggregate whey protein content (AWP) and bound whey protein content (BWP). The sources of variation tested were pH, temperature (T) and the interaction of pH and temperature (pH x T). The effect of replications is not shown in Table 6.2, as there was no significance in this variable. Results presented are supplementary, and in some cases will be compared to light backscatter maximum intensity (at ~570 nm), particle size mean radium (Z-value) by dynamic light scattering and native whey protein content (NWP) results reported in Taterka and Castillo (2015). Significance was observed in the case of light backscatter and particle size with respect to pH and temperature whereas native whey protein content showed significance only with temperature, as pH does not affect whey protein denaturation to a large degree in the pH range of this study (Table 5.1). Aggregate whey protein content did not show significance with any variables, it was observed that

bound whey protein content is significant with pH, thus supporting the idea that micellar binding is related to milk pH.

Table 6.2. Analysis of variance and *F* statistic for dependent variables[a]

			Variation source		
	Model		pH (2DF)	T (1DF)	pHxT (2DF)
	R^2	F	F	F	F
AWP	0.568	1.50ns	2.77ns	0.89ns	0.49ns
BWP	0.791	4.33*	6.95*	0.4ns	3.58ns

T, temperature; R^2, determination coefficient; F, ANOVA F-statistic; DF, degrees of freedom; *P<0.05, **P<0.01, ***P<0.001, ns not significant; N = 18.

In order to characterize the potential of the light backscatter sensor to measure whey protein denaturation, we looked at correlations with bound and aggregate protein content (Table 6.3). Bound whey protein content exhibited a strong negative, significant correlation with pH, which is likely related to the large shift in particle size (Figure 6.3A) and light backscatter intensity (Figure 6.3B). On the other hand, soluble aggregate formation exhibited a positive and significant correlation with pH, the opposite of bound whey, as these two relationships are complimentary. As expected, we observed a significant and positive correlation between bound whey protein and both light backscatter and particle size (Table 6.3), which we attribute to the attachment of denatured whey proteins to the surface of the casein micelle causing an increase in particle size (Figure 6.3A, 6.3C) and intensity of light scatter (Figure 3B, 3D). In the case of whey protein aggregates, we saw a negative, significant correlation with light backscatter, however no correlation with particle size. This can be explained by the observation that light backscatter intensity is affected to a greater extent from binding than from the formation of soluble aggregates. Therefore, the formation of more aggregates at pH 7.1 is likely to correspond to a significantly lower light scatter response (Figure 6.3B) as the potential increase in LB due to aggregates formation is extensively compensated by the decrease of LB due to the smaller presence of bound whey proteins. The wavelength used for this analysis (570 nm) corresponds to the maximum intensity, and it should be noted that from preliminary analysis a lower wavelength (~270-350 nm) was found to better correspond with the formation of aggregates. Thus, as total whey protein denaturation can be calculated as a sum of the whey proteins that have attached to the casein

micelle and aggregates which remain in the serum, the wavelength chosen for this analysis better corresponds to bound formations and may be missing the entire scope.

Table 6.3. Pearson Correlation between native-, aggregate-, and bound whey protein content with independent and dependent variables.

	LB	PS	T	pH
AWP	-0.60*	-0.37ns	0.25ns	0.58**
BWP	0.70**	0.60*	0.05ns	-0.69**

T, temperature; LB, light backscatter intensity at 570 nm; PS, particle size radius; AWP, aggregate whey protein content; BWP, bound protein content; * P<0.05, **P<0.01, ***P<0.001, ns not significant.

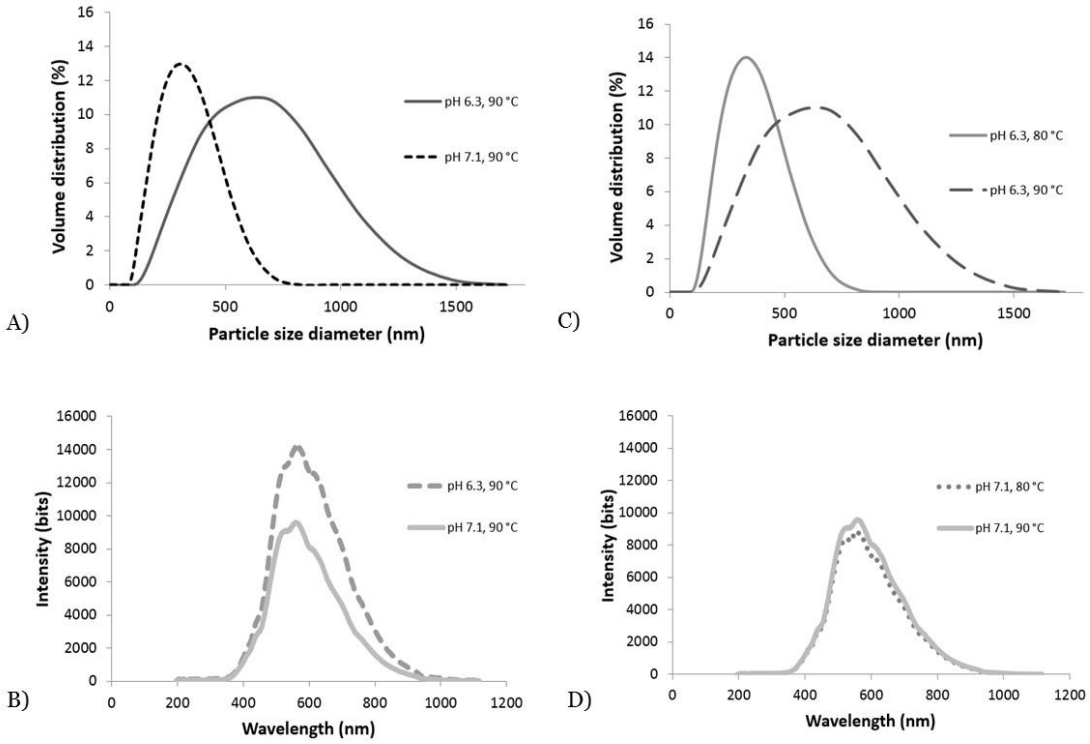

Figure 6.3**.** The effect of pH on A) Particle size distribution B) Light backscatter intensity and the effect of heat treatment temperature on C) Particle size volume distribution D) Light backscatter intensity.

6.3.2 Bound, aggregate and native whey protein content by protein type and variant as a function of temperature and pH

It was also of interest to calculate the estimated bound and aggregate content of each major whey protein, *a*-LA and *β*-LG and its variants (*β*-LG A and *β*-LG B). Protein content (mg mL^{-1}) of the acid separated and centrifuged samples was quantified by HPLC and bound and aggregate content were calculated using Eqns. (6.2) and (6.3). Changes with respect to pH and temperature of heat treatment were summarized to study the preference of the whey protein variants for binding and/or soluble aggregate formation (Figure 6.4, 6.5). Both bound *a*-LA and *β*-LG content decreased with increasing milk pH [pH 6.3, 6.7, 7.1 (*a*-LA: 0.11, 0.10, 0.06; *β*-LG B: 0.96, 0.86, 0.42; *β*-LG A: 0.50, 0.40, 0.26) mg mL^{-1}, respectively] (Figure 6.5A), as binding is the preferential mode at pH 6.3 and this tendency decreases with increasing pH. On the other hand, soluble aggregate content increased with increasing milk pH [pH 6.3, 6.7, 7.1 (*a*-LA: 0.005, 0.02, 0.13; *β*-LG B: 0.04, 0.14, 0.50; *β*-LG A: 0.08, 0.16, 0.23) mg mL^{-1}, respectively] (Figure 6.4A). This trend was also reported by Oldfield et al. (2000) where pH 6.48 milk heated at 90°C for 10 min demonstrated 55 and 95% attached *a*-LA and *β*-LG, respectively, compared to pH 6.83 milk which exhibited an attachment of 20 and 60%. Interestingly, in our study, the percentage of bound whey protein variants at each respective pH remains relatively constant [pH 6.3, 6.7, 7.1 (*a*-LA: 7, 7, 8%; *β*-LG B: 61, 63, 58%; *β*-LG A: 32, 30, 35%) mg mL^{-1}, respectively] (Figure 6.4B), whereas the percentage of soluble aggregate variants increased in the case of *a*-LA and *β*-LG B and decreased in *β*-LG A with increasing pH [pH 6.3, 6.7, 7.1 (*a*-LA: 4, 6, 15%; *β*-LG B: 29, 44, 58%; *β*-LG A: 67, 50, 27%) mg mL^{-1}, respectively] (Figure 6.5B).

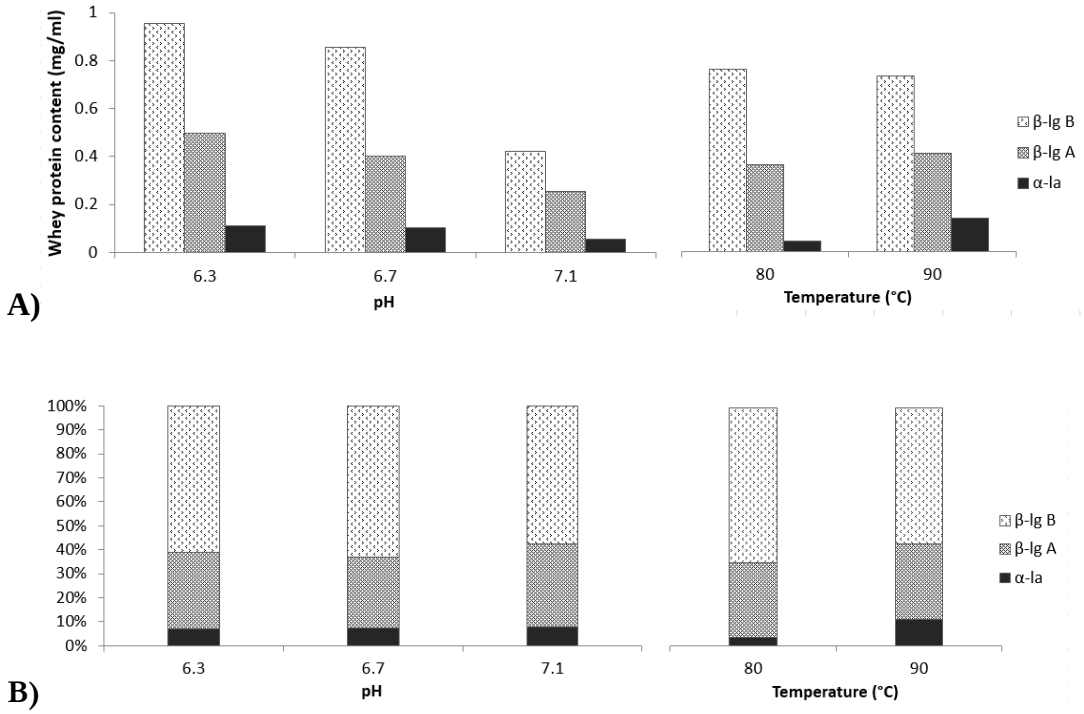

Figure 6.4. Bound content by whey protein variant separated by pH and temperature (A) whey protein variant content (B) whey protein variant percent.

Our work shows the prevalence of whey protein types in the bound portion as *β*-LG B > *β*-LG A > *α*-LA, independent of pH and temperature (Figure 6.4A). Assuming that attachment is based on a similar mechanism for all variants of whey proteins [i.e., disulfide bridge and hydrophobic interactions (Jean et al., 2006; Oldfield et al., 1998)], the distribution of whey proteins found in the bound portion should follow the heat stability and reactivity of each respective protein and protein variant. In our study whey proteins with a greater frequency to unfold and react are found in the largest proportion of the bound portion. It has been observed that the B variant of *β*-LG denatures to a greater extent than *β*-LG A (Anema & McKenna, 1996). Furthermore, it has been suggested that the amino acid substitution Ala/Val118 of the B variant causes a cavity from the loss of two methyl groups which increases access to the sulfide group of Cys121, resulting in a greater reactivity of the B variant compared to the A variant (de la Fuente et al., 2002; Qin et al., 1999). In the case of rennet gel formation (Meza-Nieto et al., 2013, 2007) variant B was found to be predominant in the internal structure of the gel made from pasteurized milk. This may infer that *β*-LG B is involved in colloidal interactions to a greater extent than the A variant of *β*-LG. Alternatively, the lower E_a and ΔH values of *β*-LG A are related to a preference for

aggregation (Anema & McKenna, 1996). As a result, it may be possible that *β*-LG B promotes attachment (Figure 6.4A), and *β*-LG A has greater tendency to form aggregates (Figure 6.5A).

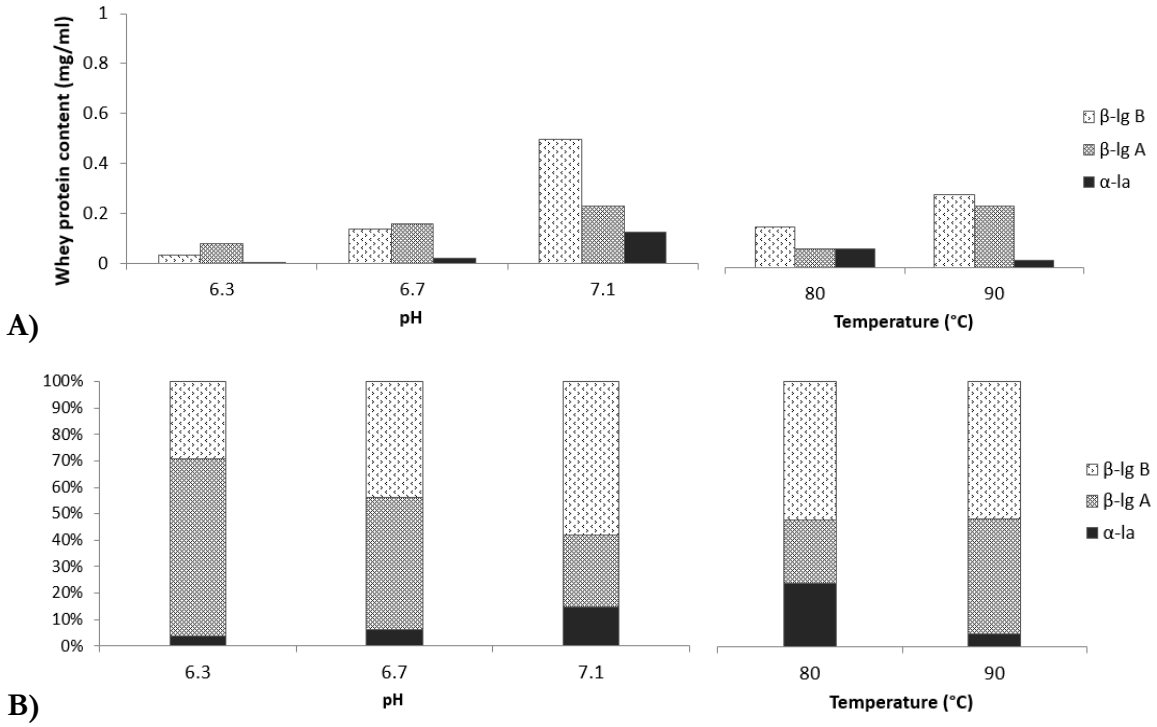

Figure 6.5. Aggregate content by whey protein variant separated by pH and temperature (A) whey protein variant content (B) whey protein variant percent.

The pH dependence of the formation of soluble aggregates observed in our study at pH 6.3 and 6.7 (Figure 6.5A) is as follows: *β*-LG A > *β*-LG B > *a*-LA, whereas at pH 7.1 the order of prevalence is *β*-LG B > *β*-LG A > *a*-LA. In agreement with our results, it has been observed that *β*-LG forms more soluble serum aggregates (Vasbinder & de Kruif, 2003) than *a*-LA. In milk at pH 6.35 heated for 10 min at 80°C only 5 and 2% of *a*-LA and *β*-LG were found as soluble whey protein aggregates, respectively, whereas in the same treatment conditions using milk at pH 6.9, 30 and 45% of *a*-LA and *β*-LG were found as soluble aggregates (Vasbinder & de Kruif, 2003). Since at pH 7.1 denatured whey proteins exhibit a greater preference for the formation of aggregates; the larger quantity of denatured *β*-LG B, as compared to variant A (which is less heat sensitive as mentioned before), might be the cause of the change in the dominant mechanism of *β*-LG B in samples at pH 7.1. Moreover,

Bello et al. (2011) has suggested that variant A has a greater tendency to form aggregates (self-association and κ-CN complex formation), however variant B was found to be involved to a greater extent in the formation of large protein aggregates (Manderson, Hardman, & Creamer, 1998). Notable observations of our study are in accordance with this notion as β-LG A was found as the abundant whey protein involved in aggregation in the serum portion at pH 6.3 and 6.7 (Figure 6.5A). On the other hand the formation of large aggregates is preferential at pH 7.1 and in these samples β-LG B was found in greater abundance in the serum aggregate portion (Figure 6.5A). Conversely, in the case of a study done by Bauer et al. (2000) it was observed that the B variant resulted in a characteristic formation of tetramers, whereas on the other hand the A variant lead to the formation of pentamers. Still, it has been established that more non-covalent bonding is involved in the formation of β-LG A aggregates than β-LG B aggregates, which may have an effect on the reversibility of these linkages; (Manderson et al., 1998; Schokker, Singh, & Creamer, 2000) furthermore promoting the potential for larger complexes in β-LG B aggregates compared to β-LG A.

Since we have observed that the ratio of the three whey protein variants in the bound portion does not change (Figure 6.4B), this may suggest that attachment is less a result of the pH-influenced ionic and structural changes on the whey protein environment, and instead due to an alteration in the preference for κ-CN to act as a nucleation site for the formation and/or reattachment of the complex to the casein micelle surface. The dissociation of κ-CN into the serum portion has been found to play a role in the preferential formation of micellar complexes or soluble serum aggregates. It has been observed that at pH 6.5 only 10% of κ-CN dissociates into the serum, whereas at pH 7.1 around 70% κ-CN was found in the serum phase (Anema, 2007). Thus, the preferential formation of soluble aggregates at pH 7.1 has been attributed to the idea that κ-CN in solution has a higher diffusion rate and therefore a higher number of potential collisions with denatured whey proteins (Anema, 2008a; Anema, 2007; Donato et al., 2007). For instance, it has been suggested that β-LG availability is the limiting factor in the attachment mechanism (Donato & Guyomarc'h, 2009; Guyomarc'h et al., 2003), however the amount of bound β-LG remains relatively constant with an increase in temperature treatment. Additionally, we see that with an 80 °C, 10 min heat treatment most denatured β-LG attached to the casein micelle, however at 90 °C we see a 2% total increase in bound β-LG and a 125% increase in aggregate β-LG. Thus, further heat-induced denaturation of β-LG appears to promote the formation of soluble whey protein aggregates, instead of the formation of whey protein/κ-CN complexes. Another observation is that the

formation of aggregate *β*-LG increases with temperature (Figure 6A), whereas bound *β*-LG content remains hardly unchanged (Figure 6.4A). If the relatively unchanged amount of bound *β*-LG content from 80 to 90°C (Figure 6.4A) is due to the fact that all *β*-LG was already completely denatured at 80°C, we would not observe a change in aggregate content with increased heat treatment temperature (Figure 6.5A).

Trends and correlations statistics were analyzed in order to observe potential relationships with respect to the various protein variant types in a bound or soluble aggregate state, with respect to light scatter techniques (Table 6.4). Both bound *β*-LG A and B exhibited a positive correlation with light backscatter and a negative correlation with pH. This falls in line with the generally accepted idea that binding occurs primarily between *β*-LG and *κ*-CN (Anema, 2008a; Anema, 2007; Guyomarc'h et al., 2003). As well, Lamb et al. (2013) observed a correlation between the light backscatter signal and *β*-LG denaturation, which was attributed to micellar binding. Alternatively, *α*-LA aggregates display a negative correlation with respect to light backscatter and a positive correlation with pH. It is likely that the negative correlation with light backscatter is a result of the large alteration in light backscatter signal with binding, whereas an increase in soluble aggregation formation would result in significantly less light scatter. As well, this relationship could be explained if we assume that soluble aggregates do not play a significant role in the light backscatter response, until reaching the point where very large aggregates are formed. Since the mechanism of binding and soluble aggregate formation is highly dependent on pH, these correlations are alike, however opposite, in the case of pH (Table 6.3).

Table 6.4. Pearson correlation between *α*-LA-, *β*-LG B-, and *β*-LG A aggregate and bound whey protein content with independent and dependent variables.

	LB	PS	T	pH
α-LA, AWP	-0.71**	-0.37ns	-0.34ns	0.64**
β-LG B, AWP	-0.50ns	-0.30ns	0.17ns	0.47ns
β- LG A, AWP	-0.39ns	-0.30ns	0.53*	0.44ns
α- LA, BWP	0.32ns	0.30ns	0.67**	-0.26ns
β- LG B, BWP	0.65**	0.49ns	-0.09ns	-0.65**
β- LG A, BWP	0.62*	0.58**	0.06ns	-0.61*

T, temperature; LB, light backscatter intensity at 570 nm; PS, particle size radius; AWP, aggregate whey protein content; BWP, bound protein content; * P<0.05, **P<0.01, ***P<0.001, ns not significant.

6.4 Conclusions

Our study investigated the previous hypothesis of Lamb et al. (2013) and Taterka and Castillo (2015) that suggested the increase in light backscatter response with heat treatment is a result of the pH-dependent binding of denatured whey proteins to the casein micelle surface. In line with our hypothesis, we observed that the light backscatter response exhibited correlations with bound whey protein (Table 6.3), however did not show any correlation with whey protein denaturation. We attributed this to the fact that the binding mechanism is highly dependent on pH, whereas there is no significant differences in whey protein denaturation in the pH range of our study (Oldfield et al., 1998, Figure 6.4). Additionally, we investigated trends for whey protein variant denaturation, binding and soluble aggregate formation. From our observations, it is probable that β-LG variant A has a greater potential to form soluble aggregates, whereas β-LG B is more involved in binding (except at pH 7.1 in which there may be a preference toward the formation of soluble aggregates). The mechanism of β-LG /κ-CN binding is not well understood, however it has been suggested that limiting factor of binding is the amount of available β-LG (Donato & Guyomarc'h, 2009; Guyomarc'h et al., 2003). On the contrary, our study showed that an increase in heat treatment temperature did not greatly affect the amount of bound β-LG, however β-LG continued to form soluble aggregates with increased temperature treatment. Thus, it is likely that an alteration in the ability for κ-CN to act as a binding site is instead responsible for the change in the preference for binding. This investigation formed useful correlations between the light scatter methodology and the mechanism of binding and/or aggregation providing essential information toward the development of an optical sensor for the determination of denatured whey proteins in heat treated milk.

CHAPTER 7: Prediction models of casein micelle particle size as a function of light backscatter intensity at different milk pH and heat treatment temperatures

7.1 Introduction

In-line monitoring of liquid milk products has potential for implementation in the dairy industry for process control and time and cost savings. To that end, the monitoring of various milk product manufacturing steps such as changes during the cheese making process (Castillo, Payne, & Lopez, 2005; Fagan et al., 2007) and determination of milk gelation mechanisms (Castillo, Payne, Wang, & Lucey, 2006) has been investigated using light scatter techniques. On the other hand, near infrared (NIR) spectroscopy has been widely used in milk to determine absorption in the infrared region (780- 2500 nm) of bonds and chemical groups to quantify various milk components (García Olmo, 2004). Robert et al. (1987) was able to establish specific wavelengths corresponding to changes in fat, protein and lactose content in milk, however noted that some interference was observed as a result of large water absorption and light scattering of fat particles. As well, it was observed by Diaz-Carrillo et al. (1993) that NIR spectroscopy could be used to successfully quantify protein, fat and total casein in goat´s milk. NIR spectroscopy has also been used to develop prediction equations for the determination of a number of milk attributes. For example, for the differentiation of different heat treatments in milk (Downey, Robert, Bertrand, & Kelly, 1990), detection of adulteration by the addition of whey powder to milk powders (Giangiacomo, Braga, & Galliena, 1991) or addition of NaCl and skim milk powder to milk (Pedretti, Bertrand, Semenou, Robert, & Giangiacomo, 1993). Sørensen and Jepsen (1997) used NIR spectroscopy to detect cheese defects as a result of *Clostridium tyrobutyricum*.

Development of prediction models has also been accomplished using both previously mentioned technologies, NIR and light scatter techniques, to predict cheese making characteristics. Castillo, Payne, Hicks, and Lopez (2000) used NIR light backscatter for developing simple prediction models using only optical parameters for the determination of cutting and clotting time. Light sidescatter and transmission were also used to estimate whey fat concentration, where sidescatter produced models with a higher R^2 (>0.95) than

corresponding transmission models (<0.5)(Castillo et al., 2005). Fagan, Castillo, O'Donnell, O'Callaghan, and Payne (2008) modeled cheese manufacturing indices such as whey fat, curd yield and curd moisture content using light backscatter sensor technology achieving R^2 values of 0.90 or more for the prediction models. In particular, their work was mainly aimed toward the determination of curd moisture content as a function of time in order to improve final moisture content during cheese making. Initial models were determined from a total of 40 parameters; however successful models utilized a combination of the parameters: temperature, percentage of protein, milk fat, and milk solids as well as milk fat protein ratio and light backscatter intensity ratios, which contain coagulation and syneresis information. Other studies have investigated whey protein denaturation and the subsequent attachment of whey proteins (WPs) to the surface of the casein micelle (Lamb, Payne, Xiong, and Castillo, 2013), however the strong pH effect of this mechanism has not been thoroughly investigated for optical sensor development.

We hypothesize that particle size may be used as an indirect measure of whey protein denaturation in heat treated milk. Particularly because the increase of particle size has been shown to be a good indicator of the extent of binding of denatured whey proteins to the surface of the casein micelle (Anema & Li, 2003a). However, this mechanism is affected to a large degree by milk pH such that a maximum in denaturated whey protein binding to the casein micelle has been found to occur at pH ~6.3, whereas the formation of soluble whey protein aggregates is the preferential mechanism at higher pH (max. at pH 7.1) (Donato & Guyomarc'h, 2009). Moreover, milk pH also affects the light backscatter signal as it has been exhibited that bound/soluble aggregate formation is highly dependent on pH and corresponds significantly to the intensity of light backscatter signal (Taterka & Castillo, 2015). Another important factor is the temperature of heat treatment, which significantly increases the amount of denatured whey protein, resulting in bound and/or soluble serum aggregates, depending on pH. Since the previous models obtained by Lamb et al. (2013) did not take into account the pH dependence of the binding reaction or the temperature x pH interaction, it is of interest to look further into modeling the light scatter signal with respect to the changes in particle size in heat treated milk, while taking into consideration the effect of milk pH in combination with temperature.

7.2 Materials and Methods

Data for this chapter is part of the experimental work of Experiment I, and no further analysis was completed, except in the case of statistical analysis and interpretation of data into graphical form. Single wavelength models (Section 7.3.1)(models 1-5) were developed using the PROC REG function in "Statistical Analysis System" (SAS, version 9.2, SAS Institute Inc., Cary, NC, USA, 2013). A more in-depth summary of models is described in Section 7.3.1. Models 6-10 utilized a technique of waveband ratios using a grouping of two wavebands portions of the spectra, determined by SAS code from Lamb et al. (2013). Wavebands were defined as 35 nm portions of the spectra, thus all grouping of waveband ratios yielded 27 distinct combinations. From our prior studies on the behavior of particle size, it has been considered that in a nonlinear regression model the response variable (particle size) is an exponential function as a function of pH (Taterka & Castillo, 2014). The NLIN function from SAS was used to form nonlinear regression models, assuming that the response variable follows an exponential model. From this, waveband ratios were developed with the objective of modeling the radius of the casein micelle versus pH and temperature. Supplementary information regarding wavelength ratios can be found in Section 7.3.2.1.

7.3 Results and Discussion

7.3.1 Single wavelength prediction models

A model for particle size as a function of light backscatter intensity at 570 nm (single wavelength model) was developed. Figure 7.1 shows the trends for both light backscatter at 570 nm and z-average particle size as a function of pH and temperature. Models were "separated" between heat treatment temperatures (80 and 90 °C), temperature "integrated" or temperature ¨combined¨. Temperature "integrated" models were developed as a function of temperature, whereas temperature combined used all data points but did not include temperature in the prediction equation. Two types of models were obtained: linear models with the form ($y = ax + b$) and quadratic models in the form ($y = ax^2 + bx + c$). As a first modeling approach, both light backscatter and particle size were modeled as a function of pH and/or T as follows:

$$LB = \beta_0 + \beta_1 pH \quad \text{(Eqn 7.1)}$$

$$LB = \beta_0 + \beta_1 pH + \beta_2 T \quad \text{(Eqn 7.2)}$$

$$PS = \beta_0 + \beta_1 pH + \beta_2 pH^2 \quad \text{(Eqn 7.3)}$$

$$PS = \beta_0 + \beta_1 pH + \beta_2 pH^2 + \beta_3 T \quad \text{(Eqn 7.4)}$$

where *LB* is the light backscatter intensity (bits) measured at the maximum intensity wavelength encountered within the wavelength range between 200 and 1100 nm (i.e., 570 nm), *PS* is the particle size z-average (nm), *T* is the heat treatment temperature (°C) and *β*0-3 are regression coefficients.

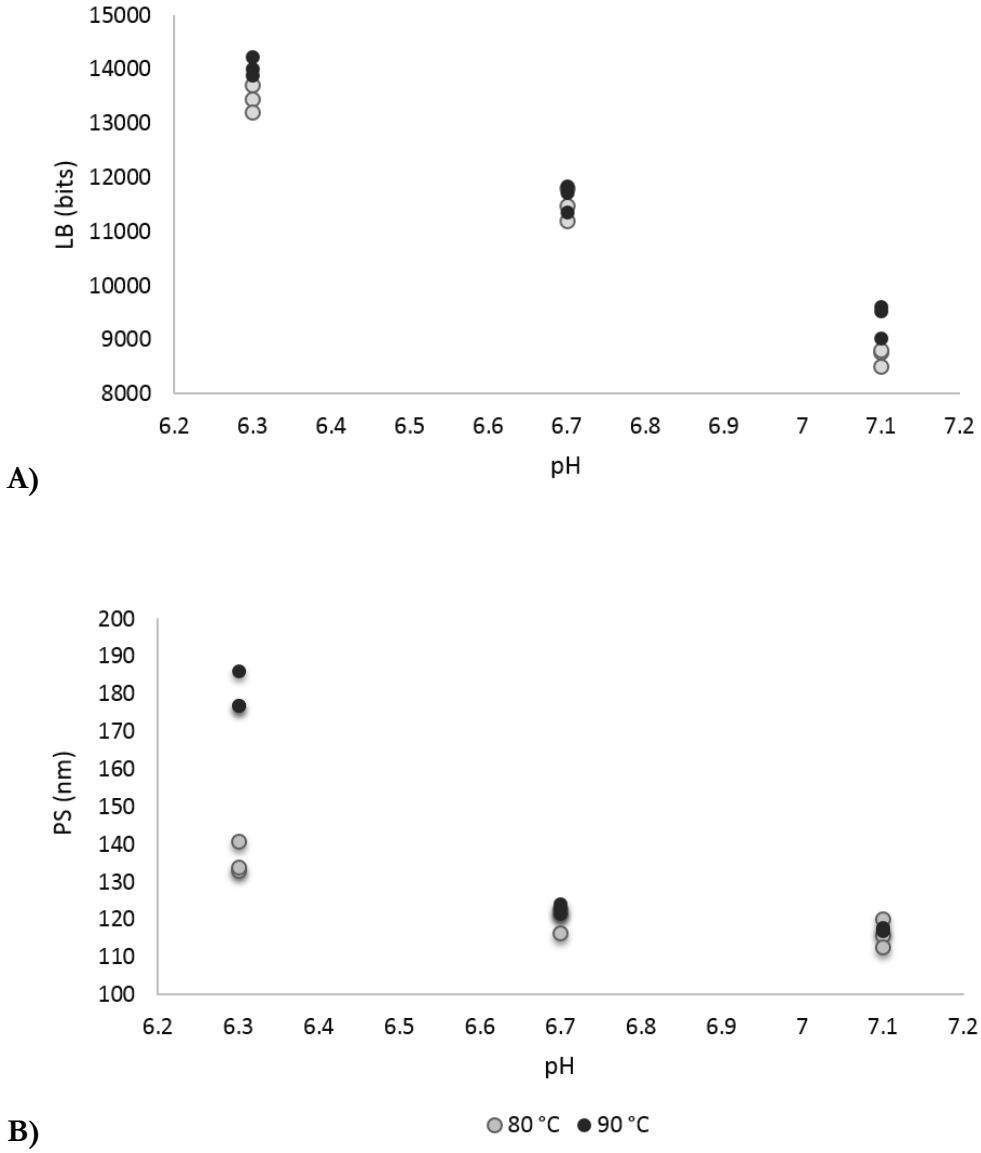

Figure 7.1. A) Light backscatter maximum intensity (LB) as a function of pH at 80 and 90 °C; B) Particle size z-average as a function of pH at 80 and 90 °C.

Light backscatter and particle size experimental data was fit to both linear and quadratic mathematical models to estimate regression coefficients and summary statistics using the PROC REG function in Statistical Analysis System (SAS version 9.2, SAS Institute Inc., Cary, NC, USA, 2013). In all cases, higher R^2 values were observed in quadratic models, however those models which did not show a large difference in R^2 between quadratic and linear models were simplified into the linear model form. Also, in some "integrated" models, temperature (*T*) was used for the model as the R^2 value increased markedly in some models

when including the *T* variable. Models in which the addition of *T* did not increase the R^2 value to a large extent were simplified into temperature combined models in order to maintain degrees of freedom (DF) for the model. Table 7.1 shows the various models that were developed and their summary statistics. Temperature "separated" models and temperature "integrated" models were developed to predict light backscatter maximum intensity as a function of pH and temperature (model 1 and 2) (Figure 7.2) and particle size z-average as a function of pH and temperature (model 3 and 4) (Table 7.1) (Figure 7.3). Model 1 utilizes a simple linear model using only pH as an independent variable, yet still results in high R^2 values for both 80 and 90 °C models (R^2 = 0.979 and 0.988, respectively) (Table 7.1) (Figure 7.2A). In the case of the temperature "integrated" model (model 2) (Figure 7.2B), all temperature data points were considered (DF=15) and a high R^2 value of 0.984 was obtained.

Table 7.1. Predictive models 1-4.

Model	Prediction equation	Temperature	DF err	Regression coefficient		s	SSE	R^2	SEP
1	$LB = \beta_0 + \beta_1 pH$	80 °C	7	β_0 =	-5.11· 10^4	2.19· 10^3	718974	0.979	320
				β_1 =	5.95 · 10^3	327			
		90 °C	7	β_0 =	-5.07· 10^4	1.61· 10^3	387167	0.988	235
				β_1 =	5.82· 10^3	240			
2	$LB = \beta_0 + \beta_1 pH + \beta_2 T$	Integrated	15	β_0 =	4.68· 10^4	1.71· 10^3	1114887	0.984	273
		(80 and 90 °C)		β_1 =	-5.88· 10^3	197			
				β_2 =	47.7	12.9			
3	$PS = \beta_0 + \beta_1 pH + \beta_2 pH^2$	80 °C	6	β_0 =	1.97· 10^3	760	88.4	0.881	3.8
				β_1 =	-526	227			
				β_2 =	37.4	17.0			
		90 °C	6	β_0 =	7.87· 10^3	630	60.6	0.992	3.2
				β_1 =	-2.23· 10^3	188			
				β_2 =	161	14.0			
4	$PS = \beta_0 + \beta_1 pH + \beta_2 pH^2 + \beta_3 T$	Integrated	14	β_0 =	4.78· 10^3	1.64· 10^3	1919	0.791	11.7
		(80 and 90 °C)		β_1 =	-1.38· 10^3	490			
				β_2 =	99.1	36.6			
				β_3 =	1.60	0.552			

N=18; DF err, degrees of freedom for error; $\beta_{0\text{-}3}$, prediction coefficients; s, standard error of the estimate for coefficients; SSE, sum of squares for error; R^2, determination coefficient; SEP, standard error of prediction for the model: LB (bits), PS (nm)

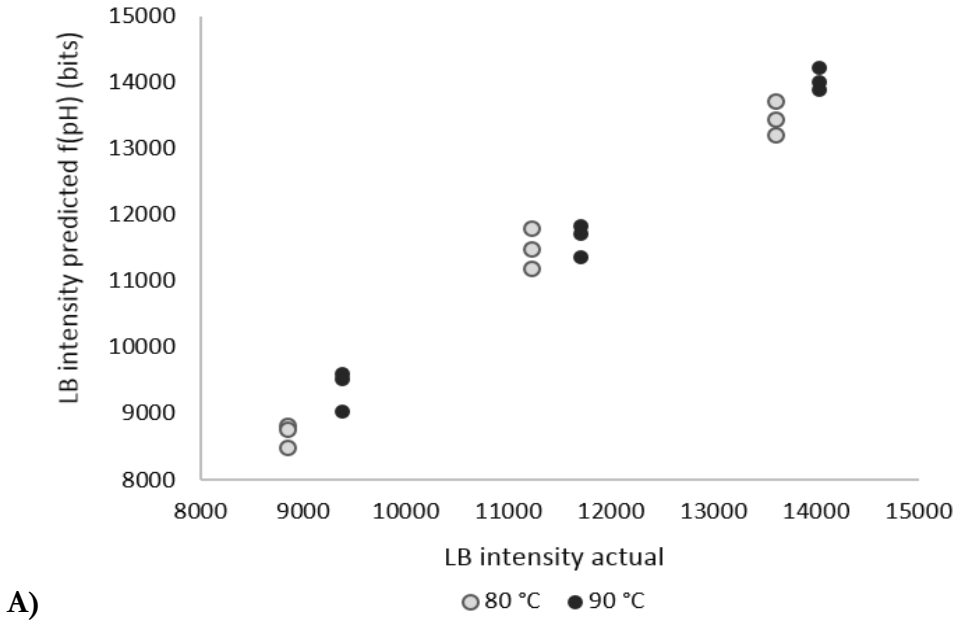

A)

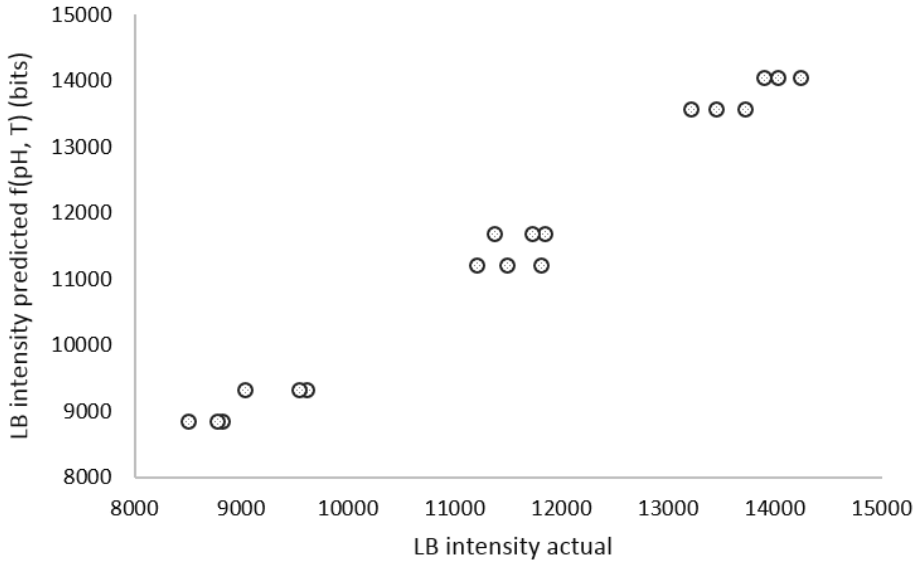

B)

Figure 7.2. A) Model 1: Light backscatter maximum intensity modeled as a function of pH at 80 and 90 °C; B) Model 2: Light backscatter maximum intensity modeled as a function of pH and temperature.

For the temperature "separated" models (model 3) (Figure 7.3A) R^2 values of 0.881 and 0.992 were obtained for 80 and 90 °C models, respectively, whereas the temperature

"integrated" model (model 4) (Figure 7.3B) had a slightly lower R^2 value of 0.791. In general, we can see that light backscatter showed a consistent linearly decreasing trend with pH (Figure 7.1A), whereas changes in particle size tended to show a more quadratic response as a function of pH, where 90 °C samples showed greater changes with pH than 80 °C samples (Figure 7.1B).

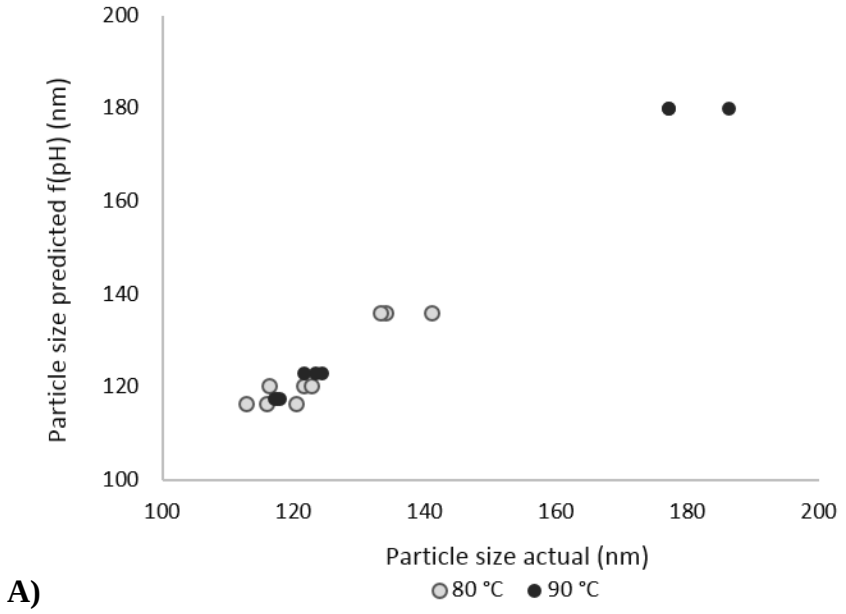

A)

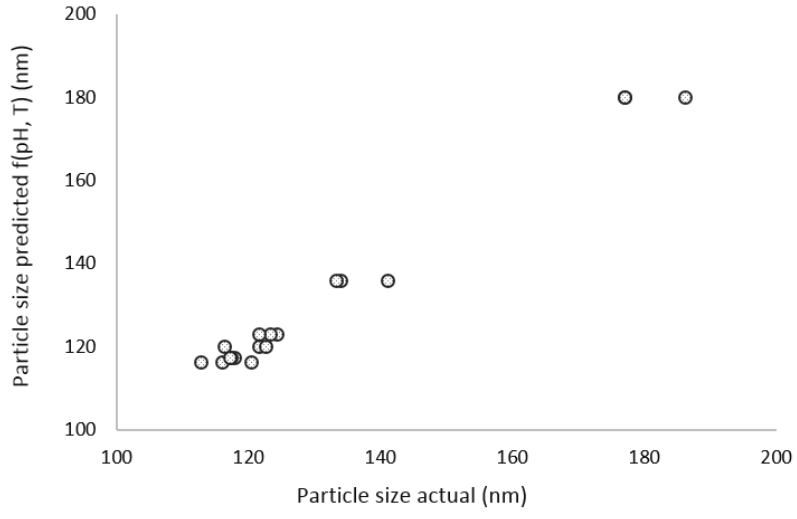

B)

Figure 7.3. A) Model 3: Particle size z-average modeled as a function of pH at 80 and 90 °C; B) Model 4: Particle size z-average modeled as a function of pH and temperature.

Trends for changes in particle size and light backscatter maximum intensity were investigated and prediction models were developed with high R^2 values as a function of milk pH (Models 1-4). As the technique to measure particle size can be time consuming and costly, the light backscatter method could be a good alternative to particle size measurements in milk as it is inexpensive and nondestructive, and can easily be implemented for in-line application. Initial work by Anema and Li (2003) presented a strong correlation of denatured whey proteins attached to the casein micelle and changes in particle size. As well, previous work in our group has shown good correlation between both the light backscatter maximum intensity (r = 0.77) (Taterka & Castillo, 2015) and bound whey protein (r = 0.70) (Taterka & Castillo, 2014) to changes in casein micelle particle size. A model of particle size as a function of light backscatter intensity would enable in-line monitorization of the extent of changes in denaturation in heat treated milk. Since in-line process control shows promise toward optimization of the manufacturing process of milk and milk products such as cheese and yogurt, a simple, non-invasive, quick and inexpensive technique providing real time information about the binding of denatured whey proteins to the casein micelle and/or soluble aggregate formation would be highly advantageous to the dairy industry. From our work, we were able to develop a relatively simple equation for the prediction of particle size as a function of the light backscatter maximum, as follows:

$$PS = \beta_0 + \beta_1 LB + \beta_2 LB^2 \qquad \text{(Eqn 7.5)}$$

Model 5 (Table 7.2) used a quadratic form, and yielded high R^2 values in the case of 80 and 90 °C models (R^2 = 0.847 and 0.992, respectively) (Figure 7.4A) and temperature "integrated" models (R^2 = 0.825) (Figure 7.4B). As it can be observed in Table 7.1 and 7.2, temperature separate models had higher R^2 and lower standard error of prediction (SEP) in nearly all models (except in the case of the temperature "integrated" Model 2, which has a higher R^2 and lower SEP value than Model 1 temperature separated at 80 °C). However, all temperature "integrated" models maintained an R^2 value higher than or equal to 0.791 and all 80 and 90 °C models with R^2 greater than 0.847 (Table 7.1, 7.2).

Table 7.2. Predictive model 5 using maximum LB intensity-570 nm.

Model	Prediction equation	Temperature	DF err	Regression	coefficient	s	SSE	R^2	SEP
5	$PS = \beta_0 + \beta_1 LB + \beta_2 LB^2$	80 °C	6	β_0 =	219	64.9	114	0.847	4.4
				β_1 =	-0.0221	0.0121			
				β_2 =	$1.18 \cdot 10^{-6}$	$5.47 \cdot 10^{-7}$			
		90 °C	6	β_0 =	572	52.4	58.5	0.992	3.1
				β_1 =	-0.0899	0.00914			
				β_2 =	$4.41 \cdot 10^{-6}$	$3.89 \cdot 10^{-7}$			
		Integrated	15	β_0 =	479	103	1599	0.825	10.3
		(80 and 90 °C)		β_1 =	-0.0725	0.0185			
				β_2 =	$3.59 \cdot 10^{-6}$	$8.14 \cdot 10^{-7}$			

N= 18; DF err, degrees of freedom for error; $\beta_{0\text{-}2}$, prediction coefficients; s, standard error of the estimate for coefficients; SSE, sum of squares for error; R^2, determination coefficient; SEP, standard error of prediction for the model (nm).

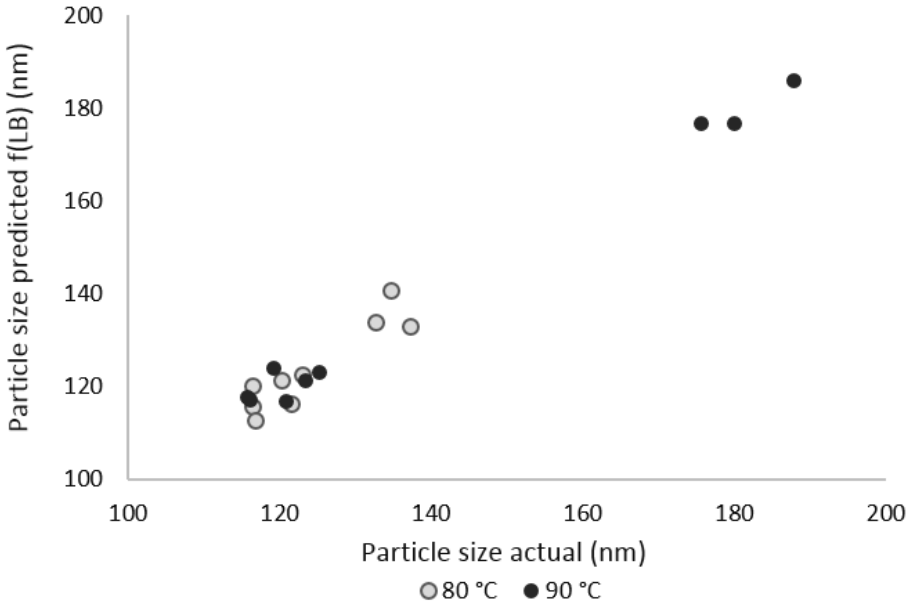

A)

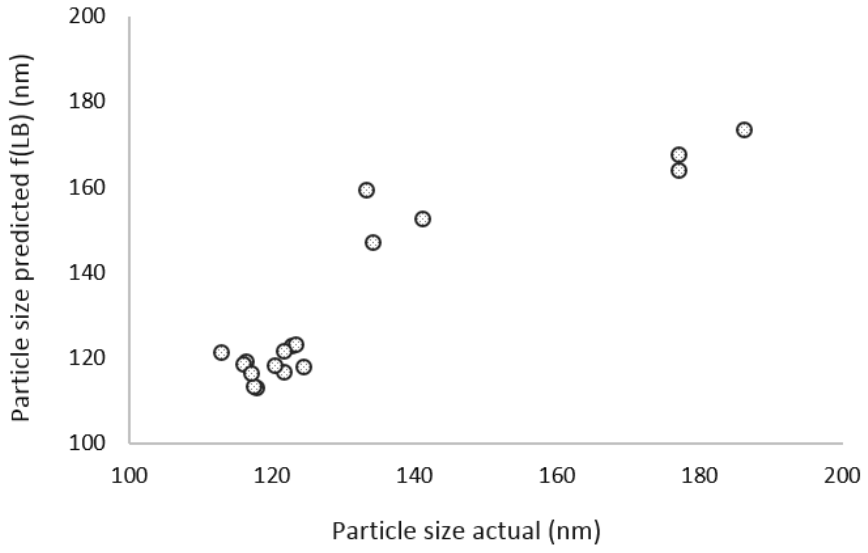

B)

Figure 7.4. A) Model 5 temperature separated: Particle size z-average modeled as a function of light backscatter maximum intensity; B) Model 5 temperature combined: Particle size z-average modeled as a function of light backscatter maximum intensity.

Other authors have looked at various characteristics of milk using NIR (780- 2500 nm) or mid-infrared (MIR) (2500- 15000 nm) spectroscopy techniques (Iñón, Garrigues, & de la Guardia, 2004; Wu, Nie, He, & Bao, 2011) by incorporating a combination of chemometric techniques for analyzing the range of spectral data in order to form useful prediction models. The NIR region is widely used in milk analysis and therefore the spectral regions which correspond to moisture content, milk fat, protein, lactose and other milk components are

well-characterized (Kamishikiryo-Yamashita, Oritani, Takamura, & Matoba, 1994; Laporte & Paquin, 1999; Robert et al., 1987; Tsenkova et al., 1999). However, it should be noted that although the light backscatter spectral range (20-1100 nm) has been studied with respect to milk particulate components, such as the fat globule and casein micelle (Castillo, Payne, López, et al., 2005; Fagan et al., 2008; Lamb et al., 2013), regions that correspond to specific characteristic and or physicochemical changes in milk have yet to be fully characterized.

7.3.2 Ratio prediction models

7.3.2.1 Waveband ratio selection

In this study, we have observed good modelization for particle size as a function of light backscatter maximum intensity (model 5). However Lamb, Payne, Xiong, and Castillo (2013) found improved predictions when using an alternative technique of waveband ratios for modeling whey protein denaturation as a function of light backscatter intensity. Lamb et al. (2013) defined waveband ratios as the average intensity at each 25 nm portion of the light backscatter spectra, and created waveband ratio combinations, which were used to form predictive models. Implementing a technique of ratios, or a combination of parameters, has been used successfully in prediction models found in the literature (Castillo et al., 2000; Castillo, Payne, López, et al., 2005; Fagan et al., 2008), which in certain cases was found to improve the accuracy of modeling. In addition, a technique of ratios has been used to decrease the number of variables used in the model by combining certain parameters, such as in the case of Fagan et al. (2008), which incorporated a non-optical milk-fat protein ratio into the model for curd moisture content. Therefore in order to pursue a higher level of accuracy for predictive models, we also tested a method of waveband ratios for our study. Note that Fagan et al. (2008) tested Partial Least Squares (PLS) regression analysis for use in optical sensor development and found little improvement in models when compared to individual wavelength and waveband ratio models. In addition, complex model development techniques are inherently more complicated and expensive as they require sensors that use multiple wavelength analysis and, as a result, we opted out of using any more than two wavelength combinations for the development of models in this study.

Table 7.3. R^2 top 10 ratios for modeling particle size.

ratio	numerator	denominator	R^2 PS f(LB ratio)	R^2_{avg} PS f(LB ratio)	R^2 LB ratio f(pH,T)	R^2_{avg} LB ratio f(pH,T)
6_18	388	808	0.979	0.952	0.991	0.993
6_17	388	773	0.979	0.951	0.992	0.993
6_16	388	843	0.978	0.949	0.993	0.993
7_16	388	738	0.977	0.949	0.992	0.993
7_15	458	773	0.977	0.948	0.992	0.993
6_19	458	738	0.980	0.954	0.987	0.989
7_17	458	703	0.978	0.951	0.989	0.991
6_15	458	808	0.976	0.948	0.991	0.992
6_20	388	878	0.981	0.955	0.982	0.985
7_18	388	703	0.976	0.951	0.986	0.989

R^2, determination coefficient; R^2_{avg}, average determination coefficient of 80 and 90 °C; LB, light backscatter intensity; T, temperature of heat treatment; PS, particle size z-average; numerator and denominator (nm).

Initially, wavebands of 15, 25 and 35 nm portions of the light backscatter spectra (from 200-1100 nm) were investigated in preliminary models, however no major differences were observed. As a result, wavebands were defined as an average of the intensity for each 35 nm portion of the spectra. Thus, we obtained a total of 27 waveband regions. The wavebands were then combined, using each waveband combination in both the numerator and denominator, to come up with all possible ratios. Predictive models were determined using the pre-selected waveband ratios that were found to best correspond to changes in particle size as a function of pH (i.e., assuming an exponential function). Table 7.3 summarizes the top 10 ratios, which exhibited the highest R^2 values used for the model development and based on the total R^2 value from a sum of the four models which used waveband ratios (Models 6 (80 °C), 6 (90 °C), 7 and 10). Figure 7.5 illustrates the typical light backscatter profile obtained from 200-1100 nm scans. Highlighted are the two sections of

wavebands which were used to obtain the best models. Wavebands 6 and 7 (range of 388-458 nm) were selected as numerator values that corresponded with models showing the highest R^2 values. The number of denominators that corresponded to the highest R^2 values for the models was larger, wavebands 15-20 (range of 703-878 nm). All ratios in the top 10 models fell within the previously described numerator and denominator ranges. Numerator values that produced the 10 highest R^2 represent a region with relatively little change among the different samples at various experimental conditions (pH and temperature of heat treatment), whereas denominator values tended to lie in a region with more notable changes (Figure 7.5). The technique of using numerator and denominator values presented as a ratio and/or as individual values is further investigated in Section 7.2.

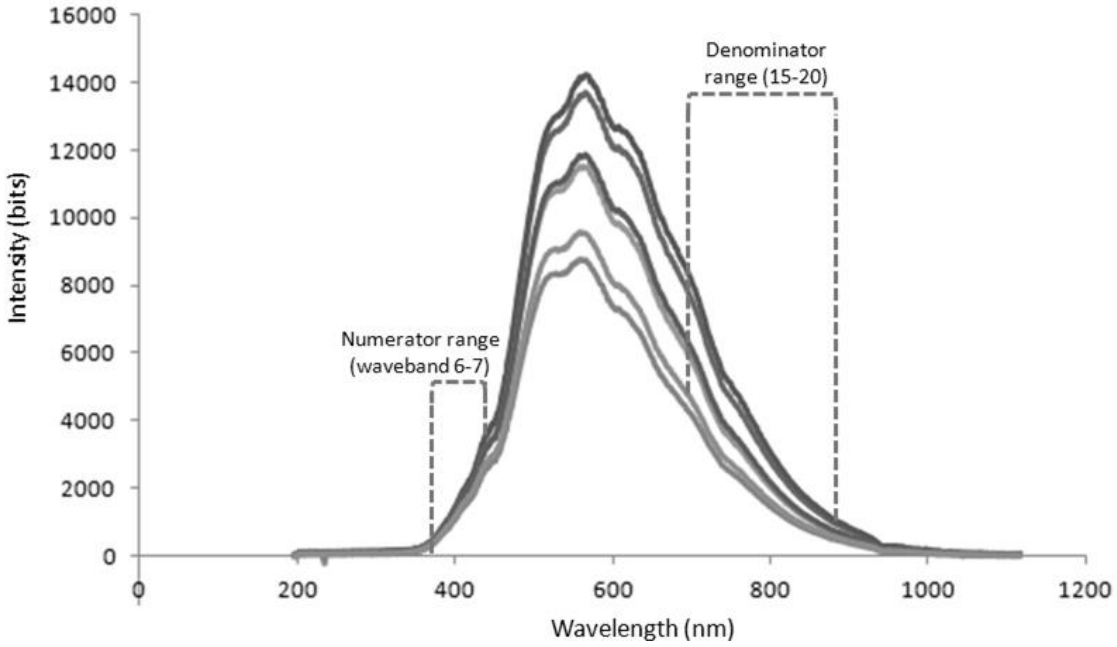

Figure 7.5. Light backscatter spectra showing selected numerator and denominator regions used for modeling.

7.3.2.2 Ratio models

Using the ratio (*R6,18*) which yielded the highest R^2 for particle size, prediction models were developed for particle size (z-average) and light backscatter waveband ratio (*R6,18*) as a function of pH in temperature "separated" and temperature "integrated" models (Table 7.4) (Figure 7.6, 7.7). In comparison to models that were developed to determine $R_{6,18}$ (models 6-7; Eqn 7.6, 7.7) (Figure 7.6), models for z-average (models 8-9; Eqn 7.8, 7.9)

(Figure 7.7) incorporated an exponential factor into equations. As mentioned previously and visualized in Figure 7.1B, particle size z-average tends to follow a more exponential curve with respect to pH when compared to light backscatter maximum intensity, which follows a linear trend with pH (Figure 7.1A). Equations for predictions are as follows:

$$\frac{I_n}{I_d} = \beta_0 + \beta_1 pH \quad \text{(Eqn 7.6)}$$

$$\frac{I_n}{I_d} = \beta_0 + \beta_1 pH + \beta_2 T \quad \text{(Eqn 7.7)}$$

$$PS = \beta_0 + e^{(\alpha_0 + \alpha_1 pH)} \quad \text{(Eqn 7.8)}$$

$$PS = \beta_0 + e^{(\alpha_0 + \alpha_1 pH + \alpha_2 T)} \quad \text{(Eqn 7.9)}$$

where I_n is the light backscatter intensity at the pre-selected numerator, I_d is the light backscatter intensity at the pre-selected denominator, PS is the particle size z-average, T is the heat treatment temperature, and $\beta_{0\text{-}2}$ and $a_{0\text{-}2}$ are prediction coefficients.

Table 7.4. Models 6.9 using $R_{6,18}$.

Model	Prediction equation	Temperature	DF err	Regression	coefficient	s	SSE	R^2	SEP
6	$\frac{I_n}{I_d} = \beta_o + \beta_1 pH$	80 °C	7	β_0 =	0.454	0.0253	$9.55 \cdot 10^{-5}$	0.991	$3.69 \cdot 10^{-3}$
				β_1 =	-0.103	$3.77 \cdot 10^{-3}$			
		90 °C	7	β_0 =	0.488	0.0176	$4.61 \cdot 10^{-6}$	0.996	$2.57 \cdot 10^{-3}$
				β_1 =	-0.106	$2.62 \cdot 10^{-3}$			
7	$\frac{I_n}{I_d} = \beta_o + \beta_1 pH + \beta_2 T$	Integrated (80 and 90 °C)	15	β_0 =	0.383	0.0197	0.0214	0.993	0.0377
				β_1 =	-0.104	$2.26 \cdot 10^{-3}$			
				β_2 =	$-1.03 \cdot 10^{-3}$	$1.48 \cdot 10^{-4}$			
8	$PS = \beta_o + e^{(\alpha_0 + \alpha_1 pH)}$	80 °C	24	β_0 =	115	2.27	292	0.871	3.49
				a_0 =	-25.2	7.53			
				a_1 =	3.52	1.21			
		90 °C	21	β_0 =	117	1.28	201	0.988	3.09
				β_1 =	-41.2	4.31			
				β_2 =	5.87	0.687			
9	$PS = \beta_o + e^{(\alpha_0 + \alpha_1 pH + \alpha_2 T)}$	Integrated (80 and 90 °C)	47	β_0 =	117	0.827	517	0.976	3.32
				a_0 =	-29.7	3.46			
				a_1 =	5.78	0.576			
				a_2 =	0.121	$6.93 \cdot 10^{-3}$			

N= 18 (I_n/I_d models), N=54, DF err, degrees of freedom for error; $\beta_{0\text{-}2}$ and $a_{0\text{-}2}$, prediction coefficients; s, standard error of the estimate for coefficients; SSE, sum of squares for error; R^2, determination coefficient; SEP, standard error of prediction for the model: LB (bits), PS (nm).

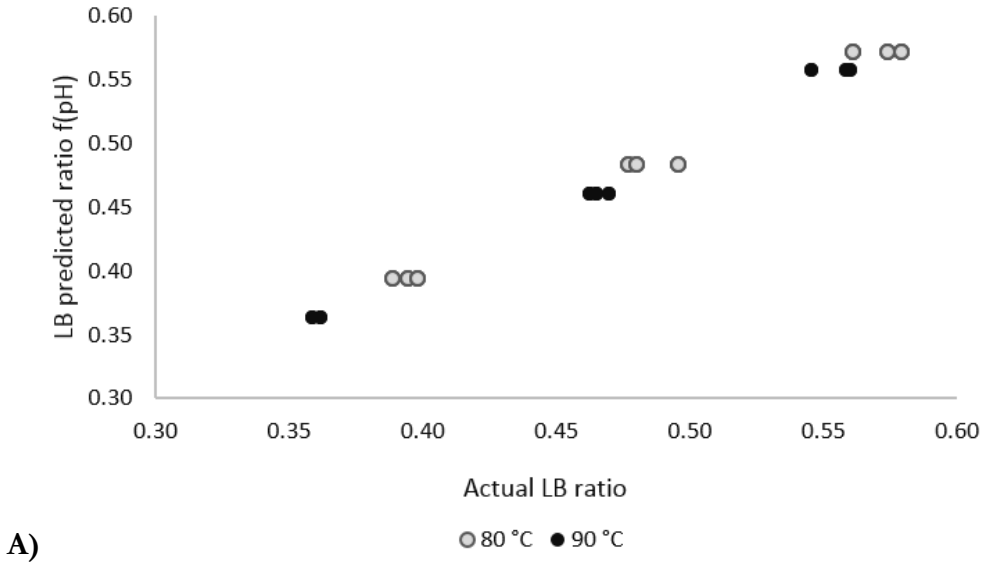

A)

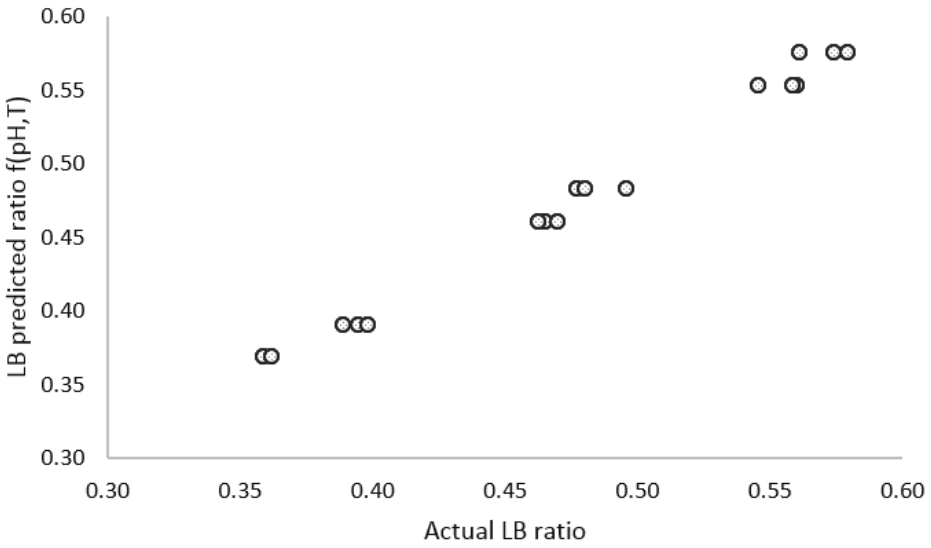

B)

Figure 7.6. A) Model 6: Light backscatter ratio $R_{6,18}$ modeled as a function of pH; B) Model 7: Light backscatter ratio $R_{6,18}$ modeled as a function of pH and temperature, LB units (dimensionless).

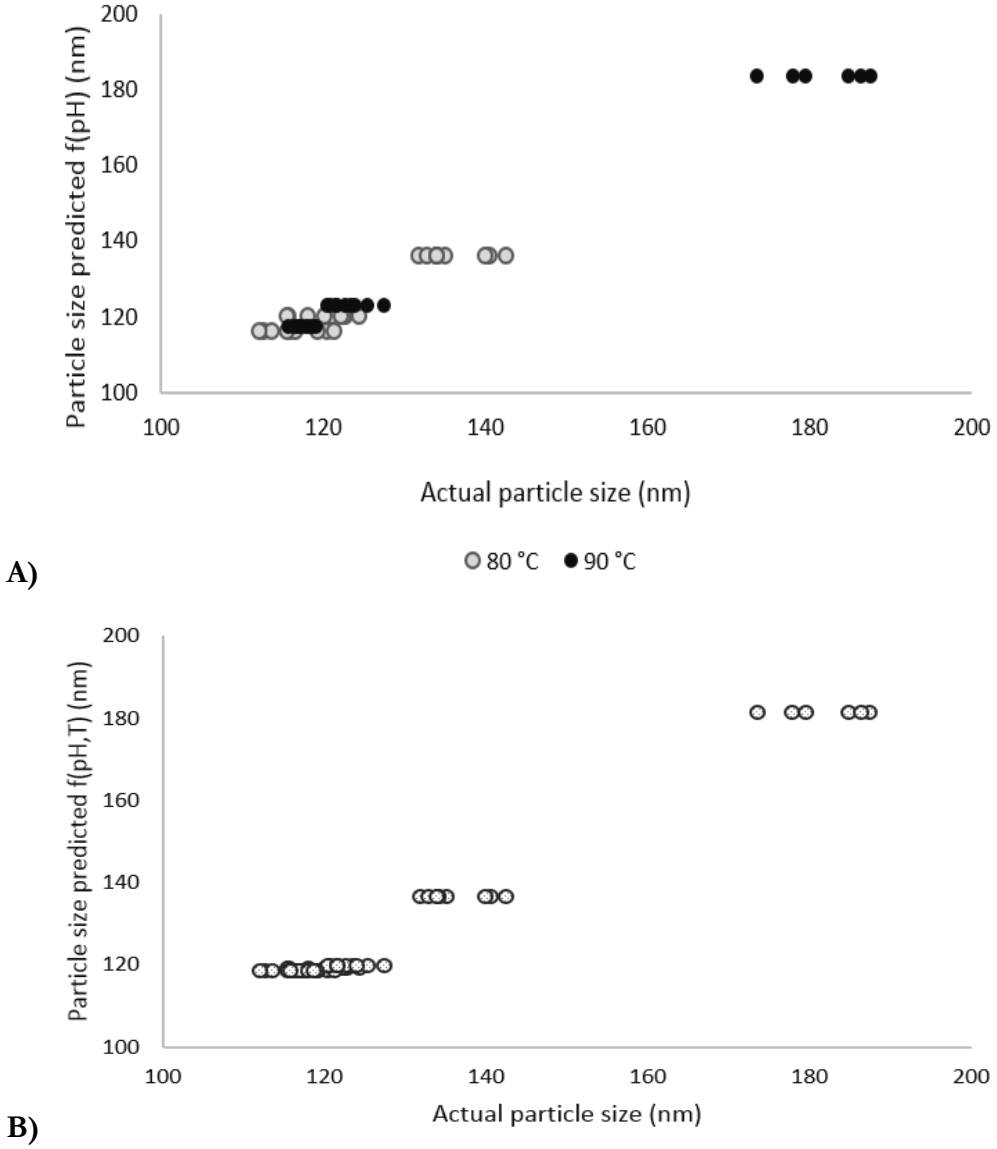

Figure 7.7. A) Model 8: Particle size z-average modeled as a function of pH B) Model 9: Particle size z-average modeled as a function of pH and temperature.

Our previous work has shown that changes in light backscatter signal and particle size have been found to be highly correlated to pH (Taterka & Castillo, 2015). Thus in model development it is reasonable that pH has been found to be a critical factor. Castillo et al. (2000) developed models for cutting time prediction in cottage cheese manufacture also using pH as a variable for predictions, whereas reasonably accurate prediction models using pH as a variable have been developed by Toffanin, De Marchi, Lopez-Villalobos, and Cassandro (2015) in order to determine characteristics of milk quality and coagulation properties using MIR analysis. As pH is a useful tool in our study for the determination of particle size and

light backscatter intensity, it may be complementary to utilize a simple technique of milk pH measurement for the determination of changes in the milk matrix with heat treatment. Unfortunately, simple laboratory pH meters generally contain glass components and other reagents that are not approved for in-line use in the food industry (Wesstrom, 1992). Preliminary work in our research group (Arango, 2015) has exhibited that optical sensors are useful for the replacement of pH meters during acid-coagulation of milk in which pH predictions as a function of light scatter techniques were developed successfully with great accuracy ($R^2 > 0.99$). Thus, the incorporation of an optical technology for the determination of pH-specific denaturation mechanisms may be of interest for investigation in our study. As a result, models for particle size using the light backscatter spectrum have been developed with good correlations. Utilizing the ratio values showed to greatly improve R^2 when comparing model 5, which did not use ratio values, (Table 7.2) (Figure 7.4) to model 10, which did (Table 7.5) (Figure 7.8). Model 10 is presented below, utilizing $R_{6,18}$ in an exponential type equation to model particle size changes.

$$PS = \beta_0 + e^{(\alpha_0 + \alpha_2 \frac{I_n}{I_d})} \quad \text{(Eqn 7.10)}$$

An interesting finding in prediction models for particle size z-average (Model 8-10) (Figure 7.6, 7.7, 7.8) is that the coefficient β_0 lies within the range of the initial casein micelle particle radius (~112-120 nm, Tables 7.4, 7.5) (Figure 7.5). The remainder of the prediction equation includes an exponential factor of other predictors (Eqn 7.8-10), which for Model 10 corresponds to a waveband ratio.

Table 7.5. Predictive Model 10.

Model	Prediction equation	Temperature	DF err	Regression	coefficient	s	SSE	R^2	SEP
10	$PS = \beta_0 + e^{(\alpha_0 + \alpha_2 \frac{I_n}{I_d})}$	80 °C	24	β_0 =	115	1.87	201	0.911	2.89
				a_0 =	-9.22	1.61			
				a_1 =	15.6	4.27			
		90 °C	21	β_0 =	117	1.03	117	0.993	2.36
				a_0 =	-12.5	0.803			
				a_1 =	23.2	2.26			
		Integrated	48	β_0 =	119	0.553	443	0.979	3.04
		(80 and 90 °C)		a_0 =	-17.5	0.700			
				a_1 =	37.0	1.94			

N=27, DF err, degrees of freedom for error; $\beta_{0\text{-}2}$ and $a_{0\text{-}2}$, prediction coefficients; s, standard error of the estimate for coefficients; SSE, sum of squares for error; R^2, determination coefficient; SEP, standard error of prediction for the model (nm).

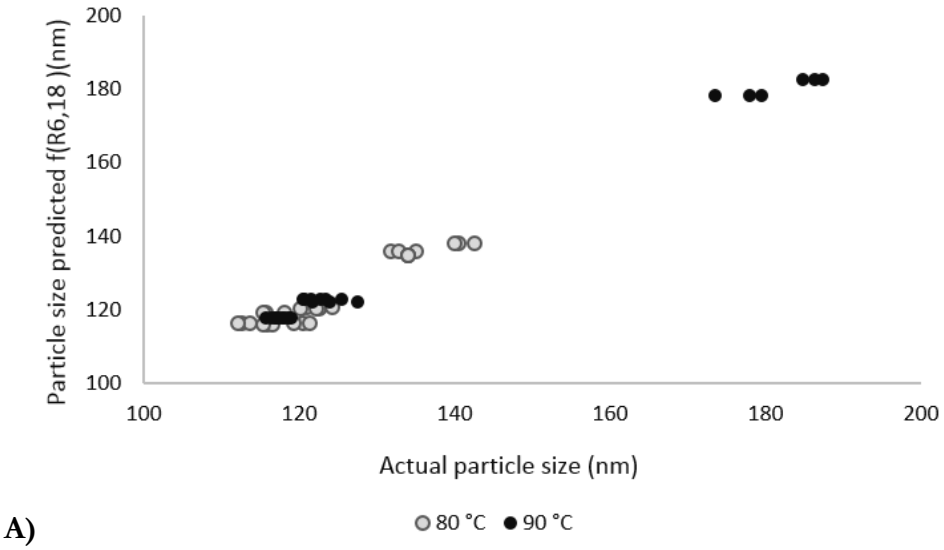

A)

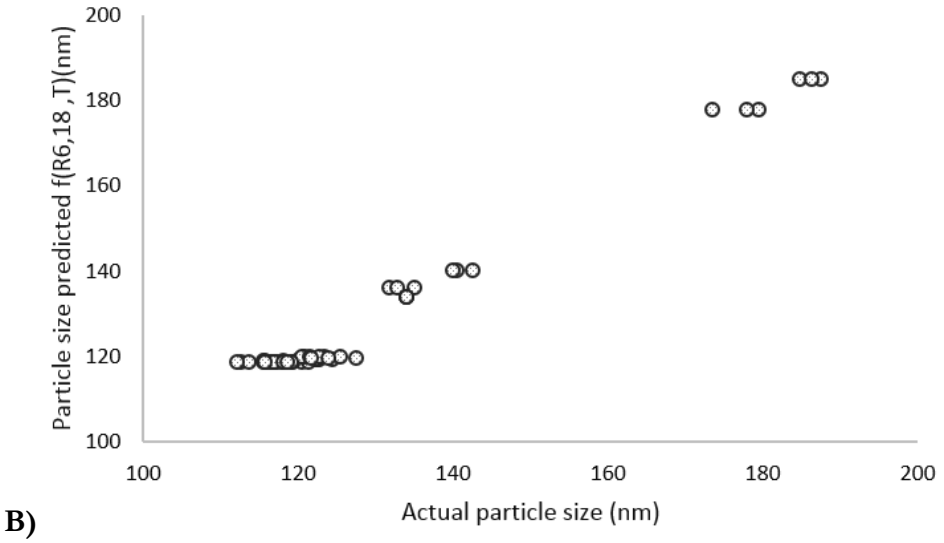

B)

Figure 7.8. A) Model 10: Particle size z-average modeled as a function of light backscatter ratio $R_{6,18}$ B) Model 10 (temperate combined): Particle size z-average modeled as a function of light backscatter ratio $R_{6,18}$.

Since binding has been found to be the main contributor in the increase in particle size, it may be suggested that the binding reaction follows an exponential growth curve. Thus, using the average initial casein micelle particle size plus some exponential increase as a result of attachment and/or aggregation, it may be possible to predict denaturation as a function

of particle size increase. From our study we saw an average radius of 119.7 nm using reconstituted milk from the same lot, comparable to average diameters reported in Martin, Williams, and Dunstan (2007) which saw an average diameter of 231.0 ± 1.6 nm in reconstituted skim milk stirred for 35 min. However it should be noted that casein micelle average size varies significantly depending on batch and thus this hypothesis should be tested using different milk batches.

7.3.3 Comparison of single wavelength and ratio models

Two sets of models have been developed and discussed in this section: models developed using the maximum light backscatter intensity (I_m) (Tables 7.1, 7.2) and models using ratio $R_{6,18}$ and an exponential factor in z-average models (Table 7.4, 7.5). Models from Table 7.1 are complimentary to models from Table 7.4 as such: Model 1 and 6, 2 and 7, 3 and 8, 4 and 9; and 5 and 10 in Table 7.2 and Table 7.5, respectively. In most cases, using a ratio value and/or adding an exponential factor to particle size prediction models acted to increase the R^2 value of the model, except model 3 compared to model 8 where adding an exponential factor gave a slightly lower R^2 for both 80 °C (model 3: 0.881, model 8: 0.871) and 90 °C models (model 3: 0.992, model 8: 0.988). This may be due to the fact that there is a large increase from 80 °C to 90 °C in particle size at pH 6.3. This difference makes it necessary for temperature "integrated" models to include an exponential factor (R^2 = 0.791 (Table 7.1) versus 0.976 (Table 7.4) with exponential factor), whereas temperature "separated" models using a simpler equation still maintain a high R^2 value for the models (R^2 = 0.881 and 0.992 (Table 7.1) versus 0.871 and 0.988 (Table 7.4)).

For the modelization of particle size z-average as a function of light backscatter intensity, model 5 and model 10 use light backscatter intensity values (model 5: I_m, model 10: $R_{6,18}$). Both models show high R^2 values, however we can see that the addition of an exponential factor, as well as using $R_{6,18}$ in model 10, acts to increase R^2 in both temperature "separate" and integrated models (R^2 for 80 °C, 90 °C and "integrated" models were 0.847, 0.992, 0.825 for model 5: and 0.911, 0.993, 0.979 for model 10, respectively). We also see this effect in the case of the temperature "integrated" models (4 and 9) in which the exponential addition greatly increases the R^2 from 0.791 to 0.976. On the other hand, when comparing Model 3 with Model 8, the simple quadratic form yields a prediction with a higher R^2 (80 °C: 0.881, 90 °C: 0.992) than when the exponential form is added to the equation (80 °C: 0.871,

90 °C: 0.988). In this case, models that are produced at each respective temperature separately, using a linear model, supports each prediction sufficiently and to a better extent than the exponential model. Nonetheless, there is a good correlation between actual and predicted values in all models, thus the light backscatter technique shows promise toward the prediction of particle size changes as a function of milk pH and temperature treatment. Since changes in particle size have been mainly found to be a result of the binding reaction of denatured whey proteins attaching to the surface of the casein micelle, this gives a relevant insight into aspects of whey protein denaturation in milk.

7.3.4 Analysis based on various portions of $R_{6,18}$

Since we have implemented two techniques for modeling, one using a single intensity at the maximum value (I_m), and the other using a ratio of intensities ($R_{6,18}$), which acted to improve the models in most cases, it was of interest to test whether using only the numerator or denominator of the ratio $R_{6,18}$ (I_n or I_d, respectively) may also yield good predictions individually. Note that a single wavelength prediction is always more convenient for industrial implementation of a sensor technology. Thus, in order to confirm the need for ratios in the development of prediction models, model 5 was tested using the maximum intensity (I_m), the intensity used in the numerator (I_n) of $R_{6,18}$ (model 11), and the intensity of the denominator (I_d) used in $R_{6,18}$ (model 12),. As summarized in Table 7.6, we can see that both I_m (R^2 = 0.847 and 0.992) and I_d (R^2 = 0.889 and 0.994) showed good R^2 for both 80 and 90 °C models, respectively. On the other hand, I_n yielded less reliable R^2 values (R^2 = 0.465 and 0.773). In temperature "integrated" models I_d was the model with the highest R^2 (0.890) and lowest SEP (8.20 nm), compared to I_m and I_d models (R^2 = 0.825, 0.491, SEP = 10.3, 17.6 nm, respectively). As I_n, in general, shows poor correlation of predicted and actual values in models, it leads us to believe that it may not be necessary for model development. A possible reason for this will be introduced below. In fact, I_d yields even higher R^2 values than I_m; possibly showing more potential in the corresponding portion of the spectrum (808 nm) for the determination of various changes in milk with heat treatment and varying milk pH as compared with the peak of maximum intensity (570 nm). Previous work in the literature (Lamb et al., 2013) found it useful to form ratios for predictive models however in our study the regions of I_m and I_d used individually appear to be much more important than I_n, at least in the case of models for particle size as a function of light backscatter intensity. Models used for comparison (Table 7.6) do not include an exponential factor, as it was not

possible to model individual intensity values without modifying the exponential equation. Since little change in intensity occurs between sample treatments in the regions where numerators with the highest R^2 for models occur (Table 7.3, Figure 7.5), it is suggested that the portion of the spectrum corresponding to the denominators (703-878 nm) is in fact representing the particle size information while numerator values act as a normalization factor for models. Additionally, exponential models tend to yield high R^2 values and include the coefficient β_0, which may be representative of the initial particle size ratio values. Considering these two observations, it is proposed that development of an in-line sensor using only one wavelength plus some predetermined normalization factor (for example, replacing the numerator with a constant) implemented into an exponential equation should yield a considerably accurate model, and in addition, would be less costly and complicated than a dual wavelength optical sensor.

Table 7.6. Models using individual wavelength values to model particle size as a function of I_m, I_n and I_d.

Model	Prediction equation	Temperature	DF err	Regression	coefficient	s	SSE	R^2	SEP
5	$PS = \beta_0 + \beta_1 I_m + \beta_2 {I_m}^2$	80 ^{O}C	6	β_0 =	$1.18 \cdot 10^{-6}$	$5.47 \cdot 10^{-7}$	114	0.847	4.36
				β_1 =	0.0221	0.0121			
				β_2 =	219	64.9			
		90 ^{O}C	6	β_0 =	$4.41 \cdot 10^{-6}$	$3.89 \cdot 10^{-7}$	58.5	0.992	3.12
				β_1 =	0.0899	0.00914			
				β_2 =	572	52.4			
		Integrated	15	β_0 =	479	103	1599	0.825	10.3
		(80 and 90 ^{O}C)		β_1 =	-0.0725	0.0185			
				β_2 =	$3.59 \cdot 10^{-6}$	$8.14 \cdot 10^{-7}$			
11	$PS = \beta_0 + \beta_1 I_n + \beta_2 {I_n}^2$	80 ^{O}C	6	β_0 =	$-2.44 \cdot 10^{-5}$	$3.58 \cdot 10^{-4}$	398	0.465	8.14
				β_1 =	-0.110	0.591			
				β_2 =	49.9	242			
		90 ^{O}C	6	β_0 =	$-1.36 \cdot 10^{-3}$	$9.60 \cdot 10^{-4}$	$1.65 \cdot 10^{3}$	0.773	16.6
				β_1 =	-1.99	1.62			
				β_2 =	847	679			
		Integrated	15	β_0 =	436	412	$4.66 \cdot 10^{3}$	0.491	17.6
		(80 and 90 ^{O}C)		β_1 =	-0.920	0.996			
				β_2 =	$6.60 \cdot 10^{-4}$	$5.97 \cdot 10^{-4}$			
12	$PS = \beta_0 + \beta_1 I_d + \beta_2 {I_d}^2$	80 ^{O}C	6	β_0 =	$4.18 \cdot 10^{-6}$	$2.07 \cdot 10^{-6}$	83.0	0.889	3.72
				β_1 =	0.0231	0.0159			
				β_2 =	148	29.2			
		90 ^{O}C	6	β_0 =	$1.36 \cdot 10^{-5}$	$1.27 \cdot 10^{-6}$	40.5	0.994	2.60
				β_1 =	0.0879	0.0107			
				β_2 =	258	21.5			
		Integrated	15	β_0 =	216	35.5	$1.01 \cdot 10^{3}$	0.890	8.20
		(80 and 90 ^{O}C)		β_1 =	$4.46 \cdot 10^{-5}$	$9.85 \cdot 10^{-6}$			
				β_2 =	-0.134	0.0385			

N=18, DF err, degrees of freedom for error; $\beta_{0\text{-}2}$, prediction coefficients; s, standard error of the estimate for coefficients; SSE, sum of squares for error; R^2, determination coefficient; SEP, standard error of prediction for the model (nm)

7.4 Conclusions

Two prediction models were developed to estimate particle size z-average as a function of the intensities of a single wavelength/waveband combinations on the light backscatter spectra (Model 5 and 10) both showing good correlation between actual and predicted values (Table 7.2, 7.5). Improvements were found with the incorporation of $R_{6,18}$ and the addition of an exponential factor (Model 10) compared to the quadratic model using I_m (Model 5). As changes in particle size diameter have been found to be primarily a result of the attachment of denatured whey proteins to the surface of the casein micelle, this model provides useful information regarding the potential modelization of WP denaturation. However, our previous work also suggests that spectral data from a light backscatter technique contains useful information regarding the quantification of not only whey proteins that have attached to the casein micelle, but also the formation of soluble whey protein aggregates, as it should be considered that total whey protein denaturation can be quantified as a sum of these two values. Taking into account the investigated models, the suggested model for particle size as a function of light backscatter intensity would include both an exponential component, an initial intercept which corresponds to an approximate value of initial particle size and a light backscatter normalized value or a waveband ratio. Further work may give more insight into a more improved model. Nonetheless, this experiment yields useful preliminary information toward the development of a comprehensive model for the determination of whey protein denaturation with the potential for implementation of an in-line optical sensor for in plant processed milk.

CHAPTER 8: Light backscatter and fluorescence spectral analysis of the preferential formation of aggregates and micellar bound whey proteins for the development of an optical sensor

8.1 Introduction

Milk heat treatment is a key step in dairy industrial processes which may result in the partial denaturation of whey proteins. As a result, exposed sulfide groups are available to react with other components of the milk matrix and generally result in the formation of serum aggregates and/or bound whey proteins when they attach with κ-CN on the surface of the casein micelle. Denatured whey protein micellar binding is largely a function of milk pH. For the most part, it has been reported to be the primary reaction mode of denatured whey proteins at pH 6.3, whereas the formation of serum whey protein aggregates occurs more commonly at pH 7.1 (Anema and Li, 2003a; b; Vasbinder and de Kruif, 2003; Anema et al., 2004b; Anema, 2007; Kethireddipalli et al., 2010). For instance, Anema (2007) observed that in reconstituted milk heated at 90 °C for 20-30 min; ~85% denatured whey proteins associated with the casein micelle at pH 6.5 and only ~15% were associated at pH 7.1. Kethireddipalli, Hill, & Dalgleish (2010) heat treated milk at 90 °C for 10 min and reported bound protein percentages of 82%, 30%, and 0-5% at pH 6.3, 6.7, and 7.1, respectively.

It is well-known that the formation of a whey protein/casein micelle complex on the surface of the casein micelle has the potential to increase casein micelle particle size (up to 30-35 nm change in diameter) (Anema and Li, 2003a; Vasbinder and de Kruif, 2003; Vasbinder et al., 2003; Anema et al., 2004a; Kethireddipalli et al., 2010; Kethireddipalli et al., 2011). And as the binding reaction occurs to a greater extent at low pH, such does the increase in particle size (Kethireddipalli et al., 2010; Vasbinder & de Kruif, 2003). Based on these principles, studies have been carried out to observe trends between changes in light backscatter signal as a result of changes in particle size and/or whey protein denaturation, while taking into consideration the light scatter properties of the casein micelle in the spectral range of 200-1100 nm (Lamb et al., 2013; Taterka & Castillo, 2015). Utilizing a simple and inexpensive light backscatter sensor, Lamb, Payne, Xiong, & Castillo (2013) were able to observe a correlation between β-lactoglobulin (β-LG) denaturation and ratios of specific

regions of the light backscatter spectra. Taterka & Castillo (2015) observed good correlation between light scatter spectra and particle size at various milk pHs at 80 and 90 °C and developed useful models for this relationship with an $R^2 > 0.9$ (Chapter 7) with an aim toward the development of an in-line optical sensor for the determination of whey protein denaturation in milk processing.

Fluorescence technology has also been used to characterize quality changes in milk/dairy products. By altering the measurement angle (30-60°), studies have shown that changes in quality characteristics in milk can be measured directly, without sample manipulation, using front-face fluorescence (Dufour & Riaublanc, 1997; Wold, Jørgensen, & Lundby, 2002; Kulmyrzaev et al., 2005; Schamberger & Labuza, 2006), which may present the potential for use of this technology for inline implementation. For example, Kulmyrzaev et al. (2005) implemented front-face fluorescence (FFF) to model %*β*-LG versus fluorescence intensity with regression coefficients of 0.67-0.68 and Boubellouta, Galtier, & Dufour (2009) used FFFS to determine changes in micelle structure as a result of the addition of phosphate, calcium and citrate and found these differences to be due to the formation of mineral complexes on the surface of the micelle. As well, Birlouez 1998, 2002 used the FAST method (Fluorescence of Advanced Maillard products and Soluble Tryptophan) to characterize milk heat treatments, however this method required sample modification to pH 4.6.

8.2 Materials and Methods

The experiment consisted of a 2x6 factorial design with milk pH values of 6.3 and 7.1 and six heat treatment times: 0, 3, 5, 7 12 and 25 min. The complete work plan for Experiment II can be found in Section 3.1.2. Fresh raw skim milk was obtained from the University of Minnesota Food Science and Nutrition pilot plant and pH adjustment can be found in Section 4.1.2. A heat treatment temperature of 80 °C was constant in all measurements. Each treatment was replicated three times. Milk heat treatment was accomplished using a CombiPAL GC Autosampler (CTCAnalytics, Zwingen Switzerland) (Figure 4.2) by transfer of vials via magnetic arm to an isolation chamber at 80°C with an agitation speed of 500 rpm, summarized in Section 4.2.2.

Native whey proteins were fractionated via acid-induced precipitation by pH adjustment to 4.6 (Section 4.6.1) and soluble whey protein fractions (native whey protein and soluble whey protein aggregates) were fractionated using ultracentrifugation at 100 g (Section 4.6.3). Whey protein concentration was determined by *Bicinchoninic Acid* (BCA) assay for all protein fractions and is summarized in Section 4.7.2. Soluble aggregate whey proteins (AWP) and bound whey proteins (BWP) were calculated using Eqns 4.2 and 4.3 (Section 4.8), respectively.

Analytical techniques used in Experiment II include: optical light backscatter, particle size z-average and tryptophan front-face fluorescence. Optical analysis was accomplished using the system described in Section 4.3.2 and can be visualized in Figure 4.4. Light backscatter intensity at 540 nm was recorded and used for further analysis. Milk samples for particle size measurements were suspended in a Ca/imidazole buffer (20 mM-imidazole, 5 mM $CaCl_2$, 30 mM NaCl, pH 7.0) and z-average was measured using the BIC ZetaPALS system (Brookhaven Instruments Corporation, New York USA (Section 4.4.1)). A Perkin Elmer Fluorescence Spectrometer LS-50B (Serial #36275, Perkin-Elmer Ltd., Beaconsfield, U.K.) (Section 4.5.1) (Figure 4.7A) with front-face accessory (60°) (Figure 3.7B) with an excitation slit attenuation filter of 2% was used to measure tryptophan flurorescence at an excitation wavelength of 290 nm recording emission spectra from 305-450 nm (Schamberger and Labuza, 2006).

Kinetic rate constants were estimated using Excel for changes in whey protein fractions (native, bound and aggregate), light backscatter intensity, casein particle size and tryptophan fluorescence intensity, by fitting curves to first-order kinetics, similar to Verheul et al. (1998) which used first-order for measuring initial denaturation and particle size of β-LG. Statistical analysis guided these calculations such that residual plots were used to ensure that there was a normally distributed data set. Kinetic rate constants and R^2 values are summarized in Table 2. Statistical differences were determined using non-overlapping 95% confidence intervals between pH levels. In most cases, rate constants were determined with a high degree of certainty by R^2, however in the case that R^2 was less than 0.70, determination of significance was not reported as values were considered unreliable. Data was also analyzed by CORR using "Statistical Analysis System" (SAS, version 9.2, SAS Institute Inc., Cary, NC, USA, 2013) and considered significant when $P < 0.05$.

8.3 Results and Discussion

8.3.1 Whey protein denaturation: native, bound and aggregate formation

Figure 8.1A shows changes in native whey protein (NWP) content as a function of heat treatment time at 80 °C in both pH 6.3 and 7.1 milk. A consistent decrease in NWP is observed with heat treatment time at both pH values, therefore NWP does not appear to be pH-dependent (Figure 8.1A). It should be noted that an increase in milk pH is generally associated with an increase in denaturation rate (Law & Leaver 2000), however the pH values of our study fall within a range in where very little difference in denaturation of β-LG an α-LA is found to occur (Law & Leaver 2000). From this it is possible to assume that total denatured whey protein is comparable at each respective heat treatment time interval of our study in pH 6.3 and pH 7.1 milk.

Bound (BWP) and aggregate (AWP) whey protein were calculated in this study using an ultracentrifuge separation technique (Section 4.6.3) and protein quantification by the BCA protein assay (Section 4.7.2). In assuming that the serum from the ultracentrifuge technique (CP) contains both NWP and AWP (Figure 4.10), we are able to calculate AWP and BWP using Eqn 4.2 and 4.3, respectively. It appears that little to no aggregates were formed at pH 6.3 during heat treatment, since the curve of CP in Figure 8.1B at pH 6.3 is nearly identical to that of NWP in Figure 8.1A. An additional observation is that CP content at pH 7.1 is greater than both the initial CP content at pH 6.3 (which we assume contains only NWP) and the acid-separated whey samples in Figure 8.1A. Due to this observed increase in CP, it is likely that CP at pH 7.1 contains other proteins, such as κ-CN and/or other caseins. This is expected, as other authors have also observed small amounts of casein in serum, which was attributed to a larger degree of κ-CN dissociation at high milk pH (Ménard, Camier, & Guyomarc'h, 2005) and in some instances the presence of small quantities of α_s-CN (Donato & Dalgleish, 2006). Even so, only small amounts of α_s-CN (from approximately 5-12%) have been reportedly observed in heat-treated milk serum in the pH range 6.3 to 7.1 (Anema & Li, 2000; Anema & Klostermeyer, 1997; Donato & Dalgleish, 2006; Ménard et al., 2005). Thus, AWP (Eqn 4.2) may result in an overestimation due to the presence of residual casein particles in pH 7.1 milk, however as this is likely to constitute only a small portion of the serum protein content, we do not consider it to negatively affect the interpretation of this data.

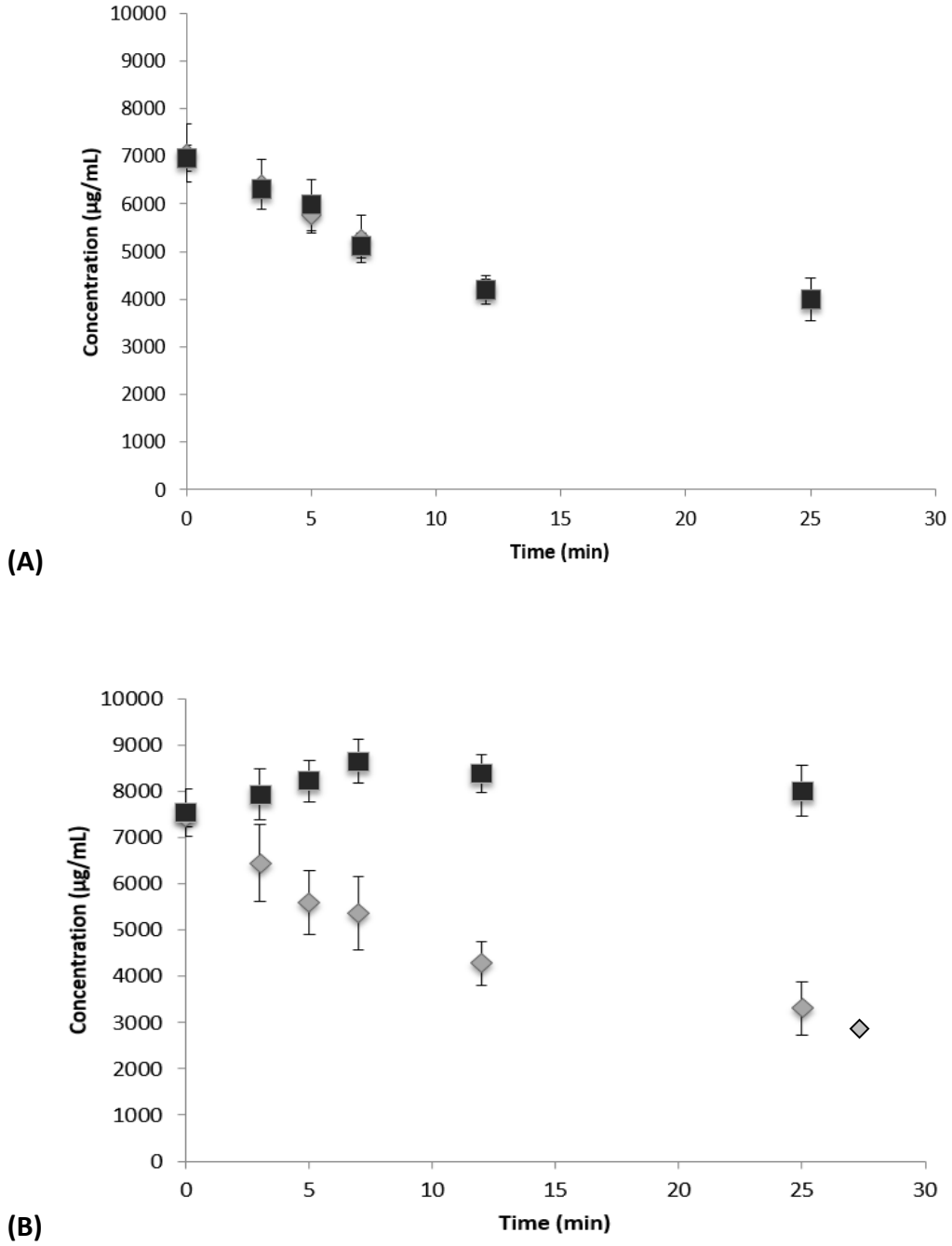

Figure 8.1. Changes in (A) native (NWP) (B) native and soluble aggregate (serum whey from ultracentrifuge separation) (CP) whey protein concentration in milk during heat treatment at pH 6.3(◇) and 7.1(■).

Calculated bound (BWP) and aggregate whey protein (AWP) content are presented as a function of heat treatment time at pH 6.3 and pH 7.1 (Figure 8.2). AWP at pH 7.1 and

BWP at pH 6.3 show a large increase with heat treatment, supporting the idea that the preferred mechanism is binding at pH 6.3 and soluble aggregate formation at pH 7.1. Although it appears that slightly more aggregates are formed at pH 7.1 than bound at 6.3, a linear plot of these two yield an equation of $y = 1.3827x + 843.04$ with $R^2 = 0.975$ (no graph shown), which may imply that their trends are in good agreement. Another factor for the observation of a higher quantity of aggregates may well be the potential for soluble casein fractions ($\varkappa$-CN, a_s-CN) to dissociate from the micelle and remain in the serum, as mentioned previously. Therefore, if we consider that this could result in a slight error in the calculation of AWP at pH 7.1, it is possible that the actual AWP is slightly lower at all respective time intervals, meaning that this curve may in fact lie closer to that of BWP at pH 6.3 than Figure 8.2 suggests.

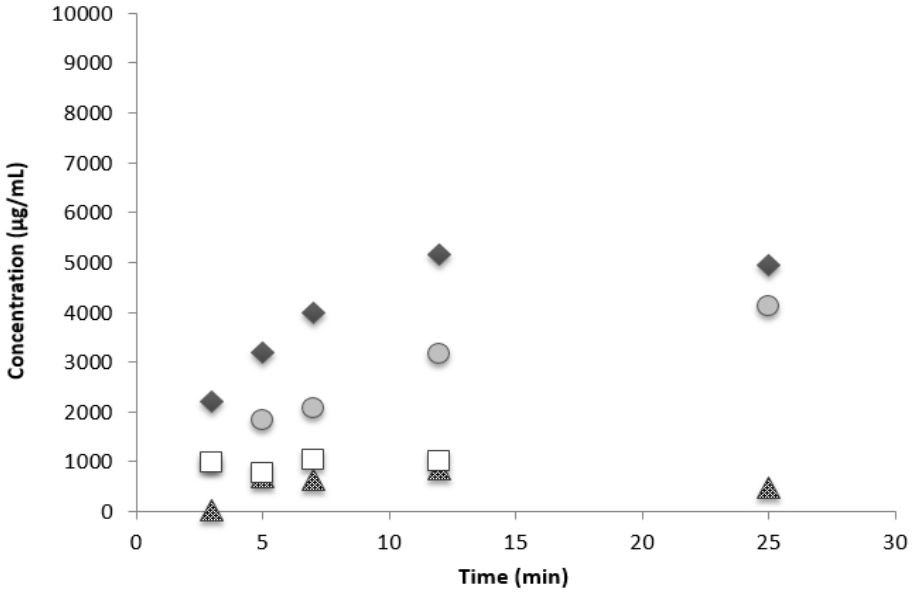

Figure 8.2. Changes in average bound and aggregate whey protein concentration in milk during heat treatment at pH 6.3 (○ BWP, □ AWP) and 7.1 (▲ BWP, ◆ AWP).

Figure 8.3 illustrates changes in total percent of whey protein in each configuration (NWP, BWP and AWP) at pH 6.3 and 7.1 at each respective heat treatment time. Our previous study (Section 6.3.1) found ~40% NWP (taking into account all pH values) after a 10 min heat treatment at 80 °C (Figure 6.2), whereas the value in this study was slightly larger; between 40-60%, if we consider that it lies somewhere in the range of 7 and 12 min of heat

treatment (Figure 8.3). The difference may be accounted for given that this study used raw skim milk and our first experiment (Chapter 5-7) used reconstituted skim milk, since reconstituted milk should initially contain some denatured whey proteins from processing damages. Percent BWP and percent AWP correspond with previously observed trends in which an increase was observed with an increase in heat treatment temperature at pH 6.3 and 7.1 (Figure 8.3 and 6.2). Our Chapter 6 summary of previous authors' observation of BWP at a range of milk pH is also in accordance with our observations (6.3- 82%, 6.7- 30-50%, 7.1- 0-5%, Table 6.1). On the other hand, %AWP is less often reported in the literature. Vasbinder and de Kruif (2003) observed ~35-40% AWP with 10 min at 80 °C in pH 6.9 milk, which is comparable to our 40-50% (estimating that this value lies somewhere between 7 and 12 min treatments) at pH 7.1, and 1-3% at pH 6.35 compared to the ~10% observed in our study at pH 6.3. Although literature reports do vary, this deviation appears to be slight, and in all of the studies reviewed, the general trend appears to follows that as %BWP decreases, %AWP increases notably with increasing pH.

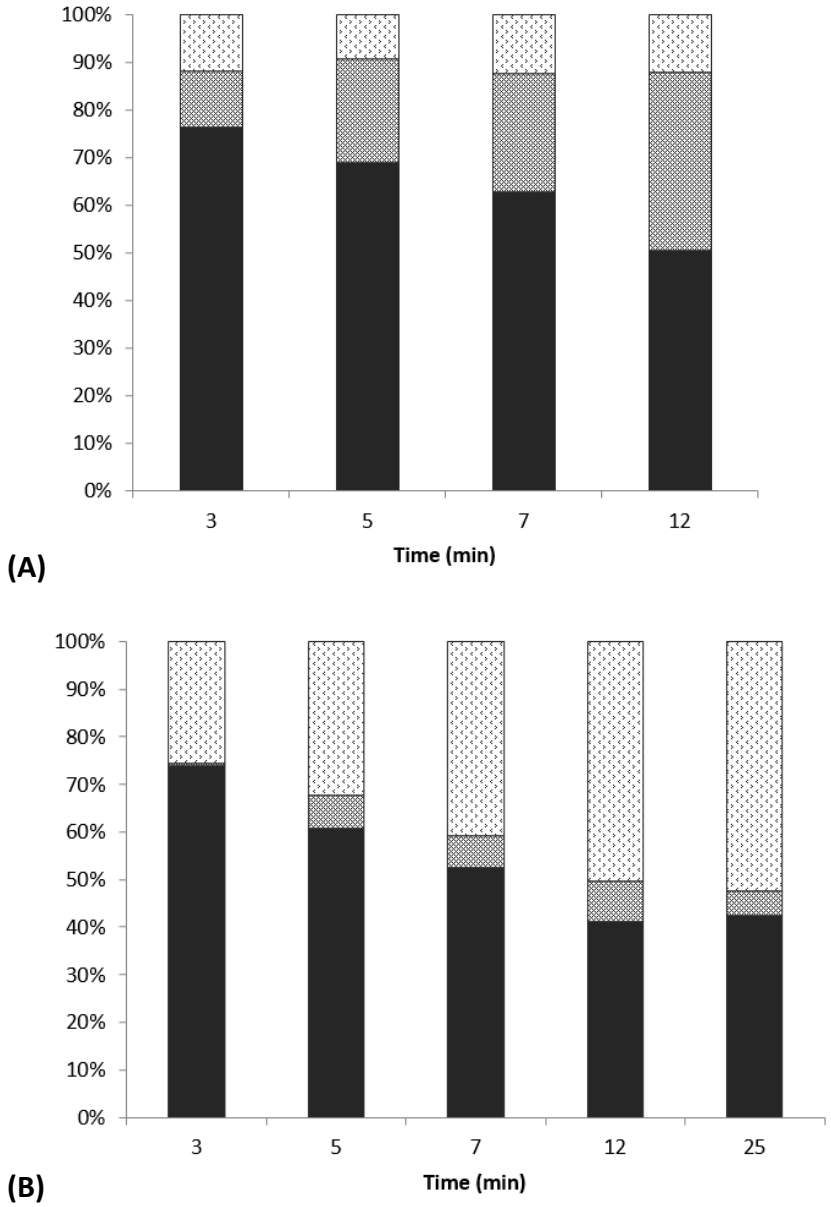

Figure 8.3. Average percent NWP (black), AWP (dotted) and BWP (grey) whey protein at (A) pH 6.3 at 3, 5, 7 and 12 min and (B) pH 7.1 at 3, 5, 7, 12 and 25 min heat treatment at 80 °C.

8.3.2 Particle size

Particle size z-average (PS) measurements are shown in Figure 8.4. An increase in PS was observed at pH 6.3 with heat treatment, whereas minimal changes occurred at pH 7.1. These observations are consistent with the literature as other authors have also reported an increase in PS in low-pH heat treated milk and relatively less changes with higher milk pH (Anema & Li, 2003b; Anema et al., 2004). As well, in our previous study (Chapter 5) a

significant negative correlation was found among pH and PS (Table 5.2). Anema & Li (2003a) found a poor correlation when relating these heat-induced differences in PS to the denaturation of whey proteins but found an improved correlation relating PS changes to bound proteins. In fact, several studies have observed significant correlations with PS and BWP, where this relationship is also pH-dependent (Anema & Li, 2003b; Anema et al., 2004; Anema, 2007; Taterka & Castillo, 2015) (Chapter 5-7). These authors observed that PS increases to a greater extent at low milk pH when compared to high pH milk. Vasbinder and de Kruif (2003) used diffusing wave spectroscopy (DWS) to monitor PS changes as a result of milk pH and presented trends in agreement to our observations. They proposed that the increase in PS was due to a decrease in κ-CN sites available on the micelle causing the formation of relatively larger than average non-uniform surface complexes in low pH milk. This may suggest that more κ-CN dissociates in the serum at low pH, yet other authors (del Angel & Dalgleish, 2006; Donato & Dalgleish, 2006) saw more κ-CN dissociation at high pH milk, which was suggested to result in more AWP with smaller diameters. As Guyomarc'h et al. (2003) has found evidence in pH 6.7 milk that some κ-CN micellar sites may be unreactive, the limitation of binding sites may also be cause for formation of larger micellar surface complexes.

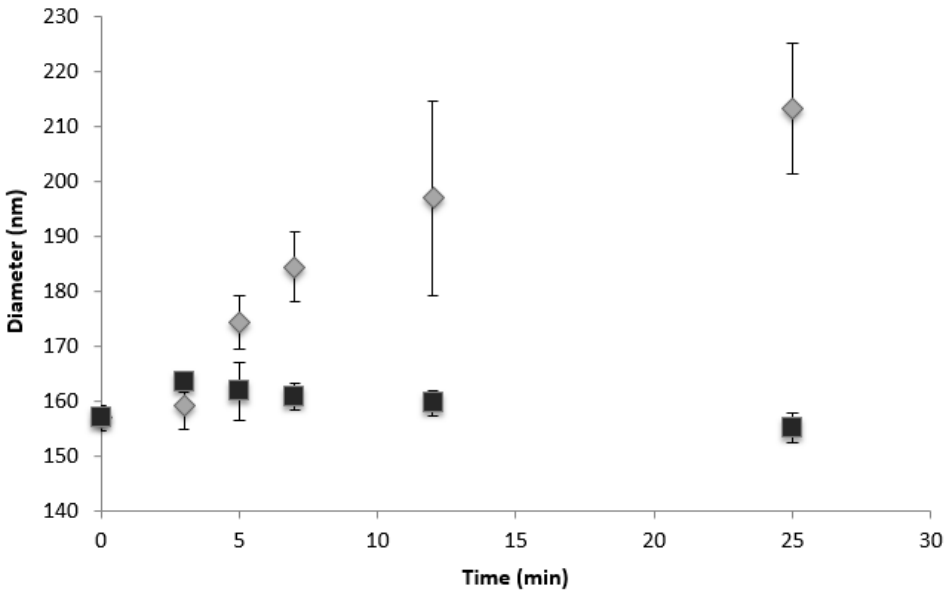

Figure 8.4. Particle size diameter (nm) as a function of heat treatment time at pH 6.3(◆) and 7.1(■).

When comparing BWP (Figure 8.2) and PS (Figure 8.4) curves at pH 7.1, both exhibit a slight initial increase until 3-5 min followed by a slow decrease. This trend was also found to occur in the work of Anema et al. (2004a) in which PS in pH 6.7 milk (the highest pH of their study) was found to increase initially up to 7 min and then leveled off. Assuming that κ-CN dissociation from the micelle should increase with heat treatment intensity, it may well be possible that, even at pH 7.1, binding is initially favored until a larger degree of κ-CN is dissociated into the serum portion, which then allows for the formation of serum complexes (AWP). As Sinaga et al. (2016) also reported that alkaline pH corresponds to a decrease in micelle gel strength, another hypothesis may be that complexes are formed on the micelle initially, however the weakening of the micelle surface the dissociation of surface κ-CN at pH 7.1 (Anema & Klostermeyer, 1997; Donato & Dalgleish, 2006) may results in bound complexes which are not strong enough to maintain their structure, thus liberating them to the serum portion. In proposing this, it must be assumed that the formation of AWP does not have a considerable effect on the changes observed in PS measurements. Previous reports have found AWP to have a diameter of approximately 60-70 nm (Jean et al., 2006; Vasbinder & de Kruif, 2003), which is in the range of the capabilities of the BIC ZetaPALS instrument (1 nm to 100 μm diameter, sample dependent). However, as we did not observe numerous peaks in the DLS spectra, we may assume that the formation of aggregates does not greatly affect the reported values in Figure 8.4, and as such any increases in PS are likely due to the formation of BWP.

8.3.3 Light backscatter

As in Chapter 5 and 6, all data presented on light backscatter intensity is taken on or near the wavelength corresponding to the maximum intensity of the light backscatter spectra. To reinstate our purpose, our primary goal was to find useful relationships using only one wavelength in order to develop the simplest sensor possible. The use of numerous spectral wavelengths may indeed increase correlative data, however in our previous study we did not observe greater data fitting when using a ratio of wavebands for model formation (Chapter 7). Thus, in Figure 8.5 only the approximate maximum intensity (wavelength 540 nm) (LB) is plotted at each respective pH and heat treatment time. The general trends are quite similar to that of PS (Figure 8.4), in that there is a noticeable increase in LB with time at pH 6.3, and at pH 7.1 there are little to no observable changes. In our previous study (Section 5.3.1), a

negative correlation was found to exist with LB and pH (Table 5.2), but at pH 7.1 no correlation existed between LB and temperature (Table 5.2).

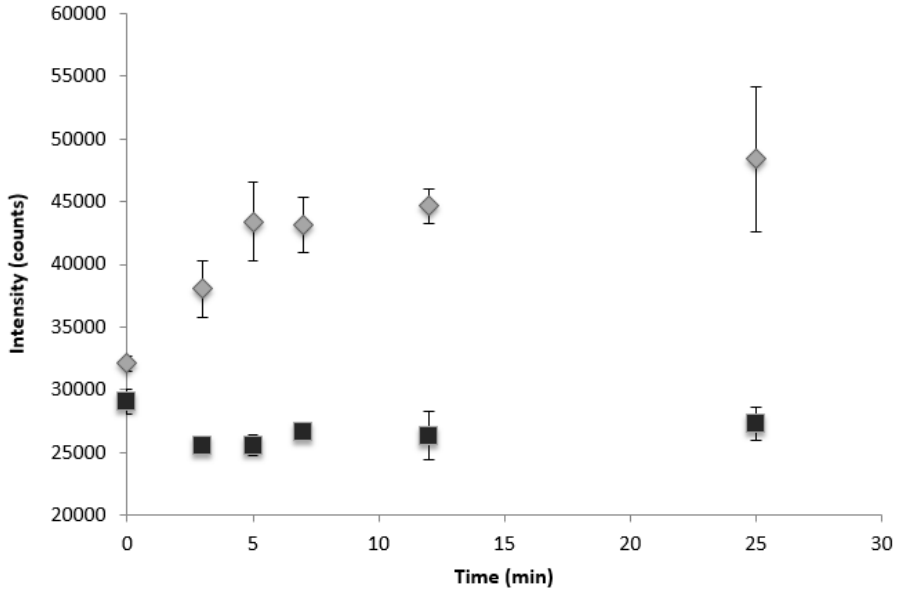

Figure 8.5. Light backscatter intensity at 540 nm as a function of heat treatment time at pH 6.3 (◆) and 7.1(■).

In order to utilize the LB signal for modeling of the whey protein denaturation mechanism, both the formation of BWP and AWP should be considered. Considering the similarities in trends in BWP (Figure 8.2), PS (Figure 8.4) and LB at pH 6.3 (Figure 8.5), there may be some potential for use of PS or LB as a useful tool in measuring BWP. On the other hand, PS and LB curves at pH 7.1 show relatively little change with an increase in heat treatment time. However, where pH 7.1 curves of PS show an initial increase (Figure 8.4), LB curves show an initial decrease and then leveling off (Figure 8.5). If we consider that κ-CN dissociation has been found to occur to a greater extent at pH > 6.7 with an increase in heat treatment intensity (Anema & Klostermeyer, 1997; Donato & Dalgleish, 2006), perhaps the decrease in LB observed in initial pH 7.1 milk is due to a decrease in surface κ-CN. Using a similar light backscatter optical setup, Blanco (2016) observed a significant decrease in LB signal at 880 nm in untreated refrigerated milk and attributed this to the micellar loss of β-CN which has been found to occur during refrigerated milk storage, and also may cause to a lesser extent κ-CN and α_s-CN release (Eck, 1990). On the other hand, this idea is contrary to

PS results, as previously mentioned, since this initial decrease was not observed in PS at pH 7.1 (Figure 8.4), however it should be noted that an increase in casein micelle size at pH 7.0 was also observed by Sinaga et al. (2016) as a result of increased casein dissociation. Another observation is that LB curve at pH 6.3 does not follow an incremental increase, which is observed for BWP and PS at pH 6.3, as there is a break around 7 min and then a further increase (Figure 8.5). Nonetheless, if we take into account the error bars associated with PS (Figure 8.4) and LB (Figure 8.5), these tendency differences may be negligible.

8.3.4 Front-face fluorescence

Fluorescence analysis was also investigated for inline implementation in comparison to or as a complementary technique to the optical light backscatter system. Implementation of front-face fluorescence (FFF) is also a possibility for inline sensor development as it can be used directly with turbid samples and protein fluorescence may be useful to provide more detailed information regarding protein configuration changes. The primary amino acid fluorophore is tryptophan (Trp) and its fluorescence can be interpreted mainly by differences in intensity as a result of availability, or by the observation of red/blue shift from a change in the location of the fluorophore. It is generally assumed that during whey protein denaturation a red-shift is observed as Trp residues become exposed and move from a nonpolar (folded) to a polar (unfolded) environment, whereas proteins which embed into a micelle may result in a blue-shift (Caputo & London, 2003). In addition, Trp residues may be affected by their proximity to quenching compounds, resulting in a decreased fluorescence intensity.

Fluorescence intensity at 340 nm is shown in Figure 8.6 where at pH 6.3 an increase with time is observed. In the case of FFF at pH 7.1, a slight but relatively steady increase occurs with heat treatment time (Figure 8.6), which is uniquely different than PS and LB where no noticeable changes occurred. The initial intensity increased by 3.7 units from t_0 - t_7 at pH 6.3 and 1.7 units at pH 7.1. Further intensity increases up to t_{25} were only 0.3 units at both pH values, totaling 4 and 2 unit for pH 6.3 and 7.1, respectively (Figure 8.6). These observations are in accordance to those of Liu, Powers, Swanson, Hill, & Clark (2005) who observed notable increases in FFF intensity up to 2.5 min of High Hydrostatic Pressure (HHP) in whey protein concentrate (WPC) and only a slight increase in intensity after 5 min, suggesting the majority of changes in the Trp environment occurred within 2.5-5 min of HHP treatment. The fluorescence studies of Rahimi Yazdi & Corredig (2012) and

Boubellouta & Dufour (2008) also observed an increase in Trp fluorescence intensity in heat treated milk, however the majority of literature studies observed a decrease in FFF after treatment (Dufour & Riaublanc, 1997; Birlouez-Aragon et al., 1998; Birlouez-Aragon et al., 2002; Kulmyrzaev et al., 2005). Schamberger & Labuza (2006), however, observed no changes in FFF intensity, except at their highest heat treatment combination (140 °C, 30 s) where a decrease in intensity was also observed. Nonetheless, a study by Ayala (2012) observed a trend in heat treated milk in which an increase in Trp fluorescence was found to occur up to t_{45} min and then decrease at t_{60} min at 80 °C, which supports our observations, whereas more intense heat treatment (90 °C and 100 °C) resulted in a decrease at all time intervals of the study.

Another noteworthy observation is that other studies using pH-altered milk observed an increase in fluorescence intensity with decreasing milk pH (Boubellouta & Dufour, 2008). Chakraborty & Basak (2007) investigated Trp fluorescence in casein subunits (a_s-CN, β-CN and κ-CN) and found a sharp increase in intensity from pH 7 to pH 6. Trp fluorescence intensity also increased in β-LG variants (from 70-90 °C, 10 min) with greater increases occurring at lower pH values (Manderson et al., 1999). In particular, FFF intensity increased only slightly at pH 7.4, whereas at pH 6.7 large increases in FFF intensity were observed in both β-LG A and B from 70-80 °C, even though at 80-90 °C β-LG-A FFF intensity decreased while β- LG B showed little change in FFF intensity. Manderson et al. (1999) proposed this decrease in β-LG A intensity to be due to their observation of a higher content of unfolded β- LG A from SDS-PAGE analysis. Interestingly this notion may be related to our previous findings where β-LG A was found to be involved in the formation of soluble aggregates to a greater extent at pH 6.3 and 6.7 than β-LG B (Chapter 6, Figure 6.5), as per its greater affinity for aggregation, as reported in the literature (Anema & McKenna, 1996; Bello et al., 2011).

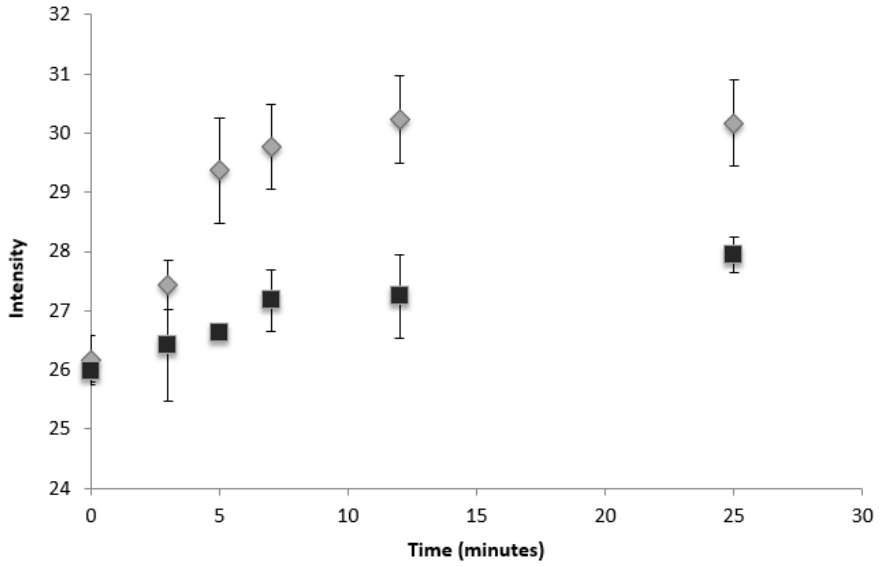

Figure 8.6. Tryptophan fluorescence at max wavelength (~340 nm), angle of 60˚, excitation at 290 nm, emission 305-450 nm, at pH 6.3(◆) and 7.1(■).

Calculation of the maximum intensity wavelength at each respective heat treatment time showed that at pH 6.3 there was a slight blue shift, which was the largest at 3 min (0.83 nm), however remained relatively unchanged with further heat treatments (Table 1.). Our results follow similarly to those found by Rahimi Yazdi & Corredig (2012) in which a small blue shift was observed during curcumin binding to the casein micelle, along with an increase in Trp fluorescence intensity after heat treatment (80 °C, 10 min). This study also gave insight into the binding capacity of casein micelles in whey protein-free milk, in which the addition of increased curcumin concentration acted to quench Trp almost entirely, which they suggested was due to curcumin binding to the casein micelle. Although these results appear to be contrary to our observed increase in FFF at pH 6.3, when Rahimi Yazdi & Corredig (2012) studied heated skim milk they found curcumin fluorescence to be higher (11 units) than in whey protein-free milk, and suggested that this is a result of an increase in casein micelle binding of curcumin due to the attachment of whey proteins to the casein micelle. Thus, the observed blue shift due to binding is expected, however the increase in intensity at pH 6.3 is still difficult to explain if we consider the potential for Trp fluorescence quenching during the formation of a *κ*-CN/whey protein complex on the surface of the micelle. Still, it is possible that the unfolded whey proteins attached to the micelle remain in their reactive form, resulting in exposed Trp residues from the layer of whey proteins on the micelle

surface. The slight decrease in FFF intensity observed at t_{25} (Figure 8.6) may support this idea as this decrease corresponds to a leveling off of BWP (Figure 8.3) which we may assume is the result of residues becoming buried as the binding reaction proceeds with heat treatment.

Table 8.1. Fluorescence intensity shift during heat treatment of milk at 80 °C.

			Time (min)				
			3	5	7	12	25
pH	6.3	Max wavelength (nm)	339.00	339.50	340.00	339.17	339.83
		Shift (nm)	-0.83	-0.33	0.17	-0.67	0.00
		Red/blue	blue	blue	red	blue	n/a
	7.1	Max wavelength (nm)	340.33	343.50	343.33	342.50	344.25
		Shift (nm)	0.67	3.83	3.67	2.83	4.58
		Red/blue	red	red	red	red	red

At pH 7.1 we also observe a gradual increase in FFF intensity, however at a lower intensity than the pH 6.3 curve (Figure 8.6). As whey protein denaturation progresses at pH 7.1, it is assumed that whey proteins unfold and primarily self-associate or form soluble aggregates with with κ-CN as heat treatment time increases. Although whey protein unfolding should considerably increase fluorescence intensity from exposure to Trp residues, Renard et al. (1998) observed self-quenching to occur in β-LG due to monomer-dimer association as a result of heat-induced aggregation formation. As well, Kulmyrzaev et al. (2005) has proposed that the shielding effect from protein-protein aggregates has a greater effect to decrease FFF intensity than does the increase in intensity as a result of protein unfolding. The red shift observed at pH 7.1 is an interesting finding (Table 8.1.) and may be well-explained if we consider that during denaturation whey proteins unfold and move from a nonpolar native state to an unfolded polar state (Moro et al., 2001; Liu et al., 2005). This is in contrast to the slight to the blue shift observed at pH 6.3, which we consider to occur when unfolded whey proteins bind to the hydrophobic portions of the casein micelle (Rahimi Yazdi & Corredig, 2012). In studying the effect of HHP on WPC, Liu et al. (2005) also observed a red shift up to 2.5 min of treatment and minimal changes in maximum intensity wavelength with further treatment. Our results are complementary to this study in which the initial red shift (4 nm, t_5) is prominent whereas any further shifting is slight with a shift of only 1 nm occurring from 7- 25 min (Table 8.1.).

8.3.5 Kinetics and correlation statistics

Kinetic rate constants were estimated for each respective technique, and separated by pH for all tested methods. In forming any recommendations for sensor development, we considered both the kinetic rate constants (Table 8.2) and reliability of that data, as well as the Pearson correlations between each respective measurement technique (Table 8.3). One limitation is that in some cases low R^2 for the rate constants resulted in uninterpretable conclusions from this work. However, this mainly occurred in techniques which were expected to see very little change with increase in heat treatment temperature, for example in pH 6.3 AWP and pH 7.1 BWP, LB and PS. As a result, these values will not be discussed in much detail as we considered these results to be inconclusive due to low R^2 (less than 0.70) (Table 2).

Table 8.2. Kinetic analysis of apparent first-order model fit for native, bound, aggregate whey protein, particle size, light backscatter and fluorescence changes in milk.

			k x 10^2 (min^{-1})	R^2	± 95% CL	Lower 95% CL	Upper 95% CL	Significance		
	6.3	NWP	5.37	0.93	1.02	4.35	6.39	*a*		
		BWP	11.62	0.87	13.5	-1.86	25.1	*a*	*b*	*c*
		AWP	1.17	0.12	9.32	-8.19	10.5	*		
		PS	2.07	0.93	1.03	1.04	3.10		*b*	
		LB	2.71	0.71	3.17	-0.47	5.88	*a*	*b*	*c*
		FFF	1.23	0.82	1.06	0.17	2.29		*b*	*c*
	7.1	NWP	5.42	0.95	0.913	4.51	6.33	*a*		
		BWP	28.21	0.49	87.8	-59.5	116	*		
		AWP	8.88	0.90	4.06	4.82	12.9	*a*		
		PS	0.05	0.02	1.35	-1.31	1.40	*		
		LB	0.38	0.50	1.16	-0.77	1.54	*		
		FFF	0.41	0.88	0.285	0.13	0.70			*c*

NWP, native whey protein content; BWP, bound protein content; AWP, aggregate whey protein content; LB, light backscatter intensity at 540 nm; FFF, Tryptophan fluorescence intensity at 340 nm; PS, particle size diameter. Equation fit to first-order kinetic model, formulas with the same letter are not significantly different at $p < 0.05$; ± 95% CL, mid-point of confidence interval; * too low R^2 to be interpretable.

NWP content follows a nearly identical curve (Figure 8.1A) at both pH values and the rate of change (k) was not significantly different between pH 6.3 and pH 7.1 (Table 2).

In addition, there were no observable correlations (Table 3) in NWP with any variables other than time, which is of course expected considering heat treatment time will result in a considerable less NWP content. Lamb et al. (2013) measured the rate of *β*-LG and *a*-LA according to first-order kinetics and found rate constants of $9.4x10^{-2}$ min^{-1} and 2.4 $x10^{-2}$ min^{-1}, respectively. Considering the majority of WP is *β*-LG (~65%) with *a*-LA comprising ~25% (Haug et al., 2007), the rate observed in our study ($k_{6.3}$ = $5.37x10^{-2}$ min^{-1}, R^2= 0.93 and $k_{7.1}$ = $5.42x10^{-2}$ min^{-1}, R^2= 0.95) would still be smaller than the rate of Lamb et al. (2013). Yet it is may be comparable if we take into account the different heat treatment, quantification technique (SDS-PAGE vs. HPLC), and consider that in their study a heat pre-treatment was implemented.

BWP at pH 6.3 should relatively corresponds to AWP content at pH 7.1 if we assume that the primary mechanisms at pH 6.3 and 7.1 are binding and soluble aggregate formation, respectively. This assumption falls in line with our data as the kinetic rate constant of BWP at pH 6.3 ($11.62x10^{-2}$ min^{-1}, R^2= 0.87) is not statistically different to that of aggregate at pH 7.1 ($8.88x10^{-2}$ min^{-1}, R^2= 0.90) (Table 8. 2) and these two are also not statistically different from the rates of decrease in NWP ($k_{6.3}$ = $5.37x10^{-2}$ min^{-1}, R^2= 0.93 and $k_{7.1}$ = $5.42x10^{-2}$ min^{-1}, R^2= 0.95). Even though this relationship has not been clearly shown in any current published work, it has been suggested to occur. For example, Vasbinder & de Kruif (2003) reported bound *β*-LG at pH 6.35 to be in the highest proportion (~80%) compared to *β*-LG soluble aggregates composing the majority at pH 6.9 (~50%). Contrary to this study, we observed a higher %AWP at pH 7.1 (~52%) than %BWP at 6.3 (~38%) (Figure 8.3). Nonetheless it should be considered that Vasbinder & de Kruif (2003) reported %NWP to be slightly lower than our value (at 80 °C, 10 min: ~20-25% native *β*-LG and ~58-62% *a*-LA calculated value versus ~40-60% of this study), which may help explain this discrepancy.

Thus, considering our objective to implement optical techniques (LB and FFF) for modeling total whey protein denaturation, we also determined the kinetic rate constants for these three techniques at each respective pH. In comparing rate constants at pH 6.3 for PS, LB and FFF, R^2 values greater than 0.70 were observed in all cases and were found to be statistically similar (2.07, 2.71, $1.23x10^{2}$ min^{-1}, respectively) (Table 8.2). As well, the rate constant of FFF at pH 7.1 ($0.41x10^{2}$ min^{-1}) is not statistically different from FFF at pH 6.3 ($1.23x10^{2}$ min^{-1}). LB and BWP at pH 6.3 are not statistically different from any of the rate constants with $R^2 > 0.70$ (Table 8.2). From this, we may suggest that the similar rate constants observed for LB, PS and FFF to be useful in sensor implementation, as they are particularly

comparable to BWP at pH 6.3. Nonetheless, as some kinetic rate constants were not compared, further interpretation of this data will be discussed from the Pearson correlations of Table 8.3.

Table 8.3. Pearson Correlation of native, bound and aggregate whey protein content with independent variables and dependent optical variables.

	pH	t	NWP	BWP	AWP	LB	FFF
t	0.28ns						
NWP	0.17ns	0.85**					
BWP	0.80*	0.01ns	0.30ns				
AWP	0.87**	0.58ns	0.53ns	0.61ns			
LB	0.98***	0.17ns	0.01ns	0.88**	0.83**		
FFF	0.79*	0.19ns	0.37ns	0.93***	0.56ns	0.90***	
PS	0.70*	0.11ns	0.19ns	0.93***	0.66ns	0.80**	0.86**

N=6; NWP, native whey protein content; BWP, bound protein content; AWP, aggregate whey protein content; LB, light backscatter intensity at 540 nm; FFF, Tryptophan fluorescence intensity at 340 nm; PS, particle size diameter; t, time; * $P<0.05$, ** $P<0.01$, *** $P<0.001$, ns not significant.

Pearson correlations were also determined to look at comparisons between analysis techniques (PS, LB, FFF) and protein portions (NWP, BWP, AWP) (Table 8.3). As expected, all variables, except NWP, showed positive and significant correlations with pH as these reactions have been observed to be pH-dependent. More notable are the correlations found which may suggest that optical techniques may be used to measure changes in whey protein denaturation, in particular that of BWP and AWP. LB showed significant correlations with both BWP and AWP, whereas PS and FFF only showed significant correlations with BWP (Table 8.3). This observation was found in our previous study, in that only LB showed any relationship with AWP (CORR, r= -0.60) (Table 6.3), even though this CORR is negative likely as a result of the study parameters (pH 6.3, 6.7, .7.1 heated for 10 min at both 80 and 90 °C). It should be considered that as Pearson correlations were determined including all pH values they cannot necessarily represent specific changes at each pH, but a summary of the total change in heat treatment variables at all pH values. As well, a strong correlation was observed between LB and FFF (Table 8.3), which gives confirmation that these two techniques are likely monitoring similar phenomena. Nonetheless, this is the first study of this dissertation which considered FFF analysis, and we should take into account that these

observations utilize a single wavelength intensity, and thus are likely to be improved with further investigation into the numerous points on both the FFF and LB spectra. Further work in this area is to be presented in the upcoming chapter (Chapter 9). Even so, with the information of our current studies, LB appears to be the more comprehensive method for potential measurement of changes in whey protein denaturation of both BWP and AWP. Nevertheless, we do not wish to insinuate this until we look into the full spectra and develop methodologies for modeling BWP and AWP. It is necessary to highlight that this study was used as a preliminary look between the relationship of BWP, AWP and NWP content with respect to various optical techniques, and an important part of the data analysis using a combination of spectral wavelengths (in the case of LB and FFF data interpretations), rather than just a single wavelength, will be discussed in the next section of this work (Chapter 9).

8.4 Conclusions

The milk pH values that were selected for this study were intended to represent a majority of binding (pH 6.3) and a majority of soluble aggregate formation (pH 7.1), which have been well represented in the literature to occur primarily in these pH ranges (Vasbinder and de Kruif, 2003; Donato and Guyomarc'h, 2009; Kethireddipalli et al., 2010). The purpose was to compare BWP and AWP to the analytical techniques of particle size, light backscatter and tryptophan fluorescence for work toward the development of an inline optical sensor for the determination of total whey protein denaturation in heat-treated milk. Our study suggests that BWP formation at pH 6.3 has potential to be measured using the optical techniques (LB, PS, FFF). In the case of AWP, however, only LB showed statistically similar rate constant and Pearson correlation (Tables 2, 3), however FFF at pH 7.1 showed a clear red shift, which should be further investigated.

It should be noted that these trends are compiled using the maximum intensity information, where other authors (Kulmyrzaev et al., 2005; Boubellouta and Dufour, 2008; Boubellouta et al., 2009) used multiple variable analysis, such as principle component analysis (PCA) and parallel factor analysis (PARAFAC), combined with FFF technology. In light backscatter the use of multiple wavelengths intensity regions for modeling has in certain cases shown increased correlations in whey protein denaturation (Lamb et al., 2013). It is possible that by incorporating chemometric techniques improvements might be found in our spectral analysis. However, this study is intended to be a preliminary assessment of the

potential for an optical sensor in which the use of one or two light detectors facilitates sensor convenience and cost. Chapter 9 looks further into various regions on the spectra for the development of models for estimation of BWP, NWP and AWP.

CHAPTER 9: Variables of whey protein denaturation prediction models utilizing specific regions of the light backscatter and tryptophan fluorescence spectra

9.1 Introduction

As mentioned in Chapter 8, modeling of whey protein denaturation variables of Experiment II is of interest to complement the models of Chapter 7, which used a constant time and variable temperature (80 and 90 °C) of heat treatment, and as well to compare with the study of Lamb, Payne, Xiong, & Castillo (2013) which used a similar light backscatter optical sensor set-up to model *β*-LG denaturation in milk.

As denatured whey proteins may either attach to the surface of the casein micelle or form soluble whey protein aggregates in the serum portion of the milk, it is uncertain the specific effect these interactions may have on the quality of milk products. To gain information about the specific configurations of whey proteins in denatured milk; model equations were determined for both whey protein interactions, BWP and AWP, that occur as a result of thermal treatment. Implementing a sensor which not only measures total denaturation of whey proteins, but in addition, the respective configuration of further interactions upon heating, could be useful to distinguish milk batches based on their specific reactivity based on their location (bound to casein micelle, in serum as soluble aggregates) in the milk matrix during cheese or yogurt manufacturing. As in Chapter 7, both maximum intensity wavelength and ratio models will be discussed.

9.2 Materials and Methods

9.2.1 Maximum wavelength models

Prediction models were developed to further demonstrate the effectiveness of LB and FFF for implementation into an optical sensor to define the whey protein denaturation parameters in milk. Maximum wavelength models were compiled using the intensity values associated with the approximate maximum wavelengths from LB (540 nm) and FFF (340 nm). All results were obtained using SAS software version 9.3 (SAS System, Cary, NC, USA, 2013). Models were determined using PROC GLM with LB and FFF as independent

variables and PS, NWP, BWP and AWP as dependent variables. For each modelization, both linear and quadratic equations were tested, following the format of Eqn 4.4 and Eqn 4.5, respectively, with x representing independent variables and y representing dependent variables. Successful models were evaluated by R^2 at each respective pH.

All models were calculated using average experimental values for the variables. Averages were taken due to the fact that each sample technique was uniquely independent and therefore the number of samples did not directly correspond to those that were measured with a different quantitative technique (Table 9.1). Sample replications are shown in Table 9.1. Each average represents a total of eight measurements for NWP, BWP and AWP (using BCA protein analysis) and nine measurements for PS, LB and FFF. Another important aspect is that milk samples were pH-adjusted and heat treated separately for each measurement of light backscatter, fluorescence, whey protein configurations and particle size. Considering potential sampling error that may occur from pH-adjustment and heat-treatment procedures, individual sample adjustments were used to ensure that any improper adjustment did not affect all variables in the replication. If the experiment were to be done using only one heat treatment/adjustment for all measurements in a replication, improper pH-adjustment and/or heat treatment would be dispersed through all the analytical techniques. Therefore the preferred method for milk preparation was individual pH-adjust and thermally treat each individual milk sample.

Table 9.1. Replications and scans per replications for each analytical technique (represented by average values in this study).

Technique	replications	scans/rep	**Total values averaged**
BCA	4	2	**8**
PS	3	3	**9**
LB	3	3	**9**
FFF	3	3	**9**

9.2.2 Ratio models

The objective of this portion of analysis was to model the diameter of the casein micelle and the characteristics of the whey protein configurations after denaturation (NWP, BWP and AWP) based on the spectrum (either LB or FFF) versus time for each pH. The average data points from each respective technique have been fit to determine the models with the highest R^2 by identifying the specific spectral regions which best describe the

evolution of each response variable. Variables were categorized as either Ratio Spectrum models or Dependent Variable models. Ratio Spectrum (RS or ratio) models were determined to measure the consistency of the spectrum of both LB and FFF spectra with time as the independent variable, and separated by pH. On the other hand, the Dependent Variable models, named further DV or by the specific dependent variable of interest (PS, NWP, BWP, AWP), used the light backscatter and fluorescence spectra as the independent variable with the dependent variable PS, NWP, BWP and AWP. Linear (Eqn 4.4), quadratic (Eqn 4.5) and cubic (Eqn 4.6) models were tested in RS models as a function of time; linear, quadratic and exponential (Eqn 4.7) models were tested for PS, NWP, BWP and AWP as a function of LB and FFF ratio. All models were separated by milk pH.

All results were obtained using SAS software version 9.3 (SAS System, Cary, NC, USA, 2013). Statistical significance has been carried out using a significance level of 0.05. Ratios were determined for both light backscatter and fluorescence spectra following the procedure explained in Section 7.3.2.1 where wavebands in groups of 5, 15, 25, 35, 45 units of wavelength were modeled against each respective waveband. The majority of top five ratios in each variable model were from ratios of 5 nm wavebands, as determined from the highest coefficient of determination (R^2), and therefore, in this study, all top models were formed using a 5 nm waveband criteria.

The goal of RS models was to determine the initial quality of each specific ratio combination, and then implement ratios into DV models. Each DV model first considered the ratio combinations which had R^2 values >0.65 in the RS model and then used those selected ratios for implementation into a DV model. An example of the initial spread R^2 values of the RS model of BWP are shown in Figure 9.1A and many ratios with high R^2 were observed. Then models were cross referenced between RS model ratios and DV model ratios. Models with significant parameters (R^2 values >0.65) in both the DV model (in this case BWP f(LB)) and the RS model as a function of time for each pH are shown in Figure 9.1B. The top five models (considering models with significant explanatory variables) are shown in Table 9.2 for both LB and FFF models. Models are ranked according to the R^2 of both RS and PS models. The numbers in the Ratio Spectrum column represent the region of the spectra where the ratio was taken, and will be described further in Section 9.3.2.1.

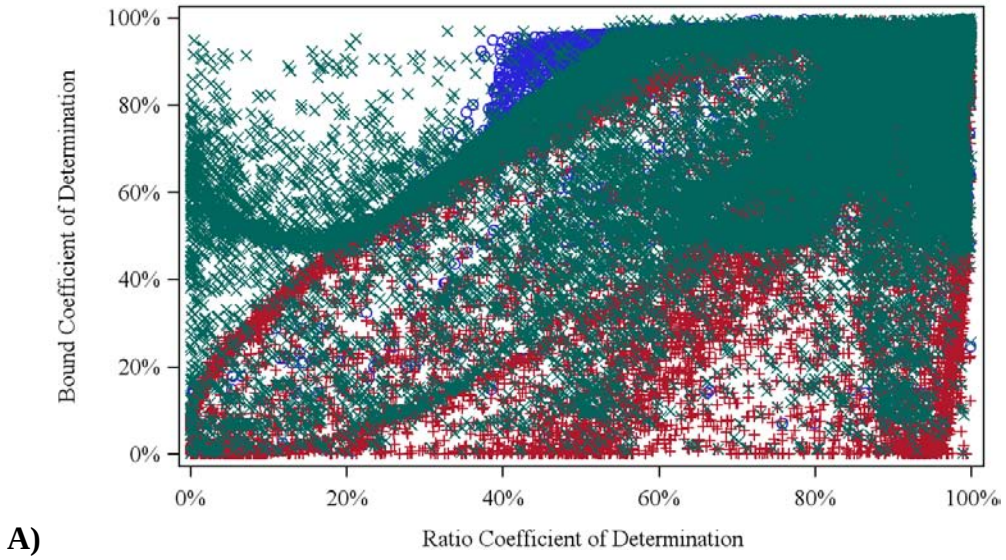

A)

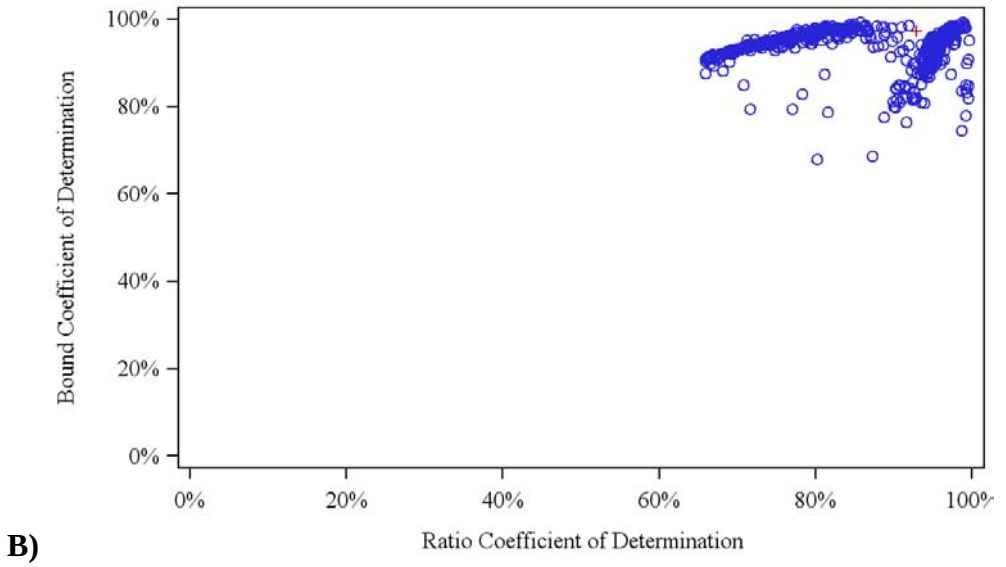

B)

Figure 9.1. A) All possible combinations of BWP versus Ratio model R^2 values and B) BWP versus Ratio model where R^2 is higher than 65% in LB and FFFS models at pH 6.3 of 5 nm waveband models; (green) exponential; (blue) linear; and (red) quadratic models.

Table 9.2. Top five ratios of LB considering both BWP and Ratio models with highest R^2 at pH 6.3 of 5 nm waveband models.

Ratio Spectrum	BWP Model	R^2	Ratio Model	R^2
LB_32_150	Linear	0.993	Quadratic	0.989
LB_29_162	Linear	0.988	Quadratic	0.999
LB_4_150	Linear	0.983	Quadratic	0.991
LB_32_159	Linear	0.986	Quadratic	0.988
LB_4_159	Linear	0.985	Quadratic	0.988
FFF_2_11	Linear	0.975	Quadratic	0.975
FFF_2_12	Linear	0.942	Linear	0.935
FFF_2_17	Linear	0.983	Linear	0.879
FFF_2_10	Linear	0.940	Linear	0.920
FFF_2_16	Linear	0.895	Linear	0.960

9.3 Results

9.3.1 Maximum wavelength models

The approximate maximum wavelengths determined for LB (LB_{max}= 540 nm) and FFF (FFF_{max} = 340 nm) were implemented into models for the determination of denaturation factors (PS, NWP, BWP, AWP) measured in the study. All response variables were modeled as a function of both LB_{max} and FFF_{max} into linear and quadratic pH-separated models and pH-integrated models.

Figure 9.2 shows the plot of the models for particle size as a function of LB_{max} in a linear model (Figure.9.2A) and as a function of FFF_{max} in a quadratic model (Figure 9.2B) considering all data at both pH values (integrated model). Integrated models were tested, however will not be thoroughly discussed in this section. Instead, it was of interest to considering the extreme pH values (6.3 and 7.1) used in this study for the purpose of finding models to determine BWP and AWP. Even though some integrated models displayed relatively good R^2 values, it can be observed that more than 50% of the data points (likely due to pH 7.1 where there is little response) lie in a saturated region. In particular, Figure 9.2A and 9.2B show that the majority of data points for pH 7.1lie between 160-165 nm. Thus, taking this into consideration, it is unfit to characterize pH-integrated models and is

further assumed that these models should be investigated using more pH values, as pH 7.1 has exhibited relatively little change with heat treatment in nearly all analytical techniques (Figure 8.2, 8.4, 8.5). Accordingly, integrated models will not be thoroughly discussed in this section.

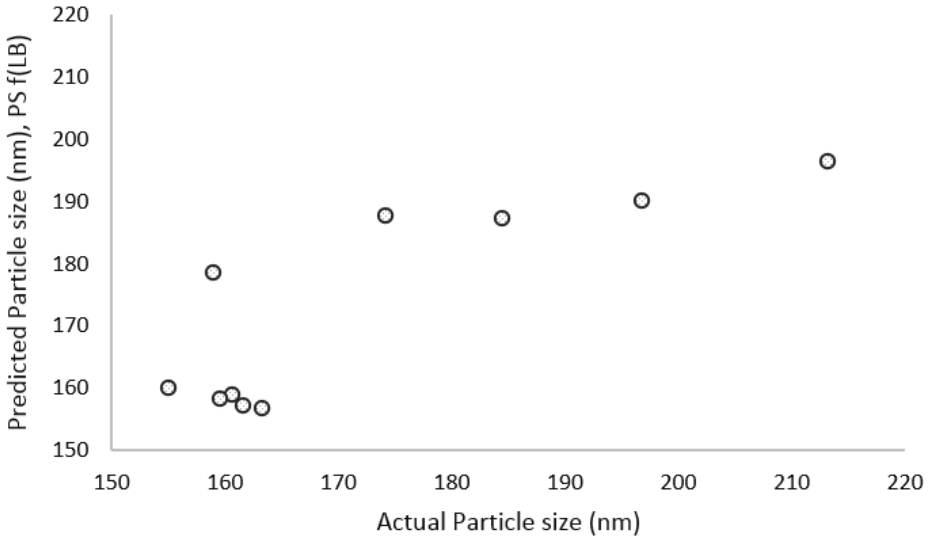

A)

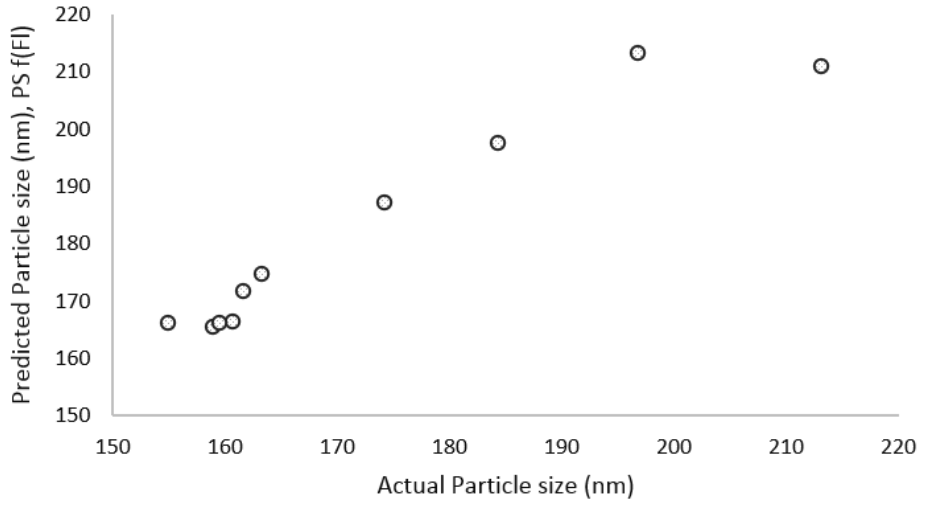

B)

Figure 9.2. Particle size pH-integrated prediction models A) PS f(LB), linear model (y = 113 + 0.0017x, R^2 = 0.707), B) PS f(FFFS), quadratic model (y = 402 +0.0016x + 0.0000006x^2, R^2 = 0.927).

Coefficients and regressions statistics for all models are found in Tables 9.3-9.6. Tables are separated by dependent variable, where Table 9.3 represents all PS_{max} models, Table 9.4 represents all NWP_{max} models, Table 9.5 BWP_{max} and Table 9.6 AWP_{max} models.

Table 9.3 Prediction models using approximate maximum wavelength intensity to model particle size as a function of LB and FFF.

	pH	Eqn type	DF_{err}	Regression coefficients		s	SSE	R^2 model	SEP model
PS f(LB)	6.3	linear	3	β_0 =	-46.1	41.9	153	0.911	7.13
				β_1 =	$5.32x10^{-3}$	$9.59x10^{-4}$			
		quadratic	2	β_0 =	252	525	131	0.924	8.10
				β_1 =	$-8.62x10^{-3}$	$2.45x10^{-2}$			
				β_2 =	$2.00x10^{-7}$	$3.00x10^{-7}$			
PS f(FFF)	6.3	linear	3	β_0 =	-273	153	429	0.751	12.0
				β_1 =	15.6	5.19			
		quadratic	2	β_0 =	$8.19x10^3$	$5.39 x10^3$	192	0.888	9.79
				β_1 =	-573	375			
				β_2 =	10.2	6.51			

N=5, DF err, degrees of freedom for error; $\beta_{0\text{-}2}$, prediction coefficients; s, standard error of the estimate for coefficients; SSE, sum of squares for error; R^2, determination coefficient; SEP, standard error of prediction for the model: PS (nm).

Table 9.4 Prediction models using approximate maximum wavelength intensity to model native whey protein as a function of LB and FFF.

	pH	Eqn type	DF_{err}	Regression coefficients		s	SSE	R^2 model	SEP model
NWP f(LB)	6.3	linear	3	β_0 =	$1.59x10^4$	$2.99x10^3$	$7.77x10^5$	0.812	509
				β_1 =	-0.247	0.068			
		quadratic	2	β_0 =	$1.24x10^4$	$4.03x10^4$	$7.74x10^5$	0.813	622
				β_1 =	-0.082	1.88			
				β_2 =	$-2.00x10^{-7}$	$2.00x10^{-5}$			
	7.1	linear	3	β_0 =	$3.69x10^4$	$1.01x10^4$	$1.00x10^6$	0.766	578
				β_1 =	-1.21	0.386			
		quadratic	2	β_0 =	$4.21x10^4$	$5.39x10^5$	$7.94\ x10^6$	0.815	630
				β_1 =	-30.8	40.9			
				β_2 =	$6.00x10^{-4}$	$8.00x10^{-4}$			
NWP f(FFF)	6.3	linear	3	β_0 =	$2.79x10^4$	$7.22x10^3$	$9.59x10^5$	0.769	565
				β_1 =	-774	245			
		quadratic	2	β_0 =	$-4.84x10^5$	$1.19x10^5$	$9.33x10^5$	0.977	216
				β_1 =	$3.48x10^4$	$8.27x10^3$			
				β_2 =	-618	144			
	7.1	linear	3	β_0 =	$4.88x10^4$	$1.01x10^4$	$5.93\ x10^5$	0.862	444
				β_1 =	$-1.61x10^3$	373			
		quadratic	2	β_0 =	$6.57x10^5$	$5.47x10^5$	$3.66\ x10^5$	0.915	428
				β_1 =	$-4.64x10^4$	$4.03x10^4$			
				β_2 =	823	823			

N=5, DF err, degrees of freedom for error; $\beta_{0\text{-}2}$, prediction coefficients; s, standard error of the estimate for coefficients; SSE, sum of squares for error; R^2, determination coefficient; SEP, standard error of prediction for the model: NWP (μg/mL).

Table 9.5 Prediction models using approximate maximum wavelength intensity to model bound whey protein as a function of LB and FFF.

	pH	Eqn type	DF_{err}	Regression coefficients		s	SSE	R^2 model	SEP model
BWP f(LB)	6.3	linear	3	β_0 =	-1.11×10^4	2.64×10^3	6.06×10^5	0.898	450
				β_1 =	0.311	0.060			
		quadratic	2	β_0 =	1.72×10^4	2.95×10^4	4.15×10^5	0.930	455
				β_1 =	-1.01	1.38			
				β_2 =	2.00×10^{-5}	2.00×10^{-5}			
BWP f(FFF)	6.3	linear	3	β_0 =	-2.33×10^4	1.01×10^4	1.89×10^6	0.682	794
				β_1 =	875	345			
		quadratic	2	β_0 =	5.41×10^5	3.57×10^5	8.42×10^5	0.859	649
				β_1 =	-3.84×10^4	2.48×10^4			
				β_2 =	682	431			

N=5, DF err, degrees of freedom for error; $\beta_{0\text{-}2}$, prediction coefficients; s, standard error of the estimate for coefficients; SSE, sum of squares for error; R^2, determination coefficient; SEP, standard error of prediction for the model: BWP (μg/mL).

Table 9.6 Prediction models using approximate maximum wavelength intensity to model soluble aggregate whey protein as a function of LB and FFF.

	pH	Eqn type	DF_{err}	Regression coefficients		s	SSE	R^2 model	SEP model
AWP f(LB)	6.3	linear	3	β_0 =	-3.10×10^4	1.48×10^4	2.13×10^6	0.651	842
				β_1 =	1.33	0.562			
		quadratic	2	β_0 =	-7.66×10^5	7.12×10^5	1.39×10^6	0.772	833
				β_1 =	57.2	54.1			
				β_2 =	-1.10×10^{-3}	1.00×10^{-3}			
AWP f(FFF)	6.3	linear	3	β_0 =	-4.49×10^4	1.60×10^4	1.48×10^6	0.757	702
				β_1 =	1.80×10^3	589			
		quadratic	2	β_0 =	-1.27×10^6	6.72×10^5	5.52×10^5	0.909	526
				β_1 =	9.23×10^4	4.94×10^4			
				β_2 =	-1.66×10^3	910			

N=5, DF err, degrees of freedom for error; $\beta_{0\text{-}2}$, prediction coefficients; s, standard error of the estimate for coefficients; SSE, sum of squares for error; R^2, determination coefficient; SEP, standard error of prediction for the model: AWP (μg/mL).

In particular, PS_{max} models exhibited high R^2 for all variables (>0.75) (Table 9.3). Figure 9.3 shows both pH 7.1 (black dots) and pH 6.3 (dotted circles) in a single graph. Data from models for pH 7.1 may in fact exhibit a slight upward trend, nonetheless, after considering that at pH 7.1, PS did not represent a consistent trend, and changes in PS are likely due to various actions of the casein micelle due to pH and *κ*-CN dissociation (Figure 8.4). As a result, it is considered that PS at pH 7.1 is not reliable for model implementation. Models at pH 7.1 had a large portion of their data points isolated, regardless of heat treatment time, with the exception of AWP models, where the opposite was observed (isolated data points at pH 6.3), and NWP curves where no significant difference have been found with pH (Figure 8.1A). In fact, this is expected if we consider that our previous work has suggested that PS measurements may show the potential to observe BWP formation, but likely do not respond to AWP. As a result of these observations, further discussion in this section will be focused only on the models which show a response to time, and will therefore consist of models at pH 6.3 for PS, BWP and NWP, and at pH 7.1 for NWP and AWP.

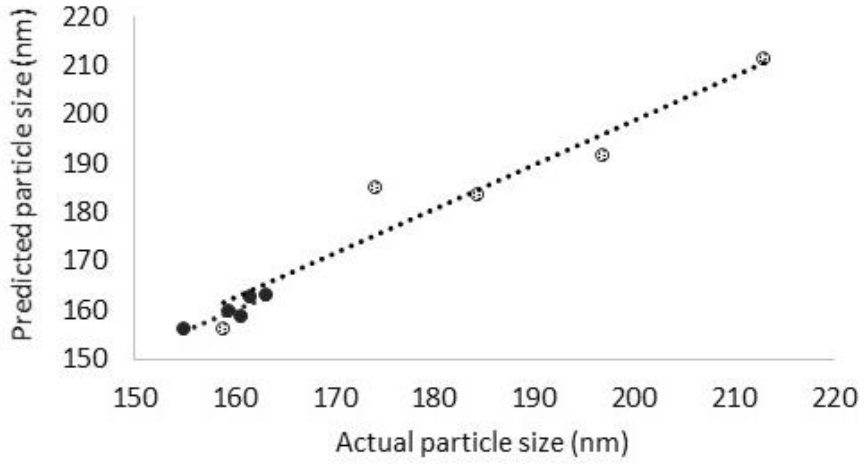

Figure 9.3. Prediction models of pH separated particle size, PS_{avg} f(LB) (6.3 (white circles): y = 0.911x + 16.49; R^2 = 0.911; 7.1 (black circles): y = 0.845 + 24.84; R^2 = 0.845).

When comparing models using linear and quadratic equations, quadratic models exhibited higher R^2 values in all cases (Table 9.3-9.6). Nonetheless, it should be considered that in most cases linear models showed R^2 values greater than 0.65, which we considered to be a fair model representation. In fact, there were only five models where the quadratic equation increased the R^2 by more than 10 percentage points compared to the linear model. Even so, some models showed significant increases using the quadratic model. One example is the AWP model f(FFF_{max}) where the linear model exhibited an R^2 of 0.757 and the quadratic model notably improved the fit (R^2 = 0.909) (Table 9.6). Other than the previously mentioned model, other quadratic models in which R^2 particularly increased were PS f(FFF_{max}) at pH 6.3 (R^2_{lin} = 0.751, R^2_{quad} = 0.888), NWP f(FFF_{max}) at pH 6.3 (R^2_{lin} = 0.769, R^2_{quad} = 0.977) and AWP f(LB_{max}) at pH 7.1 (R^2_{lin} = 0.651; R^2_{quad} = 0.772, respectively) (Table 9.3, 9.4, 9.6). All remaining models increased their R^2 value by less than 0.06 percentage points from linear to quadratic models. In these cases, linear models are preferred due to model simplicity and larger DF (Tables 9.3-9.6).

Considering the DV models at pH 6.3, it was observed that f(LB_{max}) models for PS prediction had higher R^2 at pH 6.3 (R^2_{lin} = 0.911, R^2_{quad} = 0.924) compared to f(FFF_{max}) models (R^2_{lin} = 0.751, R^2_{quad} = 0.888) (Table 9.3). All linear NWP_{max} models represented relatively good models, with R^2 values from 0.76-0.86 (Table 9.4) and also showed high R^2 in their kinetic rate constants (Table 8.1). As we observed a similar curve in both pH 6.3 and pH 7.1 plots of NWP versus time (Figure 8.1A), we would expect models to behave similarly. It is interesting to note that most NWP models improved using a quadratic regression by 5

percentage points in their R^2 values, or more. The only exception was in the case of the pH 6.3 NWP f(LB_{max}) model which did not show any improvements using a quadratic model (R^2_{lin} = 0.812, R^2_{quad} = 0.813).

BWP_{max} models exhibited $R^2 > 0.65$ in all pH 6.3, LB and FFF (Table 9.5). However, LB models proved to fit this variable with higher statistical success, as the R^2 of the linear LB model (0.898) was more than 20 percentage points higher than the FFF linear model (R^2 = 0.682) and the quadratic LB model was near 10 percentage point higher than that of the FFF model R^2 (BWP $f(LB)_{6.3}$, R^2_{quad} = 0.930, BWP $f(FFF)_{6.3}$, R^2_{quad} = 0.859) (Table 9.5). This gives further support to our previously suggested idea that LB_{max} may be useful for BWP determination at pH 6.3. It has also been proposed that AWP may be more effectively modeled using FFF spectra, and fittingly AWP models were found to exhibit higher R^2 f(FFF) than f(LB) (Table 9.6). Actually, the R^2 value of FFF models were more than 10 percentage point larger than LB models, in both the linear and quadratic form (AWP $f(LB)_{7.1}$, R^2_{lin} = 0.651, AWP $f(FFF)_{7.1}$, R^2_{lin} = 0.757 and AWP $f(LB)_{6.3}$, R^2_{quad} = 0.772; AWP $f(LB)_{6.3}$, R^2_{quad} = 0.909) (Table 9.6).

Considering this analysis uses only the approximate maximum wavelength of both the LB and FFF spectra, models maintained relatively high R^2 values to describe most of the explanatory variables. In general, DV models measuring PS exhibited consistently high R^2 values, and in general linear models were preferred as they were not notably different from quadratic models. NWP models for LB_{max} and FFF_{max} also exhibited high R^2 at both milk pH values, however in most cases the quadratic form appeared to show a slightly better relationship to NWP content. Where BWP models exhibited high R^2 at pH 6.3, AWP models showed high R^2 at pH 7.1 (Tables 9.5, 9.6), as expected from their complementary relationship. In general the preferred model is the quadratic form. BWP appeared to be better represented as a function of LB_{max} and AWP as a function of FFF_{max}. Considering the high BWP prevalence at pH 6.3 and aggregate at pH 7.1, this may give evidence to support the notion that LB is useful for determining BWP and FFF for AWP in heat treated milk. However, it should be noted that these are preliminary observations using the approximate maximum wavelength, and further investigation into the whole spectra will be presented in in the upcoming section (Section 9.3.2.1).

9.3.2 Ratio models

The top linear, quadratic and exponential models compiled using ratios of intensities of the LB and FFF spectra are summarized in Tables 9.7- 9.10, for models which show a response to time (pH 6.3 for PS, NWP and BWP; pH 7.1 for NWP and AWP), as previously explained. Tables are separated by explanatory variable, where Table 9.7 represents all PS_{ratio} models, Table 9.8 represents all NWP_{ratio} models, Table 9.9 BWP_{ratio} and Table 9.10 AWP_{ratio} models. Only models which were significant for both DV and RS models (R^2 greater than 0.65) are shown. If no significant models were observed for the variable, no model is shown. Top models were determined by calculating all possible ratios on the LB and FFF spectra, as explained in detail in Section 9.2. The ratios which proved to result in the highest R^2 are shown in each respective table for each respective variable equation.

Table 9.7. Prediction models using pre-selected wavelength ratio intensities to model particle size as a function of LB and FFF.

	pH	Eqn type	Ratio	DF_{err}	Regression coefficients		s	SSE	R^2 model	SEP model
PS f(LB)	6.3	linear	150,168	4	β_0 =	-423	7.19	17.2	0.993	2.07
					β_1 =	581	6.93			
		quadratic	47,51	3	β_0 =	$6.68x10^4$	714	3.94	0.999	1.15
					β_1 =	$-1.70 x10^5$	$1.84 x10^3$			
					β_2 =	$1.08 x10^5$	$1.18 x10^3$			
		exponential	65,167	3	β_0 =	155	0.654	25.3	0.992	2.90
					α_0=	-12.9	0.594			
					α_1=	0.696	0.024			
PS f(FFF)	6.3	linear	7,9	4	β_0 =	$2.93x10^3$	51.2	36.4	0.983	3.02
					β_1 =	$-2.70x10^3$	50.4			
		quadratic	7,9	3	β_0 =	$-3.61x10^4$	$6.77x10^3$	23.0	0.990	2.77
					β_1 =	$7.44x10^4$	$1.34x10^4$			
					β_2 =	$-3.80x10^4$	$6.60x10^3$			
		exponential	16,26	3	β_0 =	148	5.29	202	0.917	8.21
					α_0=	-48.1	9.79			
					α_1=	9.88	1.84			

N=6, DF err, degrees of freedom for error; $\beta_{0\text{-}2}$ and $\alpha_{0\text{-}1}$, prediction coefficients; s, standard error of the estimate for coefficients; SSE, sum of squares for error; R^2, determination coefficient; SEP, standard error of prediction for the model: PS (μg/mL).

Table 9.8. Prediction models using pre-selected wavelength ratio intensities to model native whey protein as a function of LB and FFF.

	pH	Eqn type	Ratio	DF_{err}	Regression coefficients		s	SSE	R^2 model	SEP model
NWP f(LB)	6.3	linear	34,151	3	β_0 =	$-2.95x10^3$	316	$1.71x10^5$	0.978	239
					β_1 =	$3.35x10^3$	289			
	7.1	linear	76,82	4	β_0 =	$9.25x10^4$	$5.40x10^3$	$2.09x10^3$	0.986	23
					β_1 =	$-8.69x10^4$	$5.11x10^3$			
NWP f(FFF)	6.3	linear	4,21	3	β_0 =	$-1.15x10^4$	$1.02x10^3$	$9.59x10^4$	0.979	179
					β_1 =	$3.02x10^3$	253			
	7.1	linear	6,21	4	β_0 =	$-5.76x10^3$	588	$4.97x10^3$	0.967	35.3
					β_1 =	$1.35x10^3$	124			

N=5 (pH 6.3); N=6 (pH 7.1), DF err, degrees of freedom for error; $\beta_{0\text{-}2}$, prediction coefficients; s, standard error of the estimate for coefficients; SSE, sum of squares for error; R^2, determination coefficient; SEP, standard error of prediction for the model: NWP (μg/mL).

Table 9.9. Prediction models using pre-selected wavelength ratio intensities to model bound whey protein as a function of LB and FFF.

	pH	Eqn type	Ratio	DF_{err}	Regression coefficients		s	SSE	R^2 model	SEP model
BWP f(LB)	6.3	linear	32,150	4	β_0 =	4.11×10^3	167	1.63×10^3	0.993	20.2
					β_1 =	-4.26×10^3	178			
BWP f(FFF)	6.3	linear	2,11	4	β_0 =	1.24×10^4	993	5.98×10^3	0.975	38.7
					β_1 =	-2.46×10^4	1.98×10^3			

N=6, DF err, degrees of freedom for error; $\beta_{0\text{-}2}$, prediction coefficients; s, standard error of the estimate for coefficients; SSE, sum of squares for error; R^2, determination coefficient; SEP, standard error of prediction for the model: BWP (μg/mL).

Table 9.10. Prediction models using pre-selected wavelength ratio intensities to model soluble aggregate whey protein as a function of LB and FFF.

	pH	Eqn type	Ratio	DF_{err}	Regression coefficients		s	SSE	R^2 model	SEP model
AWP f(LB)	7.1	linear	1,21	4	β_0 =	-4.30×10^4	1.54×10^4	7.56×10^4	0.667	138
					β_1 =	4.36×10^4	1.54×10^4			
AWP f(FFF)	7.1	linear	11,18	4	β_0 =	3.23×10^4	1.08×10^4	7.18×10^4	0.684	134
					β_1 =	-1.27×10^4	4.32×10^3			

N=6, DF err, degrees of freedom for error; $\beta_{0\text{-}2}$, prediction coefficients; s, standard error of the estimate for coefficients; SSE, sum of squares for error; R^2, determination coefficient; SEP, standard error of prediction for the model: AWP (μg/mL)

PS_{ratio} models exhibited high R^2 in all models (>0.91) (Table 9.7). LB models at pH 6.3 showed R^2 values higher than 0.99 for all three equations (linear, quadratic and exponential). In all PS_{ratio} models the quadratic equation exhibited very high R^2, greater than 0.99 ($LB_{6.3}$: R^2_{quad} = 0.999; $FFF_{6.3}$: R^2_{quad} = 0.990). Exponential models did not significantly improve R^2 compared to quadratic models. Even though quadratic models exhibited the highest R^2 values, in most cases linear models prove to have sufficiently high R^2 values, and are preferred due to simplicity.

Of all the NWP_{ratio} models tested, only linear models expressed R^2 values >0.65 for both DV and RS models. Nonetheless, all linear NWP_{ratio} models had an R^2 greater than 0.95, which we consider to represent strong models (Table 9.8). In fact, all NWP_{ratio} models show similar R^2 values at each respective pH in both LB and FFF models (Table 9.8). Linear BWP_{ratio} models were also the only models shown in Table 9.9, as no quadratic or exponential models fit with an R^2>0.65 (Table 9). All linear BWP_{ratio} and AWP_{ratio} yielded an R^2 value greater than 0.97 and 0.66, respectively. LB ratios were more successful at modeling BWP than FFF, whereas the opposite was observed for the formation of AWP, where FFF ratio models ($FFF_{7.1}$: R^2_{lin} = 0.684) exhibited higher R^2 compared to LB ($LB_{7.1}$: R^2_{lin} = 0.667). As mentioned before, BWP was also modeled with higher R^2 values in LB_{max} models, whereas AWP was modeled with higher R^2 for FFF_{max} models (Table 9.5, 9.6). This may give further evidence to support the notion that LB is useful for determining BWP and FFF for AWP in heat treated milk. However, it is of interest to investigate which specific regions on the LB and FFF spectra best correspond to each of the model predictors (i.e. ratios selected as predictors in the different models).

9.3.2.1 Waveband regions which correspond to significant models

9.3.2.1.1 Light backscatter

Table 9.11 and Figure 9.4 show the portions of the LB spectra which yielded the highest R^2 values for the models. In Table Figure 9.4, numerator values are shown as a red vertical line and denominators are black vertical lines, each corresponding to their respective wavelength. Models for specific variables are labeled by colored letters where PS is in black, NWP in blue, BWP in orange and AWP in green. Similar description methodology has been used in Figure 9.5 (FFF). If the same waveband was used for more than one model, more

than one variable, as well as pH value and numerator/denominator, is listed (Table 9.11 and Table 9.12)

Three out of seven LB numerators were found to lie in a region with relatively low intensity value (from 200- 400 nm) and 2 out of 7 are near the maximum intensity wavelength (569-626 nm) (Figure 9.4, Table 9.11). The majority of denominators were found to lie in a low-intermediate intensity area (5 out of 7 at 556 nm and from 960-1033 nm) (Table 9.11, Figure 9.4).

Table 9.11. Waveband regions corresponding to light backscatter models predictors (PS, NWP, BWP and AWP) with $R^2 > 0.65$.

Avg wavelength (nm)	Waveband	Numerator or denominator	Dependent variable	pH
203	**1**	**n**	**AWP**	**7.1**
323	**21**	**d**	**AWP**	**7.1**
387	**32**	**n**	**BWP**	**6.3**
399	**34**	**n**	**NWP**	**6.3**
471	**47**	**n**	**PS**	**6.3**
493	**51**	**d**	**PS**	**6.3**
569	**65**	**n**	**PS**	**6.3**
626	**76**	**n**	**NWP**	**7.1**
656	**82**	**d**	**NWP**	**7.1**
963	**150**	**n,d**	**PS, BWP**	**6.3,6.3**
967	**151**	**d**	**NWP**	**6.3**
1029	**167**	**d**	**PS**	**6.3**
1033	**168**	**d**	**PS**	**6.3**

n, ratio numerator values (red); d, ratio denominator value (black); PS (black); NWP (blue); BWP (orange); AWP (green).

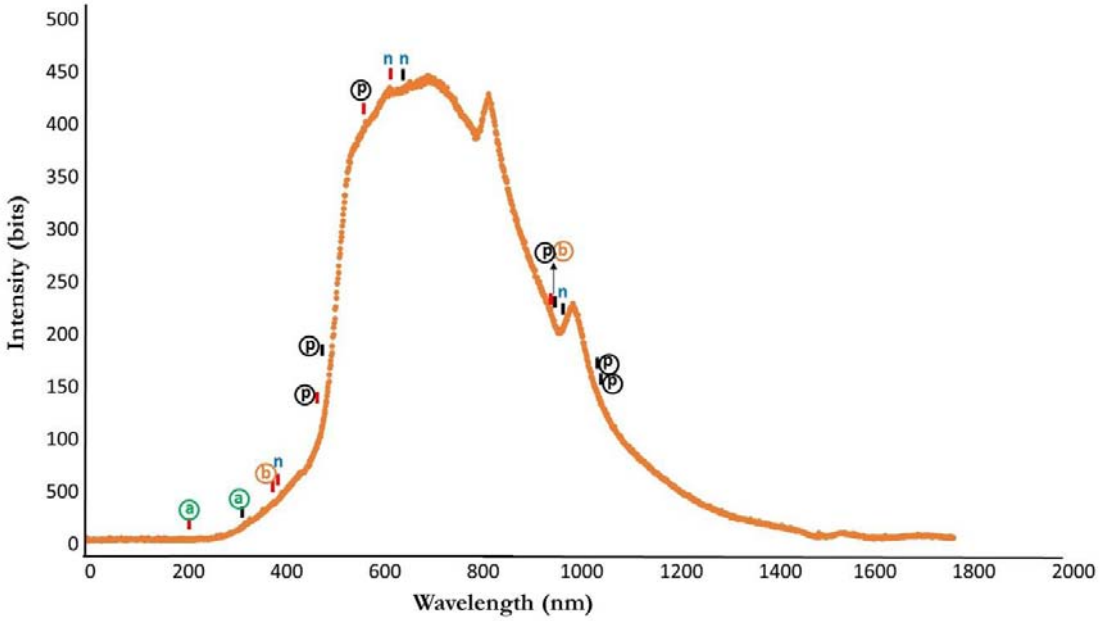

Figure 9.4. Regions corresponding to the highest R^2 for LB models. Numerator values are show in red and denominator regions in black. Each red or black line represents one model which used that spectral region. PS is represented by p (black), NWP by n (blue), BWP by b (orange) and AWP by a (green).

Of particular interest are the regions which correspond to dependent variables which show a large response with time (i.e. $AWP_{7.1}$, $BWP_{6.3}$ and $PS_{6.3}$), following our previous assumptions that:

1. Denatured whey proteins are predominantly found as AWP at pH 7.1
2. Denatured whey proteins are predominantly found as BWP at 6.3
3. Any changes in PS_{avg} is a result of BWP and not affected by AWP.

Then it may be considered that these regions correspond to their respective phenomena (AWP at 7.1→whey protein aggregation spectral region, BWP, PS at pH 6.3→bound denatured whey proteins). In Figure 9.4 models which correspond to these regions are circled. From Figure 9.4 and Table 9.11, $AWP_{7.1}$ ratios correspond to regions of low wavelength intensity (numerator 203 nm, denominator 323 nm) that fall in the UV region (100-400 nm) of the spectra, whereas the BWP/PS ratios contain a numerator in the visible range of the spectra (387, 471, 569 nm) and denominator in the IR portion (963, 1029, 1033 nm). Exceptions occur in the numerator (963 nm) of the PS linear model which is in the IR

region and the denominator (493 nm) of the PS quadratic model which is the visible region of the spectra (Figure 9.4, Table 9.10).

9.3.2.1.2 Front-face fluorescence

Table 9.12 and Figure 9.5 show the portions of the fluorescence spectra which yielded the highest R^2 values for the models. The majority of wavebands (6 out of 10) that were used to develop successful models lie around the maximum wavelength at a range of 337-356 nm and are mixed between numerator (3 out of 6) and denominator (3 out of 6). The remaining numerator and denominator values lie in the low-intermediate range (3 out of 10) on both ends of the spectra of fluorescence intensity (Figure 9.5), and only one denominator lies in a somewhat low intensity region (405 nm).

Table 9.12. Waveband regions corresponding to fluorescence models predictors (PS, NWP, BWP and AWP) with $R^2 > 0.65$.

avg wavelength (nm)	waveband	Numerator or denominator	Predictor	pH
312	**2**	**n,n**	**BWP**	**6.3**
322	**4**	**n**	**NWP**	**6.3**
332	**6**	**n,n**	**NWP**	**7.1**
337	**7**	**n,n**	**PS,PS**	**6.3,6.3**
346	**9**	**d,d**	**PS,PS**	**6.3,6.3**
356	**11**	**d,n**	**BWP,AWP**	**6.3,7.1**
381	**16**	**n**	**PS**	**6.3**
390	**18**	**d**	**AWP**	**7.1**
405	**21**	**d,d,d,d**	**PS, NWP , NWP**	**6.3,7.1, 7.1**
410	**22**	**d**	**PS**	**7.1**

n, ratio numerator values (red); d, ratio denominator value (black); PS (black); NWP (blue); BWP (orange); AWP (green). Each line represents one model which used that spectral region.

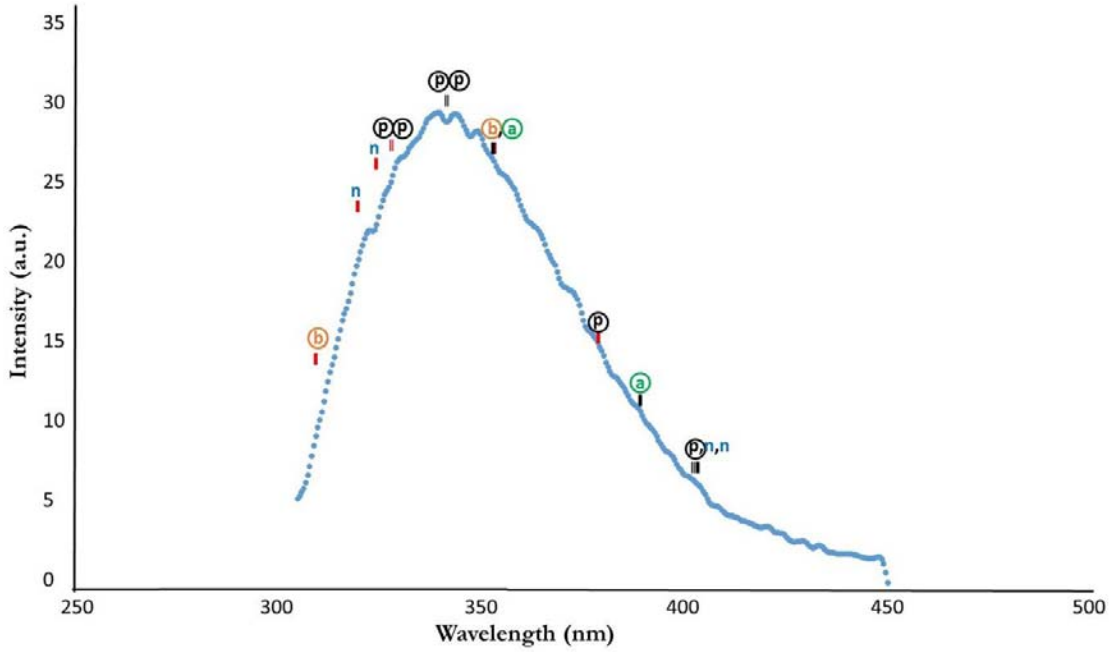

Figure 9.5. Regions corresponding to the highest R^2 for FFF models. Numerator values are show in red and denominator regions in black. Each red or black line represents one model which used that spectral region. PS is represented by p (black), NWP by n (blue), BWP by b (orange) and AWP by a (green).

The model with the highest R^2 for $AWP_{7.1}$ included a numerator near the maximum wavelength (at 356 nm) and a denominator in a low-intermediate intensity region (at 390 nm). In fact, the ratios corresponding to $BWP_{6.3}$ were in quite opposite regions with the numerator in a low-intermediate intensity region on the other side of the FFF curve (at 312 nm) and the denominator at (356 nm), which is the same wavelength as the numerator of $AWP_{7.1}$. The $PS_{6.3}$ models showed good consistency with both the numerator at 337 nm and denominators at 346 nm for both linear and quadratic models. However, in the case of the exponential model we see the numerator in an intermediate range (at 381 nm) and denominator in a relatively low range (405 nm) of intensity from the fluorescence curve.

9.4 Discussion

Both linear and quadratic models were implemented into various model equations. As R^2 values were generally similar for quadratic and linear models, linear models tend to be the preferred equation form as they contain a greater number of degrees of freedom. Exponential models were also implemented for ratio models, however were not particularly

successful, except in the case of PS ratio models where $R^2 > 0.91$ occurred in both LB and FFF models at pH 6.3. In general ratio models represented stronger models (higher R^2 values), when comparing top models (maximum wavelength models and ratio models), in nearly all cases (Table 9.13). The only exception is the quadratic maximum wavelength model AWP $f(FFF)_{7.1}$ which exhibited an R^2 of 0.909 compared to the highest ratio models (FFF_{lin}) with an R^2 of 0.684 and (LB_{lin}) R^2 of 0.667 (Table 9.13). However, it should be considered that maximum wavelength models use only one portion of the spectrum, whereas Ratio models consider all possible combinations to form a model containing a ratio of two points on the spectra. Nonetheless, it is not certain that models improve when implementing a ratio, and perhaps further investigation with single wavelengths, taken at all possible regions of the spectra, may in fact improve a final model of whey protein denaturation, as we saw in Chapter 7 when models using single denominator values in models improved R^2 compared to using a single intensity value near the maximum for model formation (Table 7.6).

The two analytical techniques (LB and FFF) were both implemented into successful models for estimating PS, NWP, BWP and AWP, however LB models were generally better at modeling most variables, where 3 out of 5 models with the highest R^2 were LB models (Table 9.13). It should be noted, however, that FFF models still exhibited high R^2, only slightly lower than that of LB models (Tables 9.3-9.10). On the other hand, when FFF yielded the highest R^2 for the model, LB models generally exhibited a lower R^2. From Table 9.13 we can see that the two models in which FFF was most successful at modeling the variable of interest were the linear equation for modeling NWP at pH 6.3 and AWP at pH 7.1. However, the pH 6.3 NWP model using LB has an R^2 of 0.978, only 0.001 units less than the FFF model (Table 9.8). In the case of AWP, the quadratic FFF model at pH 7.1 has a markedly larger R^2 (0.909) compared to LB models at pH 7.1 (LB_{lin} ratio model: R^2=0.667; LB $\lambda_{max,lin}$: R^2=0.651, $\lambda_{max,quad}$: R^2=772), and in general, AWP models using the FFF spectra have higher R^2 values (FFF linear Ratio model: R^2=0.684; LB $\lambda_{max,lin}$: R^2=0.757) than LB models (Tables 9.6, 9.10).

Table 13. Summary of best models for prediction of response variables.

pH	variable	best fit model	Region	Wavelength (n,d)(nm)	R^2	LB/FFF
6.3	PS	quadratic	$LB_{47,51}$	471,493	0.999	LB
	NWP	linear	$FFF_{4,21}$	322,405	0.979	FFF
	BWP	linear	$LB_{32,150}$	387,963	0.993	LB
7.1	NWP	linear	$LB_{76,82}$	626,656	0.986	LB
	AWP	quadratic	FFF_{max}	340	0.909	FFF

R^2, determination coefficient; n, numerator waveband; d, denominator waveband; LB, model as a function of light backscatter ratios; FFF, model as a function of tryptophan fluorescence.

In the case of LB, we observed the most successful models for $AWP_{7.1}$ with numerator and denominator regions at an low intensity region (203-323 nm), whereas $BWP_{6.3}$ numerators had low-intermediate intensities in the visible range of the spectra (387- 569 nm) and denominators on the other end of the spectrum, also in a low-intermediate intensity region (963- 1033 nm) (Figure 9.4). On the other hand, fluorescence ratio models in general had numerator and denominators near the maximum (340 nm), except $AWP_{7.1}$ which showed a numerator near the maximum (356 nm) and a denominator at a relatively low-intermediate intensity wavelength (390 nm) (Figure 9.5).

It is interesting to note that our observations exhibit some similarities with the work of Lamb, Payne, Xiong, & Castillo (2013) in which waveband ratios of LB spectra near the maximum yielded high R^2, along with ratios of one waveband near a low intensity wavelength region over a region near the maximum also proved to exhibit high R^2 for the modelization of β-LG denaturation. The models of Lamb et al., (2013) may be comparable to that of NWP models, which represent changes as a result of total whey protein denaturation, which exhibited best models (R^2 = 0.986, 0.978) and with the ratio of two wavebands near the maximum ($R_{76,82}$) with the numerator near an area of relatively low intensity and denominator near an intermediate intensity region ($R_{34, 151}$), respectively.

The top models for FFF ratio in general had numerator/denominator around the maximum intensity for tryptophan fluorescence, with 6/10 numerators and denominators near 340 nm, the region in which tryptophan fluorescence is often measured experimentally (Diez et al., 2008; Hougaard et al., 2013; Schamberger & Labuza, 2006). Even so, the maximum intensity wavelength can be shifted depending on the polarity and proximity to other fluorescent protein residues as the alteration in the maximum wavelength occurs as a

result of protein unfolding and/or other protein-protein reactions, however it may be suggested that a large number of protein conformational changes appear in the spectrum in the region near the maximum tryptophan fluorescence intensity (~340 nm), and that this region is useful for the development of model equations in this study.

One potentially interesting finding of this study, which is in accordance with our previous model development work (Chapter 8), is the observation of PS ratio models to exhibit exponential characteristics. The form of the exponential equations tend to follow a pattern in which PS is modeled as a function of LB or FFF. As previously suggested, PS appears to follow an exponential trend, where the intercept value is representative of the initial particle size in unheated milk. Using the formula of Eqn 4.7, the value of the coefficient β_0 (β_0= 148-155 (Table 9.7)) is near that of the initial PS (157 nm (Figure 8.4)) in unheated milk. As we have found PS to be mainly a factor of binding, it is proposed that this equation may follow in the form of ($PS_{heated} = PS_{initial} + e^{BWP}$), or some other exponential-type equation, where BWP represents an optical predictor containing information about BWP. This is only a hypothesis and is based on preliminary observations from model equations (Table 9.7), and should be tested with further data sets in order to make any clear conclusions.

Ultimately, this experiment was aimed toward determining regions of the spectra associated with soluble aggregate whey proteins, and confirming the assumption that $AWP_{7.1}$ is better represented using a FFF technique and $BWP_{6.3}$ and $PS_{6.3}$ using LB, and as a whole, this study continues to support this hypothesis. Specific regions of the spectra may give some insight into total whey protein denaturation model development, and therefore it is considered that these regions are of great interest to further develop prediction equations of whey protein denaturation, in particular, as a function of the two whey protein forms after denaturation (BWP and AWP).

9.5 Conclusions

Both maximum wavelength and ratio models were investigated for modeling the response variables (PS, NWP, BWP at pH 6.3 and NWP, AWP at pH 7.1), and, in general, successful models were observed for all variables. Considering the factors which are most likely attributed to binding (PS and BWP), LB models proved to exhibit the highest R^2, and generally ratio models used numerators which had low-intermediate intensities around 387-569 nm and denominators on the other end of the spectrum, also in a low-intermediate intensity region around 963- 1033 nm. AWP models were more successful using the FFF

spectra, and the region around the maximum intensity appeared to be most frequently used in models, however AWP used a denominator in a low-intermediate intensity area at 390 nm. To our knowledge, no current models have been developed which successfully incorporate both the attachment of whey proteins to the surface of the casein micelle (binding) or the formation of denatured whey protein aggregates to predict total whey protein denaturation in head-treated milk.

CHAPTER 10: The effect of fat on the amount of light scatter in milk by light backscatter and particle size measurements

10.1 Introduction

Experiment I and II have shown consistent trends with regard to skim milk changes as a result of thermal treatment at a range of temperature and pH values. In general, heat treatment has been found to result in an increase in PS, as well as in LB and FF intensity near the maximum intensity wavelength. These changes have been measured at various pH levels, where changes in whey protein denaturation variables (likely as a result of binding) occur to a great extent at pH 6.3, and minimal changes were found to occur at pH 7.1. One aspect of this study, which has not yet been investigated, is the effect of fat on these observed changes.

The addition of fat milk complicates the model for prediction of whey protein denaturation, as it has been reported in the literature that denatured whey proteins can also bind to the milk fat globule membrane (MFGM) surface during heat treatment (Cano-Ruiz & Richter, 1997; Lee & Sherbon, 2002; Ye et al., 2004). These linkages are likely formed as a result of disulphide bonding, as whey proteins were observed in the MFGM after isolation on SDS-PAGE only under reducing conditions (Lee & Sherbon, 2002; Ye et al., 2004). Caseins may also attach to the MFGM via disulphide bonding, and have been reported to compose of approximately 70% of the proteins in the MFGM after heating, with more whey proteins attaching at increased heat treatment temperature (Cano-Ruiz & Richter, 1997). In order to determine if the attachment of denatured whey proteins to the MFGM plays a significant role in the observed LB and FFF spectra, skim milk studies should be compared to milk containing fat.

10.2 Materials and Methods

The experiment consisted of a 3x6 factorial design with three milk fat levels: skim (less than 0.5%), reduced-fat (1.3%) and whole (3.7%) milk and six heat treatment times: 0, 3, 5, 7 12 and 25 min. The design was replicated three times. The complete work plan for Experiment III can be found in Section 3.1.3. Milk was obtained from the Universitat Autonoma de Barcelona pilot plant. Fat was first removed and then re-added at the

appropriate concentrations to achieve all three fat levels. Milk fat percentages were verified three times using the Gerber Method (AOAC, 2002). Milk heat treatment was accomplished using a parallel plate heating vessel and an OvanTherm C water bath maintaining proper temperature control using an OvanTherm TC00 unit (resolution 0.1, stability ±0.1°C) (Suministros Grupo Esper, S.L., Badalona, Spain). A heat treatment temperature of 80 °C was constant in all measurements. The heat treatment technique is further summarized in Section 4.2.1.

Analytical techniques used in Experiment III include: optical light backscatter, particle size z-average and tryptophan front-face fluorescence. Optical analysis was accomplished using the system described in Section 4.3.2 and can be visualized in Figure 4.4. Light backscatter intensity at 600 nm was recorded and used for further analysis (Section 4.3.2). Milk samples for particle size measurements were suspended in a Ca/imidazole buffer (20 mM-imidazole, 5 mM $CaCl_2$, 30 mM NaCl, pH 7.0) and z-average was measured using the Zetasizer 4 system (Malvern Instruments Ltd., Malvern, Worcs., UK) (Section 4.4). A Cary Eclipse Fluorescence Spectrophotometer (Agilent Technologies) was used to measure tryptophan flurorescence at an excitation wavelength of 290 nm using emission spectra from 305-450 nm (Schamberger and Labuza, 2006) (Section 4.5.2).

10.3 Results

Figure 10.1 shows the approximate maximum of the light backscatter intensity taken from 200-1100 nm in skim, reduced-fat and whole milk samples. It is clear that fat has a large influence on the amount of light scatter observed as we see a separation (more than 10,000 bits) between curves of skim (<0.5%) to reduced-fat (1.3%) and reduced-fat (3.7%) to whole milk samples. The increase did not linearly correspond to fat percentage, as a greater increase in light backscatter was observed between skim milk (<0.5%) and reduced-fat (1.3%) than from reduced-fat to whole, approximately 15,000 and 13,500 bit increase, respectively.

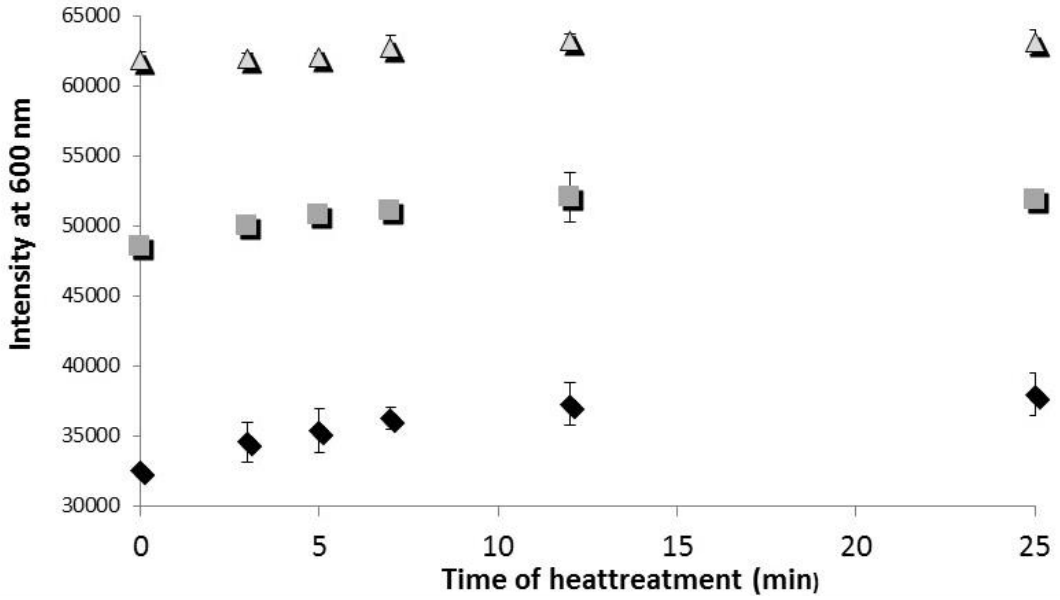

Figure 10.1. LB intensity, Black-skim, grey-reduced fat, triangle-whole. Error bars not shown as all data points are overlapping.

Similar to other experiments, LB spectra followed a trend in which average intensity increased with heat treatment time, however changes appear to be less marked with an increase in fat percentage (Figure 10.1). First-order rate constants were determined for light backscatter in skim, reduced-fat and whole milk and are summarized in Table 10.1. The observed rate for skim milk shows the highest rate (0.89×10^{-2} min^{-1}) and decreases with increasing fat percentage, with high R^2 values for all observations (Table 10.1). Even with the trend of decreasing rate with increasing fat percentage, none of the rate constants were significantly different by overlapping 95% confidence limits (Table 10.1).

Table 10.1. Kinetic analysis of light backscatter increase as a result of heat treatment and milk fat content.

	$k \times 10^{-2}$ (min^{-1})	R^2	Upper limit	Lower limit	Significance
Skim milk	0.89	0.91	1.4	0.38	a
Reduced-fat milk	0.63	0.98	0.87	0.38	a
Whole milk	0.31	0.83	0.57	0.06	a

Particle size z-average measurements show an evident increase with increasing fat content, in which nearly 100 nm difference is seen from skim milk to whole milk (Figure 10.2). The curve of particle size was bimodal, however better trends were observed in using the z-average value of the total milk sample than measuring individual milk peaks. Average PS values for skim milk corresponded similarly to our Experiment II, in which the average initial PS was 157 nm. We did not consider Experiment I to compare to this study as reconstituted milk was used and therefore a larger average of 239.4 nm was observed, which could be due to the drying process which has been suggested to result in more optically dense micelles (Martin et al., 2007). As well, whole milk samples (average of 283 nm) are similar to that of Sharma and Dalgleish (1994), where they observed an average of 285 nm after heat treatment for 10 min at 80 °C.

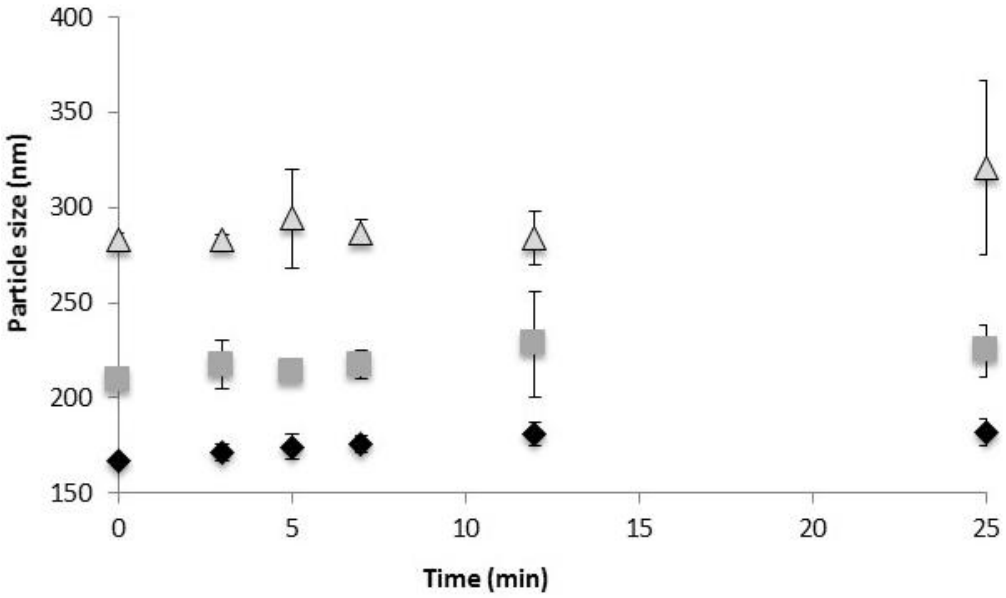

Figure 10.2. PS z-average, Black-skim, grey-reduced fat, triangles-whole. Error bars not shown as all data points are overlapping.

With respect to the PS first-order rate constants, no significant differences were observed between skim and reduced-fat milk, however whole milk presented a significantly lower rate than skim and reduced-fat milk (Table 10.2). Considering the larger surface area of the MFGM compared to the casein micelle, MFGM attached whey proteins would likely

result in a lower rate of change than micellar bound whey proteins. Denatured whey proteins attached to the MFGM may also be more evenly distributed than on casein micelles, where the formation of non-uniform surface complexes can greatly influence particle size (Vasbinder & de Kruif, 2003), and the PS rate constant. Nonetheless, a higher rate constant is observed in reduced-fat milk than skim milk, however the two rates are not significantly different, so no clear conclusions can be proposed regarding these observed rate differences (Table 10.2).

Table 10.2: Kinetic rate constants of particle size as a result of heat treatment and milk fat content.

	k x 10^{-2} (min^{-1})	**R^2**	**Upper limit**	**Lower limit**	**Significance**
Skim milk	0.64	0.98	0.80	0.49	a
Reduced-fat milk	0.68	0.86	1.17	0.18	a
Whole milk	0.03	0.79	0.07	0.002	b

Tryptophan fluorescence was also measured, however trends for this experiment did not follow previously observed trends of a clear increase in intensity with heat treatment time (Figure 10.3). Instead, changes with heat treatment appear to go through step-wise changes resulting in either an increase or decrease in intensity, however no clear trend is observed with respect to milk fat (Figure 10.3). The general trend in skim and whole milk are upward, except for the initial decrease in intensity observed in skim milk. On the other hand, reduced-fat milk exhibits an increase up to 3 min, then a decrease until 7 and further increases until leveling off at 25 min (Figure 10.3). From these observations, the relationship between fat and fluorescence measurements is not clear, which may be as a result of the combined effect of several factors affecting fluorescence of tryptophan. For the purpose of this study, we will not discuss fat content as determined by tryptophan fluorescence.

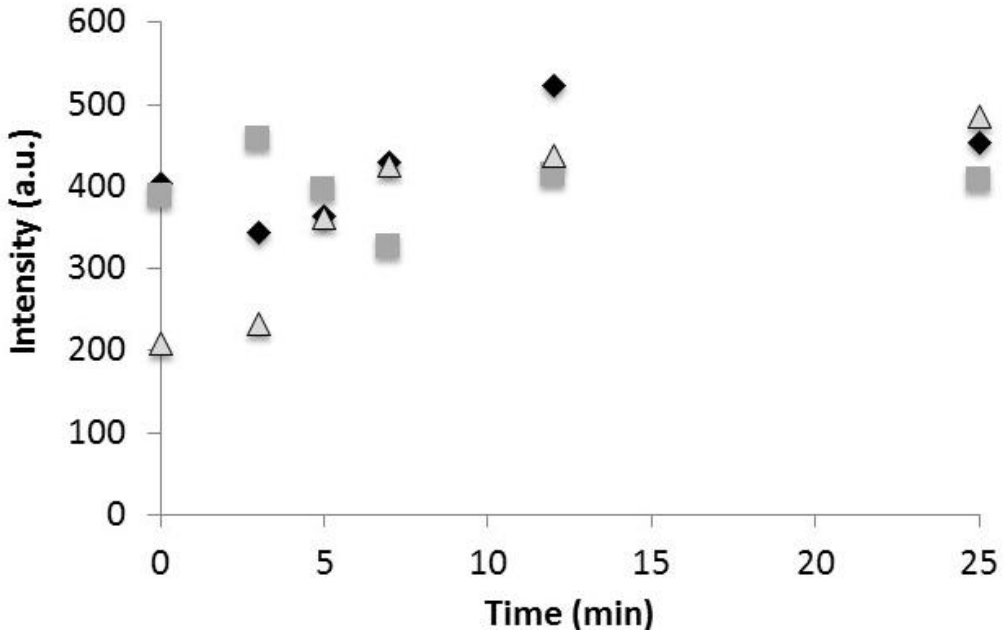

Figure 10.3. FFF intensity, Black-skim, grey-reduced fat, triangles-whole. Error bars not shown as all data points are overlapping.

An exponential trend in relation to particle size and light backscatter was also observed, as in Experiment I and II, where an exponential relationship was observed in models of PS f(LB). Figure 10.4 shows a plot of PS versus LB at the three milk fats fitting exponential trend lines, increasing with heat treatment time and milk fat.

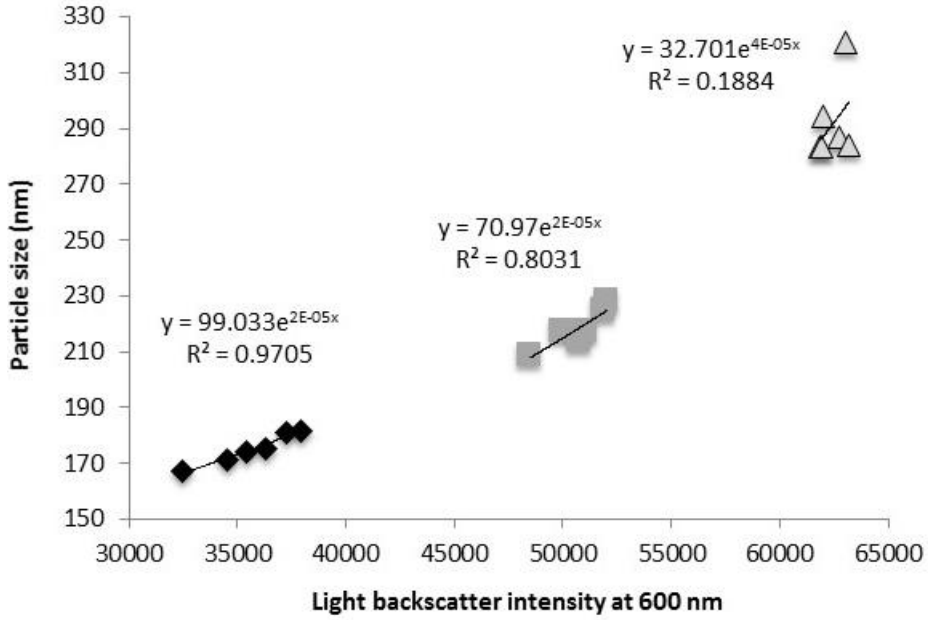

Figure 10.4. Particle size z-average versus light backscatter intensity at 600 nm; black-skim, grey-reduced fat, triangles-whole. Error bars not shown as all data points are overlapping.

10.4 Discussion

Results showed good trends with heat treatment time and fat content for both light backscatter and particle size (Figure 10.1, 10.2). In the case of light backscatter analysis, we can see that fat largely increases the response signal intensity (Figure 10.1), likely as a result of the contribution of fat globules to scatter more light as they are in general significantly larger than casein micelles (0.1-10 μm and 20-500 nm, respectively) (Table 2.2) and in higher proportion in milk (4.0 and 2.6 %w/w, respectively) (Table 2.1). However, the reaction rate is inversely related to signal intensity in which skim milk has the highest rate, and full milk the lowest. This may be a result of whey proteins acting to attach to the fat globules. However, as proteins may attach to the surface of fat particles via different mechanisms (i.e. disulfide bonds (Sharma & Dalgleish, 1994) and/or via casein micelles which have adsorbed onto the MFGM during homogenization (Ye, Singh, Oldfield, & Anema, 2004)), quantification of the specific binding patterns may be difficult to determine.

Fat has been reported to impart a protective effect on *β*-LG denaturation (Pellegrino, 1994), whereas other authors have reported an increase in denaturation with increasing milk

fat content at heat treatment temperatures >72 °C (Claeys, Van Loey, & Hendrickx, 2002). In this study the rate of change was mostly higher in skim milk compared to whole milk, however there were no significant difference observed between skim and reduced-fat milk (Table 10.3). Still, the trend was a lower rate with an increase in milk fat for both LB and PS, except in the case where reduced-fat milk has a slightly higher rate than skim milk, however not significant (Table 10.3). Considering the larger size and surface area of fat globules, it may be difficult to observe the increase in size of casein micelles as a result of the attachment of denatured whey protein to the casein micelle surface in fat milk compared to skim milk where only casein micelles are present. And in fact, it is still more likely that the preferred mode of denatured proteins is attachment to the casein micelle. It has been reported that only approximately 0.6 mg *β*-LG per gram fat interacts with the fat globule after 10 min of heat treatment at 85 °C and 0.2 mg/g fat of *a*-LA, only accounting for < 1% of total serum protein in milk (Corredig & Dalgleish, 1996).

Table 10.3. Kinetic rate comparison of light backscatter and particle size as a result of heat treatment and milk fat content

		k x 10^{-2} (min^{-1})	R^2	Upper limit	Lower limit	Significance
Skim milk	**PS**	0.03	0.79	0.07	0.002	a
	LB	0.31	0.83	0.57	0.06	ab
Reduced- fat milk	**PS**	0.68	0.86	1.17	0.18	b
	LB	0.63	0.98	0.87	0.38	b
Whole milk	**PS**	0.64	0.98	0.80	0.49	b
	LB	0.89	0.91	1.4	0.38	b

An exponential trend was observed relating particle size and light backscatter, which we propose may lead to successful prediction models of PS and LB in fat milk, similar to the ones that have been developed in Experiment I and II. As well, there is the potential for development of a LB sensor for determination of fat content, as we saw very clear trends for LB with respect to fat content (Figure 10.1). Even so, further research about the effect of heat treatment on the development of an optical sensor in milk with fat is warranted in order to gain the full scope.

CHAPTER 11: Combined-experiment prediction model

In this supplementary section, LB maximum intensity data from Experiment II (pH 6.3 and 7.1) was combined with data from Experiment III (pH 6.7) in skim milk samples heated at 80 °C for 0, 3, 5, 7, 12 and 25 min. As binding is the preferred mechanism at pH 6.3 and soluble aggregate formation at pH 7.1; pH 6.7 may represent an intermediate level consisting of a combination of these two forms. Therefore incorporating these three pH values illustrates a range of the potential attachment mechanisms of denatured whey proteins (Figure 11.1). It should be noted that this is not new data, only a compilation of the previous work in a combined pH-graph (Figure 11.1, Table 11.1, and Figure 11.2).

In Figure 11.1, we can see that the distribution of data points with respect to pH level appears to be in accordance with previous observations, in which pH 6.3 yields the highest light scatter response, pH 6.7 an intermediate response and pH 7.1 with little to no response.

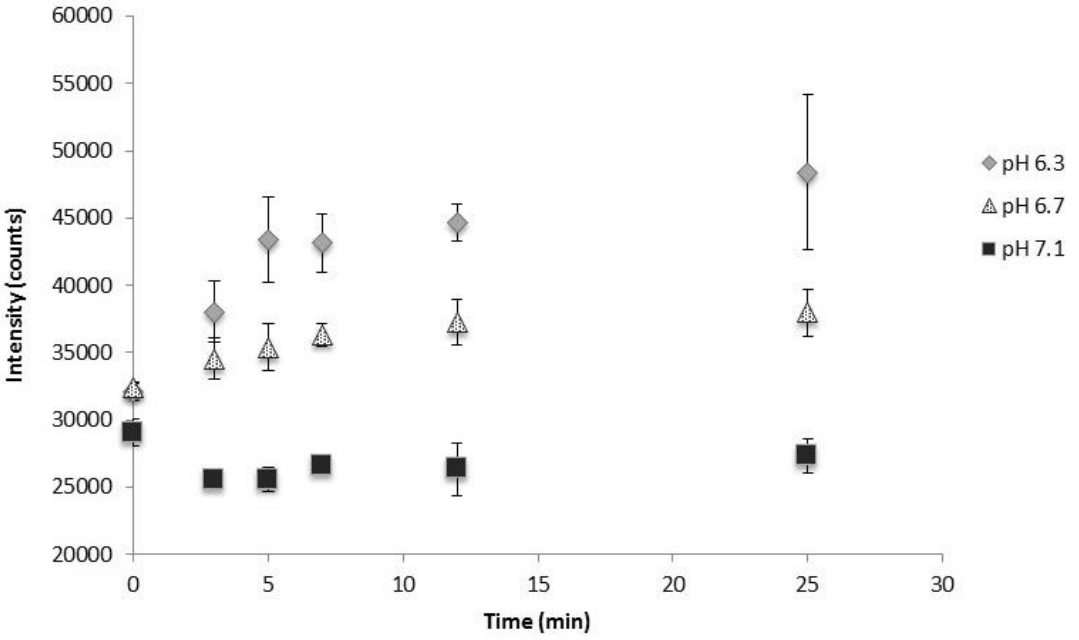

Figure 11.1. Combined graph of light backscatter relative maximum intensity at 540 nm (pH 6.3 and 7.1), and at 600 nm (pH 6.7), versus time.

Similarly, first-order kinetic rates follow the trend in which pH 6.3 has the largest rate, which decreases with increasing pH (Table 11.1). Even so, the rates are not significantly different according to overlapping 95% CI (Table 11.1).

Table 11.1: Kinetic analysis of light backscatter during skim milk heat treatment at 80 °C.

	k x 10^{-2} (min^{-1})	**R^2**	**Lower limit**	**Upper limit**	**Significance**
6.3	2.71	0.71	-0.47	5.88	a
6.7	0.89	0.91	0.38	1.4	a
7.1	0.38	0.50	-0.77	1.54	a

Finally, it was of interest to use a pH-integrated model equation using all the pH values to test the model in order to determine the success based on these 3 pH values. Data was fit to a linear pH-integrated model, developed using data from Experiment II, with an equation of PS f(LB) = 113 + 0.0017x . Using only pH 6.3 and 7.1, the R^2 of this model was 0.71, however we can see the addition of pH 6.7 milk from Experiment III increases the R^2, if only slightly (Figure 11.2). Figure 11.2 shows good fit (R^2 = 0.72), yet even so, it is possible that R^2 could improve by removing pH 7.1 as it has been established to show little response in PS and LB measurements; or by adding a few more pH values within the range of the study. As well, quadratic equations have, in general, improved R^2 compared to linear PS maximum intensity models.

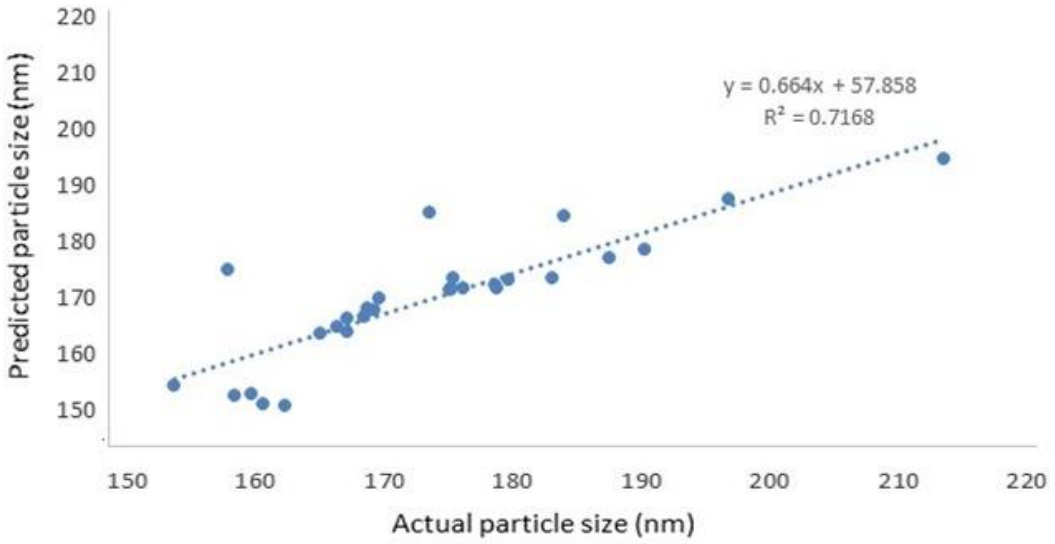

Figure 11.2. Combined experiment prediction model using the linear maximum wavelength equation for prediction of PS as a function of maximum light backscatter intensity at 540 nm (pH 6.3 and 7.1), and at 600 nm (pH 6.7), versus time.

Additional studies would be useful to confirm the possibility to use a single model equation to determine PS f(LB) at a range of pH values, however all of our studies thus far have supported this possibility. Fluorescence techniques may not yield as successful models, however this should be further investigated. As well, the potential to model other variables (NWP, BWP and AWP) has been demonstrated, however would benefit from studies among a wider range of pH in order to test the pH-dependent mechanisms of whey protein denaturation that may occur.

CHAPTER 12: Final Conclusions

1. Light backscatter measurements exhibited a consistent positive correlation with particle size measurements. This relationship was most accurately defined at pH 6.3, the pH where denatured whey proteins are more likely to form complexes with κ-casein on the surface of the casein micelle. In this sense, it was established that:

    a. Increasing heat treatment time acted to increase both light backscatter and particle size intensity, however an increase in the heat treatment temperature (from 80-90 °C) did not notably affect LB, although there was a large increase in particle size observed at 90 °C compared to 80 °C in pH 6.3 milk.

    b. Particle size showed consistent positive correlations with BWP, most significantly at pH 6.3, which suggests that particle size may be a good determinant of the attachment of whey proteins via κ-casein on the surface of the casein micelle to increase casein particle size.

2. Our study showed a significantly greater formation of BWP at pH 6.3 and AWP at 7.1, which is well supported in the literature.

    a. The whey protein variant which was more likely to form complexes on the surface of the casein micelle was β-LG B, whereas evidence seemed to show that β-LG A was involved to a greater extent in the formation of soluble whey protein aggregates.

    b. Light backscatter maximum intensity showed a correlation with both BWP and AWP at a range of pH values

    c. Particle size was shown to exhibit a correlation with BWP, no clear relationship has been established with AWP

    d. FFF shows a correlation with BWP, however does not exhibit a statistical correlation with AWP, nonetheless, a clear red shift was observed in FFF

measurements with time at pH 7.1, which may be attributed to the unfolding of whey proteins and subsequent formation of soluble whey protein aggregates. On the other hand, there was a slight blue shift at pH 6.3, which is more suggestive binding, as blue shifting may occur when the location of tryptophan is in close proximity to a micelle.

3. Particle size, front-face fluorescence and light backscatter all show a positive and significant correlation among each other.

4. The whey protein denaturation variables tested were highly pH-dependent.

    a. PS, LB, FFF and BWP all increased with heat treatment at pH 6.3.

    b. AWP increased with heat treatment at pH 7.1.

    c. NWP was the only variable which was not pH-dependent and showed a decrease with heat treatment at all the pH levels tested.

5. Many models were best-fit to quadratic equations, however the majority of variables were sufficiently modeled ($R^2 > 0.75$) using a linear equation, which may be preferred due to simplicity.

    a. Exponential models, in general, did not improve R^2 to a great extent compared to linear and quadratic forms, however PS exponential models f(LB) and f(FFF) exhibited an intercept representative of the approximate calculated initial PS corresponding to the specific milk batch characteristics. This shows potential for PS predictions using simple, direct FFF and/or LB measurements.

    b. In general, wavelength maximum models were quite successful at modelling all dependent variables, however ratio models showed improvement in R^2 as they

combined a range of spectral regions in order to find the best-fit for each variable.

c. The LB spectra exhibited the best characteristics to model BWP. Regions which corresponded to BWP/PS included a numerator between 387-569 nm and denominator from 963-1033 nm, both at low-intermediate intensity regions, however on opposite ends of the spectrum.

d. The FFF spectra was implemented into models which best predicted AWP. Regions which corresponded to AWP had numerator values near the maximum intensity and a denominator in a low-intermediate intensity range around 390 nm. In the case of f(FFF) models, most variables were chosen close to the maximum wavelength (340 nm).

6. Milk fat percentage was related to a large increase in LB and PS measurements, however in FFF there was no observable trend. Changes in LB and PS had a negative correlation with fat, in that first-order reaction rates increased with decreasing fat content. A clear relationship between LB and PS was also observed in milk with fat.

7. A pH-integrated model of PS f(LB) using skim milk measurements at pH 6.3, 6.7 and 7.1 from two independent experiments was successfully formed with a relatively good R^2 of 0.72, showing further potential for a total integrated model for the determination of PS f(LB).

CHAPTER 13: References

Alexander, & Dalgleish. (2006). Dynamic Light Scattering Techniques and Their Applications in Food Science. Food Biophysics, 1(1), 2–13.

Alimentaria. (2007). La utilización de leche cruda para la elaboración de quesos con un tiempo de maduración inferior a sesenta días.

Alloggio, Caponio, Pasqualone, & Gomes. (2000). Effect of heat treatment on the rennet clotting time of goat and cow milk. Food Chemistry, 70(1), 51–55. http://doi.org/10.1016/S0308-8146(00)00065-0

Anema, & McKenna. (1996). Reaction Kinetics of Thermal Denaturation of Whey Proteins in Heated Reconstituted Whole Milk. Journal of Agricultural and Food Chemistry, 44(2), 422–428.

Anema, S. G. (1997). The effect of chymosin on κ-casein-coated polystyrene latex particles and bovine casein micelles. International Dairy Journal, 7(8), 553–558.

Anema, S. G. (2007). Role of kappa-casein in the association of denatured whey proteins with casein micelles in heated reconstituted skim milk. Journal of Agricultural and Food Chemistry, 55(9), 3635–42.

Anema, S. G. (2008a). On heating milk, the dissociation of kappa-casein from the casein micelles can precede interactions with the denatured whey proteins. The Journal of Dairy Research, 75(4), 415–21.

Anema, S. G. (2008b). The whey proteins in milk: thermal denaturation, physical interactions and effects on the functional properties of milk. In H. Singh, M. Boland, & A. Thompson (Eds.), Milk Proteins (pp. 239–281). San Diego, CA: Elsevier.

Anema, S. G., Kim Lee, S., & Klostermeyer, H. (2007). Effect of pH at heat treatment on the hydrolysis of κ-casein and the gelation of skim milk by chymosin. LWT - Food Science and Technology, 40(1), 99–106.

Anema, S. G., & Klostermeyer, H. (1997). Heat-Induced, pH-Dependent Dissociation of Casein Micelles on Heating Reconstituted Skim Milk at Temperatures below 100 °C. Journal of Agricultural and Food Chemistry, 45(4), 1108–1115.

Anema, S. G., Lee, S. K., Lowe, E. K., & Klostermeyer, H. (2004). Rheological properties of acid gels prepared from heated pH-adjusted skim milk. Journal of Agricultural and Food Chemistry, 52(2), 337–43.

Anema, S. G., & Li, Y. (2003a). Association of denatured whey proteins with casein micelles in heated reconstituted skim milk and its effect on casein micelle size. The Journal of Dairy Research, 70(1), 73–83.

Anema, S. G., & Li, Y. (2003b). Effect of pH on the association of denatured whey proteins with casein micelles in heated reconstituted skim milk. Journal of Agricultural and Food Chemistry, 51(6), 1640–6.

Anema, S. G., Lowe, E. K., & Lee, S. K. (2004). Effect of pH at heating on the acid-induced aggregation of casein micelles in reconstituted skim milk. LWT - Food Science and Technology, 37(7), 779–787.

Anema, S. G., Lowe, E. K., & Li, Y. (2004). Effect of pH on the viscosity of heated reconstituted skim milk. International Dairy Journal, 14(6), 541–548.

Anema, S., & Li, Y. (2000). Further Studies on the Heat-induced, pH-dependent Dissociation of Casein from the Micelles in Reconstituted Skim Milk. LWT - Food Science and Technology, 33(5), 335–343.

AOAC. (2002). 33.2.27A AOAC Official Method 2000.18 Fat Content of Raw and Pasteurized Whole Milk. AOAC International.

Arango, O. (2015). Aplicación de dispersión de luz de infrarrojo próximo en la producción de derivados lácteos bajos en grasa con inulina.

Ayala, O. (2012). Formación de lactulosa durante el tratamiento térmico de la leche y su correlación con marcadores autofluorescentes. Modelización cinética. Universitat Autònoma de Barcelona.

Barman, T. E., & Perry, R. A. (1977). On the reactivities of the tryptophan residues of human alpha-lactalbumin to 2-hydroxy-5-nitrobenzyl bromide. Biochimica et Biophysica Acta, 494(2), 314–8.

Bauer, R., Carrotta, R., Rischel, C., & Ogendal, L. (2000). Characterization and isolation of intermediates in beta-lactoglobulin heat aggregation at high pH. Biophysical Journal, 79(2), 1030–8.

Beja-Pereira, A., Caramelli, D., Lalueza-Fox, C., Vernesi, C., Ferrand, N., Casoli, A., … Bertorelle, G. (2006). The origin of European cattle: evidence from modern and ancient DNA. Proceedings of the National Academy of Sciences of the United States of America, 103(21), 8113–8.

Beliciu, C. M., & Moraru, C. I. (2009). Effect of solvent and temperature on the size distribution of casein micelles measured by dynamic light scattering. Journal of Dairy Science, 92(5), 1829–39.

Bello, M., Portillo-Téllez, M. D. C., & García-Hernández, E. (2011). Energetics of ligand recognition and self-association of bovine β-lactoglobulin: differences between variants A and B. Biochemistry, 50(1), 151–61.

Berg, J. M., Tymoczko, J. L., & Stryer, L. (2002). Biochemistry. W H Freeman.

Birlouez-Aragon, I., Nicolas, M., Metais, A., Marchond, N., Grenier, J., & Calvo, D. (1998). A Rapid Fluorimetric Method to Estimate the Heat Treatment of Liquid Milk. International Dairy Journal, 8(9), 771–777.

Birlouez-Aragon, I., Sabat, P., & Gouti, N. (2002). A new method for discriminating milk heat treatment. International Dairy Journal, 12(1), 59–67.

Blanco, L. (2016). Evaluación del efecto de la refrigeración sobre la coagulación de la leche mediante dispersión de luz NIR. Universitat Autònoma de Barcelona.

Bottomley, R., Evans, M., & Parkinson, C. (1990). Whey proteins. Food Gels.

Boubellouta, T., & Dufour, É. ´ (2008). Effects of mild heating and acidification on the molecular structure of milk components as investigated by synchronous front-face fluorescence spectroscopy coupled with parallel factor analysis. Applied Spectroscopy, 62(5), 490–496.

Boubellouta, T., Galtier, V., & Dufour, E. (2009). Effects of added minerals (calcium, phosphate, and citrate) on the molecular structure of skim milk as investigated by mid-infrared and synchronous fluorescence spectroscopies coupled with chemometrics. Applied Spectroscopy, 63(10), 1134–41.

Bremer, L. G. B., van Vliet, T., & Walstra, P. (1989). Theoretical and experimental study of the fractal nature of the structure of casein gels. Journal of the Chemical Society, Faraday Transactions 1: Physical Chemistry in Condensed Phases, 85(10), 3359.

Brew, K. (2003). α-Lactalbumin. Advanced Dairy Chemistry—1 Proteins.

Cano-Ruiz, M. E., & Richter, R. L. (1997). Effect of Homogenization Pressure on the Milk Fat Globule Membrane Proteins. Journal of Dairy Science, 80(11), 2732–2739.

Caputo, G. A., & London, E. (2003). Cumulative effects of amino acid substitutions and hydrophobic mismatch upon the transmembrane stability and conformation of hydrophobic alpha-helices. Biochemistry, 42(11), 3275–85.

Castillo, M., Payne, F. ., Hicks, C. ., & Lopez, M. . (2000). Predicting cutting and clotting time of coagulating goat's milk using diffuse reflectance: effect of pH, temperature and enzyme concentration. International Dairy Journal, 10(8), 551–562.

Castillo, M., Payne, F. A., López, M. B., Ferrandini, E., & Laencina, J. (2005). Optical sensor technology for measuring whey fat concentration in cheese making. Journal of Food Engineering, 71(4), 354–360.

Castillo, M., Payne, F., & Lopez, M. (2005). Preliminary evaluation of an optical method for modeling the dilution of fat globules in whey during syneresis of cheese curd. Appl. Engineering in Agriculture, 21(2), 265–269.

Castillo, M., Payne, F., Wang, T., & Lucey, J. (2006). Effect of temperature and inoculum concentration on prediction of both gelation time and cutting time. Cottage cheese-type gels. International Dairy Journal.

Chakraborty, A., & Basak, S. (2007). pH-induced structural transitions of caseins. Journal of Photochemistry and Photobiology B: Biology, 87(3), 191–199.

Christensen, J., Nørgaard, L., Bro, R., & Engelsen, S. (2006). Multivariate Autofluorescence of Intact Food Systems.

Claeys, W. L., Van Loey, A. M., & Hendrickx, M. E. (2002). Kinetics of alkaline phosphatase and lactoperoxidase inactivation, and of β-lactoglobulin denaturation in milk with different fat content. Journal of Dairy Research, 69(04), 541–553.

Corredig, M., & Dalgleish, D. G. (1996). Effect of temperature and pH on the interactions of whey proteins with casein micelles in skim milk. Food Research International, 29(1), 49–55.

Corredig, M., & Dalgleish, D. G. (1999). The mechanisms of the heat-induced interaction of whey proteins with casein micelles in milk. International Dairy Journal, 9(3), 233–236.

Creamer, L. K., Bienvenue, A., Nilsson, H., Paulsson, M., van Wanroij, M., Lowe, E. K., … Jiménez-Flores, R. (2004). Heat-induced redistribution of disulfide bonds in milk proteins. 1. Bovine beta-lactoglobulin. Journal of Agricultural and Food Chemistry, 52(25), 7660–8.

Creamer, L. K., Loveday, S. M., & Sawyer, L. (2011). β-lactoglobulin. In Milk Proteins (pp. 787–794).

Crofcheck, C. L., Payne, F. A., Hicks, C. L., Mengüç, M. P., & Nokes, S. E. (2000). Fiber optic sensor response to low levels of fat in skim milk. Journal of Food Process Engineering, 23(2), 163–175.

Croguennec, T., Bouhallab, S., Mollé, D., O'Kennedy, B. T., & Mehra, R. (2003). Stable monomeric intermediate with exposed Cys-119 is formed during heat denaturation of beta-lactoglobulin. Biochemical and Biophysical Research Communications, 301(2), 465–71.

D'Allemand, G. (1994). Centrifuges. In M. Haven, G. Tetrault, & J. Schenken (Eds.), Laboratory Instrumentation (Fourth, pp. 31–40). New York: John Wiley & Sons.

Dairy processing handbook. (1995).

Dalgleish, D. G. (1990). The effect of denaturation of β-lactoglobulin on renneting : a quantitative study. Milchwissenschaft, 45(8), 491–494.

Dalgleish, D. G. (2011). On the structural models of bovine casein micelles—review and possible improvements. Soft Matter, 7(6), 2265

Dalgleish, D. G., Horne, D. S., & Law, A. J. R. (1989). Size-related differences in bovine casein micelles. Biochimica et Biophysica Acta (BBA) - General Subjects, 991(3), 383–387.

Dannenberg, F., & Kessler, H.-G. (1988). Reaction Kinetics of the Denaturation of Whey Proteins in Milk. Journal of Food Science, 53(1), 258–263.

Davies, D. T., & Law, A. J. R. (1983). Variation in the protein composition of bovine casein micelles and serum casein in relation to micellar size and milk temperature. Journal of Dairy Research, 50(01), 67–75.

de Kruif, C. G. (1998). Supra-aggregates of Casein Micelles as a Prelude to Coagulation. Journal of Dairy Science, 81(11), 3019–3028.

de la Fuente, M. A., Singh, H., & Hemar, Y. (2002). Recent advances in the characterisation of heat-induced aggregates and intermediates of whey proteins. Trends in Food Science & Technology, 13(8), 262–274.

De Marchi, M., Bittante, G., Dal Zotto, R., Dalvit, C., & Cassandro, M. (2008). Effect of Holstein Friesian and Brown Swiss breeds on quality of milk and cheese. Journal of Dairy Science, 91(10), 4092–102.

de Moreno, M. R., Smith, J. F., & Smith, R. V. (1986). Mechanism studies of coomassie blue and silver staining of proteins. Journal of Pharmaceutical Sciences, 75(9), 907–911.

del Angel, C. R., & Dalgleish, D. G. (2006). Structures and some properties of soluble protein complexes formed by the heating of reconstituted skim milk powder. Food Research International. Elsevier Science.

Diaz, O., Gouldsworthy, A. M., & Leaver, J. (1996). Identification of Peptides Released from Casein Micelles by Limited Trypsinolysis. Journal of Agricultural and Food Chemistry, 44(9), 2517–2522.

Diaz-Carrillo, E., Muñoz-Serrano, A., Alonso-Moraga, A., & Serradilla-Manrique, J. M. (1993). Near infrared calibrations for goat's milk components: protein, total casein, αs-, β- and k-caseins, fat and lactose. J. Near Infrared Spectroscopy.

Diez, R., Ortiz, M. C., Sarabia, L., & Birlouez-Aragon, I. (2008). Potential of front face fluorescence associated to PLS regression to predict nutritional parameters in heat treated infant formula models. Analytica Chimica Acta, 606(2), 151–158.

Donato, L., & Dalgleish, D. G. (2006). Effect of the pH of heating on the qualitative and quantitative compositions of the sera of reconstituted skim milks and on the mechanisms of formation of soluble aggregates. Journal of Agricultural and Food Chemistry, 54(20), 7804–7811.

Donato, L., & Guyomarc'h, F. (2009). Formation and properties of the whey protein/κ-casein complexes in heated skim milk – A review. Dairy Science and Technology, 89(1), 3–29.

Donato, L., Guyomarc'h, F., Amiot, S., & Dalgleish, D. G. (2007). Formation of whey protein/κ-casein complexes in heated milk: Preferential reaction of whey protein with κ-casein in the casein micelles. International Dairy Journal, 17(10), 1161–1167.

Downey, G., Robert, P., Bertrand, D., & Kelly, P. M. (1990). Classification of Commercial Skim Milk Powders According to Heat Treatment Using Factorial Discriminant Analysis of Near-Infrared Reflectance Spectra. Applied Spectroscopy, 44(1), 150–155.

Dufour, E., & Riaublanc, A. (1997). Potentiality of spectroscopic methods for the characterisation of dairy products. I. Front-face fluorescence study of raw, heated and homogenised milks. Le Lait, 77(6), 657–670.

Duggan, D. E., Bowman, R. L., Brodie, B. B., & Udenfriend, S. (1957). A spectrophotofluorometric study of compounds of biological interest. Archives of Biochemistry and Biophysics, 68(1), 1–14.

Dupont, D., & Muller-Renaud, S. (2006). Quantification of proteins in dairy products using an optical biosensor. Journal of AOAC International, 89(3), 843–8.

Dupont, D., Rolet-Repecaud, O., & Muller-Renaud, S. (2004). Determination of the heat treatment undergone by milk by following the denaturation of alpha-lactalbumin with a biosensor. Journal of Agricultural and Food Chemistry, 52(4), 677–81.

Eck, A. (1990). El queso. Paris: Ediciones Omega.

Euber, J. R., & Brunner, J. R. (1982). Interaction of κ-Casein with Immobilized β-Lactoglobulin. Journal of Dairy Science, 65(12), 2384–2387. -5

European Commission. (2015). EU agricultural product quality policy - Agriculture and rural development.

Fagan, C. C., Castillo, M., O'Donnell, C. P., O'Callaghan, D. J., & Payne, F. A. (2008). On-line prediction of cheese making indices using backscatter of near infrared light. International Dairy Journal, 18(2), 120–128.

Fagan, C. C., Leedy, M., Castillo, M., Payne, F. A., O'Donnell, C. P., & O'Callaghan, D. J. (2007). Development of a light scatter sensor technology for on-line monitoring of milk coagulation and whey separation. Journal of Food Engineering, 83(1), 61–67.

Farrell, H. M., Jimenez-Flores, R., Bleck, G. T., Brown, E. M., Butler, J. E., Creamer, L. K., Swaisgood, H. E. (2004). Nomenclature of the proteins of cows' milk--sixth revision. Journal of Dairy Science, 87(6), 1641–74.

Farrell, R. E. (2005). Appendix N – Polyacrylamide Gel Electrophoresis. RNA Methodologies. Elsevier.

Fiber Optic Cables. (2016). Retrieved February 16, 2016, from http://www.paigeelectric.com/lovo/fiber.optic/fiber.optic.cable.facts.html

Fox, P. F. (2000). Fundamentals of Cheese Science. Springer Science & Business Media.

Fox, P. F. (2002). Cheese Overview. In Encyclopedia of Dairy Sciences (pp. 252–261). Elsevier.

Fox, P. F., & McSweeney, P. L. H. (1998). Dairy Chemistry and Biochemistry.

Fox, P. F., & McSweeney, P. L. H. (2003). Advanced Dairy Chemistry.

García Olmo, J. (2004). Aplicaciones de la tecnología NIRS en la industria agroalimentaria. Nuevas tecnologías para el control de proceso y de producto en la industria alimentaria. Secretariado de Publicaciones e Intercambio Editorial.

Gaucheron, F. (2005). The minerals of milk. Reproduction, Nutrition, Development, 45(4), 473–83.

Giangiacomo, R., Braga, F., & Galliena, C. (1991). Use of near-infrared spectroscopy to detect whey powder mixed with milk powder. In Near Infrared Spectroscopy, Making Light Work (pp. 399–407).

Goff, D. H. (2016). The Dairy Science and Technology eBook | Food Science. Retrieved from https://www.uoguelph.ca/foodscience/book-page/dairy-science-and-technology-ebook

Guyomarc'h, F., Law, A. J. R., & Dalgleish, D. G. (2003). Formation of soluble and micelle-bound protein aggregates in heated milk. Journal of Agricultural and Food Chemistry, 51(16), 4652–60.

Haenlein, G. F. . (2004). Goat milk in human nutrition. Small Ruminant Research, 51(2), 155–163.

Hamosh, M., Peterson, J. A., Henderson, T. R., Scallan, C. D., Kiwan, R., Ceriani, R. L., … Hamosh, P. (1999). Protective function of human milk: The milk fat globule. Seminars in Perinatology, 23(3), 242–249.

Haug, A., Høstmark, A. T., Harstad, O. M., Bringsvar, T., Saxelin, M., Korpela, R., … Morgan, C. (2007). Bovine milk in human nutrition – a review. Lipids in Health and Disease, 6(1), 25.

Herbert, S., Riou, N., & Devaux, M. (2000). Monitoring the identity and the structure of soft cheeses by fluorescence spectroscopy. Le Lait.

Horiba. (2007). Fluorescence on Small or Solid Samples.

Hougaard, A. B., Lawaetz, A. J., & Ipsen, R. H. (2013). Front face fluorescence spectroscopy and multi-way data analysis for characterization of milk pasteurized using instant infusion. LWT - Food Science and Technology, 53(1), 331–337.

HowStuffWorks. (2015). History of Pasteurization. Retrieved December 29, 2015, from http://science.howstuffworks.com/life/cellular-microscopic/pasteurization1.htm

IDF. (2005). ISO 13875:2005 (IDF 178: 2005) - Liquid milk -- Determination of acid-soluble beta-lactoglobulin content -- Reverse-phase HPLC method.

Iñón, F. A., Garrigues, S., & de la Guardia, M. (2004). Nutritional parameters of commercially available milk samples by FTIR and chemometric techniques. Analytica Chimica Acta, 513(2), 401–412.

Jayat, D., Gaudin, J.-C., Chobert, J.-M., Burova, T. V, Holt, C., McNae, I., … Haertlé, T. (2004). A recombinant C121S mutant of bovine beta-lactoglobulin is more susceptible to peptic digestion and to denaturation by reducing agents and heating. Biochemistry, 43(20), 6312–21.

Jean, K., Renan, M., Famelart, M.-H., & Guyomarc'h, F. (2006). Structure and surface properties of the serum heat-induced protein aggregates isolated from heated skim milk. International Dairy Journal, 16(4), 303–315.

Jensen, H. B., Poulsen, N. A., Møller, H. S., Stensballe, A., & Larsen, L. B. (2012). Comparative proteomic analysis of casein and whey as prepared by chymosin-induced separation, isoelectric precipitation or ultracentrifugation. The Journal of Dairy Research, 79(4), 451–8.

Kamishikiryo-Yamashita, H., Oritani, Y., Takamura, H., & Matoba, T. (1994). Protein content in milk by near-infrared spectroscopy. Journal of Food Science (USA).

Katzenstein, G. E., Vrona, S. A., Wechsler, R. J., Steadman, B. L., Lewis, R. V, & Middaugh, C. R. (1986). Role of conformational changes in the elution of proteins from reversed-phase HPLC columns. Proceedings of the National Academy of Sciences of the United States of America, 83(12), 4268–72.

Kethireddipalli, P., Hill, A. R., & Dalgleish, D. G. (2010). Protein interactions in heat-treated milk and effect on rennet coagulation. International Dairy Journal, 20(12), 838–843.

Kethireddipalli, P., Hill, A. R., & Dalgleish, D. G. (2011). Interaction between casein micelles and whey protein/κ-casein complexes during renneting of heat-treated reconstituted skim milk powder and casein micelle/serum mixtures. Journal of Agricultural and Food Chemistry, 59(4), 1442–1448.

Kittel, C. (1986). Introduction to Solid State Physics. Retrieved from http://hyperphysics.phy-astr.gsu.edu/hbase/tables/semgap.html

Krasaekoopt, W. (2004). Comparison of texture of yogurt made from conventionally treated milk and UHT milk fortified with low-heat skim milk powder. Journal of Food Science, 69 (6), 276-280.

Kulmyrzaev, A. A., Levieux, D., & Dufour, E. (2005). Front-face fluorescence spectroscopy allows the characterization of mild heat treatments applied to milk. Relations with the denaturation of milk proteins. Journal of Agricultural and Food Chemistry, 53(3), 502–7.

Kwan, S. (2002). Principles of Optical Fibers.

Lakowicz, J. (2013). Principles of Fluorescence Spectroscopy. Springer Science & Business Media.

Lamb, A., Payne, F., Xiong, Y. L., & Castillo, M. (2013). Optical backscatter method for determining thermal denaturation of β-lactoglobulin and other whey proteins in milk. Journal of Dairy Science, 96(3), 1356–65.

Laporte, M.-F., & Paquin, P. (1999). Near-Infrared Analysis of Fat, Protein, and Casein in Cow's Milk. Journal of Agricultural and Food Chemistry, 47(7), 2600–2605.

Law, A. J. R., & Leaver, J. (2000). Effect of pH on the Thermal Denaturation of Whey Proteins in Milk. Journal of Agricultural and Food Chemistry, 48(3), 672–679.

Lee, & Sherbon. (2002). Chemical changes in bovine milk fat globule membrane caused by heat treatment and homogenization of whole milk. Journal of Dairy Research, 69(04), 555–567.

Lee, W. J., & Lucey, J. A. (2010). Formation and Physical Properties of Yogurt. Asian-Australasian Journal of Animal Sciences, 23(9), 1127–1136.

Linn, J. (1988). Factors Affecting the Composition of Milk from Dairy Cows. In Designing Foods: Animal Product Options in the Marketplace. Washington D.C.: National Academies Press (US).

Liu, X., Powers, J. R., Swanson, B. G., Hill, H. H., & Clark, S. (2005). Modification of whey protein concentrate hydrophobicity by high hydrostatic pressure. Innovative Food Science & Emerging Technologies, 6(3), 310–317.

Lomer, M. C. E., Parkes, G. C., & Sanderson, J. D. (2008). Review article: lactose intolerance in clinical practice--myths and realities. Alimentary Pharmacology & Therapeutics, 27(2), 93–103.

Lowe, E. K., Anema, S. G., Bienvenue, A., Boland, M. J., Creamer, L. K., & Jiménez-Flores, R. (2004). Heat-induced redistribution of disulfide bonds in milk proteins. 2. Disulfide bonding patterns between bovine beta-lactoglobulin and kappa-casein. Journal of Agricultural and Food Chemistry, 52(25), 7669–80.

Lowry, O., Rosebrough, N., Farr, A., & Randall, R. (1951). Protein measurement with the Folin phenol reagent. J Biol Chem.

Macheboeuf, D., Coulon, J.-B., & D'Hour, P. (2009). Effect of breed, protein genetic variants and feeding on cows' milk coagulation properties. Journal of Dairy Research, 60(01), 43.

Manderson, G. A., Hardman, M. J., & Creamer, L. K. (1998). Effect of Heat Treatment on the Conformation and Aggregation of -Lactoglobulin A , B , and C. Journal of Agricultural and Food Chemistry, 46, 5052–5061.

Manderson, G. A., Hardman, M. J., & Creamer, L. K. (1999). Effect of heat treatment on bovine beta-lactoglobulin A, B, and C explored using thiol availability and fluorescence. Journal of Agricultural and Food Chemistry, 47(9), 3617–3627.

Martin, G. J. O., Williams, R. P. W., & Dunstan, D. E. (2007). Comparison of casein micelles in raw and reconstituted skim milk. Journal of Dairy Science, 90(10), 4543–51.

Maubois, J. L., & Olliver, G. (1997). Extraction of Milk Proteins. In S. Damodaran (Ed.), Food Proteins and Their Applications (pp. 579–596). CRC Press.

McMahon, D. J., & Brown, R. J. (1984). Composition, Structure, and Integrity of Casein Micelles: A Review1. Journal of Dairy Science, 67(3), 499–512.

Ménard, O., Camier, B., & Guyomarc'h, F. (2005). Effect of heat treatment at alkaline pH on the rennet coagulation properties of skim milk. Le Lait.

Meza-Nieto, M. A., González-Córdova, A. F., Piloni-Martini, J., & Vallejo-Cordoba, B. (2013). Effect of β-lactoglobulin A and B whey protein variants on cheese yield potential of a model milk system. Journal of Dairy Science, 96(11), 6777–81.

Meza-Nieto, M. A., Vallejo-Cordoba, B., González-Córdova, A. F., Félix, L., & Goycoolea, F. M. (2007). Effect of beta-lactoglobulin A and B whey protein variants on the rennet-induced gelation of skim milk gels in a model reconstituted skim milk system. Journal of Dairy Science, 90(2), 582–93.

Modest, M. (2003). Radiative Heat Transfer (2nd ed.). Retrieved from http://store.elsevier.com/Radiative-Heat-Transfer/Michael-Modest/isbn-9780080515632/

Moro, A., Gatti, C., & Delorenzi, N. (2001). Hydrophobicity of whey protein concentrates measured by fluorescence quenching and its relation with surface functional properties. Journal of Agricultural and Food Chemistry, 49(10), 4784–4789.

Mottar, J., Bassier, A., Joniau, M., & Baert, J. (1989). Effect of Heat-Induced Association of Whey Proteins and Casein Micelles on Yogurt Texture. Journal of Dairy Science, 72(9), 2247–2256.

Mulvihill, M., & Donovan, M. (1987). Thermal Denaturation and Aggregation of Whey Proteins. Irish Journal of Food Science and Technology, 11(1), 87–100.

Noble, J. E., & Bailey, M. J. A. (2009). Quantitation of protein. Methods in Enzymology, 463, 73–95. http://doi.org/10.1016/S0076-6879(09)63008-1

Noh, B., & Richardson, T. (1989). Incorporation of Radiolabeled Whey Proteins into Casein Micelles by Heat Processing. Journal of Dairy Science, 72(7), 1724–1731.

Nollet, L. M. L. (2004). Handbook of Food Analysis: Physical characterization and nutrient analysis. CRC Press.

O'Connell, J., & Fox, P. (2003). Heat-induced coagulation of milk. In P. F. Fox & P. L. H. McSweeney (Eds.), Advanced Dairy Chemistry—1 Proteins (pp. 879–945). Boston, MA: Springer US.

O'Mahony, J. A., & Fox, P. F. (2014). Milk: An Overview. In M. Boland, H. Singh, & A. Thompson (Eds.), Milk Proteins: From Expression to Food (2nd ed., pp. 20–61).

Øgendal, L. (2013). Light Scattering Demystified Theory and Practice, (July), 129.

Oldfield, D. J., Singh, H., Taylor, M. W., & Pearce, K. N. (1998). Kinetics of Denaturation and Aggregation of Whey Proteins in Skim Milk Heated in an Ultra-high Temperature (UHT) Pilot Plant. International Dairy Journal, 8(4), 311–318.

Oldfield, D. J., Singh, H., Taylor, M. W., & Pearce, K. N. (2000). Heat-induced interactions of β-lactoglobulin and α-lactalbumin with the casein micelle in pH-adjusted skim milk. International Dairy Journal, 10(8), 509–518.

Painter, P. C., & Coleman, M. M. (2008). Essentials of Polymer Science and Engineering. DEStech Publications, Inc.

Parris, N., Purcell, J. M., & Ptashkin, S. M. (1991). Thermal denaturation of whey proteins in skim milk. Journal of Agricultural and Food Chemistry, 39(12), 2167–2170.

Pasin, G., & Miller, S. L. (2000). Sports Nutrition U . S . Whey Products and Sports Nutrition. Applications Monograph Sports Nutrition, 1–8.

Pedretti, N., Bertrand, D., Semenou, M., Robert, P., & Giangiacomo, R. (1993). Application of an experimental design to the detection of foreign substances in milk. Journal of Near Infrared Spectroscopy, 1(1), 174.

Pellegrino, L. (Milan S. U. (Italy). D. of F. S. and T. (1994). Influence of fat content on some heat-induced changes in milk and cream. Netherlands Milk and Dairy Journal (Netherlands).

Pierce Biotechnology. (2015a). Chemistry of Protein Assays.

Pierce Biotechnology. (2015b). Pierce BCA Protein Assay Kit Instructions.

Prasad, R. V., Butkowski, R. J., Hamilton, J. W., & Ebner, K. E. (1982). Amino acid sequence of rat .alpha.-lactalbumin: a unique .alpha.-lactalbumin. Biochemistry, 21(7), 1479–1482.

Qin, B. Y., Bewley, M. C., Creamer, L. K., Baker, E. N., & Jameson, G. B. (1999). Functional implications of structural differences between variants A and B of bovine beta-lactoglobulin. Protein Science, 8(1), 75–83.

Rahimi Yazdi, S., & Corredig, M. (2012). Heating of milk alters the binding of curcumin to casein micelles. A fluorescence spectroscopy study. Food Chemistry, 132(3), 1143–1149.

Regan, J. O., Ennis, M. P., & Mulvihill, D. M. (2009). Milk proteins. In Handbook of Hydrocolloids (pp. 298–358). Elsevier.

Renard, D., Lefebvre, J., Griffin, M. C. A., & Griffin, W. G. (1998). Effects of pH and salt environment on the association of β-lactoglobulin revealed by intrinsic fluorescence studies. International Journal of Biological Macromolecules, 22(1), 41–49.

Robert, P., Bertrand, D., Devaux, M. F., & Grappin, R. (1987). Multivariate analysis applied to near-infrared spectra of milk. Analytical Chemistry, 59(17), 2187–2191.

Rodríguez, F., Aguado, J., Calles, J., Cañizares, P., López, B., Santos, A., & Serrano, D. (2014). Ingeniería de la industria alimentaria (Vol 3). Madrid: Editoria Síntesis, S.A.

Roefs, S., & de Kruif, K. (1994). A Model for the Denaturation and Aggregation of β-Lactoglobulin. European Journal of Biochemistry.

Rüegg, M., Moor, U., & Blanc, B. (1977). A calorimetric study of the thermal denaturation of whey proteins in simulated milk ultrafiltrate. Journal of Dairy Research, 44(03), 509–520.

Schamberger, G. P., & Labuza, T. P. (2006). Evaluation of Front-face Fluorescence for Assessing Thermal Processing of Milk. Journal of Food Science, 71(2), C69–C74.

Schokker, E. P., Singh, H., & Creamer, L. K. (2000). Heat-induced aggregation of beta-lactoglobulin A and B with alpha-lactalbumin. International Dairy Journal, 10(2000), 843–853.

Schorsch, B. C., Wilkins, D. K., Jonest, M. G., & Norton, I. T. (2001). Gelation of casein-whey mixtures: effects of heating whey proteins alone or in the presence of casein micelles. The Journal of Dairy Research, 68(3), 471–81.

Schorsch, C., Wilkins, D., Jones, M., & Norton, I. (2001). Gelation of casein-whey mixtures: effects of heating whey proteins alone or in the presence of casein micelles. Journal of Dairy Research, 68(03), 471–481.

Sharma, S. K., & Dalgleish, D. G. (1994). Effect of heat treatments on the inocorporation of milk serum proteins into the fat globule membrane of homogenized milk. Journal of Dairy Research, 61, 375–384.

Sinaga, H., Bansal, N., & Bhandari, B. (2016). Effects of milk pH alteration on casein micelle size and gelation properties of milk. International Journal of Food Properties, 2912(March), 10942912.2016.1152480.

Singh, H. (2004). Heat stability of milk. International Journal of Dairy Technology, 57(2-3), 111–119.

Singh, H., & Waungana, A. (2001). Influence of heat treatment of milk on cheesemaking properties. International Dairy Journal, 11(4), 543–551.

Skoog, D. A., Holler, F. J., & Crouch, S. R. (2007). Principles of Instrumental Analysis. Thomson Brooks/Cole.

Smith, P. K., Krohn, R. I., Hermanson, G. T., Mallia, A. K., Gartner, F. H., Provenzano, M. D., … Klenk, D. C. (1985). Measurement of protein using bicinchoninic acid. Analytical Biochemistry, 150(1), 76–85.

Sørensen, L., & Jepsen, R. (1997). Detection of cheese batches exposed to Clostridium tyrobutyricum spoilage by near infrared spectroscopy. Journal of Near Infrared Spectroscopy, 5(1), 91.

Spectrometer Knowledge. (2015). Retrieved December 2, 2015, from http://bwtek.com/spectrometer-introduction/

Tamime, A. Y., & Robinson, R. . (1999). Yoghurt Science and Technology (2nd Edition).

Taterka, H., & Castillo, M. (2014). Analysis of the preferential mechanisms of denaturation of whey protein variants in heat treated milk as a function of temperature and pH for the development of an optical sensor. Rotterdam, the Netherlands: 7th Annual International Whey Conference.

Taterka, H., & Castillo, M. (2015). The effect of whey protein denaturation on light backscatter and particle size of the casein micelle as a function of pH and heat-treatment temperature. International Dairy Journal, 48, 53–59.

Toffanin, V., De Marchi, M., Lopez-Villalobos, N., & Cassandro, M. (2015). Effectiveness of mid-infrared spectroscopy for prediction of the contents of calcium and phosphorus, and titratable acidity of milk and their relationship with milk quality and coagulation properties. International Dairy Journal, 41, 68–73.

Tran Le, T., Saveyn, P., Hoa, H. D., & Van der Meeren, P. (2008). Determination of heat-induced effects on the particle size distribution of casein micelles by dynamic light scattering and nanoparticle tracking analysis. International Dairy Journal, 18(12), 1090–1096.

Tsenkova, R., Atanassova, S., Toyoda, K., Ozaki, Y., Itoh, K., & Fearn, T. (1999). Near-infrared spectroscopy for dairy management: measurement of unhomogenized milk composition. Journal of Dairy Science, 82(11), 2344–51.

Vasbinder, A. J., Alting, A. C., & de Kruif, K. G. (2003). Quantification of heat-induced casein–whey protein interactions in milk and its relation to gelation kinetics. Colloids and Surfaces B: Biointerfaces, 31(1), 115–123.

Vasbinder, A. J., & de Kruif, C. G. (2003). Casein–whey protein interactions in heated milk: the influence of pH. International Dairy Journal, 13(8), 669–677.

Vasbinder, A. J., Rollema, H. S., & de Kruif, C. G. (2003). Impaired rennetability of heated milk; study of enzymatic hydrolysis and gelation kinetics. Journal of Dairy Science, 86(5), 1548–1555.

Verheul, M., Roefs, S. P. F. M., & de Kruif, K. G. (1998). Kinetics of Heat-Induced Aggregation of β-Lactoglobulin. Journal of Agricultural and Food Chemistry, 46(3), 896–903.

Vivian, J. T., & Callis, P. R. (2001). Mechanisms of tryptophan fluorescence shifts in proteins. Biophysical Journal, 80(5), 2093–109.

Walstra, P. (1990). On the Stability of Casein Micelles. Journal of Dairy Science, 73(8), 1965–1979.

Walstra, P., & Jenness, R. (1984). Dairy chemistry and physics.

Walstra, P., Wouters, J. T. M., & Geurts, T. J. (2005). Dairy Science and Technology, Second Edition. CRC Press; 2 edition.

Waungana, A., Singh, H., & Bennett, R. J. (1996). Influence of denaturation and aggregation of β-lactoglobulin on rennet coagulation properties of skim milk and ultrafiltered milk. Food Research International, 29(8), 715–721.

Wedholm, A., Larsen, L. B., Lindmark-Månsson, H., Karlsson, A. H., & Andrén, A. (2006). Effect of Protein Composition on the Cheese-Making Properties of Milk from Individual Dairy Cows. Journal of Dairy Science, 89(9), 3296–3305.

Wesstrom, O. (1992). Inline pH Measurement for the Food / Dairy and Beverage Industry.

WHO, & FAO. Codex Alimentarius: Milk and milk products (2011).

Wold, J. P., Jørgensen, K., & Lundby, F. (2002). Nondestructive measurement of light-induced oxidation in dairy products by fluorescence spectroscopy and imaging. Journal of Dairy Science, 85(7), 1693–704.

Wolfbeis, O. S. (1985). Fluorescence optical sensors in analytical chemistry. TrAC Trends in Analytical Chemistry, 4(7), 184–188.

Wu, D., Nie, P., He, Y., & Bao, Y. (2011). Determination of Calcium Content in Powdered Milk Using Near and Mid-Infrared Spectroscopy with Variable Selection and Chemometrics. Food and Bioprocess Technology, 5(4), 1402–1410.

Ye, A., Singh, H., Oldfield, D. J., & Anema, S. (2004). Kinetics of heat-induced association of β-lactoglobulin and α-lactalbumin with milk fat globule membrane in whole milk. International Dairy Journal, 14(5), 389–398.

Ye, S., Singh, H., Taylor, M., & Anema, S. (2004). Interactions of whey proteins with milk fat globule membrane proteins during heat treatment of whole milk. Le Lait, 72(84), 269–283.